University of Alberta

Structural Health Monitoring of Syncrude's Aurora II Oil Sand Crusher

by

Ved Prakash Sharma ©

A thesis submitted to the Faculty of Graduate Studies and Research
in partial fulfillment of the requirements for the degree of

Doctor of Philosophy

In

Structural Engineering

Department of Civil and Environmental Engineering

Edmonton, Alberta

Fall 2007

Library and
Archives Canada

Published Heritage
Branch

395 Wellington Street
Ottawa ON K1A 0N4
Canada

Bibliothèque et
Archives Canada

Direction du
Patrimoine de l'édition

395, rue Wellington
Ottawa ON K1A 0N4
Canada

Your file Votre référence
ISBN: 978-0-494-33062-3
Our file Notre référence
ISBN: 978-0-494-33062-3

NOTICE:
The author has granted a non-exclusive license allowing Library and Archives Canada to reproduce, publish, archive, preserve, conserve, communicate to the public by telecommunication or on the Internet, loan, distribute and sell theses worldwide, for commercial or non-commercial purposes, in microform, paper, electronic and/or any other formats.

The author retains copyright ownership and moral rights in this thesis. Neither the thesis nor substantial extracts from it may be printed or otherwise reproduced without the author's permission.

AVIS:
L'auteur a accordé une licence non exclusive permettant à la Bibliothèque et Archives Canada de reproduire, publier, archiver, sauvegarder, conserver, transmettre au public par télécommunication ou par l'Internet, prêter, distribuer et vendre des thèses partout dans le monde, à des fins commerciales ou autres, sur support microforme, papier, électronique et/ou autres formats.

L'auteur conserve la propriété du droit d'auteur et des droits moraux qui protège cette thèse. Ni la thèse ni des extraits substantiels de celle-ci ne doivent être imprimés ou autrement reproduits sans son autorisation.

In compliance with the Canadian Privacy Act some supporting forms may have been removed from this thesis.

While these forms may be included in the document page count, their removal does not represent any loss of content from the thesis.

Conformément à la loi canadienne sur la protection de la vie privée, quelques formulaires secondaires ont été enlevés de cette thèse.

Bien que ces formulaires aient inclus dans la pagination, il n'y aura aucun contenu manquant.

Canada

Dedicated to my

Big Loving Family

and Inspiring Professors

ABSTRACT

Structural Health Monitoring (SHM) is an emerging tool aimed to take a structure from passive to an active state in terms of intelligence and self diagnosis. However, many issues remain to be addressed before SHM becomes a readily usable and easily accessible tool. Techniques for extracting structural signatures, managing data, and detecting structural changes or damage remain core areas of research. This research on the Aurora II oil sand crusher of Syncrude Canada Limited in Fort McMurray, Alberta, extends the application of SHM beyond the conventional boundaries of bridges and buildings to industrial structures. A range of design parameters need to be tested, more detailed loading information needs to be obtained, and long term data on real field conditions are required for future design enhancements in the structure, which this research project strives to fulfill.

The Aurora II crusher has been instrumented with a state-of-the-art data acquisition system to regularly monitor and provide a health report on demand. This research establishes a knowledge-base on crusher behaviour and the loads acting on it under different operating conditions. Structural behaviour of the crusher including strain patterns and their inter-relationship with different dump types, critical strain magnitudes, and impact factors at various locations under severe loading have been established. Dynamic properties of the structure such as fundamental frequencies of vibration and their modal damping ratios have been determined. Fatigue analysis on the structural components revealed a reasonable fatigue life in general; however, factors like higher critical stresses due to a history of loss of bolts lead to a recommendation for annual

inspection and tightening of bolts. Pontoon and hopper response are found to be quite stable whereas some of the columns are heavily stressed under extreme loading. Under similar conditions, most of the bracing members show signs of excessive bending as well as axial stresses indicating design vulnerability that could lead to issues with serviceability and fatigue. Hence, they are recommended for review in future designs of the crusher structure.

With about 1.5 GB of data produced each day, data processing and management assumed great importance. Using strain jump as the metric of dump events, a multi threshold based data processing and management algorithm has been developed to successfully reduce data by 10,000 times. The dump events identified are verified across a number of selected gauges before writing into a database of dump events. Statistical analyses were conducted to establish the parameters for monitoring the structure. A finite element model of the structure has been calibrated with field observations to propose a new field design load case. A numerical damage simulation exercise has led to decisions on suitable strategies for damage detection by monitoring the strain magnitudes and strain patterns in the vicinity of a damage. The data processing and management system, the structural behaviour and strain patterns, statistical parameters, and finite element model together constitute an SHM system that is able to provide on demand health report of the crusher, predict its remaining life and monitor its performance.

ACKNOWLEDGEMENTS

I would like to begin with special words of appreciation for my supervisor Dr. J. J. Roger Cheng, who has been the primary reason behind such an exciting research project and a great university industry partnership, for all his guidance and kind words of wisdom. The academic training and industrial exposure gained in the course of the project along with the many opportunities to share with fellow researchers at the ISIS Canada research network and its annual conferences have had a strong bearing on this research and will continue to do so in the future. Financial support received during the course of this study in the form of NSERC Industrial Postgraduate Scholarship, ISIS Canada Open Scholarship, CSCE Donald Jamieson Fellowship, Syncrude Canada Ltd. and the University of Alberta research fellowships and grants are gratefully acknowledged.

My sincere thanks to Syncrude Canada Ltd. and its research staff in particular Dr. Khaled Obaia, Jesse Neudorf and Silvia Gonzalez for their unwavering support to the research project and for providing all the logistics at site. I would also like to acknowledge the support of Krupp Canada Inc. by providing their finite element models of the hopper and the pontoons, and also the structural drawings of the crusher. Help and advice received from Dr. Alaa E. Elwi during instrumentation, testing and data analysis is gratefully acknowledged. I would also like to thank and acknowledge help received from Dr. Simaan Abourizk and his team of programmers Stephen Hague and Jon San Agustin in coding the data processing and management algorithm into Visual Basic. Special words of thanks go to Roy Gitzel, Richard Helfrich and Larry Burden for help in data collection and instrumentation. Thanks are also extended to Cara Denkhaus for help during instrumentation and some initial data processing. Many fruitful discussions and advice obtained from Dr. Nadeem Khattak, Dr. Shahab Afhami and Dr. Mohammad Behbahanifard have been quite helpful at different stages of the research project in gaining a better understanding of instrumentation, field testing and structural behaviour.

I would also like to take this opportunity to express my gratitude to Dr. Ram Krishna Yaji and Dr. K. R. Narayanaswamy Setty of the National Institute of Technology, Karnataka,

India, and Dr. Pennung Warnitchai of the Asian Institute of Technology, Bangkok, Thailand, for being there for me whenever I have needed them. Last but not the least, all this would not have been possible without the inspiration, love and support of my big family, parents, in-laws, brother and sisters, and most especially my wife Anupama and my two loving sons Vishwam and Vishruth.

TABLE OF CONTENTS

Chapter	Title	Page
	Title Page	
	Abstract	
	Acknowledgement	
	Table of Contents	
	List of Figures	
	List of Tables	
	List of Symbols and Abbreviations	
1.	Introduction	1
	1.1 Introduction to SHM	1
	1.2 Background and Motivation	2
	1.3 Objectives and Scope of Research	5
	1.4 Methodology and Layout	7
	1.5 References	8
2.	Aurora II Crusher and Oilsand Technology – A Review	10
	2.1 Background to Oilsand	10
	2.2 The Oilsand Technology	11
	2.2.1 Brief History	11
	2.2.2 Mining	12
	2.2.3 Extraction	16
	2.2.4 Upgrading	16
	2.3 The Aurora II Crusher	17

2.3.1 Introduction to the Crusher 17
2.3.2 Development of the Crusher and its Future 19
2.3.3 Structural Components of the Crusher 21
2.3.4 Structural Health of the Crusher 25
2.4 Past Researches at Syncrude 26
2.4.1 Investigations of Double Roll Crusher 7 26
2.4.2 Other Relevant Research on Crushers 29
2.4.3 Vibration and Dynamic Load Studies at Syncrude 30
2.5 References 33

3. Instrumentation and Data Acquisition 36
3.1 General 36
3.2 Introduction to Measurement and Data Acquisition 36
3.3 National Instruments DAQ Specifications 41
3.4 Sensors – Selection Specifications and Application 45
3.4.1 Weldable Strain Gauges 46
3.4.2 Accelerometers LVDT and Thermocouples 47
3.5 Instrumentation Details and Locations 51
3.5.1 Hopper Strain Gauges 52
3.5.2 Column Strain Gauges 53
3.5.3 Pontoon Strain Gauges 60
3.5.4 LVDT, Accelerometers and Thermocouples Locations 62
3.6 Field Testing 63
3.6.1 Base Data and Temperature Data Collection Oct 2003 63
3.6.2 Controlled Testing and Normal Operation - April 2004 65
3.6.3 Continuous Data Collection in June 2006 66
3.7 References 67

4. Data Processing and Management 69
4.1 Introduction 69
4.2 Data Files and Features 70

4.3 Signal Characteristics and Dump Events 74
4.4 Strain Jump as Identifier and Metric of Dump Events 77
4.5 Event Identification and Data Reduction – Needs & Review 79
4.6 Spike Detection – A Literature Review in Neuroscience 83
  4.6.1 General 83
  4.6.2 Threshold Based Spike Detection 85
  4.6.3 Other Detection Methods 87
4.7 Proposed Data Processing Algorithm 88
  4.7.1 Program Overview 89
  4.7.2 Data Processing Algorithm for Event Identification 96
  4.7.3 Minor Event Identification Algorithm 101
  4.7.4 Event Verification and Database Entry 103
4.8 Class Diagram 111
4.9 Database of Dump Events 114
4.10 Summary 117
4.11 References 118

5. Structural Behaviour of Crusher 120
5.1 General 120
5.2 Understanding the Load 120
5.3 Zero Load Readings of Sensors 123
5.4 Adequacy of Rate of Data Acquisition 124
5.5 Analysis of Thermal Data 127
5.6 Parameters for Presentation of Field Testing Results 138
5.7 Behaviour under Controlled Empty Hopper Dumping 140
  5.7.1 Strain Jump along Column Gridlines 140
  5.7.2 Pontoon Behaviour under Empty Hopper Dumping 149
  5.7.3 Hopper Behaviour under Empty Hopper Dumping 152
5.8 Impact Factor 153
  5.8.1 Definition of Impact Factor 153
  5.8.2 Factors Affecting Impact Factor 156

5.8.3 Impact Factors for the Empty Hopper Dump C1-L 157
5.8.4 Average Impact Factor on Pontoon during Normal Op. 165
5.8.5 Average Impact Factors for Columns and Hopper 171
5.9 Influence of Various Dump Parameters on Strain Jump 172
5.9.1 Empty Hopper Strain Jump vs. Full Hopper Static 172
5.9.2 Influence of Side of Dump on Strain Jump 175
5.9.3 Influence of Duration of Dump on Strain Jump 178
5.9.4 Influence of Hopper Material Level on Strain Jump 181
5.10 Displacement and Acceleration Readings 182
5.11 Summary and Conclusions 183
5.12 References 185

6. Dynamic Properties of the Crusher 186
6.1 Introduction 186
6.2 Scope of Work 187
6.3 Dynamics of the Load on Aurora II 188
6.4 Vibration Based Damage Detection 189
6.5 Signal Processing Tools for Dynamic Analysis 190
6.6 Frequency Analysis 194
6.7 Natural Frequencies of the Aurora II Crusher 197
6.8 Band Filtering for Modal Amplitude and Damping 212
6.9 Summary 222
6.10 References 223

7. Statistical Analysis of Dump Events and Fatigue Life 225
7.1 Introduction 225
7.2 Strain Jump Stats at the Critical Gauges 225
7.3 Histogram of Strain Jump at the Critical Gauges 230
7.4 Fatigue Life Calculations 239
7.5 Summary 242
7.6 References 243

8. Finite Element Modelling and Simulation 244

8.1 Introduction 244

8.2 Krupp's STAAD Pro Model 244

8.3 Model Calibration and New Field Design Load Case 246

8.3.1 Calibration by Trial and Error 246

8.3.2 The New Calibrated Design Load Case 250

8.3.3 Model Calibration Results 256

8.3.4 Plate Stresses on Pontoon Girder 258

8.3.5 Stress Hot Spots from Analysis 267

8.4 Damage Simulation 271

8.5 Summary 277

8.6 References 277

9. Summary Conclusions and Recommendations 278

9.1 Summary 278

9.2 Conclusions 287

9.3 Recommendations 289

Appendix A Sample Input File for Field Design Load Case 292

LIST OF FIGURES

Figure	Title	Page
2.1	Shovel digging and scooping oil sand at Syncrude Mine	14
2.2	Hydraulic shovel pouring oil sand into 400 ton haul truck	14
2.3	Haul truck dumping oil sand into the crusher hopper	15
2.4	Crusher oil sand transported on conveyor belt to the surge tank	15
2.5	A view of the Aurora II crusher plant from the north side	19
2.6	A view of the diamond shaped hopper from top	22
2.7	A view of the hopper and column from underneath the crusher plant	23
2.8	Finite element model of the hopper and columns	23
2.9	Picture showing the two pontoons supporting the crusher columns	24
2.10	Finite element model of the pontoons	24
2.11	Instances of past problems at crusher	26
3.1	National Instruments Data Acquisition System	41
3.2	Aliasing effects due to under sampling (National Instruments)	44
3.3	Application and protection of a weldable strain gauge	48
3.4	Different operating principles of accelerometers (Bruel and Kjaer)	49
3.5	Hopper instrumented region	52
3.6	Hopper strain gauge location	52
3.7	Hopper gauge location on drawing	53
3.8	Hopper strain gauges view	53
3.9	Aurora II plan with pontoons and column gridlines	55
3.10	Strain gauges on columns at gridline 2	56
3.11	Strain gauges and LVDT on columns at gridline 4	57
3.12	Strain gauges on columns at gridline 5	58

3.13 Strain gauges and accelerometers on columns at gridline 6 59
3.14 Pontoon gauge P53 60
3.15 Pontoon strain gauges 61
3.16 Picture of pontoon gauges 61
3.17 LVDT set up at column top 63
3.18 Accelerometers at foundation level 63

4.1 Typical impact due to a Dump Event 75
4.2 Sample strain time history with a single Dump Event 78
4.3 Strain Jump calculated on a 1 second moving window 78
4.4 Measurement of neural action potentials 81
4.5 Influence of threshold level on neural spike detection (Lewicki, 98) 86
4.6 Finding an optimum threshold level (source: Lewicki, 1998) 86
4.7 An overview of data processing algorithm 90
4.8 Flow chart for major Dump Event identification 91
4.9 Flow chart for minor Dump Event identification 92
4.10 Flow chart for Dump Event verification and database entry 93
4.11 Strain vs. time plot for the pontoon gauges –a minor dump 106
4.12 Strain vs. time plot for the selected critical gauges – a minor dump 106
4.13 Strain vs. time plot for the pontoon gauges – a major dump 107
4.14 Strain vs. time plot for the selected critical gauges – a major dump 107
4.15 Example of Dump Event not verified in one channel 108
4.16 Example of Dump Event not verified in more than one channels 108
4.17 Wrong rejection of a Dump Event 109
4.18 Wrong detection of a Dump Event 109
4.19 Strain Jump with noise greater than 18 Hz filtered out 110
4.20 Filtered out noise greater than 18 Hz 110
4.21 Class diagram for the data processing program 113

5.1 Zero oil sand load strain readings of pontoon gauges 124
5.2 Probability distribution of strain change between readings 126

5.3 Avg strain change for diff number of data points on a sinusoidal arm 126

5.4 Variation of strain with temperature per minute 129

5.5 Strain vs. temperature averaged over every 10 minutes 129

5.6 Standard deviation of Average for different averaging intervals 134

5.7 Mean of SDev for different averaging intervals 134

5.8 Standard deviation of SDev for different averaging intervals 135

5.9 Line of regression for strain variation with temperature 135

5.10 Extrapolated strain variation with temperature at pontoon gauges 137

5.11 Extrapolated strain variation with temperature at column gauges 137

5.12 Strain jump at column gauges on gridline 2 for dump C1-L 144

5.13 Strain jump at column gauges on gridline 4 for dump C1-L 144

5.14 Strain jump at column gauges on gridline 5 for dump C1-L 145

5.15 Strain jump at column gauges on gridline 6 for dump C1-L 145

5.16 Axial and bending strains separated at gridline 2 column gauges 148

5.17 Axial and bending strains separated at gridline 4 column gauges 148

5.18 Axial and bending strains separated at gridline 5 column gauges 149

5.19 Axial and bending strains separated at gridline 6 column gauges 149

5.20 Strain Jump recorded at pontoon gauges for dump C1-L 150

5.21 Absolute strain jump at pontoon gauges for dump C1-L 151

5.22 Absolute strain jump at pontoon gauges for various dump events 151

5.23 Strain jump recorded at hopper gauges for dump C1-L 152

5.24 Definition of impact factor 154

5.25 Static component of strain at gridline 6 columns for dump C1-L 155

5.26 Static and dynamic components of strain at grid 6 columns for C1-L 155

5.27 Impact factors at pontoon gauges for dump C1-L 161

5.28 Impact factors at hopper gauges for dump C1-L 161

5.29 Impact factors at column gridline 6 for control dump C1-L 162

5.30 Impact factor variation with static strain for dump C1-L 162

5.31 Impact factor variation with strain jump for dump C1-L 163

5.32 Strain jump variation with static strain for dump C1-L 163

5.33 Strain jump variation with static strain for dump C1-L 164

5.34 Strain jump variation with static strain – new slope 164
5.35 Impact factor distribution at different static strain levels 168
5.36 Impact factor at different static strain levels – a close up view 168
5.37 Impact factor at different static strain levels for different Dumps 169
5.38 Impact factor at different static strain levels for diff Dumps -3D 169
5.39 Static strain change along the pontoon for different Dump Events 170
5.40 Impact factor distribution along pontoon gauges for different dumps 170
5.41 Empty hopper strain jump vs. full hopper static strain 174
5.42 Comparison of various Dump Events along pontoon gauges 174
5.43 Strain jump along the pontoon for different control dump events 177
5.44 Normalized strain jump along the pontoon for different dump types 177
5.45 Strain jump variation with dump duration for pontoon gauges 180
5.46 Normalized strain jump plot with duration of Left dumps 180
5.47 Variation of strain jump with hopper material level 182

6.1 Ideal and real Filter Transfer Functions (National Instruments) 194
6.2 Butterworth Filter response (National Instruments) 194
6.3 Power spectrum for data collected on pontoon gauges during dump 199
6.4 Signal at gauge P52 passed through a high pass 5 Hz cut-off Filter 200
6.5 Signal at gauge P52 passed through a high pass 10 Hz cut-off Filter 200
6.6 Signal at gauge P52 passed through a high pass 15 Hz cut-off Filter 201
6.7 Signal at gauge P52 passed through a high pass 18 Hz cut-off Filter 201
6.8 Signal at gauge P52 passed through a low pass 18 Hz cut-off Filter 202
6.9 Signal at gauge P52 after passing through an 18 Hz low pass Filter 202
6.10 Signal at gauge P52 passed through a low pass 5 Hz cut-off Filter 203
6.11 Signal at gauge P52 passed through a low pass 0.1 Hz cut-off Filter 204
6.12 Power spectrum for 10 sec long data at gauges P51 and P52 206
6.13 Power spectrum for 50 sec long data at gauges P51 and P52 206
6.14 Power spectrum for 100 sec long data at gauges P51 and P52 207
6.15 Power spectrum for 200 sec long data at gauges P51 and P52 207
6.16 Power spectrum during dump C5-R at gauges P51 and P52 209

6.17 Power spectrum during multiple dumps at gauges P51 and P52 210
6.18 Power spectrum for data during severe Dump C1-L in April 2004 210
6.19 Power spectrum for data collected at pontoon gauges in June 2006 211
6.20 Power spectrum for data collected at column gauges in June 2006 211
6.21 Contribution of noise frequencies between 42 and 48 Hz to response 216
6.22 Contribution of noise frequencies between 15 and 25 Hz to response 216
6.23 Contribution of 7.81 Hz modal frequency to structural response 217
6.24 Contribution of 6.83 Hz modal frequency to structural response 217
6.25 Contribution of 6.83 and 7.81 Hz modal frequencies to response 218
6.26 Contribution of 5.86 Hz modal frequency to structural response 218
6.27 Contribution of 3.91 Hz modal frequency to structural response 219
6.28 Contribution of mixed frequencies lower than 3.5 Hz to response 219
6.29 Contribution of 2.93 and 3.42 Hz modal frequencies to response 220
6.30 Contribution of modal frequencies lower than 1.5 Hz to response 220
6.31 Contribution of 0.96 Hz modal frequency to structural response 221
6.32 Contribution of 0.49 Hz modal frequency to structural response 221
6.33 Contribution of 0.24 Hz modal frequency to structural response 222

7.1 Mean and extreme values of strain jump at different gauges 228
7.2 Mean and maximum values of strain jump at diff gauge locations 229
7.3 Mean values of Strain Jump at different gauge locations 229
7.4 Histogram of Strain Jump at column gauge C10 on grid-4 Right side 233
7.5 Histogram of Strain Jump at column gauge C5 on grid-4 Right side 233
7.6 Histogram of Strain Jump at column gauge C36 on grid-4 Left side 234
7.7 Histogram of Strain Jump at column gauge C13 on grid-5 Right side 234
7.8 Histogram of Strain Jump at column gauge C20 on grid-6 Right side 235
7.9 Histogram of Strain Jump at bracing gauge C7 on grid-4 Right side 235
7.10 Histogram of Strain Jump at column gauge C34 on grid-4 Left side 236
7.11 Histogram of Strain Jump at bracing gauge C16 on grid-5 Right side 236
7.12 Histogram of Strain Jump at bracing gauge C40 on grid-5 Left side 237
7.13 Histogram of Strain Jump at bracing gauge C24 on grid-6 Right side 237

7.14 Histogram of Strain Jump at gauge P52 on pontoon mid-span 238
7.15 Histogram of Strain Jump at gauge H61 on hopper 238

8.1 Krupp's impact design load case 247
8.2 The oil sand dumping haul truck 248
8.3 Trial uniform load case at bottom of hopper 248
8.4 Trial uniform load case at top of hopper 249
8.5 Vertical components of new design load case 252
8.6 Horizontal components of new design load case 252
8.7 Load distribution at gridline 2 254
8.8 Load distribution at gridline 4 255
8.9 Load distribution at gridline 6 255
8.10 Results matching at gridline 2 259
8.11 Results matching at gridline 4 259
8.12 Results matching at gridline 5 260
8.13 Results matching at gridline 6 260
8.14 Error between field and analysis stresses at gridline 2 261
8.15 Error between field and analysis stresses at gridline 4 261
8.16 Error between field and analysis stresses at gridline 5 262
8.17 Error between field and analysis stresses at gridline 6 262
8.18 Axial stress component matching at gridline 2 263
8.19 Bending stress component matching at gridline 2 263
8.20 Axial stress component matching at gridline 4 264
8.21 Bending stress component matching at gridline 4 264
8.22 Axial stress component matching at gridline 5 265
8.23 Bending stress component matching at gridline 5 265
8.24 Axial stress component matching at gridline 6 266
8.25 Bending stress component matching at gridline 6 266
8.26 Comparison of field and analysis strains on pontoon 267
8.27 Sectional view of pontoon plates stress contour 269
8.28 Isometric view of pontoon plates stress contour 269

8.29 Sectional view of vertical plate shear wall stresses for columns 270
8.30 Sectional view of columns braces and beam stresses 270
8.31 Influence of different damage scenarios on gauges at gridline 2 275
8.32 Influence of different damage scenarios on gauges at gridline 4 275
8.33 Influence of different damage scenarios on gauges at gridline 5 276
8.34 Influence of different damage scenarios on gauges at gridline 6 276

LIST OF TABLES

Table	Title	Page
3.1	Issues at hand for the control test	64
4.1	Dump Events in April 2004 control tests	72
5.1	Comparison of different averaging intervals for temperature readings	131
5.2	Thermal strain slopes at different column gauges (Denkhaus, 2004)	136
5.3	Thermal strain slopes at different pontoon gauges (Denkhaus, 2004)	136
5.4	Thermal strain slopes at different hopper gauges (Denkhaus, 2004)	136
7.1	Statistical properties of Dump Events at the critical gauges	227
8.1	Unit load response for calibration by trial and error	251

LIST OF SYMBOLS AND ABBREVIATIONS

Symbols

F_{max}	Maximum frequency
dF	Frequency resolution
f(n)	Data function
f(s)	Sampling rate of DAQ
g	Acceleration due to gravity
m	Number of full cycles count on a sine wave
N	Total number of data points in a time window
n	Data pointer number
p	Discrete natural frequencies
T	Time period
u_o	Magnitude of starting peak
u_{o+m}	Magnitude of mth peak after starting peak
V	Volts
dV	Small change in voltage
X_p	Amplitude of frequency component of ^{pth} mode
$\Delta\sigma_e$	Equivalent stress change
$\Delta\sigma_i$	Stress change at ith peak
ξ	Modal damping ratio

Abbreviations

C	Degree Celsius
C	Columns
C	Controlled Dumping
D	Double dump
DAQ	Data Acquisition (System)
H	Hopper
Hz	Hertz
I. F.	Impact Factor
ISIS	Intelligent Sensing for Innovative Structures
KHz	Kilo Hertz
kN	Kilo Newton
L	Left side dumping
LVDT	Linear Variable Displacement Transducer
MPa	Mega Pascal
mm	Millimetres
N	Number of cycles to fatigue failure (fatigue life)
N	Newton
P	Pontoons
R	Right side dumping
s	Seconds
SCL	Syncrude Canada Limited
SHM	Structural Health Monitoring
ton	Imperial ton (0.907 Mg)
με	Micro-strains

CHAPTER 1

INTRODUCTION

1.1 General

Civil Engineering Structures were once looked upon as "ever-lasting" and immune to almost anything, a notion proved wrong by many existing and failed structures. Innumerable bridges and other infrastructure today stand in dire need of rehabilitation or replacement in North America and other parts of the world. Current and past practice in civil engineering infrastructure has been to adopt a 'passive-reactive' approach to the maintenance and management of structures and systems. In other words, while a great deal of effort and resources are applied to the design and construction of infrastructure, very little is done after construction to actively monitor the performance and deterioration, or health, of the structure. Only after substantial damage or deterioration has taken place do engineers react and undertake what is by then a costly evaluation and repair or replacement activity. A more proactive solution is to instrument, and continuously monitor infrastructure to give immediate indication of a damage or deterioration in performance, which may affect safety, serviceability or maintenance.

Smart structures today can speak for themselves. They are smart, have a life and its heartbeat can be monitored by continuous/regular monitoring. Not only that, the emphasis is to make them smart enough to diagnose and locate their own damage or distress, and suggest a cure. Structural Health Monitoring (SHM) thus helps in efficient maintenance and management of structures, thereby extending its useful service life. It has been effectively used as a validation tool for new and innovative designs like the steel free bridge deck (Tennyson et al., 2001), new construction materials like fibre reinforced polymers (ISIS Canada, 2001), and new repair techniques like fibre sprayed concrete (Banthia & Boyd, 2000) at an accelerated pace in real life working conditions. Many bridges of national significance, pipelines, and monumental structures are currently being monitored by SHM systems. With new information and real load data, it is only appropriate that health monitoring will lead to improvements in design codes, more efficient and reliable structures, and revolutionize the design of civil engineering structures.

Health monitoring has become a choice with a reckoning for researchers and engineering professionals throughout the world, especially for monitoring aging bridges. However, scores of issues remain to be addressed before SHM could become a readily usable tool. Techniques of extracting structural signatures and detecting variations due to structural changes or damage, remains a core area of research. Vibration based (Amin et al., 2002) and video imaging based damage detection techniques (Poudel et al., in press) have been used in the laboratory with reasonable success, however, their application on complex structures in the field is still a topic of debate and needs to be researched further. There is a clear need to combine the strengths of static and dynamic measurements to complement each other for reliable damage detection. SHM also needs to expand in dimension to encompass different types and domains of structures, for most of the available literature is limited to bridges (ISIS Canada, 2001). The present research on Aurora II crusher is a step out in this direction of extending the utility, application, and benefits of SHM to the industry, where it matters every day. Variability of loads and extreme climatic conditions make the project all the more challenging. Limited test information exists about the loads acting on the structure and its actual structural behaviour as compared to the design expectations, which the current research provides to support the design of future generation of fully mobile crushers. Maintenance and management of the crusher structure will be more reliable with the SHM system keeping track of its “health” at all times. An explicit presentation of directly tangible benefits would, without a shadow of doubt, make SHM an integral part of every structure that matters.

1.2 Background and Motivation

The heart of Alberta’s economy lies in the oil sands of northern Alberta. An estimated 180 billion barrels of oil wealth lies under frozen grounds valued at nine trillion dollars at current market prices, which is second in the world only to Saudi Arabia (New York

Times, 2001). Technology is fast advancing and people are more sensitive to environmental issues now than ever. In such complex industrial and economic scenario, it is only imperative that engineers are required to come up with innovation time and again. Mining operation in the process of extraction of oil from oilsand is the costliest of all. The only way to remain competitive and yet be friendly to the earth is to cut costs and make the process more efficient and reliable. Syncrude Canada Ltd, a leading oil production company based in Fort McMurray, Alberta, devotes significant funds and resources into research to solve existing problems and target higher levels of productivity and efficiency for the future through Syncrude Research. Syncrude Canada Ltd., Krupp Canada Inc., and the University of Alberta have thus joined hands to initiate a Smart Crusher Project, which falls under the broader spectrum of Structural Reliability of Mining Equipment at Syncrude.

The crusher performs the vital function of breaking oilsand into smaller pieces so that it can be transported from mining to the extraction plant by mixing with hot water, called as hydro-transport. The Smart Structures Project has Structural Health Monitoring (SHM) of Aurora II crusher as its important component. The project aims to reduce trucking costs and crusher downtime. It is envisaged that a Fully-Mobile Crusher in the future will bring about significant reduction in haul distances of the trucks dumping oilsand into the crusher hopper, resulting in substantial savings. In a bid to move to the future generation of fully mobile crushers from the present semi-mobile ones, a range of design parameters need to be tested, more detailed loading information needs to be obtained, and long term data on real field conditions are required. The SHM project of Aurora2 crusher is envisaged to be the primary feeder of all this information on loading, boundary conditions, impact factor, and stress ranges etc. to Syncrude and Krupp Canada Inc., the vendors of the crusher. Information on real-life data from the present semi-mobile crushers would form the backbone of design in future generation of crushers for Krupp Canada Inc. The SHM system will also supplement Syncrude in managing its repair and maintenance operations in a realistic manner with continuous feedback and warning about its critical performance. Instead of reacting when a damage or distress has occurred, which is by then a costly affair, a more proactive approach would be to instrument and continuously monitor the crusher to give immediate indication of deterioration in performance.

University of Alberta has a long history of industrial partnership in education and research; and the Civil and Environmental Engineering Department has been a pioneer in research on Structural Health Monitoring of bridges and other innovative structures. Being a host to the Theme Director on SHM of the Intelligent Sensing for Innovative Structures (ISIS, Canada), a Network of Centres of Excellence Program, the university has been monitoring various bridges in Alberta and Canada under the umbrella of ISIS like the Crowchild bridge in Calgary, with innovative steel free bridge deck technology, Fort Saskatchewan bridge, Taylor bridge etc. (ISIS Canada, 2001). ISIS has also been monitoring structures of great historical value like the Golden Boy on Manitoba Legislature Building and the Confederation Bridge in PEI. Other prestigious upcoming projects like the Canadian Parliament Building in Ottawa and various pipeline monitoring applications add diversity to the theme of SHM. In line with their visions, both the university and ISIS look forward to and encourage partnerships with industries to introduce them to the benefits of SHM, and thus this unique research project – a first of its kind in structural engineering.

The focus of this research is to set up an intelligent health-monitoring scheme for the Aurora II crusher plant at Syncrude Canada Ltd. in Fort McMurray, Alberta. This crusher plant is one of the largest in the world with a receiving-hopper of 1000 ton capacity and 1400 ton in weight. It is capable of crushing 15,000 ton per hour and lumps of 3.5 m in length (Krupp Canada, 2003). With such a step out in size as well as the inherent variability in northern climate mining conditions, uncertainties in structural health are a major concern. Any possible shutdown of this crusher will cost literally millions of dollars per day. Continuous health monitoring of the plant will provide on demand reliable data pertaining to the safety and integrity of the structure, keeping track of its behaviour and "health" at all times. Technological advances in communication, sensing, data processing, and information technology, make it feasible to implement structurally integrated health monitoring systems that can actively monitor the health of a structure through its entire service life.

1.3 Objectives and Scope of Research

The following objectives have been set for this research project, which will benefit both industrial partners Syncrude Canada Ltd. and Krupp Canada Inc. by knowing their structure better and having a basis for improved design of fully mobile crushers in the future. Syncrude will also be able to monitor its crusher regularly by the Structural Health Monitoring (SHM) system in place that will provide on demand data pertaining to its behaviour and alert when there is a need for repair/maintenance. The specific objectives of this research are:

1. To design and implement a structural health monitoring system for the Aurora II Crusher
2. To understand the structural behaviour, design and performance of the structure
3. To develop an efficient data processing and management system for the SHM system
4. To conduct statistical analyses, establish fatigue characteristics, establish behaviour patterns and set up monitoring parameters.

In order to fulfill the above mentioned objectives of the research project, the following sub objectives or activities are planned to achieve the goal and define the scope of work.

- To develop and implement a structural health monitoring system for the Aurora II semi-mobile crusher of Syncrude, which can provide on demand health information.

- To study characteristics of the signal obtained from sensors; and explore most suitable ways to process, analyse and extract information from huge amounts of health monitoring data.

- To develop an algorithm for automatic and appropriate processing and management of data for the SHM project, enabling efficient data handling and archiving for long term health monitoring.

- To present structural response of the crusher under different types of loads, devise event recognition parameters, analyze its behaviour patterns, impact factors etc., and compare design with actual performance.

- To determine the dynamic properties of the structure like natural frequencies and modal damping.

- To prepare a finite element model of the structure fine tuned with field behaviour; and present a field design load case that truly represents the field behaviour for a better understanding and design in future.

- To conduct statistical analysis on the health monitoring data to establish the salient statistical features as captured by each monitoring sensor to be used for a long term monitoring based on shift in statistical features.

- To suggest ways of predicting remaining life of the structure and the stress hot spots based on fatigue analysis.

- To propose a health monitoring and damage warning system platform to be built upon in future based on the statistical information and numerical damage simulation.

The health monitoring system established by this research is envisaged to provide the basic framework for Syncrude Canada Ltd. to build upon for industrial application. The results obtained from the tests and the monitoring system are furnished to Krupp for its perusal to consider in the design of future crushers. The finite element model and damage simulation provides the industries with an opportunity to verify their design and analysis in an integrated way with a load case based on real field loading. This research aims to study and monitor the properties and behaviour of the existing structure, however, design aspects of this or the future crushers is beyond its scope.

1.4 Methodology and Thesis Layout

A brief review of the oil sand technology, the Aurora II crusher, its salient features, and past research conducted on it are given in Chapter 2 of this thesis. The crusher has been instrumented with strain gauges, thermo-couples, accelerometers, and LVDT's, totaling 82 in number. A state-of-the-art data acquisition system and communication technology from National Instruments has been used, details of the field instrumentation and testing are given in chapter 3. Intelligent data processing and management are essential for dealing with huge amounts of data and integrated structural health monitoring, which have been implemented in this project as presented in Chapter 4. This chapter gives details of the signal processing tools and techniques used and the algorithm for data reduction and archiving.

Control testing was done to establish a benchmark for the structural behaviour and to understand the influence of various parameters on its performance. It helped establish trend lines and characteristic features for comparing and evaluating performance throughout its life. Obviously, these control tests form the backbone of the SHM system being developed. Ample data has also been collected under normal operation of the crusher to establish the operating stresses and conditions. Structural behaviour of the crusher structure is analysed, and its performance under control tests and normal operation reported in Chapter 5. Parameters for performance signatures are established and influence of temperature and impact are explained. Dynamic properties of the structure like the natural frequencies and damping are also investigated and presented in Chapter 6.

Statistical analysis techniques are employed to extract salient statistical features from structural response data that aid in long term monitoring of the structure as well as carrying out fatigue analysis for the remaining life of the structure. These statistical analyses and remaining life calculations are presented in Chapter 7. Analysis of field data and test results led to the formulation of an appropriate finite element model of the structure finely tuned with experimental measurements. Appropriate damage simulation helps establish a warning and decision system for optimum repair and maintenance of the crusher. In addition, field data gives the most needed validation of design assumptions, especially with regard to handling of impact and vibration. Chapter 8 deals with the finite element modelling of the structure, presentation of a field load case, and damage simulation. Thus, a combination of the state of the art instrumentation, intelligent data processing and management techniques, structural analyses and behaviour patterns, application of statistical tools for monitoring and prediction, and a finite element modelling and simulation exercise lays the foundation for a long term structural health monitoring project for the Aurora II crusher of Syncrude Canada Ltd. The summary of findings of this research, pertinent conclusions and recommendations for future research are presented in Chapter 9 of the thesis.

1.5 References

Amin, M.S., Humar, J.L. & Soucy, Y. 2002. Experimental verification of a vibration based damage detection technique. *Sixth international Symposium on NDE for Health Monitoring and diagnostics, Proc. of SPIE Conference, Los Angeles, 4-8 February 2002.* vol. 4753 I: 428-434

Banthia, N. & Boyd, A.J. 2000. Sprayed fibre reinforced polymers for repairs. *Canadian Journal of Civil Engineering.* October 2000, 27 (5): 907-915.

ISIS Canada 2001. *Guidelines for structural health monitoring*. Winnipeg: ISIS Canada.

Krupp Canada. 2003. Design drawings and modelling of Aurora II crusher. *Personal Communication.*

New York Times. 2001. Global crude oil reserves. http://www.nytimes.com Accessed April 2004.

Poudel, U.P., Fu, G. & Ye, J. in press. Structural damage detection using digital video imaging technique and wavelet transformation. *Journal of Sound and Vibration* (Accepted for publication October 2004).

Tennyson, R.C., Mufti, A.A., Rizkalla, S., Tadros, G. & Benmokrane, B. 2001. Structural health monitoring of innovative bridges in Canada with fibre optic sensors. Journal of Smart Materials and Structures, June 2001, 10 (3): 560-572

CHAPTER 2

AURORA II CRUSHER AND OILSAND TECHNOLOGY

2.1 Background

The heart of Alberta's economy lies in the oil sands of northern Alberta. An estimated nine trillion dollars worth of oil wealth lies under frozen grounds, which is second in the world only to Saudi Arabia. The Canadian oil reserve is estimated to be 180 billion barrels, which accounts for 17% of the currently known sources of all crude oil reserves in the world amounting to 1038 billion barrels (New York Times, 2004). More than 50% of oil production in Canada comes from oil sands. In spite of such large oil reserves, oil exploration in Canada was taking a backbench until recently, primarily due to higher cost of extraction from oil sand. However, thanks to the ever-rising price of oil, now oil sand projects are profitable and hot. As per CIA (2001), Canadian production per day was 2.74 million barrels, which is about 3.6% of the world production of 75.46 million barrels, giving it a tenth rank in the world among oil producers. These figures are all set to change drastically in the coming years with many new ventures in the offing. Syncrude Canada Limited currently supplies thirteen percent of the nation's requirement, producing 0.35 million barrels of crude oil per day.

The effects of oil sand on the economy of Canada and Alberta in particular are far reaching and enormous, which has become evident over the years. With the magnitude of the things at stake, all parties seem to be seriously committed to keeping the momentum going. Technology is fast advancing and people are more sensitive to environmental issues now than ever. In such complex industrial and economic scenario, it is only imperative that engineers are required to come up with innovation time and again. The only way to remain competitive and yet be friendly to the earth is to cut costs and make the processes more efficient and reliable. This section is devoted to introducing the oil sand technology and its evolution over the years. The steps involved in turning oil sand to light crude oil and the role of the Aurora II crusher in the process is highlighted.

Syncrude invests significant resources into research and development to lead the way to innovation in the field, and so do some other companies, to remain highly competitive and profitable. A brief summary of the past research at Syncrude on oil sand mining equipment and components subjected to dynamic loads is presented. Industrial need of the current research in this light is evaluated and justified. Mining operation in the process of extraction of oil from oilsand is the costliest of all, making reliability of mining equipment a vital research area at Syncrude. Instead of reacting when a damage or distress has occurred, which is by then a costly affair, it is more appropriate to instrument and monitor the crusher. It is also envisaged that a Fully-Mobile Crusher in the future will bring about significant reduction in haul distances of the trucks dumping oilsand, resulting in substantial savings. Information and real-life data from the present semi-mobile crushers will form the backbone of design for future generation of crushers.

2.2 The Oilsand Technology

2.2.1 Brief History

Unlike oil wells in the Arab world and elsewhere, the oil in Canada is mixed with sand and water making it a sticky land mass. So, it is not possible to simply drill a hole and pump oil out; a lot more things need to be done before the crude oil is obtained. Naturally, this makes the process much more costly and cumbersome, so much so that its feasibility was under question mark for a long time. However, increasing oil prices and rising demand for sources of energy combined with advances in technology have made it all feasible and profitable. Oil sand is recognized as one of top ten engineering achievements in Canada.

The aboriginal people had been using oilsand to waterproof and repair their canoes for long before the first Europeans spotted bitumen along the banks of Athabasca River over 200 years ago, as per historical documents. Fur trader Peter Pond is named as the first European to have seen and written about the oil sands, while exploring opportunities for fur business (SCL, 2004). Economic value of the oil sand had been felt and narrated by many travelers and writers, which attracted attention of the government as well as explorers and scientists. The first government sponsored geological study of the area was conducted in1875 and was followed up after some years on several occasions. In early twentieth century about 24 wells were sunk in search of pools of oil, but none were successful in finding such pools of oil, rather they discovered salt, which became a major industry in Fort McMurray area for 50 years (SCL, 2004).

The 1920's saw a shift from the notion of oil pools to extracting bitumen from sand. From 1913 until 1945 an engineer named Sidney Ells under the federal department of mines worked extensively on economic extraction of bitumen from sand and advocated hot water flotation method. Oil sand samples were shipped out and tried as road paving material, which was successful but not economically competitive. During the same period around 1920's an entrepreneur, R. C. Fitzsimmons, and a scientist, Dr. Karl Clark were also experimenting with the hot water flotation method of separation of bitumen. Several research and commercial initiatives were undertaken to extract bitumen efficiently and produce diesel. The same hot water flotation method of bitumen extraction is still used today, which was pioneered by Ells, Fitzsimmons, and Clark and proved to be the most viable method. With the publication of an Alberta government report in 1950 indicating oil from the sands could be a profitable venture, there was an upsurge of interest. It was in 1962 that the government announced the oil sand policy to provide for orderly development; and in 1967 came the first oil sand operation by Sun Oil Company (later Suncor Energy). Syncrude Canada Limited produced its first barrel in 1978 and in 1998, produced its one-billionth barrel (SCL, 2004).

2.2.2 Oilsand Mining

Mining operation is the first step towards oil extraction from oil sand. Mining, extraction, upgrading and utilities are the four major technological areas. Most of the mines in Fort McMurray, Alberta are open pit mines. Once the topsoil and vegetation is removed, shovels are brought in to dig and scoop overburden first and then oilsand, which is filled into large haul trucks of 400 ton capacity. Oilsand lies buried 15 m or deeper below the overburden (SCL, 2004). These haul trucks carry the oilsand to the site where the crusher plant is located, and dump it into the hopper of the crusher. Fig 2.1 and 2.2 show the shovels currently used at Syncrude scooping oilsand and dumping into the haul truck. Fig. 2.3 shows the haul truck in operation, dumping oilsand into the hopper of the crusher. They give a feeling of the size of the things involved and the magnitude of the loads under consideration. The future generation of crushers is envisaged to be fully mobile, by which the haul trucks will be eliminated from the system and the shovels can directly dump oil sand into the hopper of the crusher that can move around. This will entail into significant savings on operation and maintenance of haul trucks, which at that size is obviously expensive. The hopper collects the oil sand dumped by trucks; and the apron feeder transports it to the crusher drums. Different speeds of the apron feeder and the crusher drums allow different crusher throughputs. Thus the structure supporting all these components of the crusher is subjected to considerable magnitude of impact from dumping and vibration due to moving parts and machines. Severe climatic conditions only magnify the challenge.

The crushed oilsand is dropped on to a moving conveyor belt that transports it to the surge tank (Fig. 2.4). The sized oil sand is mixed with steam, hot water, and caustic soda to condition it for bitumen extraction, creating aerated slurry. The slurry is then hydrotransported by pipeline from mining to extraction, and during transportation it is also being conditioned for extraction (SCL, 2004).

The sheer size of all the plants and equipment makes the cost of operation and maintenance substantial. Mining is the costliest of all operations with lot of abrasion, wear and tear. Every 24 hours, there is enough metal worn off the mining equipment by abrasive oilsand, to make two full-size pick-up trucks (SCL, 2004).

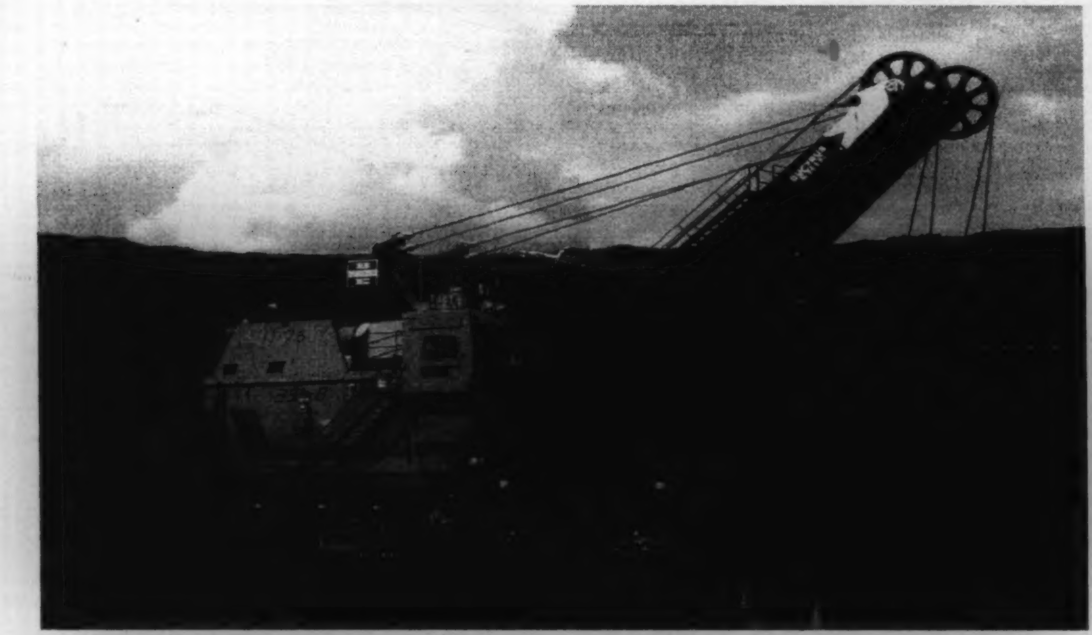

Fig. 2.1 Shovel digging and scooping oilsand at Syncrude

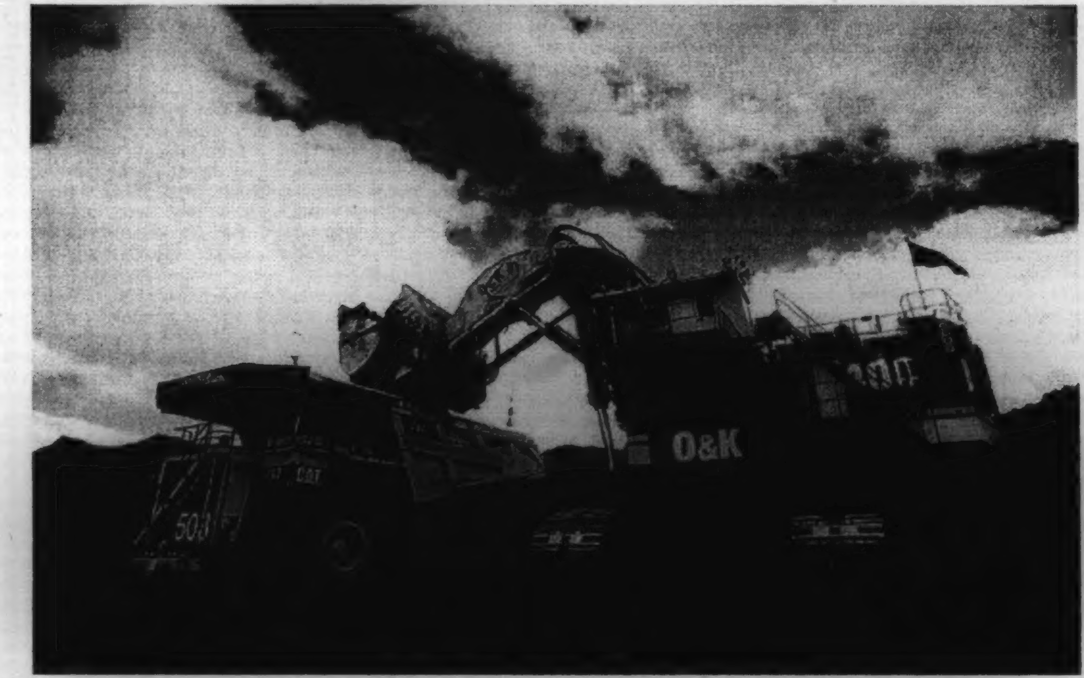

Fig. 2.2 Hydraulic shovel pouring oilsand into 400 ton haul truck (SCL, 2004)

Fig. 2.3 Haul truck dumping oilsand into the crusher hopper (Aurora II, Syncrude)

Fig. 2.4 Crushed oilsand transported on conveyor belt to the surge pile (Aurora II)

2.2.3 Extraction

Aurora II train is using newer technologies bringing about changes that make the process more efficient. In addition to having a larger crusher for mining and bigger haul trucks for ferrying oil sand, it has also introduced the indigenously developed hydrotransport technology to carry sized oil sand from mining to extraction plant. Hydrotransport is a mixing operation that combines oilsand with hot water to create slurry. The oil sand slurry is transported at the rate of 8000 ton per hour and conditioned on the way. The slurry is fed to the Primary Separation Vessels and the Auxiliary Settling Areas where the bitumen floats to the surface as primary froth and the sand settles out. The middlings and underflow streams are sent to the Tailings Oil Recovery Unit where the deep cone vessel secondary floatation plant recovers most of the remaining bitumen. The Aurora plant uses a new low energy extraction process, which operates at a lower temperature of approximately 35 degree Celsius as compared to the earlier process at 80 degrees, consumes only about one third as much energy to extract bitumen froth from the slurry. The extraction complex stands tall as a nine stories high building (SCL, 2004).

Following extraction, the bitumen froth is sent to the Upgrading unit through a 36 inch buried pipeline for froth treatment and bitumen upgrading. Froth treatment minimizes the water and solids going into the upgrader by diluting the froth with naphtha and then put through inclined plate settlers and centrifuges. The Aurora train uses natural froth lubricity to transport the froth for upgrading without using any diluent. The naphtha recovering unit recovers naphtha from all froth treatments (SCL, 2004).

2.2.4 Upgrading

The upgrading process converts viscous tar like bitumen froth to the Syncrude Sweet Blend crude oil, with the lowest sulphur content possible. The upgrading process begins with the diluent recovery units, which distill off diluent naphtha to return to the extraction plant and also distill off some light gas oil to be sent directly to the hydrotreaters for removal of sulphur (SCL, 2004).

The remaining bitumen is then subjected to a vacuum distillation unit operating under vacuum conditions; and LC-Finer hydroprocessor which breaks down bitumen feed through a catalyst assisted reaction with hydrogen. The light and heavy gas oils obtained from both these operations are then sent to the hydrotreaters, whereas residuum bitumen from each of the above processes is fed into the fluid cokers for further processing. The high temperature in the coker causes the bitumen long chain molecules to thermally crack and break down into lighter products like naphtha and oil gas, which are again sent to the hydrotreaters. Thus, the hydrotreater collects the liquid products like oil gas and naphtha, which are high in sulphur and nitrogen, from different sources mentioned above. The hydrotreater reactors induce the oil to react with hydrogen over a packed catalyst bed at high temperatures and pressures, removing sulphur and nitrogen from the oil in the form of hydrogen sulfide and ammonia byproducts. The hydrogen sulfide is converted to elemental sulphur and stored at the plant site in sulphur blocks, whereas the ammonia is burned in the utilities plant boilers as fuel. The coking plant also produces byproducts like sulphurous sour fuel gas that is again sent for sulphur removal, and coke, which is recycled in the coker plant and excess is stored in the mine area for future use (SCL, 2004).

The upgraded crude oil is sent by pipeline to three Edmonton area refineries and to terminals shipping to refineries in Canada and the United States. It takes 3 days at peak for oil to travel from Fort McMurray to Edmonton. The output coming from refineries is the gas sold in retail at gas pumps (SCL, 2004).

2.3 The Aurora II Crusher

2.3.1 Introduction to the Crusher

With a bird's eye view of the whole oil sand processing technology, the crucial role of the crusher plant being monitored becomes evident. Synonymous to its name, it does crush large lumps of oil sand up to 3500 mm in one dimension during frozen ground conditions, into smaller pieces of less than 400 mm for hydro-transportation, as mentioned earlier. The crusher structure consists of three main structural parts, namely – the hopper, columns, and pontoons. The diamond shaped hopper of 1000 ton capacity is capable of receiving oil sand dumps from two 400 ton trucks simultaneously at the Aurora II crusher plant. The hopper is supported by column groups, which in turn rest on the pontoons (Fig. 2.5). The crusher structure is symmetrical longitudinally, with one pontoon on either side of the line of symmetry. The pontoons are the base support for the crushing plant, which consist of a box girder supported on feet that transfer all loads to the foundation. Other important components of the crusher, which are not participating in the load transfer mechanism as a structure but are crucial to its operation and add an additional dead load and vibration load, can be enumerated as the apron feeder, the double roll crusher drums, the conveyor belt passing underneath, and the tower structure housing the operator's cabin. The tower structure is completely segregated from the main plant to minimise the transfer of any vibrations during operation, which can affect the electronic equipment and the operators occupying it during day-to-day inspections. There are also retaining walls around the hopper, which continue for quite some distance. The haul trucks, which cost a million dollar a piece, dump oilsand into the hopper from on top of the retaining wall. Then the oilsand chunks are transported by apron feeder to drop in between the teeth of the double roll crusher drums of 2 m in diameter. The double roll crusher, also called as DRC, rests on a solid platform supported by the pontoons (Krupp Canada, 2003 a b).

The Aurora II Crusher (Fig. 2.5) is designed to accommodate all of the static and dynamic loads imposed by the dumping and crushing of oil sands. Many different load cases were investigated and used in the design of its different components, including the temperature variation of about –50 to +40 degree Celsius. The Aurora II Crusher is a semi-mobile type of crusher costing more than 30 million dollars, which is a step up from the previous version of double roll crushers made in 1992. The crusher weighs 1400 ton and is capable of crushing lumps as large as 3.5 m in size at the throughput of 15000 ton per hour. It is 32.30 m in length, 14.25 m in width and 19 m in height (Krupp, 2003 b). With such a step out in size as well as the inherent variability in unforgiving northern

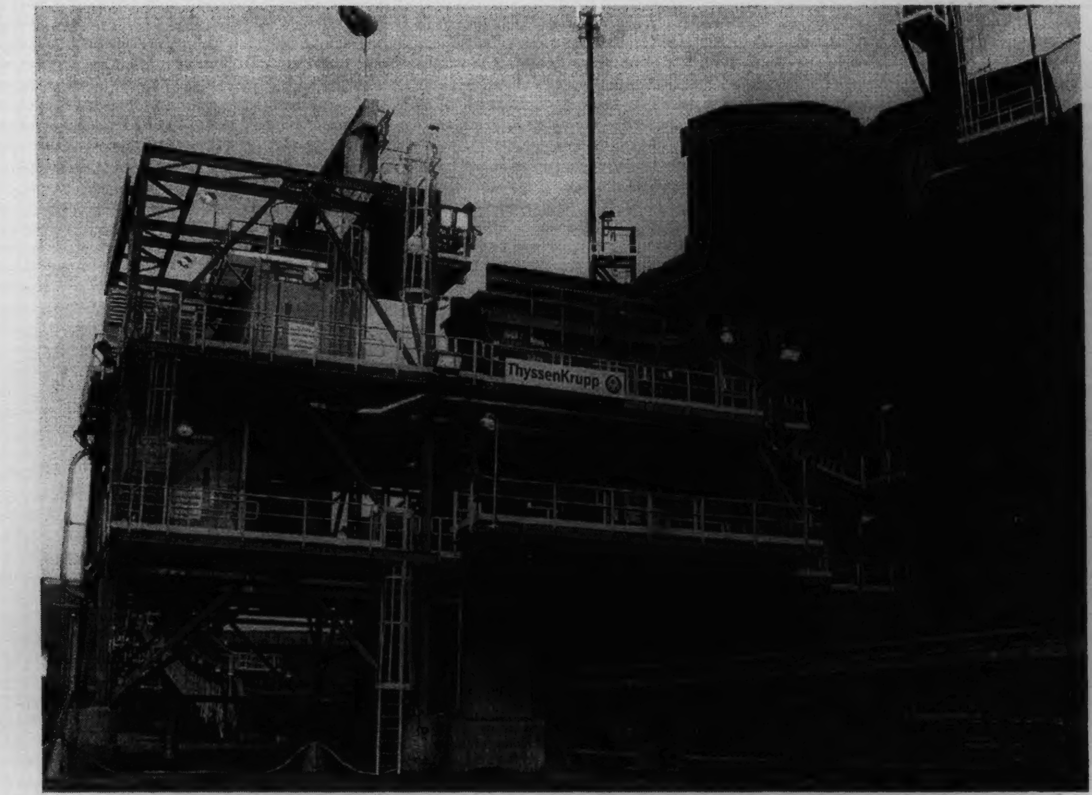

Fig. 2.5 A view of the Aurora II crusher plant from the north side

climate mining conditions, uncertainties in structural health are a major concern. Any possible shutdown of this plant will cost literally millions of dollars per day. (Krupp, 2003 b)

2.3.2 Development of the Crusher and its Future

What stands today as the state of the art Aurora II crusher at Syncrude in Fort McMurray started as the first Double Roll Crusher (DRC) in 1992, specifically designed to operate in oil sands. Prior to that date, different technology like the gyratory crushing unit was used in oil sand crushing. However, the gyratory crusher did not work successfully with the sticky oil sands, and hence another method was necessary to be found. The ability of the DRC to penetrate and shear sticky material, self clean, and still handle the hard rock impregnation proved to be a breakthrough in the philosophy of oil sand handling (Krupp, 2003 a). The first DRC used to take material from a single 240 ton truck in a receiving hopper of capacity 500 ton and a crusher throughput of 7500 ton per hour, which were exactly half of today's capacities. The rapidly changing demands in the oil sands industry led to the development of larger capacity and faster Semi-Mobile Crushing Plants, which could be relocated in approximately 72 hours. To facilitate moving the large mobile structure, the crushing components were supported on a free-standing pontoon, which is the base support for the crushing plant. The plant could be relocated by simply jacking up the pontoon structure and lowering the entire crushing plant on a suitable trailer or crawlers (Krupp Canada, 2003 a). The Aurora II belongs to this second generation of crushers with largest capacities and flexibility of relocation to a new site. The diamond shaped hopper allows two trucks to dump simultaneously into the hopper. Based on the operating experience gained so far and research at Syncrude and Krupp, the future requires the crusher to be Fully-Mobile.

The future generation of fully mobile crushers will eliminate the vast number of 400 ton haul trucks that carry the oil sand from mining site to the crusher plant, rather the shovel would mine oil sand and dump it directly into the crusher's hopper. Being mobile, the crusher can be easily located from one mining site to another as the quarry moves. Elimination of the haul trucks means significant savings in capital cost as well as maintenance and operation costs. Data and results from this health-monitoring project are expected to provide valuable information to Syncrude and the crusher's designer Krupp. Large amount of long-term data under daily operation, instead of limited data under controlled laboratory conditions, further enhances the value of the information. Information about impact factors, structural response to different loads, the history of loads, dynamic properties, adequacy of the design model, a parametric damage analysis exercise, etc. all go a long way in securing a more efficient, economical, and reliable crusher in the future.

2.3.3 Structural Components of the Aurora II crusher

The crusher plant as a whole consists of structural and non-structural components from a civil engineer's point of view. Although each moving component and supporting component of the crusher is subjected to stresses and wear due to abrasion, most of those mechanical components of the crusher plant like the crusher drum and teeth, apron feeder, conveyor belt, etc. are considered as non-structural, except for the dead load they add, and excluded from the structural model. These mechanical components subjected to heavy abrasive stresses require special monitoring methods and design considerations that are better suited to the mechanical engineering fraternity, research on which is already a part of Syncrude program. Other non-structural components like the retaining walls and the adjoining tower structure are not connected to the crusher structure in any way and hence excluded from the analysis. Thus, the main structural components considered in the structural model are the hopper, the columns, and the pontoons.

The hopper is the first to interact with the load, the oil sand dump. It is mainly subjected to impact in addition to the static weight of the dump. Of course, there are other less significant effects from other operating machinery etc. The hopper has a lining to counter the abrasion from oil sand dump. Fig. 2.6 shows a close up of the hopper from the top and Fig. 2.7 from underneath. The hopper is strategically designed to take dump from two trucks simultaneously in a diamond shape and ensures the discharge from it is approximately uniform along the width of the dump zone (SCL, 2004). The hopper lining is one of the fastest wearing parts of the crusher and is inspected and replaced every three to six months. Various load and impact cases were considered in its design. The location of impact due to dump depends on the level of material in the hopper. Operation under empty hopper condition is not recommended due to larger impact due to a fall of more than 10 m when totally empty. As the material level in the hopper rises, the level of impact and location of impact keeps changing which is difficult to exactly pinpoint.

Fig. 2.7 also shows a column supporting the hopper. There are five rows of column groups supporting the hopper on top of a pair of pontoons. During design, the hopper was modelled as a plate element, with columns and stiffeners modeled as beam elements. Fig.

2.8 shows a view of the hopper and columns modelled by the STAAD analysis software (Krupp, 2003 b). Interestingly, the columns were assumed as pinned at the bottom where they connect with the pontoon. Krupp used two different finite element models for design purposes. Thus, hopper and columns were modelled together, whereas the pontoons were modelled separately.

Fig. 2.9 shows a picture of the bottom portion of the crusher, that is the pontoons, from the North side. The pontoons, two in number, are basically steel box girders resting on concrete pedestals at each end. The concrete pedestals in turn are comfortably placed on top of pile foundations. The two pontoons are laterally braced against torsion at mid-span. Fig. 2.10 shows the finite element model of the pontoons, which have been modelled using plate elements. The support condition on the concrete pedestal was also assumed as pinned with certain spring stiffness based on pile load tests.

Fig. 2.6 A view of the diamond shaped hopper from top

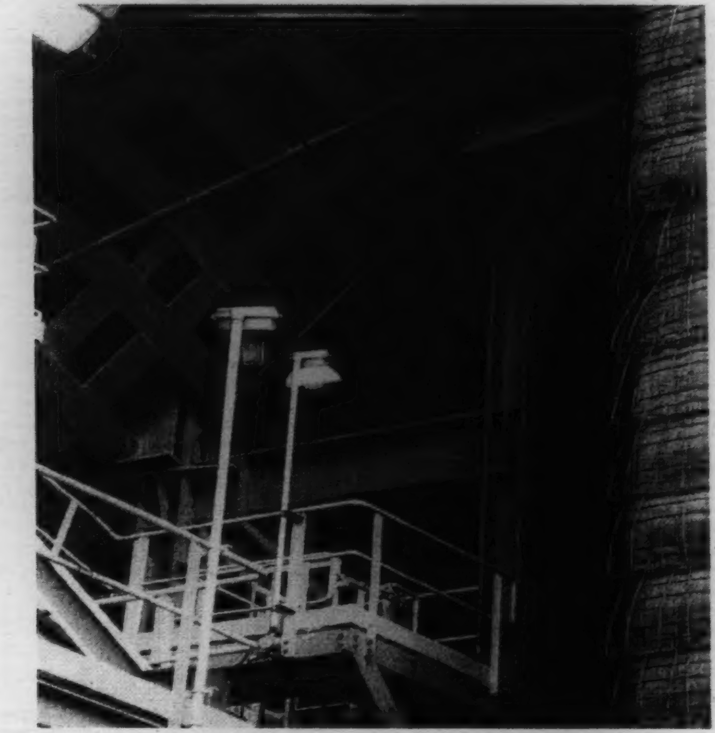

Fig. 2.7 A view of the hopper and column from underneath the crusher plant

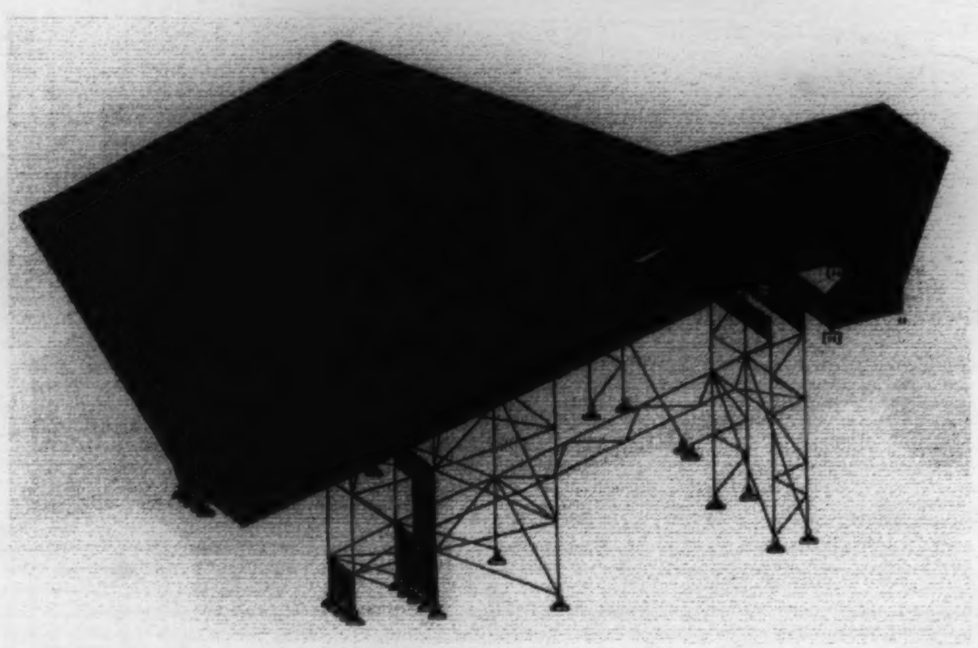

Fig. 2.8 Finite Element model of the hopper and columns – south view (Krupp, 2003 b)

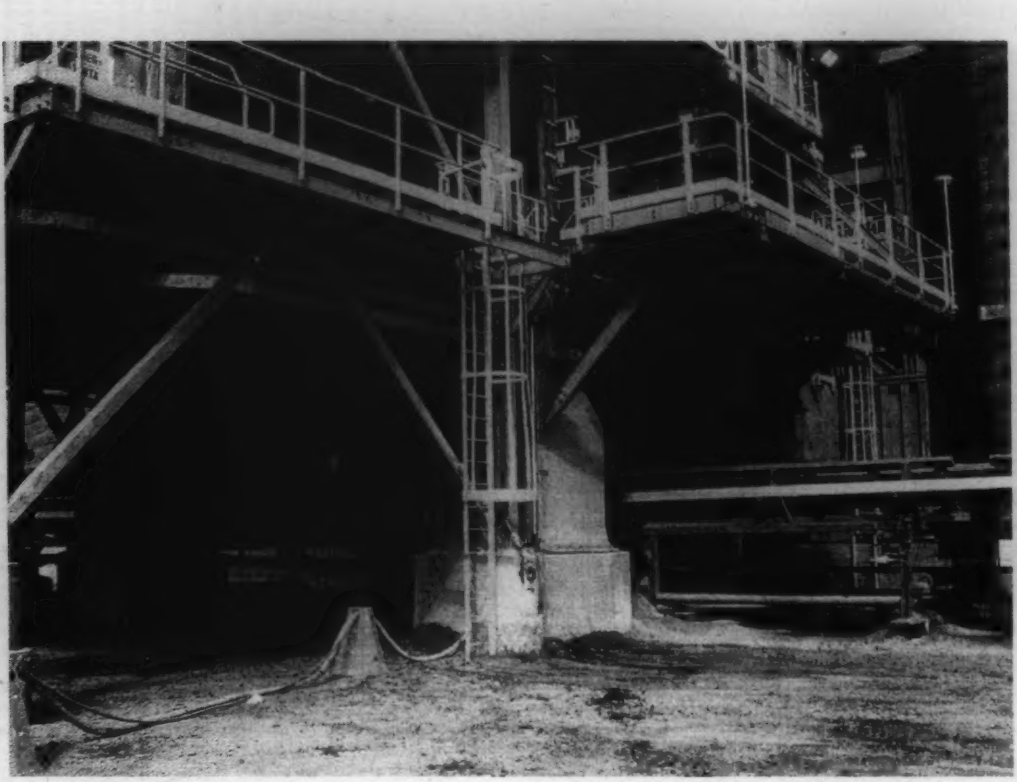

Fig. 2.9 Picture showing the two pontoons supporting the crusher columns – north view

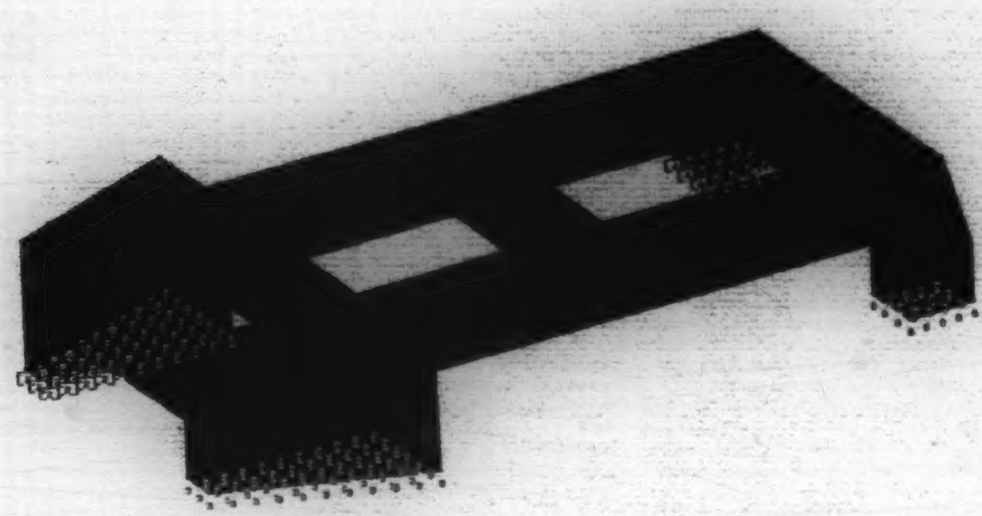

Fig. 2.10 Finite Element model of the Pontoons – south side view (Krupp, 2003 b)

2.3.4 Structural Health of the Crusher

The Aurora II crusher is quite a healthy structure in general terms. However, they do need regular maintenance and repair from time to time to keep the clock ticking for them. The major difference for this industrial structure from other civil engineering structures is the severity of working environment and presence of many mechanical wearing parts, which are integrated with the structure housing them. The nature and type of load acting on the structure is also much different from the conventional loads that a civil engineering structure is subjected to. As expected, the mechanical components deteriorate much faster due to abrasive action of oil sand, and are regularly maintained and replaced. The hopper lining and crusher drum teeth are the two fastest wearing parts of the crusher. Of course, lubrication and maintenance of machines and control systems is done as per guidelines of the equipment manufacturer. However, very little attention is given to the structure itself because it is well designed and expected to last its lifetime, which is only partially true.

Like any other structure, the crusher structure too has damage and deterioration going on, which may fail to get attention until its effects are magnified. A few examples of most common problems encountered in the past are instances of loose or missing bolts, cracks, and spalling of concrete base etc. (Fig. 2.11). Fortunately, damages observed so far have been limited to minor consequence and easily handled, mainly due to the conservative approach adopted in industrial structure design. However, rising cost of materials and the challenges of future generation of industrial structure design will take this luxury away. Inspections at site are currently limited to visual inspection at the time of machine maintenance. The short-term inspection is done at 1000 hours (about one and half months) outage, which lasts for two to three days and focuses mainly on pipes and pumps. The longer-term inspection occurs every three to six months wherein the wear tiles in hopper and drum teeth are inspected and replaced along with the general visual inspection of the structure. With visual inspection the chances of capturing damage in its early stage is highly unlikely, and hence it is waiting for the damage to grow and the structure to convey the message in some other ways, that is structural ways like excessive vibrations, large displacements, signs of distress, or even failure. Regular monitoring by an SHM system on the other hand would be able to detect the damage much earlier than naked eyes, and timely repair and maintenance would serve to guarantee and extend the continued healthy life of the structure.

Every healthy structure needs some form of monitoring for it to remain healthy for a long time in a reliable manner. This has been the driving force behind the reliability-based research at Syncrude. The Aurora II crusher will serve as the pioneering model structure to adapt and apply the benefits of structural health monitoring, which will then be extended to other structures at Syncrude.

(a) (b)

Fig. 2.11 Instances of past problems at crusher (a) Spalling of concrete base (b) Missing bolts

2.4 Past Research at Syncrude

2.4.1 Investigations of Double Roll Crusher 7

Syncrude and Krupp have carried out research on the Double Roll Crushers (DRC) at different times for different purposes. The major aims have been to gain valuable information about the design loads, impact factors, and vibrations. DRC-6 and DRC-7 are identical crushers in operation at Syncrude, however, DRC-7 showed larger displacements and vibrations as perceived by the operators. This prompted a detailed investigation into the vibration and support displacement of the DRC-7. The two test programs conducted in summer and winter measured the column-top level displacements at three locations close to the hopper (Fowler and Gonzalez, 1999). Measured values at DRC7 were found to exceed calculated values by Krupp (vendor) with assumption of fully rigid foundations, raising concerns on structural reliability. The research confirmed the higher displacement in DRC7 at the top of the crusher hopper by 1.5 to 2 times as compared to DRC6. There could be several reasons behind the difference in performance of the two crushers. The simplest would be to say that the DRC7 crusher feed was coming from richer ore and the shovels digging the oilsand affected the size and number of lumps too. Because DRC 7 has also been reported as the crusher with double the downtime owing to frozen lump jams (Fowler et al., 2000). Thus, if the load acting were bigger then the displacement would naturally be larger. However, this theory was sidelined by the assumption that the oilsand grades were comparable. The authors considered rigidity of supports as one of the likely causes of difference in displacement.

Fowler and Gonzalez (2000 b) performed second set of measurements at the same locations on the two crushers in winter conditions to assess the effect of foundation stiffening due to frozen soil. It was found that the maximum structural displacements under winter conditions were reduced to half of those in summer months. The maximum displacement at the back column reached 16.5 mm in winter as opposed to 36.4 mm in summer at the DRC7 crusher for a dump of rich ore. The maximum displacement at the same location on DRC6 was 17.8 mm in summer, which was quite close to that of DRC7 in winter. It was evident that frozen ground was leading to improvement in structural performance, but temperature was an important player as well. Shrinkage in steel members and connections due to lower temperature could have easily led to more rigid connections and a rigid foundation. The frozen ground could only make the concrete pile cap more rigid. Hence, it may not be appropriate to attribute all credit for lower displacements observed during winter months to the frozen ground alone. However, it was not possible to separate displacements due to bending and rigid body motions with the limited number of measurements taken.

Obaia and Gonzalez (2001) followed up to investigate this aspect if rigidity of supports was indeed the reason, focusing on the base of the crusher. Four LVDT's were used to measure the vertical and horizontal displacements of concrete pile cap and the steel piers with respect to a "stationary" retaining wall. Data was sampled at 10 Hz for 24 hours under normal operation and again under controlled dump on empty hopper for about 20 minutes. The displacements in general were smaller in winter month for the same type of load due to low temperature and frozen ground condition, which constrained the displacement of piles. The temperature effect on displacement was less than 0.5 mm and was more noticeable in concrete pile cap than in steel column base. Further, rich ore produced more displacement than lean ore because they discharge as one big lump and produce more impact on the crusher. Also, the vertical displacements were larger than horizontal displacements (Obaia and Gonzalez, 2001).

The maximum displacement was observed to be 0.61 mm. In all the investigations done only LVDT has been used to measure the displacements at pile cap, pier bottom and top. The accuracy of the LVDT used was +-0.25 mm, which is in the range of the measured displacements (less than 1 mm at the bottom of piers). Hence, Obaia and Gonzalez (2001) recommend viewing the results in general trend rather than their absolute values. The report remains inconclusive as to the reason behind the difference in displacements of the two crushers, however, it rules out support movement as the cause for the excessive displacement encountered at DRC7. Hence, the value of current SHM project at Aurora II crusher is further enhanced due to so many unanswered questions and limited knowledge regarding performance of these huge oil sand structures in day to day operations compared to design assumptions.

2.4.2 Other Relevant Research on Crushers

A structural performance testing of North Mine DRC6 crusher was conducted to determine if the crushing plant structure was adequate for the actual operating loads to which the structure was subjected (Givens, 1997). Strain measurements of some key structural members were done at eight locations and compared with those of the vendor's design values. No conclusions were made by the report and only the values obtained during operation were reported, the maximum stress values being in the range of 13.8 MPa.

Concerns arising from structural displacement issues with DRC7 in the North Mine prompted a structural displacement study of the new Aurora crushing plant. Displacement measurements arising out of normal and controlled dumping of oilsand into the hopper were taken with the help of LVDT's, the way done earlier for the DRC6 and DRC7 investigations. Measurements were made at three of the hopper support columns. Data was again collected at 20 Hz, which was sufficient to capture the impact displacements. Results revealed that the maximum displacements at the newly commissioned Aurora crusher were between 10% and 20% of Krupp's maximum allowable displacement values for two of the major design load cases. Hence, design values were far larger than the actual maximum displacement values (Fowler and Gonzalez, 2000 a).

One of the major non-structural issues with crushers responsible for causing big downtimes has been attributed to frozen lump jams (Fowler et al., 2000). Studies on crusher performance and event data sheets led to the revelation that there had been an equivalent downtime of 23 days in the North Mine since startup. The study also found that the DRC7 crusher downtime due to frozen lump jam was double that of DRC6. The difference between the two crushers seemed strange on the underlying assumption that both the crushers are of same design, however, differences in feed quality and the manner in which various shovel types fragment ore while digging could influence the size and number of lumps sent to the crushers (Fowler et al., 2000). In order to mitigate the problem of lump jams, the authors endorsed research into gaining better understanding of the energy requirements to break frozen lumps, which will lead to solutions for improved crusher productivity and knowledge base for better design of future crushers.

2.4.3 Vibration and Dynamic Load Studies at Syncrude

The load bearing structure of Feeder Breaker 4 (FDB#4) at Syncrude was instrumented and monitored for strains for an interpretation of the dynamic loads acting on the structure and its variability (Carroll, 1996 b). Six weldable strain gauges of 350 ohms resistance were installed on the FDB beams and columns. The statistical parameters of the data were calculated. Supplemented by video recording, spikes in strain were observed due to the dump with duration of about 2 seconds, which varied depending on the ore characteristics and dumping conditions etc. A cohesive material sliding off as a single mass into an empty hopper led to the maximum value of impact due to larger mass and a greater distance of fall. Momentum is a product of mass and velocity, and the rate of change of momentum is nothing but the force of impact. When the material was dumped slowly, then the dynamic component of the load was non-existent. The dynamic load factor on the vertical column was 1.75 (Carroll, 1996 b).

Vibration and impact can be clearly identified as the two major issues plaguing oilsand structures. Carroll (1996 a) reports the vibration analysis on a BWR#4 front end, which was showing violent oscillations and then cracks in the structural bracings. FFT operations by excel on the collected strain data revealed that frequency resonance was occurring between the bucket digging motion and the natural frequency of the structure. The author diagnosed this resonance with a low damping coefficient and overstressed bracing as the reason behind cracks and oscillations.

Investigations were also carried out to improve the reliability of the crusher dump blocks and to ascertain the magnitude of forces acting on them. Carroll et al. (1998) recorded the truck approach deceleration with the help of laser beams and multiplying it with the mass of the truck (with material) was able to give an idea of the forces acting on the dump block when the heavily loaded haul trucks were backing into them and hitting against.

Readings were taken at the frequency of 20 Hz with a 60 second data run manually. An average force of 900 KN and a maximum of 1800 KN were observed for the haul truck type 793B.

Yin et al. (2003) attributes the frequent and almost sure occurrence of cracking in heavy mining equipment to high impact loads, high fatigue cycles, low operating temperatures, and large component size. The project aimed to examine the crack management program at Syncrude for mobile equipment and to optimize it, which requires a myriad of information and knowledge. BE 395 electric shovel was picked for the study and a model was developed to predict the behaviour of fatigue cracks, which consisted of four phases. The first phase was definition of the load spectrum by field-testing the shovel under simulated and normal operating conditions. Two cable transducers were used to monitor the position of the stick during excavation and 32 strain gauges were used for strain monitoring and finite element model validation. Data was collected at 100 Hz for about a week in sessions in August 2002. Field data provided with a stress history of the structure, which was also used in validating the finite element model. Three unit load cases were used to correlate measured field data and the finite element analysis results. Material testing was done to get fatigue and material properties, and crack growth rate (behaviour) simulation was conducted (Yin et al., 2003).

Carroll (1997 a b) and Yin et al. (2003) highlighted the significance of monitoring of mining equipment at Syncrude. The magnitude and frequency of loading with 24/7 operations throughout the year naturally leads to a lot of breakdown and repairs. The industries in oil sand, including Syncrude, have to operate and maintain a large fleet of big mining equipments. Wear and tear of the equipment due to extreme temperatures, rough ground, and highly abrasive oil sand cost millions of dollars per year. Shovels and draglines repeatedly experienced cracks in its boom, which propelled research into measurement and study of structural loads on mining equipment. The track rollers of RH 200 hydraulic shovel was identified as a component posing reliability problems with significant breakdown due to overloading, costing 300K in 1996 for the replacement of rollers alone. By 2006, it was expected to reach 6 million dollars, excluding installation costs and lost production.

The real time monitoring project of the track rollers (Carroll, 1997 b) aimed to introduce operator awareness along with maintenance and appropriate design to boost reliability and high production rates. State of the art data acquisition and wireless communication technique, which required line of sight for uninterrupted transmission up to 20 km, was used to transmit data at 19.2 kb/s from a mobile shovel to a pick up truck housing the receiving wireless modem and laptop computer, at 200m, for real time processing and analysis. The signal conditioners, A/D converter, transmitting wireless modem, and a battery to power all of these equipment, were housed in a well-protected shelf in the car body. The strain gauges, which were attached to a moving part, were connected to the stationary signal conditioners through a slip ring, and then were transmitted by a wireless modem. Two channels of data from strain gauges on the inside surface of the roller were streamed at 50 Hz frequencies each, which was converted to an equivalent stress and load by a numerical model, under the assumption that all strains were within the linear elastic range. Appropriate boundary conditions were applied to the numerical model and a stress value per unit of load applied was developed for each strain gauge location. The model was not so accurate in the regions of contact stresses because those regions were not modelled by contact elements or by finer mesh. Load predictions made by the gauges differed only by 4% from each other, which confirmed the validity of the model and the monitoring for load determination, to facilitate a redesign of the roller for significant savings in roller replacement cost (Carroll, 1997 b).

BE 2570W dragline boom was another mining equipment exposed to severe dynamic loading leading to extensive fatigue cracking of its members, with outages lasting up to three days for repairs. These draglines needed to improve their operational reliability in order to maintain the production tonnage. A research was undertaken (Carroll, 1997 b) with the objective of lowering the fluctuating loads on the boom that caused fatigue, while maintaining production levels. Dragging, hoisting, dumping, and swinging are the various actions of a dragline boom that subject it to large stress cycles. The boom stress monitoring system consisted of two biaxial strain gauges installed on the outside chord of each side of the boom and a data acquisition system collecting data at 150 Hz. The swing and hoist actions were found to be the ones most affecting the boom stress. Since the motion of the dragline was very complex and undetermined with a large number of degrees of freedom, and the stresses were largely operator dependent, it was difficult to predict the loading from cycle to cycle. However, the monitoring system was designed to give the operators a real time feel of the stress level of the boom and influences of his/her operational maneuvers on the stress level. Thus, awareness is developed among the operators about the possible ways of doing the job with least stress on the boom.

The foregoing research bears much semblance to the current SHM project on Aurora II crusher in principle and objectives. In closing remarks Carroll (1997 b) suggests that continuous improvement of equipment reliability would be achieved through strain measurements on load bearing components, which would result in lower operation and maintenance costs. With addition of new equipment and continued utilization of aging equipment, the requirement to evaluate their performance and reliability, diagnose faults, and verify equipment design loads would be ever important. The author also recommends likely future monitoring and operator assistance system for the haul trucks, shovels, and dynamic load monitoring of crusher systems. Thus, the SHM project has well seamed into the overall goals and objectives of Syncrude through years of in-house research.

2.5 References:

Carroll, M., 1996 a. BWR#4 Front End Vibration Analysis. Syncrude Canada Ltd., Research Department Progress Report, 25 (2), pp. 82-89.

Carroll, M., 1996 b. FDB#4 Dynamic Load Study. Syncrude Canada Ltd., Research Department Progress Report, 25 (8), pp. 90-100.

Carroll, M., 1997 a. Dragline #4 Boom Loading Condition Monitoring. Syncrude Canada Ltd., Research Department Progress Report, 26 (5).

Carroll, M., 1997 b. Mining Equipment Monitoring at Syncrude. CIM District 5 Conference.

Carroll, M., Claus, D., Gonzalez, S., and Lipsett, M., 1998. Analysis of Forces Acting on North Mine Crusher Dump Blocks. Syncrude Canada Ltd., Research Department Progress Report, 27 (09), pp. 168-170.

Central Intelligence Agency (CIA), 2001. http://www.cia.gov. Accessed April 2004.

Fowler, C.G. and Gonzalez, S., 1999. Preliminary Investigation of DRC-7 Displacement. Syncrude Canada Ltd., Research Department Progress Report, 28 (11), pp.120-131.

Fowler, C.G. and Gonzalez, S., 2000 a. Assessment of Aurora Crusher Structural Displacement. Syncrude Canada Ltd., Research Department Progress Report, 29 (09), pp.026-034.

Fowler, C.G. and Gonzalez, S., 2000 b. Study of DRC7 Displacement During Frozen Ground Conditions.Syncrude Canada Ltd., Research Department Progress Report, 29 (05), pp.57-66.

Fowler, C.G., Kube, R., and Kamm, T., 2000.Crusher Production Limitations due to Frozen Lump Jams. Syncrude Canada Ltd., Research Department Progress Report, 29 (11), pp. 44-53.

Givens, Paul C., 1997. North Mine DRC#6 Structural Performance Testing. Syncrude Canada Ltd., Research Department Progress Report, 26 (10), pp. 53-61.

Krupp Canada, 2003 a. Research Development and Design of a Semi-Mobile Crushing Plant for a Northern Alberta Oil Sands Mine. http://www.krupp.ca. Accessed April 2003.

Krupp Canada, 2003 b. Design Drawings and Modelling of the Aurora II Crusher. Personal Communication through Syncrude.

New York Times, 2004. Global Crude Oil Reserves. http://www.nytimes.com. Accessed and searched April 2004.

Obaia, K. and Gonzalez, S., 2001. Investigation of Support Displacement of DRC7. Syncrude Canada Ltd., Research Department Progress Report, 30 (09), pp. 1-13.

Syncrude Canada Limited (SCL), 2004. http://www.syncrude.com/who_we_are/01_07.html.

Yin, Y., Grondin, G., and Elwi, A., 2003. Fatigue Crack Management in Heavy Mining Equipment. A Progress Report submitted to Syncrude Canada Ltd. Department of Civil Engineering, University of Alberta.

CHAPTER 3

INSTRUMENTATION AND DATA ACQUISITION

3.1 General

Data acquisition and signal processing lay the foundation for a Structural Health Monitoring (SHM) project. Naturally, a solid understanding in this area is a necessity for success. The structural response or "health" is measured in terms of signals generated by sensors and interpreted by the data acquisition system. Every step from here on depends on the reliability of the signals that have been collected. The way sensors "talk" and the way the data acquisition and monitoring system "hears" has to be well integrated in a seamless manner for a long period of time under harsh field environment. Of course, every electronic system has certain limitations and acceptable limits of numerical errors; this in turn assigns a corresponding limit on further interpretation of the data. An understanding of different types of sensors, their operating principles, the types of signals they produce, the signal conditioning required, and the way the data acquisition system collects and processes data, ensures the confidence level on the predictions of an SHM system. An SHM system basically consists of instrumentation and data acquisition, signal processing and analysis, data management, and finally, data interpretation and monitoring system. This section presents the various aspects related to instrumentation, data acquisition, and field-testing adopted in this project.

3.2 Introduction to Measurement and Data Acquisition

Structural response measurement is nothing new to structural engineering. Appropriate tools and instruments have been used for centuries to measure different performance indicators. Mechanical and analogue instruments with manual data recording were the first to begin with. It is only after the fifties (1950) that progress in electronics and computation triggered the shift to digital systems with automatic data acquisition by a computer. Dedicated computers for each type of instrument were needed to read and record the data for quite some time. However, with availability of software interfaces and instrument drivers, now any computer can be used as a virtual instrumentation and data acquisition system. The ever-increasing capability in digital computing with continuous high-speed data acquisition, wireless communication, and real time monitoring has made SHM feasible and affordable.

There are various types of data acquisition systems available in the market from different manufacturers. Each one of them has a certain characteristic feature or strength, and is based on a certain physical principle. There are systems that operate on acoustic emission technique, electromagnetic measurement technique, and principles of optics. Fibre optic sensors are the newest technology in structural measurements, which require separate data acquisition system that can read optical signals and also provide optical (light) excitation for the sensor to reflect back for reading. These systems are relatively pricey at the moment and have limited channel capacity, but they also have the advantage of freedom from electromagnetic noise. Electrical resistance based sensors are the longest used system with well-researched technique. These systems supply an electrical excitation voltage to the sensors and then read the voltage or its imbalance in the bridge, or measure the electrical current generated by piezoelectric sensors. The electrical data acquisition system has been selected for this project based on past experience and familiarity at both Syncrude and the University of Alberta. Hence, only items associated with this type of Data Acquisition System (DAQ) are presented in this report.

Cost of a data acquisition system is dependent on the number of input channels, types of sensors it can read from, type of signal, signal conditioning, speed of data acquisition and resolution. Every system has its own list of variables and economic size for selection. Since the absolute minimum requirement was about 60 channels with capability of dynamic measurements, only systems that were able to meet these criteria were looked into. It is worth mentioning here that no two systems are exactly equivalent to each other and each one of them have their own strengths, but they are listed here only to give a glimpse of other options available for consideration.

Campbell Scientific DAQ:

Campbell Scientific (2003), a Canadian company based in Edmonton, has a couple of data loggers in its series that are suitable for different purposes. Its data loggers are claimed to be flexible and able to measure most of the sensors by incorporating appropriate modules. CR23X Micrologger, with12 differential channels (24 single ended), is capable of scanning at 100 Hz. For a single input it could go up to a maximum of 1.5 KHz. Terminal Input Modules (TIM) are the peripheral interfaces providing completion resistors and signal conditioning to read signals from strain gauges. Each strain channel should have an independent TIM, or one of the modules has to be multiplexed for use by other strain gauges. These units with AVW1 or AVW4 modules can also read vibrating wire sensors. Accelerometers can be directly connected to these channels without any additional module. Its channel count can be expanded by using the digital input / output ports with multiplexers or Synchronous Devices for Measurements (SDM). One multiplexer can have a maximum of 32 strain channels at the cost of lower scan rate. These digital ports can also be used as control port to read 0 or 5 volts (in a binary true or false sense) to start or close a device. The CR23X data logger also has four pulse channels that can be used to record frequency data from anemometers etc., but is not of much use to us. Remote communication is possible by using NO-105 network link interface.

CR9000 is the other data logger from Campbell capable of recording data at a much faster rate of 100 KHz. This is a modular unit consisting of a base system and slots for user specified input/output modules. Adding CR 9050 modules, up to a maximum of 9 input output modules, can increase number of data channels as per requirement. Software selectable voltage ranges allow full utilization of the data logger resolution.

Optimum Instruments DAQ:

Data Dolphin of Optimum Instruments (2003) is compact and portable instrument for outdoor use. But it does not have many channels – only 4 differential inputs. It has four additional inputs which can be user selected as pulse, status or analog inputs. It is capable of measuring signals down to 90 nanovolts; hence, most sensors can be directly connected without any signal conditioning. Its low power consumption, long battery life, compact size, communication capabilities, solar power option, and high resolution of 24 bits, make it a good choice for long term health monitoring projects. However, its signal scan rate is low at 2 Hz to 100 Hz. So, it is not suitable for multipurpose laboratory use, but a good choice for static measurements. In this project with a high channel count and dynamic measurements, it is not suitable. The data dolphin was used for data acquisition at the Portage Creek Bridge. It may not be compatible with accelerometers. Optimum Instruments is again an Edmonton based Canadian company.

Roctest DAQ:

Roctest (2003) data logging system SENS-LOG 2380 MCU has direct compatibility with vibrating wire sensors, but in order to measure outputs from other sensors it needs appropriate I/O modules. These modules with user programmable measurement functions support most popular sensors used in geotechnical and structural engineering. Analog signal multiplexer (ASM) is one such I/O module. This data logger can record data at 20 readings per second, which is quite slow for the purpose of this project. Its specialty is its suitability for vibrating wire sensors, which give frequency output instead of voltage. The benefit of such sensors lies in elimination of noise due to electrical or magnetic interference that is possible with voltage based sensors like strain gauges. Primarily Roctest instruments are targeted for geotechnical measurements. ROCTEST also has fibre optic counterpart (FISO).

Vishay Measurements Group DAQ:

System 6000 Strain Smart Data System is the Measurements Group's best available data acquisition system beyond static measurements (Micro Measurements, 2003). It has data acquisition rate of 10 KHz per channel with a maximum throughput of 200 KHz, which means 20 channels at 10 KHz, or 40 channels at 5 KHz. Number of input channels can vary from 1 to 1200 and it uses different cards for strain gauges, LVDT, piezoelectric, etc. sensors. It has a built in bridge completion for 120, 350 and 1000 ohm strain gauges. Simultaneous sampling and individual analog to digital conversion for each channel, and low noise signal conditioning are some of its salient features. Micro measurement has a diverse list of products under its belt, and hence, is compatible with most sensors. A long history of strong technical support and learning system is evident from its scores of in-depth publications.

National Instruments DAQ:

National Instruments Data Acquisition Systems are modular systems, which can be expanded as per needs and is able to communicate with almost any type of sensor. Its Labview software with concept of virtual instrumentation is a popular tool across laboratories and industries. Several accessories are required for this system like chassis, terminal blocks, signal conditioners for accelerometers etc. Separate signal conditioning input modules are available for different types of sensors (Fig. 3.1). The DAQ card that converts the analogue data into digital format for computer to read and store is inserted right into the mother board of the computer, wherein stems the capability of virtual instrumentation by making use of the Labview software. Real time scan capabilities and motion control provide great strength to robotics and industrial control systems. The system has immense flexibility and expansion capabilities built into it. Channel count can be increased by adding input modules like universal strain gauge (SCXI 1520) for strain readings and by multiplexing. However, data sampling speed will be shared depending on the number of channels used in the monitoring project. Strain gauge modules have in-built completion resistors, null balancing, and separate power supply for each channel. Major cost of the system comes from the SCXI 1520 module that decides the number of channels the system can have (National Instruments, 2003). This is the one system that both Syncrude and the University of Alberta structural lab are familiar with, which has been a strong factor deciding in its favour in addition to its extraordinary features.

The data acquisition system has a chassis with capacity to hold twelve signal-conditioning modules for different types of sensors. Eight strain gauge modules were procured, each with 8 strain channels, thus making the total number of strain channels 64. Accelerometer, LVDT, and Thermocouple signals were read by using three appropriate voltage modules of 8-channel capacity each. Thus, the chassis still has an unused space for expanding the system by adding another module of 8 channels. Further expansion is possible by multiplexing at the cost of speed. However, with the number of channels available, it was expected that the data acquisition system would serve the needs of the project, which it did. Detailed specifications of the DAQ selected with a brief explanation of the terms involved are provided in the following sections.

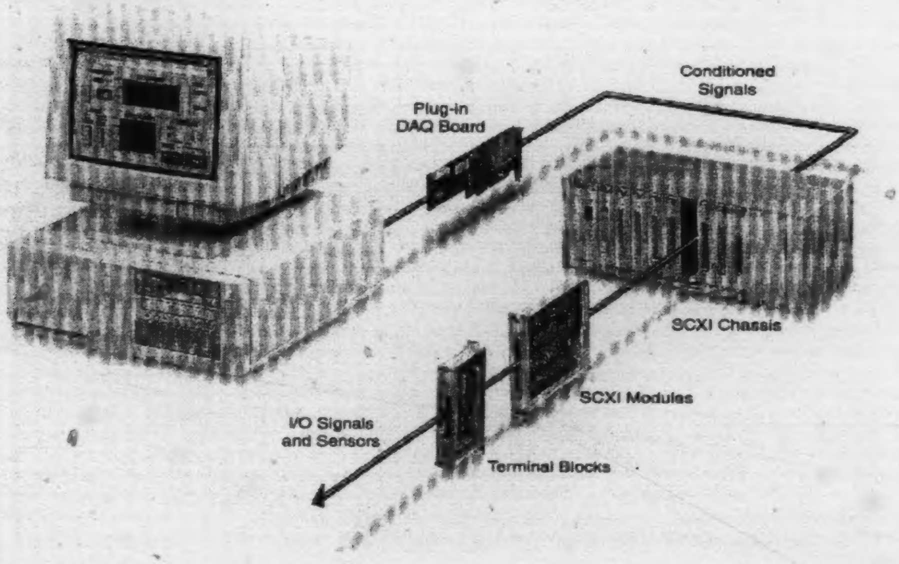

Fig. 3.1 National Instruments Data Acquisition System (Source: National Instruments)

3.3 National Instruments DAQ Specifications

E-series data acquisition boards from National instruments were deemed appropriate for the purpose of the project. The analogue to digital converters or digitizers had resolution of 12 to 16 bits. They were capable of handling 16 to 64 channels of data at speeds ranging from 200 kilo samples per second to 1250 kilo samples per second. Due to the very dynamic nature of the dump load, a faster data acquisition system would be able to capture its behaviour in a more complete sense, and hence the choice of E-series DAQ. The data measured by a data acquisition system are numbers whose quality is dependent on its value in relation to the specifications of the DAQ. Thus, choosing the right system for the right purpose is the key to reliable data acquisition.

As mentioned earlier, Resolution of a data acquisition system is an important factor determining the error associated with digitization. Currently 12 to 16 bit digitizers are available in the market, however, 32 and 64 bit resolution microprocessors have recently started coming up and could soon be the standard. Obviously, the higher the resolution the lower the error and the more reliable the data becomes, and larger the measuring capacity. Thus, a 'α' bit resolution in computer terminology means that the voltage range 'V' is divided into N equal divisions of δV, the smallest measurable change in voltage. The finer the measurement, the better the resolution and reliability of data.

Hence,

[3.1] $$\delta V = \frac{V}{2^{\alpha}}$$

Range of a DAQ board defines the selectable minimum and maximum voltage level it is capable of measuring. A bigger range would mean more liberty to err. In other words, even a small error in digitization becomes significant if the total measurable range is small as well. On the other hand, the same small error for a bigger range of voltage measurement would constitute a negligible error. The usual ranges of voltage measurements are –10 V to +10 V, which means a total voltage range of 20 V. Sometimes, a range of –5 V to +5 V with a total of 10 V signal range is used.

In many situations, the signals generated by the sensors are of very low magnitude with respect to the range of measurement at the DAQ, this is where the Gain specification comes handy. With involvement of many different types of sensors to be read by one data acquisition board, a universal range to suit all of them is seldom possible. In such a scenario, it is necessary to bring all the signals to the same level of magnitude or into the same range of measurement by conditioning the signal. Gain is a factor by which a signal is amplified before being digitized by the DAQ board. Care should be taken though that the gain is not too large to make the signal fall outside the measurable range of the DAQ. Some experience with the different types of sensors and signals produced by them is necessary to be able to decide the right amount of gain for each signal-conditioning module. Thus, each sensor channel can have a different gain to suit the signal generated by it at that location.

Sampling Rate is the most commonly used and controlled specification by users. During analogue to digital conversion at the DAQ board, digital samples of the signal are taken at a certain scan rate and then the full signal is digitally constructed based on a best fit estimate offered by the sample points or readings. The faster the scan rate or the closer the digital readings, the better the digital estimate of the signal. However, faster scan rates come at a higher cost of hardware and data processing, and beyond a certain limit for each application, increase in sampling rate does not bring about significant improvement in signal quality, whereas the cost can become prohibitive. It is this fine balance of cost and quality that is desired. In the case of structures subjected to static loads, sampling rate becomes insignificant and only as a means of reducing the noise by averaging. Whereas for structures subjected to dynamic loads, especially if frequency analysis is of any interest, the data sampling (scan) rate assumes magnanimous proportions. Insufficient number of data points may lead to distortion of signal – aliasing, if not fast enough. Fig. 3.2 shows an example of such a situation. It also restricts the number of mode shapes and frequencies that could be extracted from the data because the frequencies beyond half of the sampling frequency are not reliable. Various types of analogue to digital converters with different scan rates, channel capacity, and cost are available in the market and one needs to judiciously select the right one for a project.

A review of literature at Syncrude Research revealed that scan rates of up to 50 Hz were used in the past for cases where dynamic measurements were required (Carroll, 1997). For most of the cases, however, only static measurements were desired and obtained at a much lower scan rate. SHM research projects at the University of Alberta have in the past used data scan rates of up to 1000 Hz for low channel count short duration data collection purposes like ambient vibration test, whose objective is to estimate the natural frequencies of the structure. The higher the scan rate the more number of frequencies can be accurately predicted and the less the errors from noise and other uncertainties. More commonly, scan rates of 500 Hz were popular for ambient vibration tests and 200 Hz for other dynamic tests (Khattak, 2003; Afhami et al., 1998). For this project a scan rate of 100 Hz was selected due to large number of channels to acquire data from, and past experience with crusher dynamic tests (Obaia and Gonzalez, 2001).

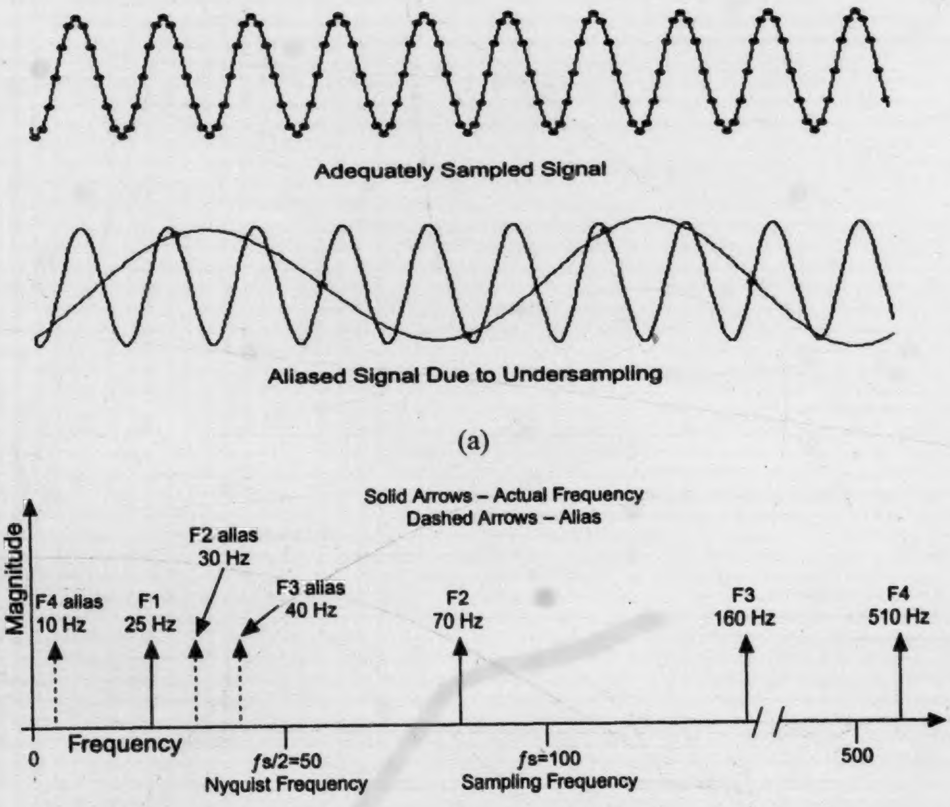
Adequately Sampled Signal
Aliased Signal Due to Undersampling
Solid Arrows – Actual Frequency
Dashed Arrows – Alias
Magnitude
F4 alias 10 Hz
F1 25 Hz
F2 alias 30 Hz
F3 alias 40 Hz
F2 70 Hz
F3 160 Hz
F4 510 Hz
Frequency
0
fs/2=50
Nyquist Frequency
fs=100
Sampling Frequency
500

(a)

(b)

Fig. 3.2 Aliasing effects due to under sampling (Source: National Instruments)

Any unwanted signal measured by the DAQ is considered as noise. Noise can be the greatest source of error and problems in data acquisition, if not properly handled. Noise can creep into the data at the point of signal generation, during transmission, and at the point of digitization. It can be due to various reasons like electromagnetic interference, ambient noise in the environment, vibrating machinery, potential difference between points, etc. The key lies in minimizing as many sources of noise as possible and then adopting a filtering mechanism to get rid of the leftover noise. It is accepted in SHM that there will always be sources of noise; hence, one needs to learn about them and find ways to live through it.

Shielded wires significantly reduce noise due to surrounding electromagnetic sources of noise (National Instruments, 2003). Taking differential voltage measurements instead of single ended measurements reduces the errors and noise due to potential difference between points. Single ended measurements are referenced to a common ground point whereas in the differential mode both lead wires from sensors are connected to DAQ board input channels. Techniques like three-wire system as compared to the two-wire system gets rid of the error due to lead wire resistance. Temperature compensation can be done to rid the data from the effects of temperature. Data averaging by sampling at higher frequency than required is also a popular method of filtering out noise. The NI DAQ boards have built in hardware and software filtering capabilities to filter out left over noise.

3.4 Sensors – Selection, Specifications and Application

The first in the line to connect a data acquisition or health monitoring system to a structure are the sensors. It can be compared to the instruments used by doctors in medical parlance of human health to record the heartbeat or other significant symptoms. Thus, it is important that the sensor generates (feels) and transmits the true and useful movements of the structure for a DAQ system to interpret accordingly. Hence, the interface between the sensor and the structure, i.e. the bond, which is dependent on the method of application / connection of the sensor to the structure, assumes great significance although least noticeable. A group or network of sensors when working together to gather data seem quite like the network of neurons in human body that sends information to the brain.

Each sensor is selected for a particular purpose at a particular location. Location of a sensor is very important in capturing important structural phenomenon, which demands some experience and imagination during instrumentation planning. Sensor sensitivity, range of measurement, compatibility with DAQ, cost, size, durability, and ease of application and use are the various factors that go into selection of a sensor and its appropriateness for a particular project. Strain gauges are the most popular of them followed by linear variable differential transducer (LVDT), accelerometers, and thermocouples, which have been employed in this project. A total of 60 weldable strain gauges, 10 LVDT, 10 accelerometers, and 2 thermocouples have been put on the structure for data collection.

3.4.1 Weldable Strain Gauges

Strain gauges are the most widely used sensors in structural and mechanical tests today. Their reliability, ease of application, durability, and accuracy of measurements due to differential measurements of Wheatstone bridge balancing make it an ideal choice. Much of the noise and measurement error is avoided by double-ended measurement of strain and the three-wire system. Based on the well-known Wheatstone principle, the strain gauge measurements can be made on a quarter-bridge, if only one gauge is active and the hardware module of the data acquisition system provides the rest of the three completion gauges. In a full bridge measurement on the other hand, all four active gauges are on the structure to give one unified reading. Obviously, more number of channels is used up in such measurements, however, the accuracy and reliability of the data is improved due to averaging of readings. Many references are available that give details of such measurement techniques and other related issues of strain gauges from manufacturers like Micro Measurements and National Instruments, and other instrumentation textbooks.

Weldable strain gauges of 350 ohms resistance from Micro Measurements were chosen over the conventional bonded gauges for concerns of durability of the glue under extreme temperatures. Once welded the gauges were quite permanent in nature suiting the nature of long term monitoring projects, and have been working satisfactorily over the last two years. The higher resistance ensures low heat generation and related errors, but the lower resistance gauges have relatively longer fatigue life and better signal to noise ratio. The application of weldable gauges started with grinding and buffing the surface to free it from any paint, dirt or uneven surface. Once smoothened up with fine buffing brush, the centre line of gauge application point was marked and the surface cleaned with de-greaser and dried in one stroke. The gauge was placed along the marked axis and a few spot welds were put on three sides to hold it in place, thereafter the manufacturer recommended welding sequence was followed to attach the gauge to the desired surface and location (Fig. 3.3 a). The strain gauge was then applied with a coat of air-drying nitrile rubber coating gel to protect it from weather and moisture, and when it dried up, a transparent Teflon tape to cover up a wider area (Fig. 3.3 b) with neoprene rubber pads underneath the lead wires. In total five protective layers were applied to the gauge. Figure 3.3 (c) shows the remaining two protective layers, a layer of rubber pad to protect the gauge from direct damage and then a heavy-duty aluminium duct tape to hold everything together. A final layer of butyl rubber sealant coating black in colour was applied to cover the entire assembly protecting from weather and damage, which hardened with time. The gauges were then wired up to the strain gauge modules, which provide signal conditioning before being digitized by the analogue to digital converters. Figure 3.3 (d) shows the data acquisitions system with various modules, the power supply and the laptop computer with the DAQ card.

3.4.2 Accelerometers, LVDT and Thermocouples

Different types and makes of accelerometers are available in the market, Bruel and Kjaer, Entran, etc. being a few leading brand names. Accelerometers can work on various principles of physics. Major categories of them being piezoelectric, spring mass type, servo force balance, or strain gauge type. Piezoelectric accelerometer is a device that uses piezoelectric material to measure acceleration. The schematic diagram of the accelerometer is shown in Figure 3.4 (a). It consists of a housing, a mass, and a piezoelectric sensing element (often a quartz crystal). A preloading spring sleeve is used to generate the initial force between the mass and the sensor. When the housing is subjected to acceleration, the force exerted by the mass on the quartz crystal is altered. This generates a charge on the crystal, which can be sensed with a charge amplifier. Piezoelectric accelerometer can be used for up to 1000g acceleration. The device can be

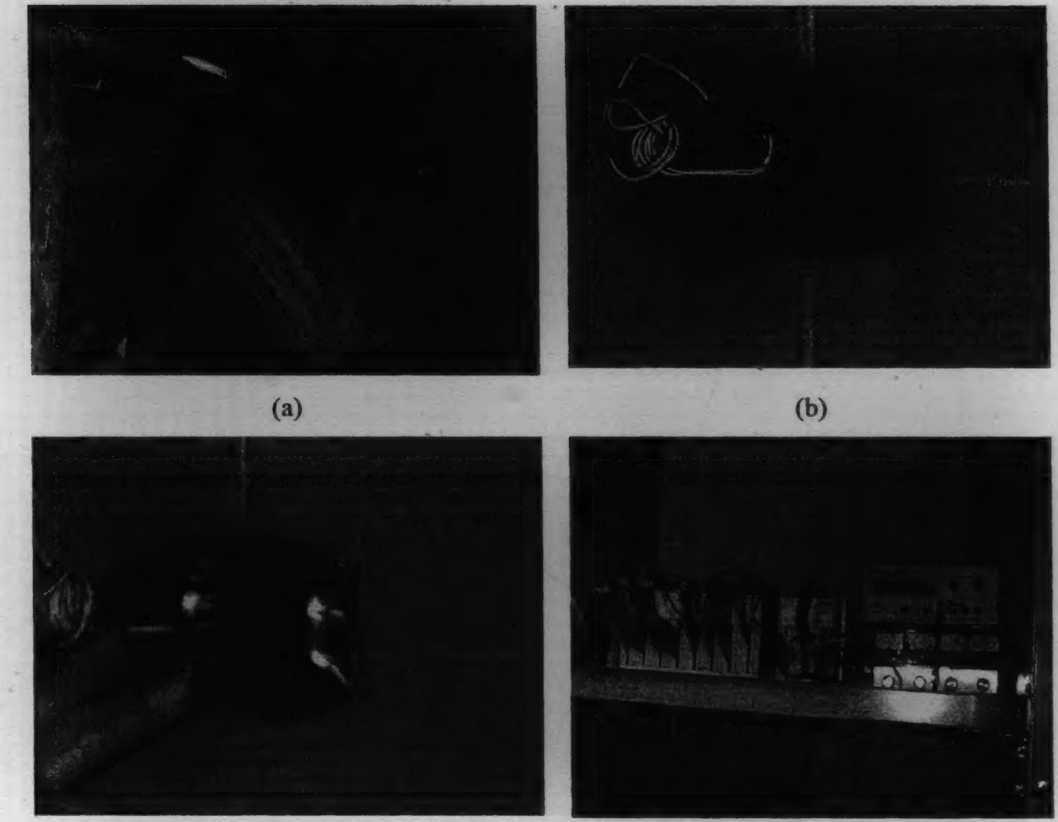

(a) (b)

(c) (d)

Fig. 3.3 Application and protection of a weldable strain gauge for measurement (a) Welding the gauge (b) Protective layer of silicon and transparent tape on the gauge (c) Gauge covered up with a layer of rubber and heavy duty silver duct tape (d) Strain modules and the data acquisition system.

used to measure frequencies up to 25 kHz if quartz crystal is used as the sensor, which has natural frequency of 125 kHz.

The strain gauge based accelerometers, which have been used in this project, use strain gauges as the sensing elements. As shown in the Figure 3.4 (b), force exerted on the mass by the accelerating body is transmitted through the cantilever beam. Bending of the beam is sensed with four active strain gauges forming a Wheatstone bridge, two on the top and two at the bottom. Damping fluid fills the housing to damp oscillations. Advantage of the strain gauge accelerometer over the piezoelectric accelerometer is that the former can respond properly to a steady acceleration. However, due to their low natural frequency they can measure frequency only up to several hundred hertz. LVDT and capacitive sensors can also measure acceleration, but are usually used for fairly low frequencies.

Mounting of an accelerometer is important in the field, which determines its ease of application and accuracy of measurements in a particular direction. The accelerometers usually come with a choice of mounting type depending upon the project need. Availability of different mounting options can greatly increase the utility of accelerometers in difficult field and laboratory conditions.

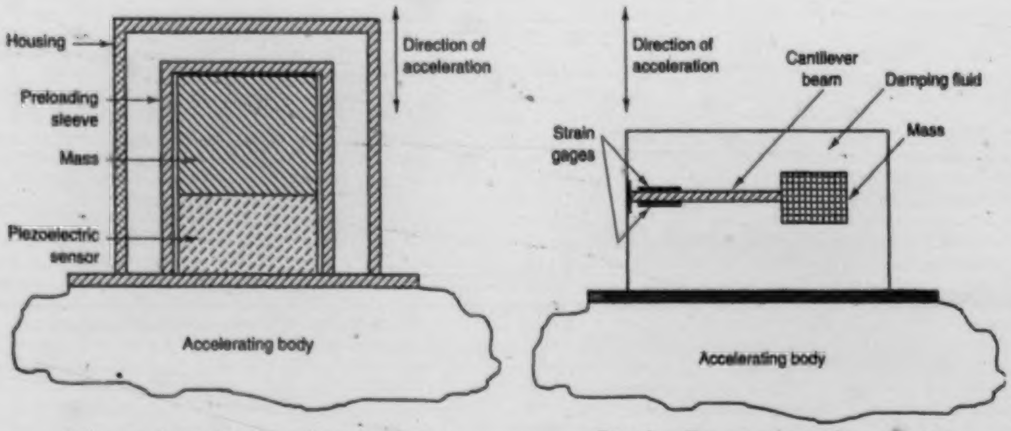
Housing
Preloading sleeve
Mass
Piezoelectric sensor
Direction of acceleration
Accelerating body
Direction of acceleration
Cantilever beam
Damping fluid
Mass
Strain gages
Accelerating body

Piezoelectric accelerometer (a)

Strain Gauge Accelerometer (b)

Fig. 3.4 Different operating principles of Accelerometers (Source: Bruel and Kjaer)

The expected acceleration level was estimated at the foundation of the crusher from the LVDT readings of previous measurements done by Syncrude. The LVDT had a sampling rate of 0.1 second (10 Hz) and an accuracy of 0.25 mm. Thus there is ample scope for differences of opinions, however, there is no doubt about the general trend. In general, the maximum acceleration obtained was less than 10 mm per square seconds (0.001 g), barring one point with acceleration of 65 mm per square seconds (0.0065 gals). The acceleration at column tops could be higher, but all data indicate that the acceleration level is expected to be less than 1 g. Hence an accelerometer with large capacity is not required, but a high sensitivity and good frequency range is. Some toughness against severe environment conditions is also desirable. The strain gauge accelerometers of Entran's high performance EGCS-A series, combing high sensitivity with heavy duty, were selected for their good frequency resolution and capacity. They have superior sensitivity as high as 2.5 V/g for a measurement range of 2 g, high frequencies up to 50 KHz for an ultra-fast dynamic response, over-range protection to 10,000 g in all three axes, and operating temperature of –40 to 120 degree Celsius. The maximum range can go up to + - 5000g and frequency will rise up to 8000 Hz, but then the sensitivity will drop down to 1 mV/g. From the available information, EGCS-A series of accelerometers with high sensitivity, heavy duty, internal amplifier, and damped, and 15 V DC excitation is a suitable option. The accelerometers were used with an output of +- 5 Volts and a calibration of 2.5 V/g.

LVDT are used to measure displacements at a point. The movement of a magnetically conductive core (shaft) inside a hollow cylinder with three transformer coil windings produces a differential voltage, which has a linear calibration with displacement of the core relative to its original position. Different sizes and ranges of LVDT with suitable core and winding size are available to measure varying degrees of movements that also affects its precision. Past research by Syncrude suggested that the maximum displacement at foundation level was less than 1 mm. Hence, LVDT with small range of 12.5 mm but higher accuracy would be good for monitoring displacement near foundation. On pontoons and columns, 50 mm range LVDT was desirable. The displacements at the top of the columns would be relatively more requiring larger range up to 150 mm, as evidenced by previous measurements on DRC7 of a maximum displacement of 55 mm. This philosophy was followed in selection of appropriate LVDT for different locations for best results. All displacements were measured with respect to the retaining wall by using small angle brackets to mount the LVDT to the pontoon or columns with magnets. Captive guided spring return LVDT were used to take care of the vibrations occurring on the crusher during operation, with output in the range of +- 5 volts and an error of +- 0.25% of the full range.

Type T thermocouples were installed at two locations on the crusher to estimate the average temperature around the crusher during the day and different seasons. The thermocouples were glued to the surface and then covered by a butyl rubber sealant coat. Surface preparation and cleaning procedures adopted were same as for the strain gauges.

3.5 Instrumentation Details and Locations

The crusher was instrumented with 82 sensors in the fall of 2003. A National Instruments data acquisition system (DAQ) with Labview based data logging program was used for obvious reasons of past experience and familiarity with the system. A 12 bit analogue to digital converter with 100 Hz scan rate per channel was used to collect data from the 82 channels, out of which 60 were strain channels, 10 LVDT's, 10 accelerometers, and 2 thermocouples. Ten minutes of data storage required 11 MB of disk space at that scan rate for the number of channels. It is important to have sufficient number of sensors to understand the behaviour of a structure and establish evaluation criteria for the monitoring system. However, practicality poses restrictions on the number of sensors that can be actually placed owing to costs involved in instrumentation and data processing. It may not be possible to achieve the best instrumentation plan in the first go; however, prior consideration does take it very close to what was contemplated. The Aurora II being a large structure, it was not possible to instrument each component extensively, hence, decisions on instrument locations were taken based on qualified judgements to fulfil the main objectives of understanding its structural behaviour, impact factors, boundary conditions, and monitoring goals. The advantage of structure having a longitudinal line of symmetry allowed to focus on one side, so the north side of the crusher was extensively instrumented. Eventually, the monitoring system would rely heavily on a number of critical sensors at strategic locations and the rest of the channels would serve as a validation tool.

3.5.1 Hopper Strain Gauges

Ten weldable strain gauges were installed on a north side panel of the hopper to monitor strain from local impacts and its distribution, where most dumps from the north side were expected to hit. Figure 3.5 shows the instrumented region of the diamond-shaped hopper. With the limited amount of instrumentation, it was not expected to get the complete behaviour of the hopper rather its relationship with the global behaviour of the whole structure would be established. Six out of the ten strain gauges were installed in a cluster with 2 on vertical stiffeners, 2 on horizontal stiffeners, and 2 directly on the hopper wall plate (Fig. 3.6). The remaining four gauges were put on the stiffeners and their junctions to monitor impact on the hopper. Figure 3.7 shows the layout of the gauges on the developed hopper drawing and Fig. 3.8 shows the close-up view of hopper gauges cluster.

The main purpose of hopper gauges was to capture the largest of impacts coming into the hopper. Information about the influence of impact on the hopper plate, the stiffeners, and

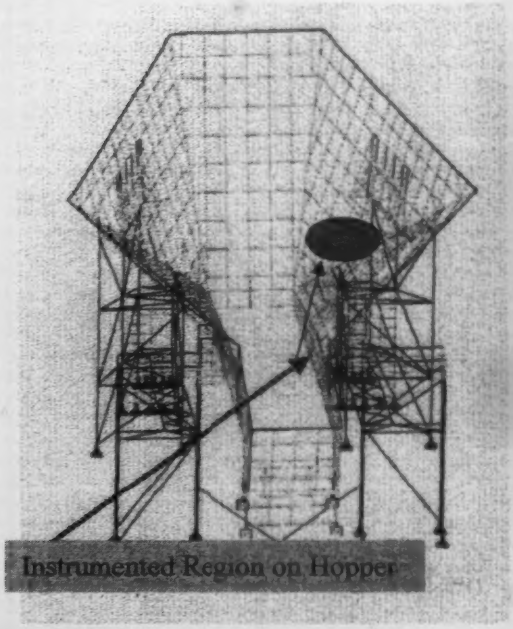

Fig. 3.5 Hopper instrumented region

Fig. 3.6 Hopper strain gauge location

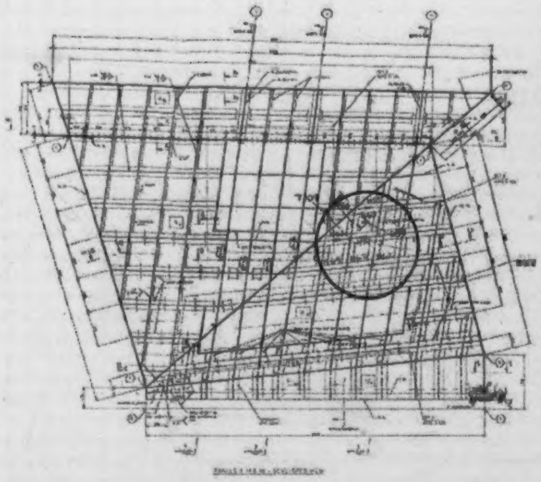

Fig. 3.7 Hopper gauge location on drawing

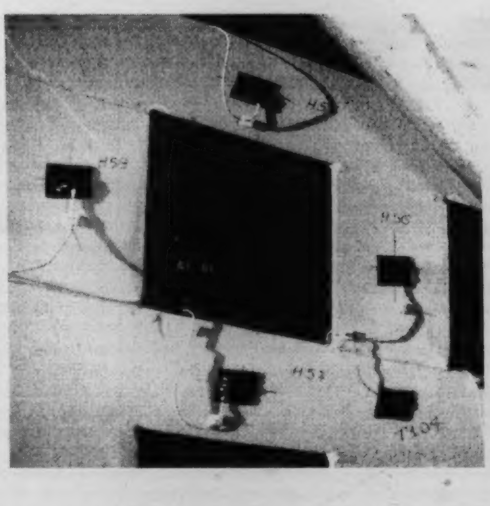

Fig. 3.8 Hopper strain gauges

their junction was desirable. This has been the governing factor behind the distribution of gauges as they are. It is also realized that the location of impact on the hopper keeps changing with the material level in the hopper. Hence, the strain or impact factor shown by the gauges may not always be the maximum being experienced by the hopper. With the size of the hopper and variation in loading environment involved, obtaining complete information about it would require excessive number of gauges, which is not practically feasible. Hence, a limited number of gauges have been chosen for a limited purpose.

3.5.2 Column Strain Gauges

Columns supporting the hopper were instrumented with forty welded strain gauges for the purpose of determining the axial and bending stresses experienced by the columns during dump events. Hence, the gauges were installed in pairs on the two flanges of the column sections at about mid height, so that they could stay away from regions of stress concentration. A pair of gauges was placed on flanges of each individual structural section in a built-up column section, such that it was possible to get longitudinal strain in columns on a transverse section. The transverse distribution of these gauges allowed for plotting of strain distribution along the column sections. Columns on four transverse sections marked as gridlines 2 to 6 were instrumented with all of the forty gauges (Fig. 3.9).

As shown in Figure 3.9, columns on gridlines 2, 3, and 4 rest directly on the foundation, whereas the columns on gridline 5 and 6 rest on the pontoons. Columns on gridline 2, 4, 5, and 6 were instrumented, but gridline 3 was not instrumented because of welded shear plates complicating the geometry. Every effort was made to keep the gauges free and away from sources of error and stress concentration. The gauges were mostly put on the vertical column flanges at mid span away from connections. Figures 3.10 to 3.13 show the gauge locations on column gridlines 2 to 6. The letter C denotes strain gauges on columns; L stands for LVDT's, and A for accelerometers. A few gauges on the columns were also placed in regions of highest expected stress concentrations where the columns met the hopper, with a view to capture extreme strains. Gauges C11 and C12 on gridline 4 (Fig. 3.11), and C29 and C30 on gridline 2 (Fig. 3.10) are the two strain gauge pairs dedicated to capturing stress concentration at top of the columns. Strain gauges were also welded to the inclined struts connecting columns to pontoons directly so that most of the loads being transferred to the pontoon could be quantified. Gauges put on inclined struts are C15, C16, C39, and C40 on gridline 5 (Fig. 3.12), and C23 and C24 on gridline 6 (Fig. 3.13). There were also a few strain gauges put on bracings to measure stress level on bracings, C7, C8, C33, and C34 being at gridline 4 (Fig. 3.11); and C17 and C18 being at gridline 6 (Fig. 3.12).

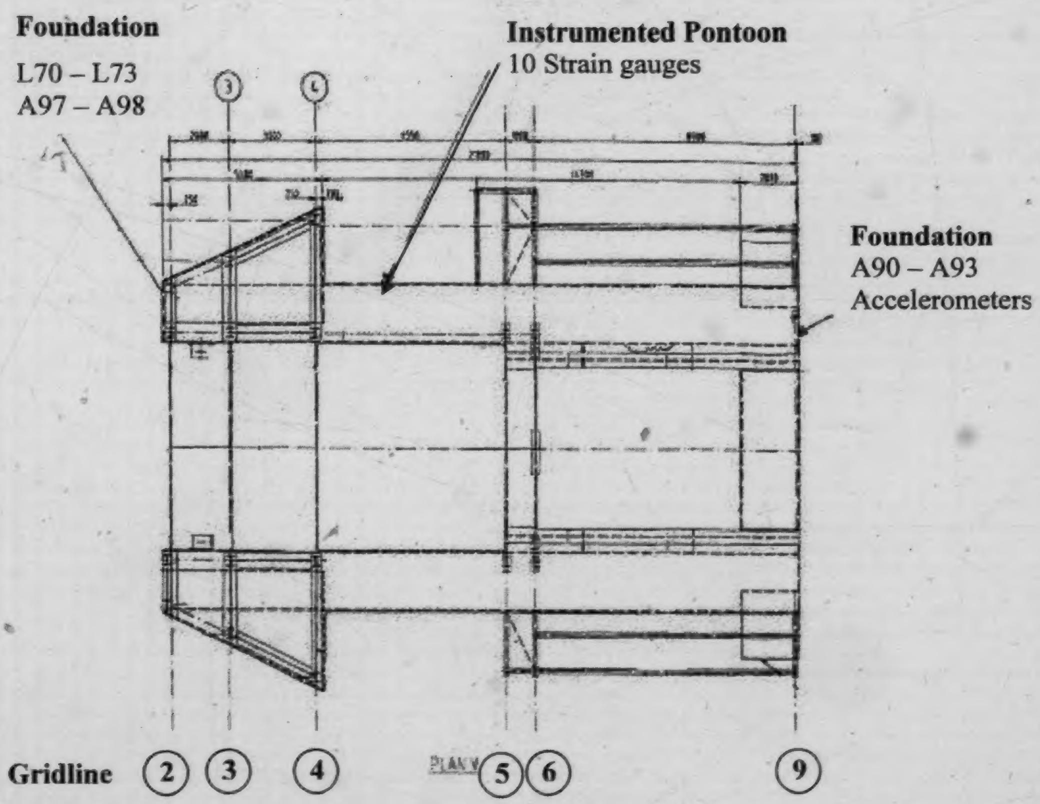

Foundation
L70 – L73
A97 – A98

Instrumented Pontoon
10 Strain gauges

Foundation
A90 – A93
Accelerometers

Fig. 3.9 Aurora II plan with pontoons and column gridlines

The column strain profile at gridline 2 will be provided by the vertical (longitudinal) strain gauges C1 to C4, and C25 to C28. Similarly, at gridline 4, C5-C6, C9-C10, and C31-C32, C35-C36 provides the strain profile. C13 to C16 and C37 to C40 are able to give the strain profile at gridline 5, whereas C19 to C24 give the strain profile at gridline 6. Thus, the gauges for strain profile, peak stresses, and inclined member stresses add up to make 40 strain gauges, which are numbered from C1 to C40 for column strain gauges. In addition to strain gauges, a few LVDT's and accelerometers were also used at certain locations on the columns, which will be discussed further in the sections to follow.

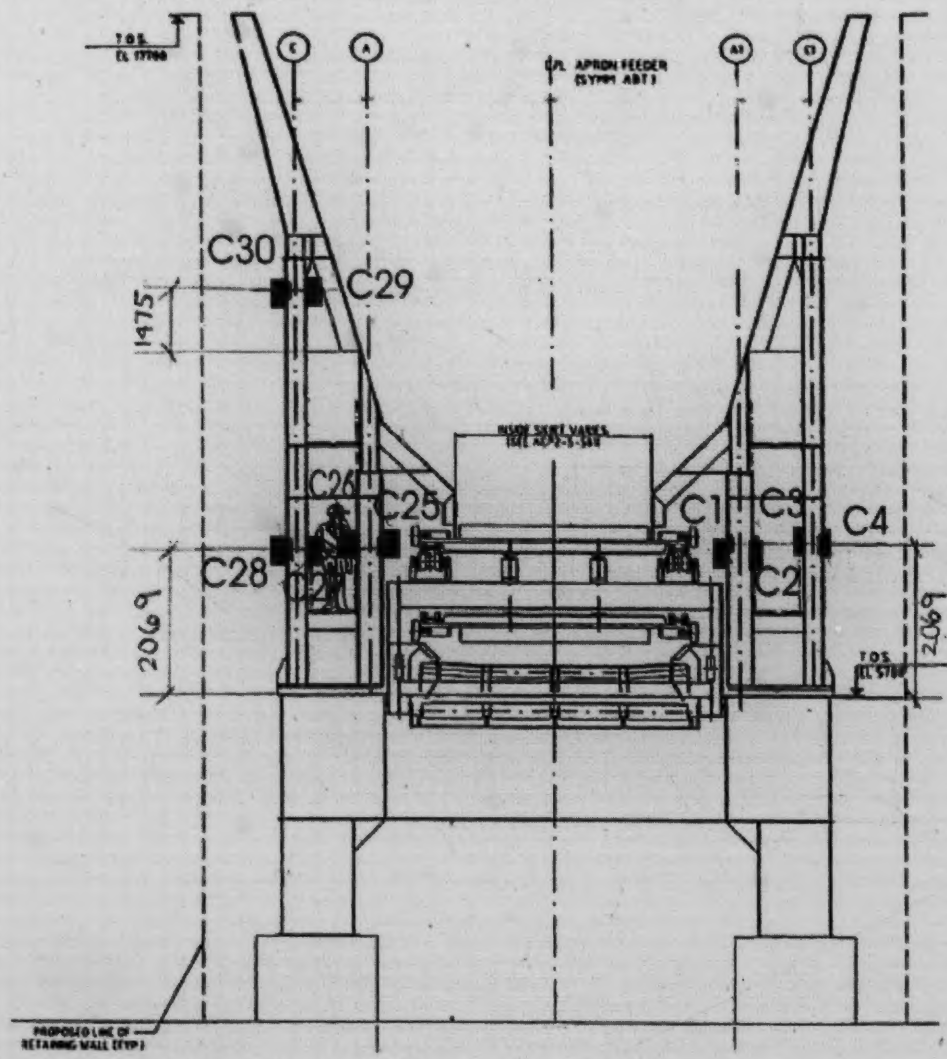
T.O.S.
EL 17700
C
A
C/L APRON FEEDER
(SYMM ABT)
A1
C1
C30
C29
1475
C26
C25
C28
C2
2069
C1
C3
C4
C2
2069
T.O.S.
PROPOSED LINE OF
RETAINING WALL (TYP)

Fig. 3.10 Strain gauges on columns at gridline 2

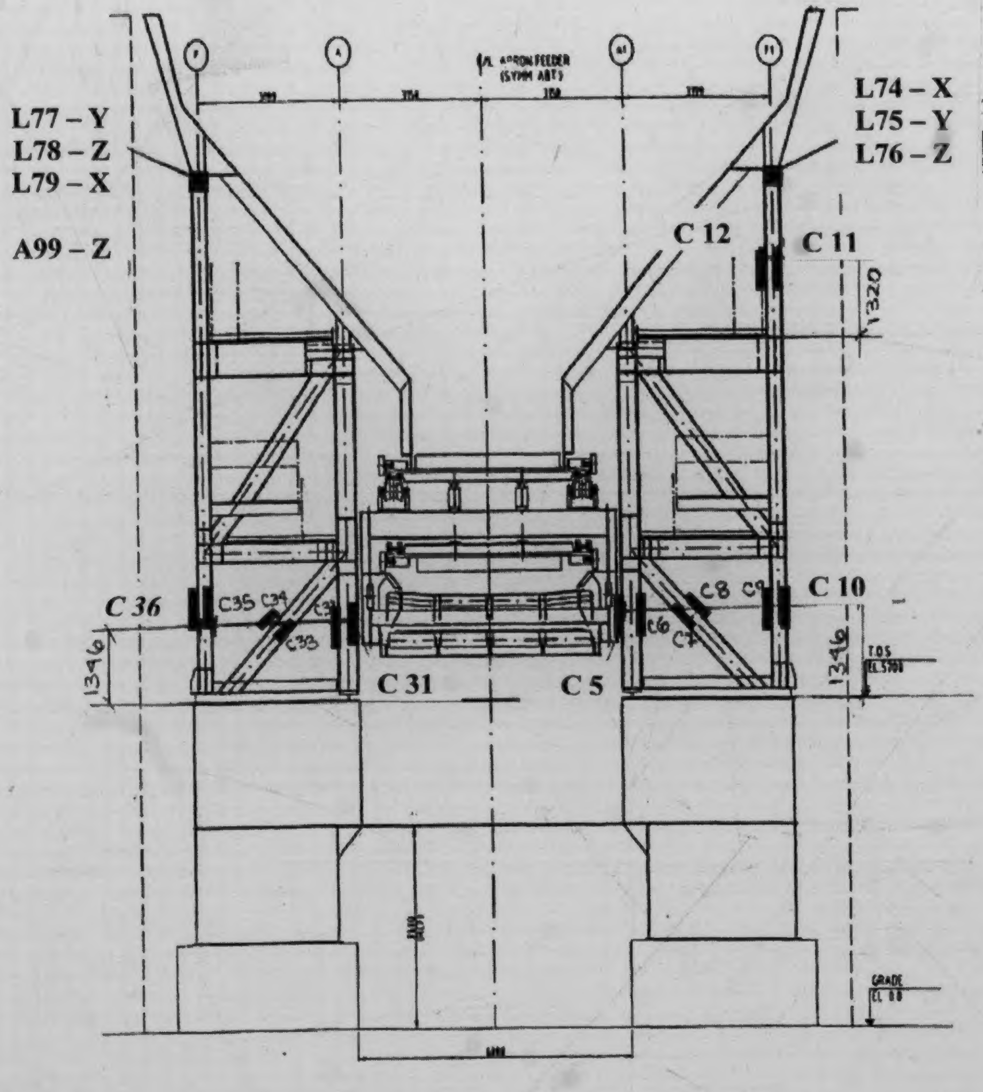
L77 – Y
L78 – Z
L79 – X
A99 – Z
L74 – X
L75 – Y
L76 – Z
C 12
C 11
1320
C 36
C35
C34
C33
C 31
C 5
C6
C7
C8
C9
C 10
1346
1346
T.O.S
GRADE

Fig. 3.11 Strain gauges and LVDT on columns at gridline 4

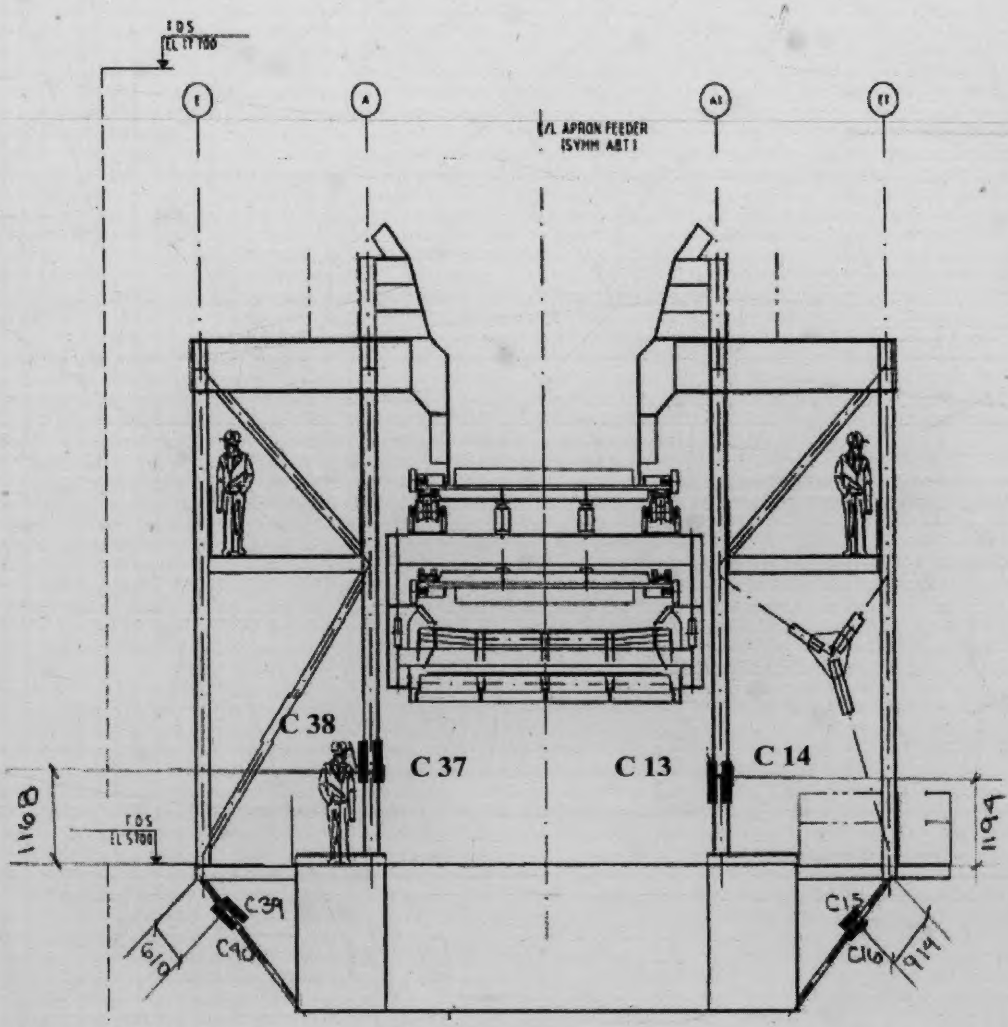
TOS
EL 17 100
E
A
A1
E1
C/L APRON FEEDER
(SYMM ABT)
C 38
C 37
C 13
C 14
1168
TOS
EL 5100
1194
C39
C40
610
C15
C16
914

Fig. 3.12 Strain gauges on columns at gridline 5

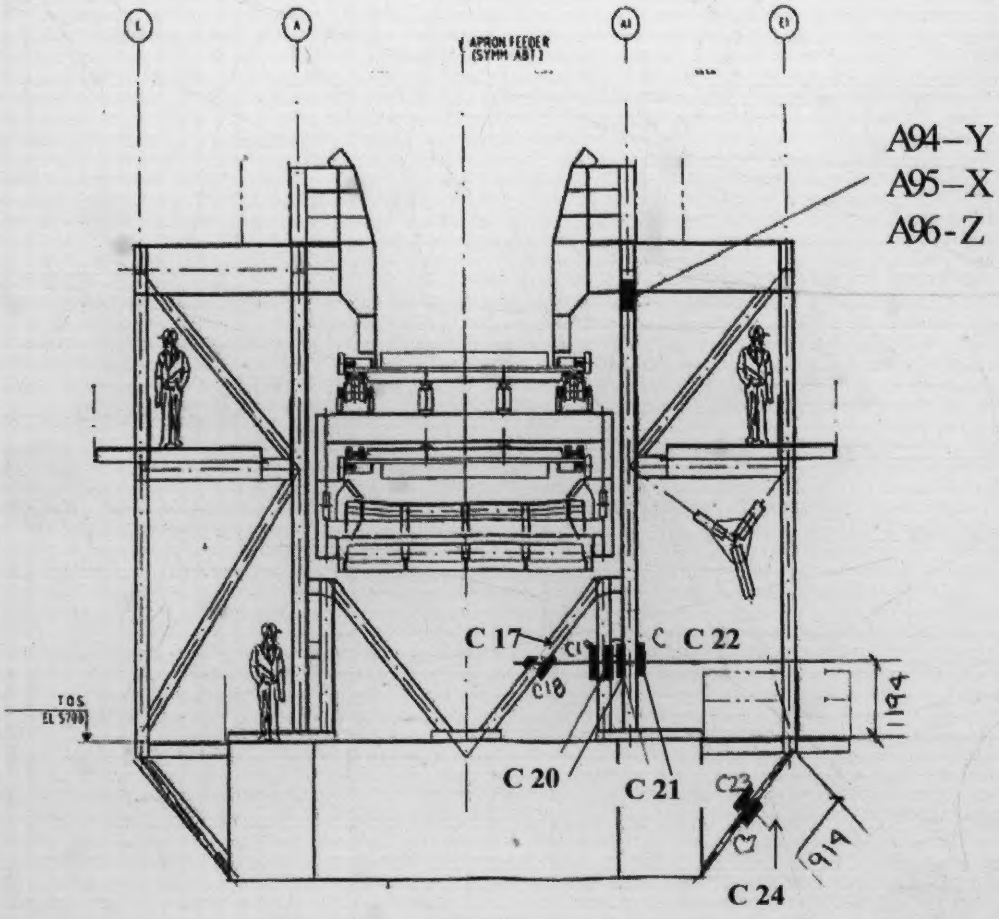
E
A
A1
E1
℄ APRON FEEDER
(SYMM ABT)
A94–Y
A95–X
A96-Z
T.O.S.
EL 5700
C 17
C1
C
C 22
C18
C 20
C 21
1194
C23
C 24
919

Fig. 3.13 Strain gauges and accelerometers on columns at gridline 6

3.5.3 Pontoon Strain Gauges

A pair of box-girder pontoons supports all the columns that carry the loads from the hopper. Pontoons also support the crusher drums, the machinery, inspection platforms, and the instrument control room, all of them adding a dead load and some dynamic load on the pontoons. Making use of the longitudinal symmetry, only one of the two pontoons was instrumented. The north side pontoon was instrumented with ten strain gauges with the objective of quantifying the stress distribution along its length and determining the boundary condition. The gauges were put in pairs as close as possible to the tension and compression flanges of the box girder at five locations along the length, three on one side of the mid-point and two on the other (Figures 3.15 and 3.16). Pontoon gauges P45 and P46 form a compression/tension strain pair, and similarly there are other pairs up to P53 - P54. Pontoon gauges P49 to P52 lie in the mid-span flexure zone, whereas the remaining gauges are located in shear prominent regions. All the gauges near the bottom flange were welded exactly 150 mm above the bottom flange. However, the same conformity could not be attained in the case of gauges at the top due to practical accessibility constraints. While three of the top gauges P45, P47, and P49 are also 150 mm below the top flange, P51 is 350 mm below the top flange and P53 is 900 mm above the bottom flange.

With this arrangement of strain gauges, it is expected that the maximum flexural stresses experienced by the pontoon would be known, and so would be the distribution of stresses along its length. It will be possible to explore the boundary conditions of the pontoon and load transfer from the columns.Fig. 3.14 shows a close-up of the gauge P53 and P54 along with their wiring.

Fig. 3.14 Pontoon Gauge P53

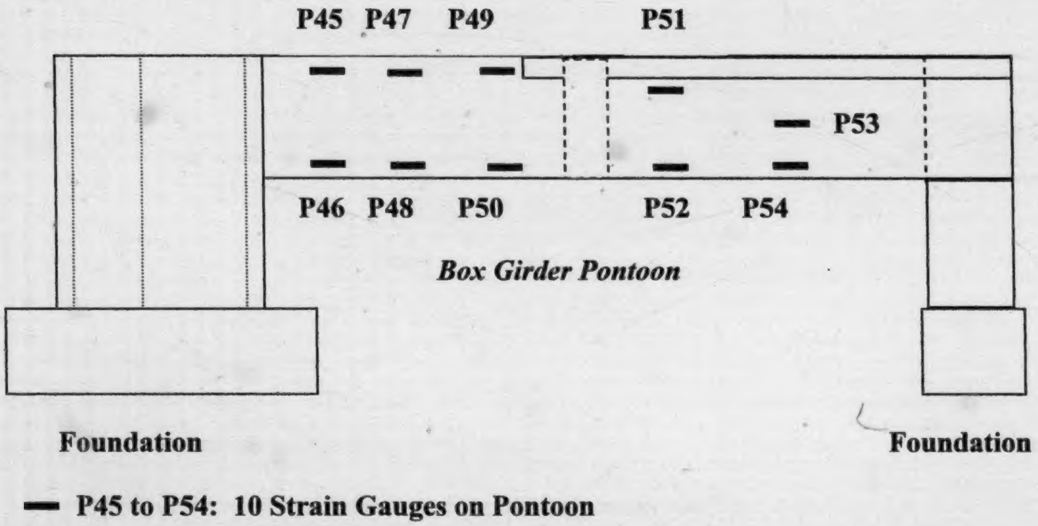
P45
P47
P49
P51
P53
P46
P48
P50
P52
P54
Box Girder Pontoon
Foundation
Foundation
P45 to P54: 10 Strain Gauges on Pontoon

Fig. 3.15 Pontoon strain gauges

Fig. 3.16 Picture of Pontoon gauges

3.5.4 LVDT, Accelerometers and Thermocouple Locations

In order to keep a watch on the structural displacements and vibrations, as experienced in the case of Double Roll Crusher7 plant (DRC7), 10 LVDT's and 10 accelerometers were also used. The displacements were measured at the probable locations of substantial deflection like top of the columns. Displacements in all three Cartesian directions were measured at gridline 4 with three LVDT's at column tops on each side of the crusher, both north and south as marked in Fig. 3.11 (L74 to L79). All measurements were made with respect to the retaining wall, which was assumed to be stationary relative to the crusher. Figure 3.17 shows a typical bracket set up for measurement of displacement at column top relative to the retaining wall. Displacements at the foot of the columns where they rest directly on the pontoon foundation and on top of the concrete pile cap were also measured with four sensitive LVDT's in two horizontal directions as marked on Figure 3.9 (L70 to L73). The vertical deformation was assumed to be negligible at those locations and hence not measured. At the far end columns on gridline 6 and the far end foundation, where retaining wall was not available for measuring relative displacement using LVDT, accelerometers were used instead. Accelerations in all three directions were measured at the top of column on gridline 6 (A94 to A96, Fig. 3.13). Accelerations in two horizontal directions at the foundation level, one at pontoon top-flange level and the other at pile cap level, were also recorded as shown on Figure 3.9 (A90 to A93). The purpose of these measurements at pontoon foundation top and pile cap level will be able to shed some light on the rigidity of supports and any possible movements or rotations of the foundation. Figure 3.18 shows a typical placement of two accelerometers to measure the two horizontal accelerations at the foundation level just above the pile cap. The accelerometers served dual purpose of monitoring vibration characteristics and displacement. Two thermocouples were used to monitor the average temperature at the structure, one on each side of the crusher. Figure 3.8 shows thermocouple T104 placed along with hopper strain gauges on the north side.

Fig. 3.17 LVDT set up at column top

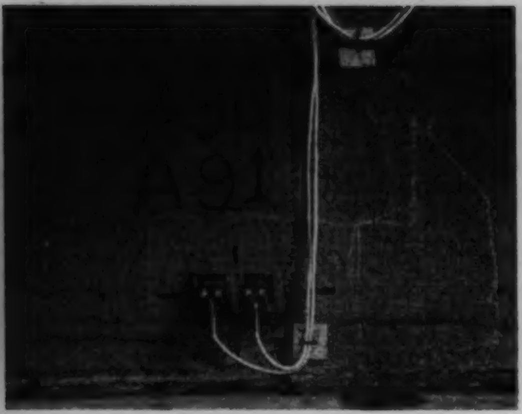

Fig. 3.18 Accelerometers at foundation

3.6 Field Testing

3.6.1 Base Data and Temperature Data Collection in Oct 2003

Field data were collected mainly under four testing conditions, namely – base data, temperature data, normal operation, and controlled testing. Aurora II being a new addition to the production line of Syncrude, its instrumentation was done just before commissioning in October 2003. Thus, base data was collected at the time under empty hopper condition as well as normal operation for 24 hours. The base data serves as the datum against which all future measurements would be compared and will serve as the benchmark for monitoring of damage and distress. Data was also collected at that time under the influence of temperature variation alone without any dumping occurring into the hopper. It helped estimate the influence of temperature on sensor readings, which will establish a certain pattern for the healthy structure. A change in this pattern with temperature at a later date would suggest change in structural parameters of the crusher.

Data under normal operation helps determine the statistical significance of each sensor reading and eventually set the guidelines for the health monitoring system. Working with data obtained from the normal test run of Aurora II in November 2003 afforded a global picture of the characteristics, strengths, and weaknesses of those data. Along came a realization of what is needed in future tests and what is not needed at the moment. The major issues of concern/importance that were noticed at that time are listed in Table 3.1 below. The required resources and test strategies to address those issues also follow thereafter. Some of the issues were related to the instruments, the data acquisition system and its operation, whereas others were related to identification of the load (event) coming on to the structure, and testing under different conditions for comparison. Synchronized video recording was proposed to address the issues mentioned and data collected in files no larger than holding 5 minutes of data during the next testing in April 2004. Influence of material level in hopper, rate of dump, grade of oil sand, type of dump, and side of dump was also planned for investigation.

Table 3.1 Issues at hand for Control Testing

Difficulties / Issues	**Action Proposed**
The size of each data file larger than the capacity of Excel chart wizard to plot data series.	Reduce the data file size from 10 min of data to 5 minutes.
Accelerometers and LVDT were not working properly.	Test in Syncrude lab.
Difficulties encountered in the following: 1. Locating the dump events. 2. Distinguishing between different types of dump whether double dump or single dump. 3. Identifying the side of dump - left or right. 4. Level of oilsand in hopper at the time of dump events. 5. Duration (speed) of each dump – fast or slow. 6. Grade of oilsand being dumped – rich or lean.	Synchronized video recording of the whole duration of testing in digital or VHS format.
Magnitude of Dump Load	Record weight of oilsand in the truck.
Is the impact factor influenced by the level of oilsand in the hopper?	Monitor the level of oilsand during each dump
Variation of pattern recognition and structural behaviour parameters with different dump conditions.	Dump under different conditions and compare

3.6.2 Control Tests and Normal Operation in April 2004

The second field-testing and data collection was undertaken in April 2004 (Sharma et al., 2004). Data was collected under normal operation and in addition some controlled tests were also conducted. Control tests, as the name signifies, are aimed to simulate laboratory-testing conditions in the field by allowing measurement and control over various parameters, which otherwise would be varying randomly. Tests in lab conditions allow great degree of freedom and control to the researcher. On the contrary, field tests are more difficult to control and many unknown factors often creep into the system to further complicate things. It is virtually impossible to control each and every parameter in the field. However, one does aim to achieve what is physically viable and economically feasible with reasonable amount of time and effort and minimum interference to operation. In the case of Aurora II, controlling the load itself was the biggest challenge because it depends on so many factors like the weight of material, grade of oil sand, speed of dump, hopper level, side of dump, etc. However, best efforts were made to control and gather information about each of these factors during the test, so that a conclusive pattern could be generated. Video footage during control tests and normal operation played an important role in recognition of patterns and determining the duration of dumps. Control testing helped establish a benchmark for the structural behaviour and understand the influence of various parameters on performance. It also helped establish trend lines and characteristic features for comparing and evaluating performance throughout its life.

The following paragraphs outline the procedure adopted for successfully carrying out the Control Tests. On 14th of April, a day before the real test, the test team did a trial run of the data acquisition system to check all their instruments are working properly and try a mock data collection. This also gave an opportunity to all the team members to get familiar with the system, understand each person's role in the test, and fix problems in advance. It was found that some of the accelerometers and LVDT's and one thermocouple were not working properly. Hence, data from those sensors were not collected. Late in the afternoon, data under normal operation was collected in two smaller files. One team member did video recording every time data was collected under normal operation or during control tests.

Control test started on April 15 at 1:30 PM. The site Coordinator was in continuous touch with the haul truck drivers from the control room, the camera operator was on top floor in full view of trucks and the hopper, and one person operated the data acquisition system. The site Coordinator was the common link to command the dumps and relay information back to data collection team. Trucks were stopped from dumping oilsand into the hopper to mark the beginning of the control test, and the hopper was allowed to empty. Thereafter, the hopper remained empty for a while, which provided the base zero load readings. The first dump on the empty hopper was made from North side (Left) and then the hopper was allowed to empty. The second dump was from South side (Right) and again the hopper was emptied. At the third dump, two trucks dumped at the same time from North and South sides followed by the hopper being emptied again. Once one set of the control test was completed, two more sets of dumps were done on the empty hopper and then normal operation was resumed. This pair of control testing and normal operation testing helped determine the influence of dumping on a full hopper versus an almost empty one. All the while video recording was done.

3.6.3 Continuous Data Collection in June 2006

Once the basic nature of the structural behaviour of the crusher was understood and the nature of loading and the response it generated at various gauge locations was established, an automated data processing and management system was developed. The data processing and management system, which is discussed in detail in Chapter 4 of this thesis, was able to considerably reduce the processing time requirement and storage space requirement. Data collection, processing and archiving became much more efficient and less time consuming. Further, the earlier tests had helped establish response patterns, the expected stress levels and parameters to look for. Thus, data could be acquired continuously without worrying about management issues. It was also important to collect sufficient amount of data could help look at them in a statistical sense, for which a large number of dump events needed to be captured. Consequently, in June of 2006 the third data collection trip to Fort McMurray was made. This time around, the largest volume of data was collected for about 3 days continuously capturing more than 1300 dump events in close to 10 GB of data. This data has been used for developing the statistical parameters and values that is presented in Chapter 7 of this thesis. During the field data collection in June 2006, no attempt was made to control the load or dumping. Data was collected primarily under normal operating condition without any interference into the crusher's operation. This is the only way the normal structural signatures could be derived and established, which can be compared to the data in subsequent years. With the availability of the data processing and management algorithm, now the data can be substantially reduced without sacrificing its quality. Hence, the structure and the health monitoring system is now in a ready state to operate continuously for monitoring its performance. The monitoring system and its processing algorithms now need to be integrated with the production and operating system of the industry to facilitate round the clock monitoring.

3.7 References

Afhami, S., Alexander, S.D.B., and Cheng, J.J.R. July 1998. "Field Instrumentation and Monitoring of Crowchild Bridge in Calgary, Alberta. SMSB V Conference in Calgary, Alberta, July 13-16.Campbell Scientific, 2003. Campbell Scientific (Canada) – Products. http://www.campbellsci.ca (accessed March 2003).

Campbell Scientific, 2003. Campbell Scientific web site, accessed in 2003.

Carroll, M., 1997 a. Dragline #4 Boom Loading Condition Monitoring. Syncrude Canada Ltd., Research Department Progress Report, 26 (5).

Carroll, M., 1997 b. Mining Equipment Monitoring at Syncrude. CIM District 5 Conference.

Entran Devices Inc., 2003. Entran Accelerometers: Accelerometer Product Families. http://www.entran.com (Accessed February 2003).

ISIS Canada. Spring 2001. "Guidelines for Structural Health Monitoring". A Design Manual published by ISIS Canada, a Network of Centres of Excellence.

Khattak, N. A. and Cheng, J. J. R. April 2003. "Assessment and Rehabilitation of FC Girder Bridges". Structural Engineering Report No. 253, Department of Civil and Environmental Engineering, University of Alberta.

Krupp Canada, 2003. Design Drawings and Modelling of the Aurora II Crusher. Personal Communication through Syncrude.

Micro Measurements, 2003. Vishay Measurements Group web site, accessed in 2003.

National Instruments, 2003. National Instruments web site, accessed in 2003.

National Instruments Corporation. 2000. "Labview Measurements Manual". National Instruments Corporation, Austin, Texas.

Obaia, K. and Gonzalez, S., 2001. Investigation of Support Displacement of DRC7. Syncrude Canada Ltd., Research Department Progress Report, 30 (09), pp. 1-13.

Optimum Instruments, 2003. Optimum Instruments web site.

Roctest, 2003. Roctest web site, accessed in 2003.

Sharma, V.P., Obaia, K., Cheng, J.J.R., & Neudorf, J. 2004. Smart structures – controlled field test of Aurora II crusher. *Syncrude Canada Limited Research Department Progress Report*. 33 (10) 1.2.

CHAPTER 4

DATA PROCESSING AND MANAGEMENT

4.1 Introduction

Structural Health Monitoring (SHM) projects produce huge amounts of data, which is its strength and also weakness, posing a big challenge of identifying useful data. In order to fulfil the objectives of health monitoring and damage detection with reasonable reliability, a considerable amount of data has to be collected at high rates, analysed for meaningful information and stored for a long period of time. An efficient and effective data processing and management system forms the backbone of a successful structural health monitoring project, though finding such a tool has proved to be the biggest road block to the growth and field application of the concepts of SHM. Manual processing of each data file to gather valuable information about the behaviour of a structure and its health becomes highly inefficient and exorbitantly expensive in the long run. In the absence of an effective value extraction tool, it also becomes quite difficult to justify the utility of storing mammoth amount of data. Automation in data processing and management, with reduction in the quantity of data without losing its quality, is the current research need for continuous monitoring of a structure and long term sustainability of SHM projects. An algorithm is presented in this chapter that detects events in data files, extracts valuable information about the events from each data channel and stores the reduced data into a database before archiving or eliminating the original data file, as per need.

The first sets of data were collected in October 2003 continuously under normal operating conditions. The initial portion of data focused on capturing zero live load reading of the gauges and influence of temperature on them. Base data with normal dump operation was also collected at that time to serve as the benchmark of structural behaviour. Thereafter, controlled tests were conducted in April 2004 and data under controlled operations and normal operation were collected. At this time, round the clock data collection had not been started due to practical data handling and management issues. Data collected from 82 sensor channels at the rate of 100 Hz in 'csv' text format amounted to 22 MB disk space for each 5-minute of data. At this rate the daily disk space requirement would be more than 6.3 GB. Thus, a 100 GB hard drive would be full in 15 days time. In addition to the storage issues, there exists an even bigger problem of processing and making sense out of the data. Processing and managing such huge amounts of structural health monitoring data can be demanding in terms of computing resources and manpower requirement. This chapter is dedicated to introducing the data files, understanding the characteristics of signals, available processing tools, techniques of event recognition and data reduction, and a database management system for data archiving and query. By using the proposed data processing algorithm, critical information about structural response can be extracted and the data reduced in size by 10,000 times before being stored in a database, that is 10 GB of data is reduced to 1 MB.

4.2 Data files and features

Data collected at different occasions were primarily similar in nature and size except that during the April 2004 data collection, a few gauges were not working properly and the size of files were reduced from 10 minutes to 5 minutes of data per file. This was done primarily to make it easy to work on excel spreadsheets. Data collected at different times had four main themes in perspective, namely – influence of temperature, base data, controlled operation, and normal operation. With each of the themes, the basic data file structure remained the same; the only change being in the operating parameters of the crusher and information about them. For example, during the data collected to assess the influence of temperature on each of the sensor readings in October 2003, no oil sand was being dumped into the crusher. Similarly, during base data collection, the first signatures of the crusher were collected under normal operation. This would serve as the benchmark for comparing future performance under normal operation of the crusher.

Data collected in April 2004 comprised of control testing as well as normal operation. Control test implied that the weight and grade of oilsand in the truck were known, the truck number and side of dump were known as well. Further, the hopper was emptied completely before and after each dump so that each dump was on an empty hopper simulating the highest impact. Video recording was done throughout the controlled test for visual validation of data and to gauge the hopper level in cases where the hopper was not completely emptied. Special permission had to be obtained to empty the hopper completely for the test since normal operating conditions require a minimum level of ore in hopper to be maintained. On the other hand, normal operating condition implied uncontrolled test. None of the parameters mentioned above were known during such normal operation test. However, from the video the side of dump and the grade of oil sand or the hopper level could be found. A few of the sensors that were not working were not used in data collection at that time. Accelerometers -A90 to A95, LVDT's – L70 to L72, L78, L79, and Thermocouple T101, were not working properly. This left a channel count of 70 sensors out of 82 that were working.

Aurora II test in April 2004 produced a video of approximately one and a half hours duration, and 15 data files in total. About one hour of video and 9 data files were obtained on 15 April, whereas 6 data files were obtained during normal operation on April 14 and 15 together with the remaining video. A total of 15 dump events were identified during the control tests and verified by video observations. Table 4.1 summarizes the details of those dumps including the date, time, dump duration, weight and grade of oilsand, side of dump, and hopper level at the time of dump. The Control dumping started on 15 April at 13:52 and the dumps were numbered with the prefix C standing for control. The letter L stands for dumps occurring from the left side corresponding to the North direction, R stands for right side dumps coming from the South side of the hopper, and D for double dumps when trucks dump from both right and left sides simultaneously.

Table 4.1 Dump Events in April 2004 Control Tests

Date	Dump Time	Side of Dump	Material Level in Hopper	Duration of Dump (sec)	Dump Weight (ton)	Comments / *file*
April 14 2004	15:50	North	80%	12 sec	--	Lean Ore – free flow of material. Large lump at the end falls on centre. *(14 Apr Normal Operation_1.xls* - @ 143.42 sec)
	15:52	South	85%	7 sec	--	Most of the material falls in the last two seconds as one large lump. *(14 Apr Normal Operation_1.xls* - @ 227.3 sec)
	15:53	North & South	80%	5 sec & 14 sec	--	Double Dump - Lumps from both sides collide and fall in the centre. North truck immediately empty, but South truck takes a while for all material to slide off. *(14 Apr Normal Operation_2.xls* - @ 354 sec)
15 April	10:08	--	--	--	--	Hopper Level at 100%, being slowly reduced. *(15Apr Normal Operation_1.xls)*
15 April 2004	10:10	North	95%	8 sec	--	North truck has to wait a while longer for some material to slide off. South truck has been waiting for a long time. *(15 Apr Normal Operation_2.xls* -@ 306 sec)
	10:52	North & South	90%	18 sec & 12 sec	--	All material yet to slide off into the hopper. Both trucks waiting. Level 100%. *(15 Apr Normal Operation_2.xls* - @ 538 sec)
	10:59	North	95%	--	--	Hopper level 100%. *(15 Apr Normal Operation_2.xls* - @ sec)
15 April 2004	13:35	--	--	--	--	Trucks stopped from dumping. 80% hopper level started emptying. (*testplan emptying hopper_1.xls*)
	13:52	North	0%	6 sec	364 T	Rich Ore. Fast Dump. Load Falls as one big lump. (testplan_1.xls) Case C1-L - @ 113.91 seconds.
	13:56	South	0%	17 sec	420 T	Lean Ore. Load falls gradually. Big impact at the end of dump. File (testplan_2.xls) Case (C2-R)
	14:01	North and South	0%	2 sec 12 sec	362 T 382 T	Double Dump. North Rich, South Lean. The rich ore falls first and hits wall. North (left) dump dominates. (testplan_3.xls) Case C3-D – @ 610 sec
	14:16	North	0%	81 sec	384 T	Rich Ore. Slow dump. Material falls on apron feeder, then on north side of skirt, then big chunk on south side. (testplan after test_1.xls) – @ 220 sec Case C4-L

Date	Dump Time	Side of Dump	Material Level in Hopper	Duration of Dump (sec)	Dump Weight (ton)	Comments / *file*
15 April 2004	14:21	South	0%	14 sec	369 T	Slow Dump but Large impact at end File (testplan after test_1.xls) – @ 396 sec Case C5-R
	14:22	North	20%	15 sec	--	Rich Ore. File (Aftertest_1.xls) – @ 447 sec. Case C6-L
	14:24	North and South	33%	17 sec 5 sec	--	Double Dump. Hopper level after dump 80% to 90%. File (Aftertest_1.xls) – @ 616 sec and 621 sec. Case C7-D
	14:28	--	66%	15 sec	--	Lean Ore. Free flowing gradual. Low impact. No impact on the other side. (Aftertest_2.xls) - @ 841 sec. Case C8-R
	14:29	--	75%	15 sec	--	Lean Ore. Gradual flow. But impacts the other side. File (Aftertest_2.xls) - @ 877 sec. Case C9-L.

It is worth mentioning here that one truck dump fills up almost one third of the hopper. During normal operation it was observed that many trucks were assigned to Aurora II crusher, such that a few had to wait in queue for their turn to dump. It is thus not surprising that most of the time the material level in hopper remained almost full (90%) under normal operation, which greatly reduces the impact from dumps. Going by the same reasoning, the duration of each dump was much longer than initially imagined, because the oil sand in the truck could not slide into the hopper until the level dropped enough. One single dump (single truck) could take up to a few minutes to complete. The dumps are all numbered from 1 to 9 starting with the letter C, which stands for control, followed by L, R, or D depending on whether they are a left, right, or a double dump.

During base data collection in October 2003, all the pertinent information about individual dump events mentioned in the table above were completely unknown. Events can be identified from change in sensor signals; however, the characteristics of the dump event such as side of dump, duration of dump, hopper level, weight of material, etc. remained unknown. This is where pattern recognition is useful to predict the unknown parameters based on strain patterns established from control tests. Unknown dump events can be compared to those patterns to classify them into appropriate category.

Identification of dump characteristics may be of interest to the designer, however for the purpose of health monitoring, more has to be read into the pattern recognition algorithms.

4.3 Signal Characteristics and Dump Events

Data was collected from the structure under normal operation of the crusher as well as under controlled field testing conditions 3 times over three years. Round the clock monitoring and data collection could not be started without an accurate and efficient data processing and management tool. The cost and time involvement in storing and processing large amounts of data in its raw state is simply prohibitive. Based on a series of data analysis and interpretation exercises conducted on data collected at different times and under different environments, it was possible to come up with an algorithm that catered to all varieties of data with confidence. The primary requirement for the program was to be able to effectively identify each dump event, quantify the dump event by a universal parameter, and then save in a reduced database. The program had to be robust enough to make sure that no false events were recorded and no true events were lost.

It is evident from the foregoing that hours of data may account for a few countable numbers of dumps. The cost of processing and storing large amounts of data combined with the efforts involved in identifying and locating dump events led to the need for data reduction and event identification algorithms. The algorithm needs to be robust enough to ensure that no significant dump event is unaccounted for and no valuable data is lost while reducing. On the other hand, it also has to be balanced enough to minimize and nullify the effect of false dump event identification. The reduced data would then be stored in a suitable database management system. Various statistical queries can be run on the reduced database to gain valuable information about the load and behaviour of the structure. Careful monitoring of the statistical information and strain patterns over the years will facilitate health monitoring of the structure.

In order to process or reduce data, it is essential to understand the basic signal characteristics and the influence of operation and environment on it. The nature of critical loading of the crusher plant and its operation indicates that impact due to falling oilsand dictates most structural response. Along the way, the crusher hopper may be completely full or totally empty, the latter case being more detrimental to the health of the structure. As the crusher is operating round the clock throughout the year, it makes sure that the hopper is rarely totally empty and most of the time partially full. Figures 4.1 and 4.2 show two examples of typical strain gauge reading during a dump event wherein a sharp peak corresponds to the moment the material hits the hopper. Thereafter, as the crusher operates and the hopper gets emptied, the strain level slowly drops with the drop in material level in the hopper. There is static strain change associated with each filling or emptying cycle of the hopper; however, they are much more gradual and slow compared to the sudden change in strain associated with a dump event. From the point of view of fatigue and remaining life considerations, the strains due to dumping activity weigh over other less significant strains, as evidenced further by the Figure 4.1, which show the difference between dynamic component of the strain due to impact and static component due to the same oil sand. The durability or life of the structure is influenced by the change in stress magnitude (strain) and its number of cycles, which is very low for static strain as compared to the dynamic component and the number of dumps in a year.

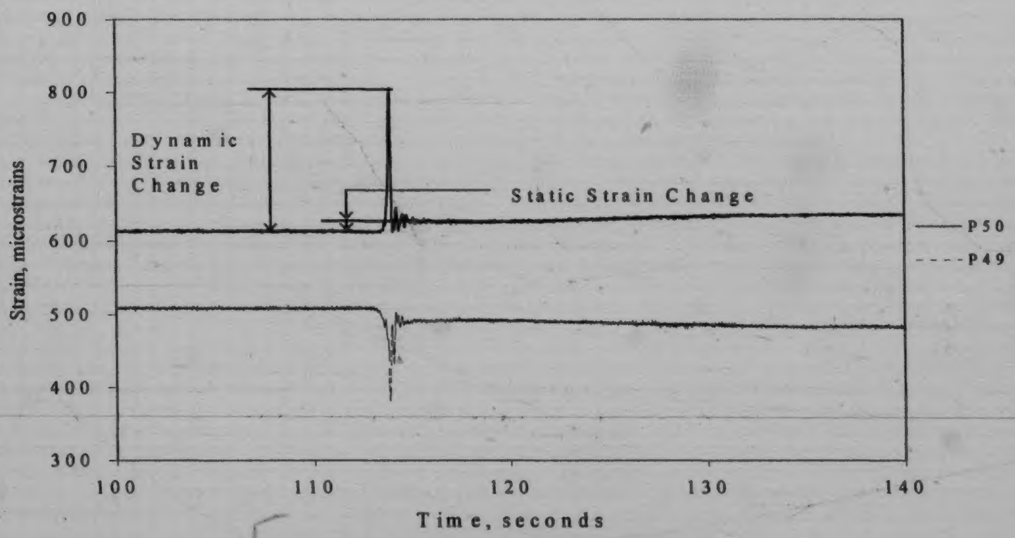

Fig. 4.1 Typical impact due to a Dump Event

The low magnitude strain cycles from high frequency operating machine parts have negligible effect on the crusher and are mostly mired along with noise within the range of 5 micro-strains. The dynamic strain change due to a severe dump event at the same location, on the other hand, could be in the range of hundreds of micro-strains. The frequency of such dump events occurring in a day at 70% of rated capacity of the crusher could be more than 500 in number. Annually, the number of dump events could easily be above 0.2 million. It should be clarified though that not all dump events lead to such high strain magnitudes, only the severest of them do. Strain change due to temperature can be significant over different seasons, however, within a day 10 to 20 degree fluctuation distributed over 24 hours period seems less significant when assessing damage or remaining life. All in all, the magnitude of suddenly and frequently changing strain due to dump events on the crusher out-weighs strain changes due to all other associated factors like temperature, machinery, static load, noise, etc. Hence, if data pertaining to all dump events are identified, measured and stored, one can safely say that nothing has been lost as far as the main features of the structural response are concerned.

Careful observation of a data file (Fig. 4.2) reveals that hardly one percent of data corresponds to the dump event capturing structural response. Remaining ninety nine percent of the data simply displays noise and gradual decrease/increase in strain due to emptying of the hopper from crusher operation. As can be seen from Figures 4.1 and 4.2, most of the influence of impact due to dumping occurs within duration of 2 seconds or so. The strain magnitude jumps to a peak and then almost instantly drops down close to its original value differentiated only by the static load effect. Thus, out of 24 hours (86,400 seconds) in a day, only 1000 seconds (500 dumps times 2 seconds) pertain to the dump events and the rest are insignificant operating strains of negligible magnitude. This leads to the fact that less than 2% of the collected data contains information of significant value and the rest 98% of data do not add much value and hence, can be done away with. However, before discarding any data or reducing its size, it is of utmost importance to extract the main information, i.e. the characteristics features of the dump. It is also important to ensure that there is limited margin of error in identification and extraction of information from dump events, and the algorithm is robust and reliable.

4.4 Strain Jump as Identifier and Metric of Dump Events

Strain Jump is introduced here as a useful parameter that helps in capturing the essence of each dump event without losing any valuable information. This parameter when effectively used has the potential to significantly reduce data size and processing time. Dump events are marked by a clear jump in strain level especially for empty-hopper dumps. Strain jump is defined as the difference between maximum and minimum values of strain reached in the vicinity of the dump. This parameter takes into account both static and dynamic effects of the load. Strain jump is calculated by taking the difference between maximum strain and minimum strain encountered in a very small window such that it is representative of the impulse response of the structure. Windows of durations from 1 sec to 20 sec were tried in order to capture the true nature of the signal collected under impact loading. When the differential window was too small, one dump event was going to be broken into two or more pieces, whereas when the window was too large like 20 sec, the maxima and minima calculations are influenced by unwanted effects in the vicinity of the dump such as rise or fall in strain due to hopper getting emptied as the crusher operates. By trial and error, a processing window of 10 seconds duration was found to give the most optimum results, and hence, strain jump parameter has been based on this widow size in all discussions henceforth. Static strain associated with any particular static load acting on a linear elastic structure is at all times constant. However, in the case of Aurora II crusher structure, the strain magnitude for the same ore weight is not constant due to variations in impact area and dynamic component of the load. Therefore, the strain jump parameter, as defined above, is better suited to quantify the structural behaviour due to dump events occurring under different operating conditions than parameters based on static strain alone. The magnitude of this strain jump is dependent on many factors such as ore weight, speed of dump, grade of oilsand, hopper level, side of dump, etc. For control dumps with hopper totally empty, the jump is considerably high, whereas in the case of normal operation these jumps are much smaller in magnitude because the hopper remains mostly close to full during such operations. Figure 4.2 shows strain reading at pontoon mid-span for a typical dump event, for which the corresponding strain jump calculated in a one second window is shown in Fig. 4.3.

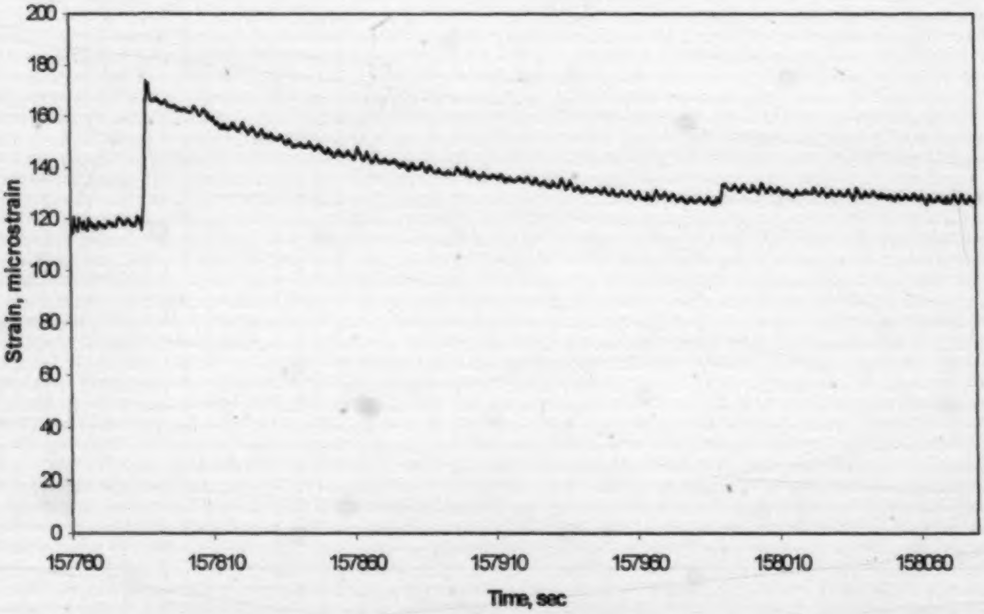

Fig. 4.2 Sample strain time history with a single Dump Event at gauge P52

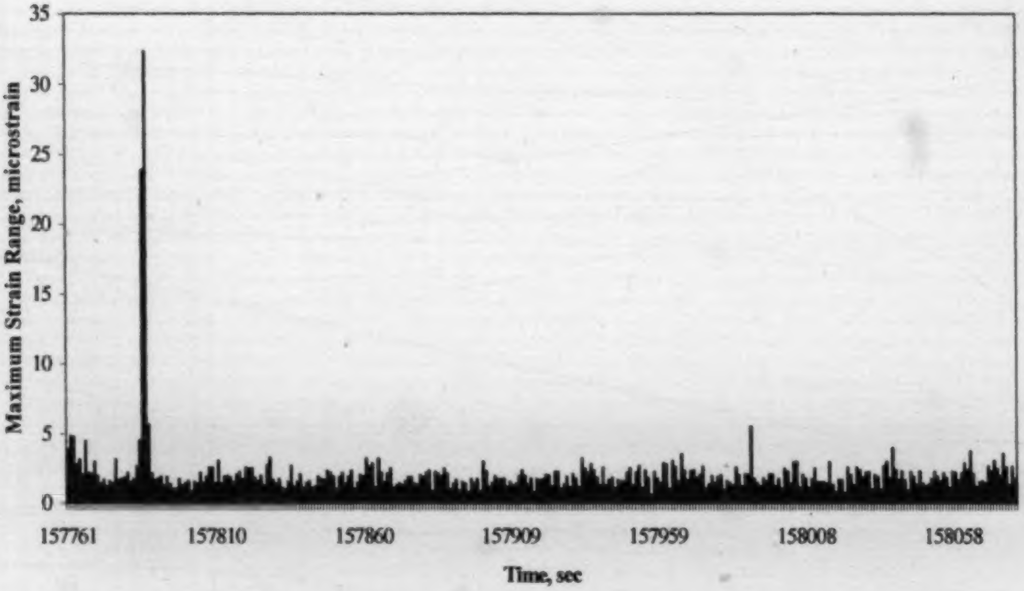

Fig. 4.3 Strain Jump calculated on a 1 second moving window at gauge P52

The strain jump at the instant of the dump event can be easily seen standing tall among other insignificant ones of much smaller magnitude, which can be classified as noise. Analysis of several strain data files reveals that the magnitudes of such "noise events" are mostly less than 5 με and remained less than 15 με even for the worst cases of noise pollution. When compared with dump events in hundreds of micro-strains, these noise magnitudes are easily detectable and separable, making the strain jump parameter attractive to use. However, there might be certain dumps under full hopper conditions, which may produce a much smaller strain jump, which is close to the noise amplitude. Event detection then poses some challenges which can be tackled by adopting a robust and flexible detection algorithm that can encompass different dump scenarios. On the other hand, if the dump events are too small, then even losing them would not be of much concern due to its low magnitude. A threshold of 15 με will in many cases suffice as the criterion for identification and separation of events from noise (non-event). When the event strain jump magnitude to noise ratio is not very good, or when the noise magnitude has increased, the algorithm should be able to learn from the history of past noise magnitudes and adapt accordingly. The magnitudes of strain jumps combined with their relative variation along different gauge locations will give an indication of operating conditions and the health of the structure. It is evident that the strain jump parameter efficiently captures the dump event, while filtering-out the non-event data. These short duration differential readings are also completely free from the effects of temperature, drift, machinery and noise. Within ten second window there are no other factors that could muddle or pollute the strain jump parameter, and hence, it remains a pure parameter at all times.

4.5 Event Identification and Data Reduction – Needs and Review

The strain jump parameter can be effectively used in an event identification and data reduction algorithm. A moving window of 10 second duration is used to scan each data file and calculate the difference between maximum and minimum strain values observed during that period. By taking differential readings in a moving window of 10 second duration, the data file size is already reduced significantly by 1000 times. Thus, a gigabyte of data has been reduced to a megabyte. Now consider discarding the non-event data completely from the system and keeping only the dump events. This step will lead to reduction in data by another 10 to 20 times, thereby only data with noticeable dump event is recorded into the database that can be queried for various statistical purposes. This means a total reduction in data size by 10,000 to 20,000 times. Thus, assuming a maximum of 4 dump events in a 10 minute data file, which contains 60,000 data points sampled at 100 Hz, the data is effectively reduced to four points. So, 10 GB of data is reduced to 1 MB by effectively utilizing the strain jump parameter.

Before reducing any data, it is important to make sure events have been properly identified with reasonable accuracy. There can be many ways of event identification based on the characteristics of the signal and structural properties. For the type of load and signal generated, a literature survey was conducted for the most appropriate ways to achieve this goal. Card and McNeill (2004), arguing in favour of the need for event identification and data reduction in SHM projects, have used unsupervised neural computation for novel event identification based on power spectrum of the signal. Although there is agreement with the authors on the needs and reasons for event identification and data reduction, power spectrum is not the best tool to fulfill the objectives of this research because it is not only less sensitive to subtle changes but also prone to manifold processing errors, especially when the mass in the hopper of the crusher can change by 1000 ton. For the particular case of strain signals from impact loading of oil sand, the task has been cut out to determine the strain jump for event identification. This is analogous to spike or peak detection. The closest examples of such spike detection algorithms were found in the field of Neuroscience. Coincidentally, the nature of signal obtained in this SHM project is quite similar to the signal obtained from neuron-scanning or heartbeat monitoring equipment. They both have occasional spikes on a noisy background. Understanding of brain structure and function is one of the biggest challenges faced by Neuroscientists and in the field of neural computation. There are countless numbers of neurons in human brain and these neurons communicate with each other by firing electrical signals called action potentials. Eggermont (1990) explains brain as a largely parallel system whose activity is induced by the functional coupling of many neurons. When the neurons fire, they produce a spike that can be measured by electrodes placed nearby. Figure 4.4(a) shows an arrangement for acquiring and measuring neural action potentials. The weak intensity neural signals are magnified by an amplifier before filtering and analog to digital conversion. This process makes the neural signals digitally detectable, but at the same time also adds some background noise into the system. Figure 4.4(b) shows a typical signal from neurons acquired by the data acquisition system (Source: Lewicki, 1998).

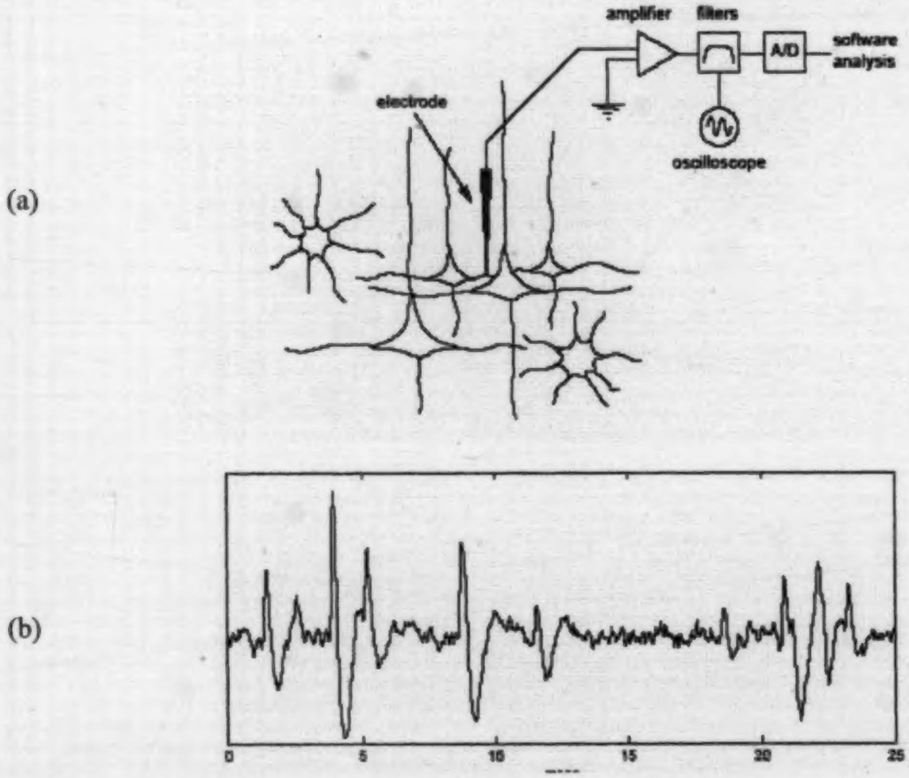

Fig. 4.4 Measurement of neural Action Potentials (a) Experimental set up (b) Measured signal with spikes (Source: Lewicki, 1998)

The neural spikes are separated from each other by some background noise and the spikes are seen clearly standing tall among noise, bearing much semblance to the strain signals due to impact loading. Strain of significant amplitudes under isolated dumps are separated by comparatively negligible amplitude strain under other operating loads like static loads, machine vibration, temperature, etc. The dumps occur in such short duration of time that other aspects of load are overshadowed by the effect of impact, just like a neuron bursting action potential. Here, strain due to a dump event bears direct semblance to a neural action potential. An electrode with larger tip is able to record signals from greater number of neurons in the neighbourhood, but too large a tip makes isolation of signals from any one particular neuron impossible. With too small a tip, on the other hand, signals may be too weak to be detected (Lewicki, 1998). An electrode in neuroscience is able to capture signals from many nearby neurons at the same time, the strongest signals being from the closest firing neuron. This necessitates the task of identifying and separating signals obtained from a group of different neurons, which is not easy but possible because each neural signal has a particular shape and characteristic. The signals from nearby neurons in many cases constitute noise rather than a spike because of weaker signals muddling up along with other sources of noise; hence, placement of the electrode and identification and separation of the action potentials from a particular neuron seems to be the focus of spike detection in neuroscience. Some of the newer techniques in neural spike detection are using multiple electrodes instead of a single electrode collecting signals from a group of neurons, which makes identification and classification more robust. In short, the neural signals have temporal as well as spatial variations recorded.

Fortunately, such a situation of peaks muddling up each other does not occur in structural engineering, for signal generated by one strain sensor does not get recorded by another sensor. Although every strain gauge is recording strain under the same dump load, they are all at different locations and do not influence each other electrically rather only by laws of structural mechanics. Thinking of each strain gauge as a neuron, in effect an independent electrode (strain gauge) is being used to measure action potentials (strain) generated by each neuron (gauge) without muddling up of peaks. The sources of noise are mainly electromagnetic and vibrating machinery; and each spike measured at the Aurora II crusher is due to a new dump. So, records from each strain sensor have only temporal variation and no spatial component. The signal to noise ratio appears to be better in the case of strain signals than the neural signals in most cases. This fact will work to advantage when selecting the event detection algorithm. In both the cases of structural strain and neural spikes, the candidate spike (event) to actual spike ratio is quite large, which makes spike (event) detection quite challenging, especially if the data is too noisy. Hence, along with many similarities between neural spikes and strain jump due to dumping, there are many subtle differences as well. The similarities and differences both have to be analysed and taken into account while coming up with a suitable spike detection algorithm.

The main concern in data reduction is to detect the spikes in a reliable manner. The strain jump (spike) due to a dump event varies significantly from one event to another, unlike the neural action potentials which retain their basic features and shape from one neural firing to another. The magnitude and shape of the strain spike varies even at the same gauge location depending on many factors like dump speed, hopper level, side of dump, oil sand grade, etc. Further, being in an industrial environment and not a well-controlled science laboratory, the nature and extent of noise is more severe in the case of signals obtained at the crusher. The neural action potentials do sometimes vary in magnitude and shape from event to event over time; however, they are rather slow and subtle in variation. In spite of all the similarities perceived between neural potentials and structural strain spikes, and due to the many dissimilarities existing, it is clear that the spike detection algorithms found in neuroscience may be used as a source of motivation and conceptual validation but there is a clear need for an algorithm that caters to the specific needs of the project with simplicity and accuracy. Hence, learning from the experience of neural spike detection techniques, an event identification and data processing algorithm is proposed using multiple layers of thresholds based on the structural behaviour.

4.6 Spike Detection – A Literature Review in Neuroscience

4.6.1 General

Gloor (1975) defined spike as "a restricted triangular transient clearly distinguishable from background activity and having amplitude of at least twice that of the preceding 5 second of background activity". Many different spike detection techniques have been devised and used over the years with each technique having its own strengths and weaknesses. A review of some of the major tools and techniques is provided here along with the proposed Strain Jump detection algorithm. In the early fifties to seventies, hardware discriminators were used to identify and classify spikes based on peak amplitude, spike duration, or conduction velocity. Advent of computers has facilitated software algorithms that use more sophisticated and intensive techniques like spike area, template matching, contour limiting, principal component analysis or Fourier spectral analysis for effortlessly and efficiently classifying spikes in more complex scenarios (Garcia et al., 1998). These methods, however, can not adapt their classification to the progressive modification of spike shape induced by the neural tissue vibration, and require prior information about epochs and shapes. This is where the recent advances in ANN based classification system proves capable of overcoming the drawbacks. ANN is capable of parallel distributed processing with highly non-linear discriminating power and stability in noisy and complex patterns. It is accurate, flexible and can perform in real time.

Wilson and Emerson (2002) broadly classifies spike detection techniques into mimetic, linear predictive and template based methods. The mimetic techniques copy the human expert, linear predictive methods use signal processing techniques to distinguish spikes from background noise, and template based methods look for match with previously selected spikes. Many detection algorithms choose to apply multiple methods for better accuracy. Mimetic and template based spike detection algorithms may work well with the neural spike detection and classification where there is little variation in magnitude and characteristics of the spike over time. However, in the case of strain jump detection due to oilsand dumping the magnitude and duration of which can vary widely depending on many operating parameters, linear predictive methods based on signal processing techniques would be more practical. The most common detection / discriminating attributes used are magnitude, slope, height to width ratio, curvature, duration, pseudoduration etc. Detection is also influenced by the patient's level of arousal in neural signals, which is analogous to the severity of dump events. Hellman (1999) developed a set of 19 attributes to discriminate spikes from non-spikes.

4.6.2 Threshold based Spike Detection

The simplest and basic step in spike detection starts with threshold detection, where the most prominent feature is the amplitude. Its obvious advantage is minimum hardware and software requirement and the disadvantage is that acceptable isolation is not always possible. Figure 4.5 shows an example of neural spikes detected from a signal from a group of neurons. It shows how lowering of the threshold from (a) to (b) leads to poor isolation in the detected spikes (Lewicki, 1998). Along with its simplicity, the threshold approach also carries many sources of error. Firstly, in the case of neural spikes, it could lead to a bias towards the neurons generating large action potentials. In the case of dump events though, the problem of bias does not occur because each strain gauge is producing independent signals. It could be a source of error only if the impact magnitudes recorded by the gauge were smaller with small peaks, and the noise was relatively large. The peak could get lost into noise. On the other hand, if the noise amplitude rose significantly, it could cross the threshold level and give the impression of too many dump events of smaller magnitude occurring repeatedly. It is important to avoid both these errors of missing a peak or false counting them. The most ideal situation would be to balance them out together. Figure 4.6 shows how setting a threshold at point A would lead to false counting of many peaks of neuron 2 (noise) and bumping the threshold up to point B would lead to missing many of the real peaks of neuron 1 (dump event). Thus, the optimum threshold lies in between the points A and B and eventually determines the trade off between missed spikes and false positives (Lewicki, 1998).

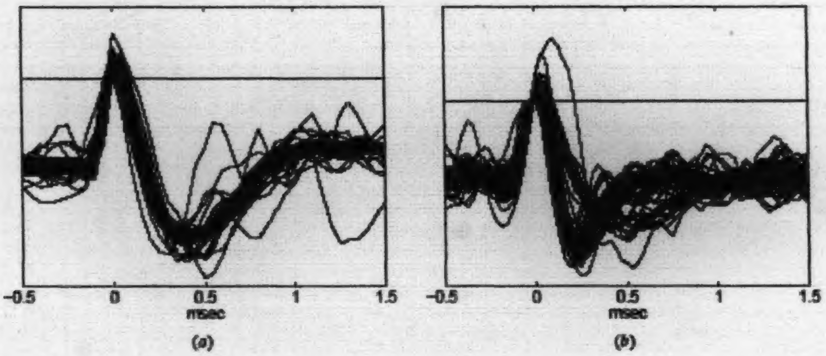

(a) (b)

Fig. 4.5 Influence of threshold level on neural spike detection (Source: Lewicki, 1998)

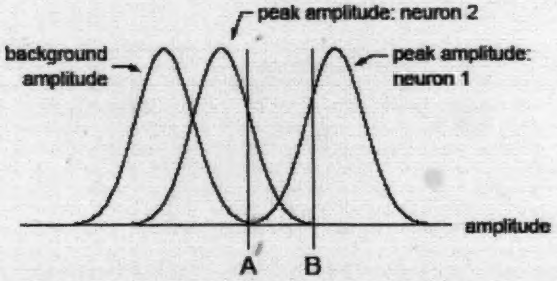

Fig. 4.6 Finding an optimum threshold level (Source: Lewicki, 1998)

There are several additional techniques which when combined with the threshold detection technique, make it more robust. For example, the spike duration or inter-spike interval histogram could serve as useful attributes for spike identification. The width to height ratio of the spikes is another criterion that lends further option. Garcia et al. (1998) used dual threshold criteria for spike detection and a five layer ANN based classification system. The absolute value of the mean of six sequential data must be over the first threshold and the absolute value of the slope of the least squares line of the six points must also be over another threshold level in order for it to be detected as a spike. The threshold levels were automatically calculated using the noise of the signal and were usually about 5 to 10% of the peak value of the signal. Further, the authors used a changing slope criterion for identification of the peak in this detection (segmentation) module. In order to avoid the influence of baseline fluctuation on spike detection and classification, all spikes were normalized after centering. In the classification module, each of the five layers had a different learning rule for classification. Detection of the spikes had lead to data reduction by more than 60 percent.

Marion-Poll and Tobin (1991) used a software filter based algorithm for detecting spikes superimposed on a fluctuating baseline. The authors used first derivative (slope) of the signal as the parameter for detection of spikes if they were larger than the threshold value. Before calculating the slope of the signal, all the high frequency content (noise) was basically filtered out such that only the fluctuating DC baseline and the spike remained. This technique will not work well in this case because of impact loading on the crusher, wherein filtering out all the high frequency content would mean losing the peak or reducing its amplitude. And filtering out partially will be of no value because it won't be possible to set a threshold slope that works. Hence, slope does not seem to be a good parameter for spike detection in short duration impulse loading, where all high frequency noise can not be filtered out.

4.6.3 Other Detection Methods

There are many other methods of varying complexities and capabilities. However, no one method stands out from the rest and the choice of a particular method mainly depends on the requirements of the project and suitability of the method in effective and efficient identification (Lewicki, 1998). Feature analysis is a technique used to classify multiple spikes simultaneously by measuring features such as shape, height, width, peak duration, or peak-to-peak amplitude. Not faced with the problem of identifying multiple spikes because each dump is independent from another and hence are never mixed up, there is no justified reason for attempting to extract too many features of the peak. Each additional feature adds an extra dimension to the detection/classification system. So, instead of having a one dimensional classification based on threshold alone, one could choose to have a two-dimensional or multi-dimensional system for better accuracy. Some authors have used principal component analysis (PCA) to choose the features automatically. The goal of PCA is to find an ordered set of orthogonal basis vectors, which is quite similar to finding the mode shapes and frequencies in Fourier analysis

(Glaser, 1971). A score is associated with each principal component and each component adds one extra dimension for classification using the Euclidean distance. Wheeler and Heetderks (1982) found that using PC as features yielded more accurate classification than other features, but less accurate than template matching. However, these methods of PCA or Fourier analysis are not much suitable in the case of the Aurora II crusher because of the fact that the mass contained in the structure is never constant and can vary by up to 1000 ton, which is significant when compared with the self weight of the structure. Hence, there will be significant variations in the components or frequencies calculated with different weight of material in the hopper, which does not lend any confidence or accuracy to the results. There are other methods like clustering that use many different clustering techniques such as nearest neighbour clustering (Hartigan, 1975). The Bayesian clustering and classification uses conditional probability concepts and performs classification with a certain probability assigned to an event being classified in each sub-category (Cheeseman and Stutz, 1988). Such clustering approaches work well in some cases, but also pose a problem in choosing the number of classes and probability distribution function. In clustering procedures, the spike templates are automatically chosen for matching (Lewicki, 1998). Some filter based methods assume that both noise power spectrum and the spike shape can be estimated accurately by the power spectrum, however, this is not very accurate, especially so when the mass is changing. Then there are the methods of independent component analysis and the artificial neural networks that are widely used.

4.7 Proposed Data Processing Algorithm

Reinforced by the findings of literature review, a multi-threshold based detection system has been proposed for detecting dump events on the Aurora II crusher. A couple of simultaneous threshold criteria have been used in line with Garcia et al. (1998) for the detection of dump events, so that the deficiencies of one threshold can be mitigated by another threshold to minimise errors. Spike amplitude, spike duration, inter-spike interval, and average noise amplitude are the parameters employed for setting optimum thresholds to ensure reliability and quality of event detection. The algorithm has been coded in Visual Basic programming language, whose brief overview is shown in Figure 4.7 and the detailed procedure in Figures 4.8 to 4.10. The program has been tested for performance in processing data collected under different operating environments and has been found to perform excellently in identifying all the genuine dump events and yet keeping it free from false dump event identification. It is able to accurately detect all types of dump events and extract a differential parameter referred to as strain jump for each gauge. Thus, continuous running of the program populates a database with strain jump recorded for each dump event at each gauge location.

4.7.1 Program Overview

As shown in Figure 4.7, the data processing algorithm begins with reading the command line arguments, verifying its syntax and creation of a database to store dump events, if necessary. If a database already exists, new events are appended into it. In addition to accuracy of the dump event identification algorithm, its efficiency is also important. With 82 data channels collecting data at 100 Hz, the importance of efficiency can not be overemphasized. However, efficiency shall not come at the cost of accuracy or quality. Since each of the 82 data channels are recording signals under the influence of the same dump at the same time (neglecting infinitesimal time lag), it can be expected that if an event can be accurately detected on one channel it should also be detected around the same time on all other channels. Hence, for the purpose of identification, six of the most sensitive channels are selected and referred to here as critical channels. After careful evaluation of all the pros and cons and the intensity of signal acquired, six gauges labelled as C10, C20, C24, C34, C36 and P52 have been selected as the critical channels. The prefix 'C' stands for gauges placed on columns and 'P' stands for gauge placed on pontoon. Detailed description of instrumentation and their location as well as the structural behaviour of the crusher has been provided in chapter 3 and Sharma et al. (2006). The selected channels not only offer better signal to noise ratio, but are also highly sensitive to dump events such that they consistently produce high peaks. The gauges have been strategically located at points of maximum stress, for example gauge

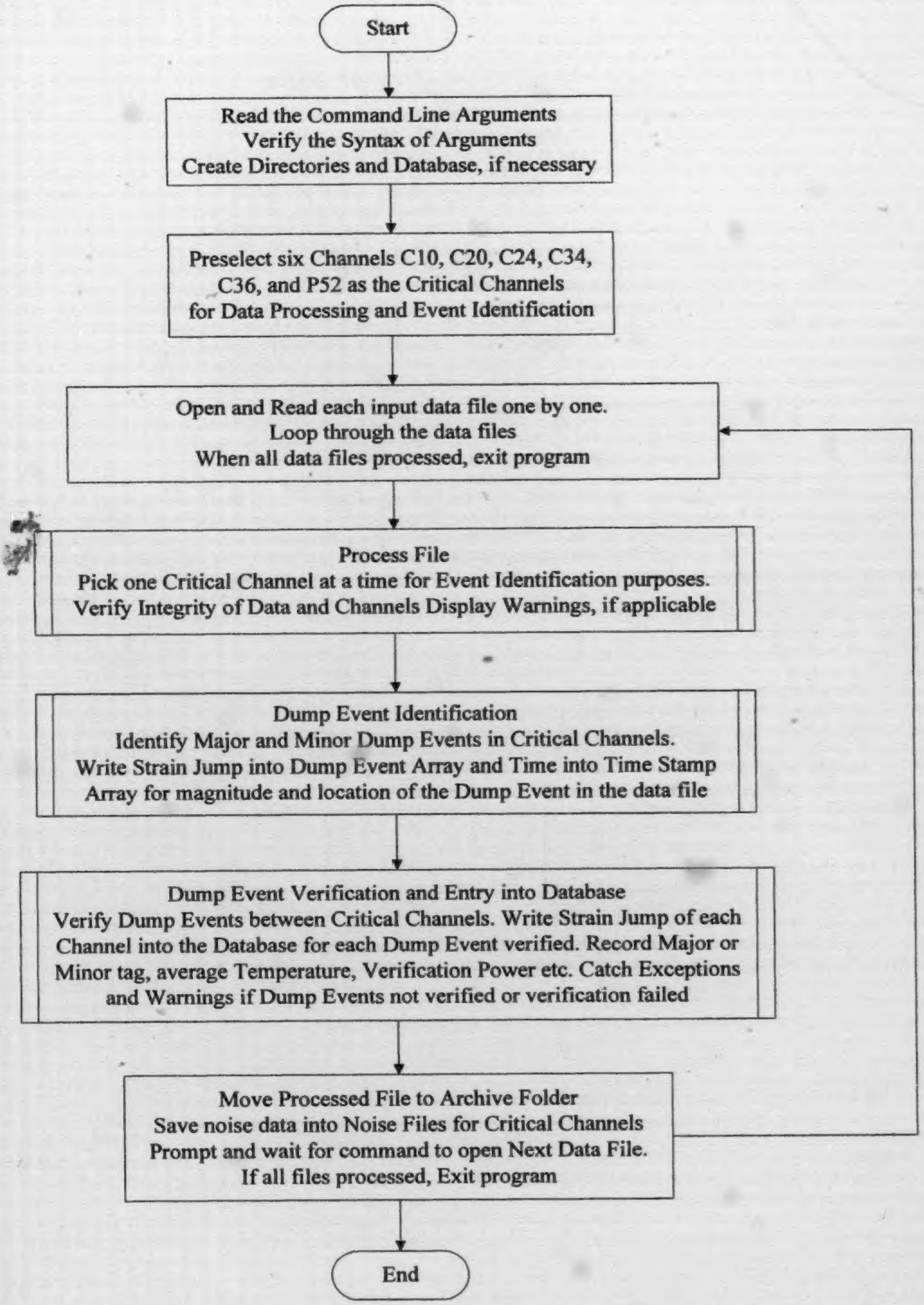
Start
Read the Command Line Arguments
Verify the Syntax of Arguments
Create Directories and Database, if necessary
Preselect six Channels C10, C20, C24, C34, C36, and P52 as the Critical Channels for Data Processing and Event Identification
Open and Read each input data file one by one.
Loop through the data files
When all data files processed, exit program
Process File
Pick one Critical Channel at a time for Event Identification purposes.
Verify Integrity of Data and Channels Display Warnings, if applicable
Dump Event Identification
Identify Major and Minor Dump Events in Critical Channels.
Write Strain Jump into Dump Event Array and Time into Time Stamp Array for magnitude and location of the Dump Event in the data file
Dump Event Verification and Entry into Database
Verify Dump Events between Critical Channels. Write Strain Jump of each Channel into the Database for each Dump Event verified. Record Major or Minor tag, average Temperature, Verification Power etc. Catch Exceptions and Warnings if Dump Events not verified or verification failed
Move Processed File to Archive Folder
Save noise data into Noise Files for Critical Channels
Prompt and wait for command to open Next Data File.
If all files processed, Exit program
End

Fig. 4.7 An overview of data processing algorithm

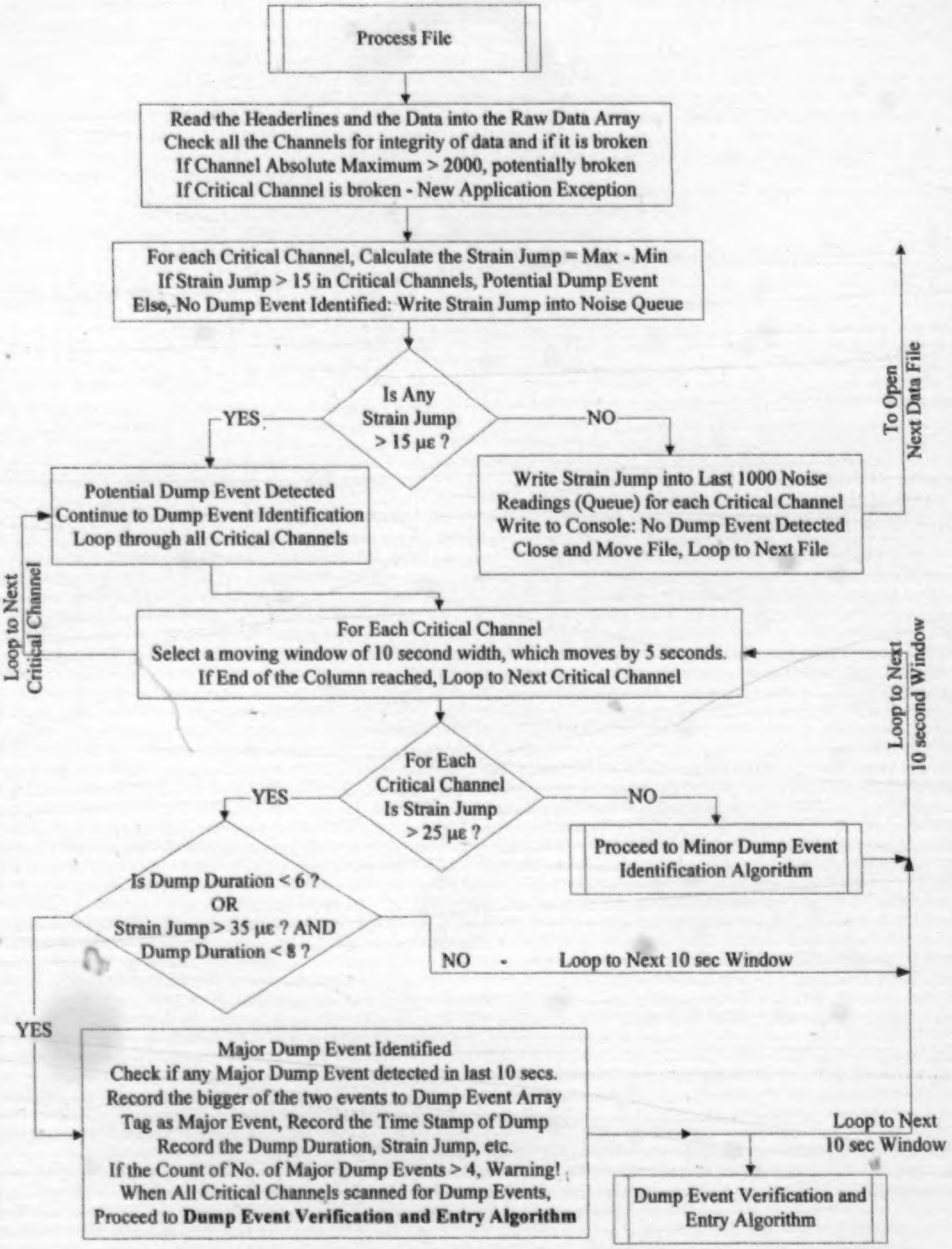
Process File
Read the Headerlines and the Data into the Raw Data Array
Check all the Channels for integrity of data and if it is broken
If Channel Absolute Maximum > 2000, potentially broken
If Critical Channel is broken - New Application Exception
For each Critical Channel, Calculate the Strain Jump = Max - Min
If Strain Jump > 15 in Critical Channels, Potential Dump Event
Else, No Dump Event Identified: Write Strain Jump into Noise Queue
Is Any Strain Jump > 15 με ?
YES
NO
Potential Dump Event Detected
Continue to Dump Event Identification
Loop through all Critical Channels
Write Strain Jump into Last 1000 Noise
Readings (Queue) for each Critical Channel
Write to Console: No Dump Event Detected
Close and Move File, Loop to Next File
To Open Next Data File
Loop to Next Critical Channel
For Each Critical Channel
Select a moving window of 10 second width, which moves by 5 seconds.
If End of the Column reached, Loop to Next Critical Channel
Loop to Next 10 second Window
For Each Critical Channel Is Strain Jump > 25 με ?
YES
NO
Proceed to Minor Dump Event Identification Algorithm
Is Dump Duration < 6 ?
OR
Strain Jump > 35 με ? AND
Dump Duration < 8 ?
NO - Loop to Next 10 sec Window
YES
Major Dump Event Identified
Check if any Major Dump Event detected in last 10 secs.
Record the bigger of the two events to Dump Event Array
Tag as Major Event, Record the Time Stamp of Dump
Record the Dump Duration, Strain Jump, etc.
If the Count of No. of Major Dump Events > 4, Warning!
When All Critical Channels scanned for Dump Events,
Proceed to Dump Event Verification and Entry Algorithm
Loop to Next 10 sec Window
Dump Event Verification and Entry Algorithm

Fig. 4.8 Flow chart for major dump event identification

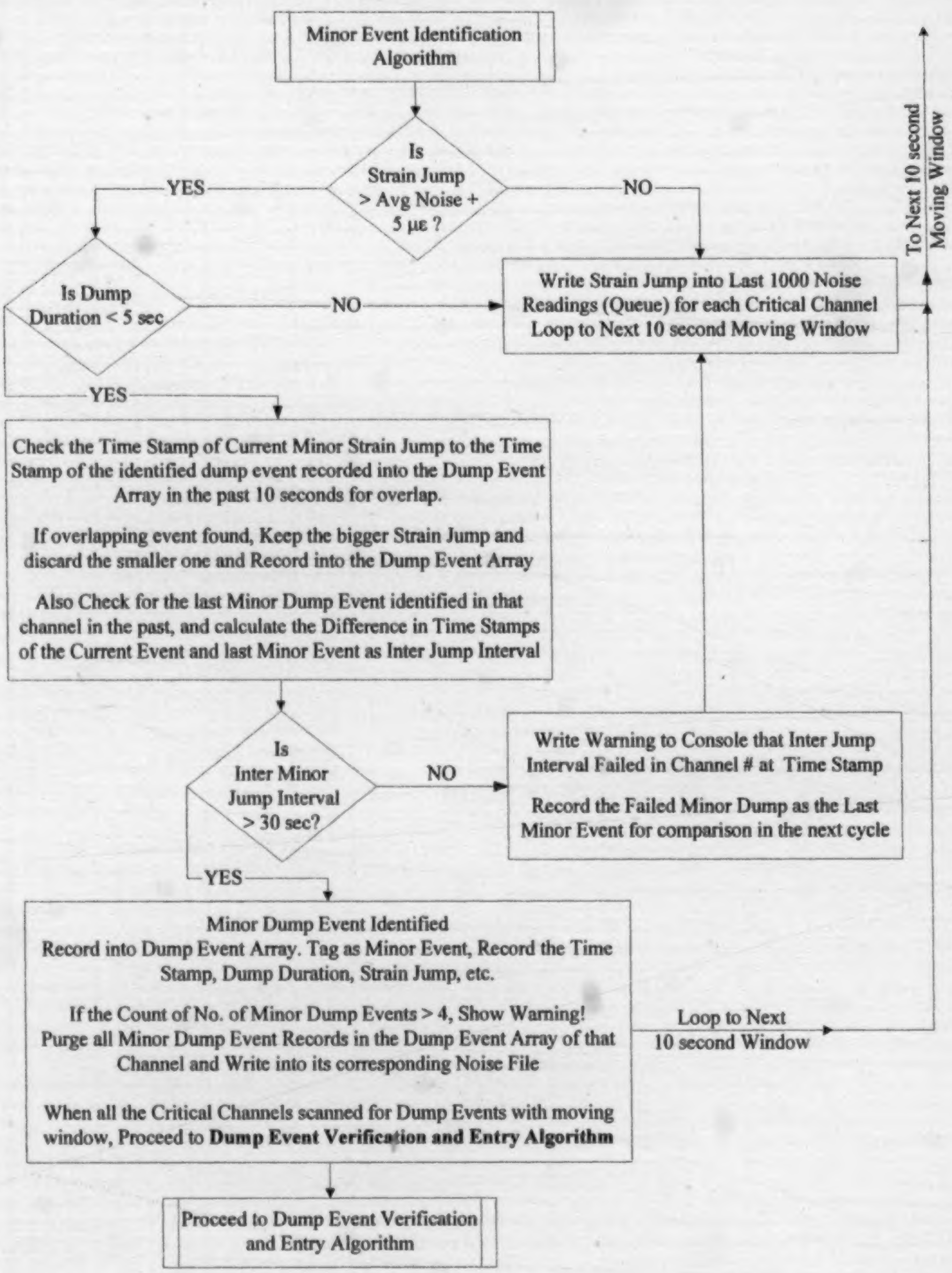
Minor Event Identification Algorithm
Is Strain Jump > Avg Noise + 5 με ?
YES
NO
Is Dump Duration < 5 sec
NO
YES
Write Strain Jump into Last 1000 Noise Readings (Queue) for each Critical Channel Loop to Next 10 second Moving Window
To Next 10 second Moving Window
Check the Time Stamp of Current Minor Strain Jump to the Time Stamp of the identified dump event recorded into the Dump Event Array in the past 10 seconds for overlap.
If overlapping event found, Keep the bigger Strain Jump and discard the smaller one and Record into the Dump Event Array
Also Check for the last Minor Dump Event identified in that channel in the past, and calculate the Difference in Time Stamps of the Current Event and last Minor Event as Inter Jump Interval
Is Inter Minor Jump Interval > 30 sec?
NO
YES
Write Warning to Console that Inter Jump Interval Failed in Channel # at Time Stamp
Record the Failed Minor Dump as the Last Minor Event for comparison in the next cycle
Minor Dump Event Identified
Record into Dump Event Array. Tag as Minor Event, Record the Time Stamp, Dump Duration, Strain Jump, etc.
If the Count of No. of Minor Dump Events > 4, Show Warning! Purge all Minor Dump Event Records in the Dump Event Array of that Channel and Write into its corresponding Noise File
When all the Critical Channels scanned for Dump Events with moving window, Proceed to Dump Event Verification and Entry Algorithm
Loop to Next 10 second Window
Proceed to Dump Event Verification and Entry Algorithm

Fig. 4.9 Flow chart for minor dump event identification

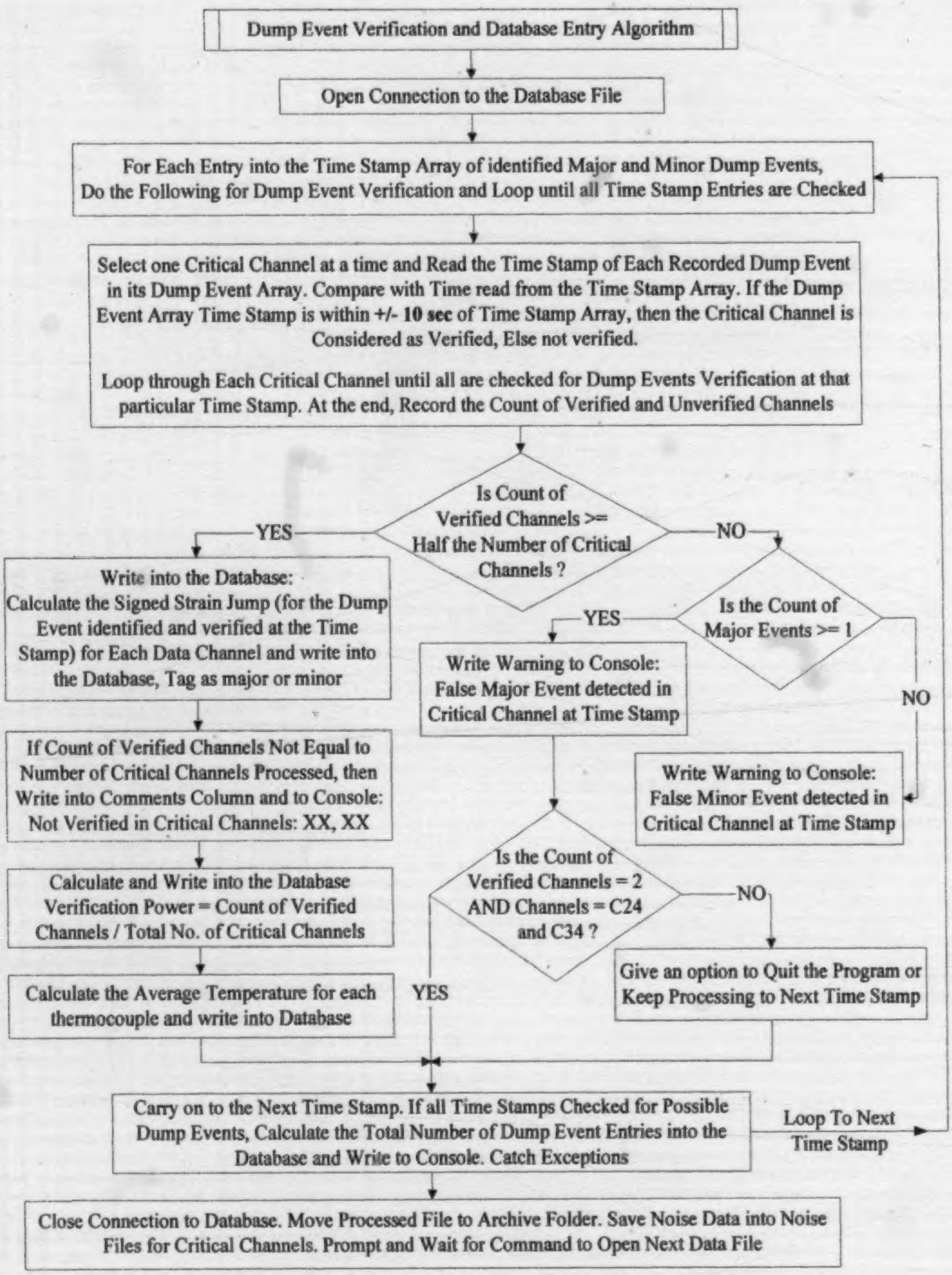
Dump Event Verification and Database Entry Algorithm
Open Connection to the Database File
For Each Entry into the Time Stamp Array of identified Major and Minor Dump Events, Do the Following for Dump Event Verification and Loop until all Time Stamp Entries are Checked
Select one Critical Channel at a time and Read the Time Stamp of Each Recorded Dump Event in its Dump Event Array. Compare with Time read from the Time Stamp Array. If the Dump Event Array Time Stamp is within +/- 10 sec of Time Stamp Array, then the Critical Channel is Considered as Verified, Else not verified.
Loop through Each Critical Channel until all are checked for Dump Events Verification at that particular Time Stamp. At the end, Record the Count of Verified and Unverified Channels
Is Count of Verified Channels >= Half the Number of Critical Channels ?
YES
NO
Write into the Database: Calculate the Signed Strain Jump (for the Dump Event identified and verified at the Time Stamp) for Each Data Channel and write into the Database, Tag as major or minor
Is the Count of Major Events >= 1
YES
NO
Write Warning to Console: False Major Event detected in Critical Channel at Time Stamp
Write Warning to Console: False Minor Event detected in Critical Channel at Time Stamp
If Count of Verified Channels Not Equal to Number of Critical Channels Processed, then Write into Comments Column and to Console: Not Verified in Critical Channels: XX, XX
Is the Count of Verified Channels = 2 AND Channels = C24 and C34 ?
NO
YES
Calculate and Write into the Database Verification Power = Count of Verified Channels / Total No. of Critical Channels
Give an option to Quit the Program or Keep Processing to Next Time Stamp
Calculate the Average Temperature for each thermocouple and write into Database
Carry on to the Next Time Stamp. If all Time Stamps Checked for Possible Dump Events, Calculate the Total Number of Dump Event Entries into the Database and Write to Console. Catch Exceptions
Loop To Next Time Stamp
Close Connection to Database. Move Processed File to Archive Folder. Save Noise Data into Noise Files for Critical Channels. Prompt and Wait for Command to Open Next Data File

Fig. 4.10 Flow chart for dump event verification and database entry

P52 is located at pontoon mid-span, where maximum bending strains occur. The five remaining gauges are located on columns at different gridlines.

Three of the five column gauges, C10, C34 and C36, are located on columns at gridline 4 and the remaining two C20 and C24 are located on gridline 6 as shown in Figures 3.11 and 3.13, where maximum influence of dump was experienced. Out of the three gauges on gridline 4, C10 is located on the right side of the line of symmetry and the other two are on the left side. Similarly, both the gauges on gridline 6 are located on the right side of line of symmetry. Thus, totally three gauges are chosen on the right side and two on the left side of the column gridlines. Such a distribution will help in capturing dump events coming from both the right and left side of the hopper. It is worth mentioning that strain gauges located on column gridline 2 were subjected to the least magnitude of strain jump, and hence, none of them feature in the list of critical gauges. Having another look at the five selected column gauges from a different angle, three of the gauges (C24, C34 and C36) are on column bracing members, whereas the other two (C10 and C20) are located on vertical column members. Thus, the selected critical gauges offer good signal to noise ratio and are widely distributed on the structure in zones of high stresses on different structural members like columns, braces and pontoon. Hence, they are truly representative of the structure in question and are balanced in terms of identifying dump events from both sides.

It has to be borne in mind though that no matter how well placed and sensitive a gauge is, it will not be equally sensitive to all types of loads. Hence, some gauges may not be able to "see" or identify some of the dump events while other critical gauges do. Figure 4.11 shows the plot of strain against time obtained at the pontoon gauges during a minor dump event. There does not seem to be any dump event happening because no peak is visible and nothing has been captured by the pontoon gauges. However, for the same minor event it can be seen in Figure 4.12 that most of the critical gauges that were selected are able to capture the dump event with clear peaks visible. Hence, the point that not all gauges are equally sensitive to all dump events is driven home. On the contrary, for another dump event a major one this time, many of the pontoon gauges as well as all of the selected critical gauges are able to detect the dump event clearly with large peaks as shown in Figures 4.13 and 4.14. This is a very natural phenomenon and expected due to the size and complexity of the structure. So, the six critical gauges work in a group and they need to verify each other in order for a dump event to be declared as identified. The gauges are located strategically such that at least 3 of the 6 gauges must see a dump event. Thus a verification power of at least 50% is mandatory. On most occasions though, the verification power is close to 100% meaning the dump event has been identified on all the six gauges. For example, in Figure 4.15 three dump events have been detected and are shown. For two of the dump events all of the gauges detect the event with a verification power of 100%. However, for one of the dump events shown in the middle and circled for identification, one gauge is not able to verify the dump event but the event still passes verification because all other gauges verify it. In the next example shown in Figure 4.16, two channels are not able to detect and verify a dump event, but the event is still rightly passed as verified. On the other hand, one false minor event that is detected by only one channel probably due to noise and not detected in any of the other channels is rejected as unverified and not written into the database. The average verification power obtained for more than 1300 identified dump events was around 80%, which draws sufficient confidence in the event detection algorithm. When the verification power is less than 50% for any potential event, then the program will throw a warning message that will be displayed on the screen console and the event in question will not be written into the database, simply ignored.

Once the set of critical channels are selected, each of the data files is read one by one and processed for data integrity and dump event identification. Warning is issued for any gauge that is behaving in a strange way. During processing, events are tagged as major or minor events depending on the magnitude of strain jump. Separate algorithms exist for identifying major and minor events as shown in Figures 4.8 and 4.9, the details of which are discussed subsequently. The events, major or minor, identified in each critical channel are passed through a verification algorithm shown in Figure 4.10. Only those events that satisfy the verification criteria are finally declared as dump events and recorded into the database. At this time, strain jump for each of the sixty strain channels are calculated and recorded into the database for every identified dump event. The processed file is finally moved into an archive folder or deleted; and the noise data encountered during processing of the file is saved in a noise queue of 1000 most recent noise data for each critical channel. Thereafter, next data file is read for processing even if no dump event was identified or verified in the file just processed. Once all the data files have been processed, the program exits. Figure 4.7 shows an overview of all these steps involved in the data processing and management algorithm. As a backup for other types of analyses, one complete data file of 5 minute duration can be permanently stored in addition to the database of dump events for each day of operation of the crusher.

4.7.2 Data Processing Algorithm for Event Identification

The processing of strain data begins with reading of the raw data and verification of its integrity at all gauges as shown in Figure 4.8. Any gauge with irrational gauge reading is accordingly reported as broken. The event identification algorithm from here on focuses only on the data in the six critical channels. This lends efficiency and a degree of predictable reliability to the algorithm. Multiple layers and varieties of thresholds have been employed for detection quality assurance, which are discussed in this section in detail. In the first layer of the detection, the algorithm takes a broad look at the data and judges if there are any possible dump events in any of the critical channels being processed. If there are none present, then there is no point in carrying further processing. The first threshold used for this purpose is 15 $\mu\varepsilon$ of strain jump magnitude. Strain jump in each critical channel is calculated for the whole data file of 300 second long window, that is the maximum and minimum in the entire file and its absolute magnitude is compared to this threshold. Looking at the whole file at once is able to save some computing time if it does not contain any dump event, so that there is no need to perform more rigorous analysis on it. A single threshold can never be able to deliver clear detection / classification for data collected in complex scenarios with many unknowns and noise. Too low a threshold will detect too many events whereas too high a threshold will fail to detect some genuine events. The solution is to use multiple thresholds with increasing degree of sophistication and increasingly stringent measures. So, the first threshold is the easiest to satisfy with possibility of many false peaks getting detected, but not leaving out any genuine dump event. The first threshold of 15 με is one such limit. It is able to provide acceptable isolation from non-events or noise, because the noise magnitude is almost always lower than 10 με value whereas the strain jump during a dump event could go into hundreds of micro-strains. Upon failing this threshold, the strain jump calculated for each critical channel is simply written into a noise queue for the channel that keeps the most recent 1000 noise readings. The purpose for keeping this noise data will be clarified shortly. After writing into noise queue, the file is closed and archived and the next data file is opened for a new analysis to begin.

If the first threshold is cleared by the data, then the algorithm moves on to next level of more rigorous scanning of the data file to look for more than one dump event in a file and also their exact times of occurrence. This is achieved by reading the data for each critical channel in a moving window of 10-second duration, for reasons already discussed. The strain jump magnitude is calculated for each moving window of 10-second duration. The centre of the moving window, however, moves by 5 seconds, thereby creating an overlap of 5 seconds between two subsequent windows. So, in effect the data file is being scanned at the centre of the 10-second windows every 5 seconds. This helps maintain a smaller window size of 5 seconds for better resolution in locating dump events; and at the same time avoids errors due to discontinuous boundaries that are at distances of 5 sec in each direction from the centre. A dump event falling at the boundary of one window may be missed by it, but the same dump event will be at the centre of the next window, and hence, will not be erroneously missed. The strain jump magnitude obtained from each window is compared against the second threshold value of strain jump magnitude, which is higher than the first threshold and has been set at 25 με for now. The strain-jumps exceeding the threshold are considered as potential major events and subjected to a series of other thresholds, whereas those falling below it are regarded as possible minor events and are processed using an algorithm developed for processing such boundary line minor events that is described in the next section.

The events passing the second threshold and labelled as possible major events are subjected to more checks to eliminate chances of certain errors. This time, in addition to the amplitude thresholds, dump duration is also used as a criterion for vetting a strain jump as a major event. Dump duration is defined here as the difference between the time stamp at the instant of maximum value of strain and that at the minimum value of strain within each ten-second window. Even though sometimes a haul truck may take much longer to empty its contents, technically the dump event would be occurring at the moment the largest chunk of material hits the hopper because the small droppings or static load produce little increase in strain. The spikes due to impact are occurring mostly within a small window of 2 to 3 seconds. Hence, the third threshold for a potential major event is set at dump duration of 6 seconds, which is well clear of the usually occurring durations and is able to accommodate slow dumps and double dumps with some time lag. In case the dump duration happens to be less than 6 seconds, with strain jump magnitude of greater than 25 $\mu\varepsilon$, then the event is classified as a major dump event and the processing continues to next 10 second window of the same channel. Once all the dump events in the channel are identified, then the same procedure is repeated for the other critical channels, thereby identifying another set of dump events (major or minor) for each critical channel, which are then taken to the verification algorithm before being entered into the database.

However, if the event under consideration fails the criterion of 6 seconds duration of dump, then the event is given one more chance to prove itself before being thrown out as a non-event and continue processing for the next 10-second window. This time around, a composite threshold of dump duration of 8 seconds and strain jump magnitude of 35 micro-strains is used as shown in the flowchart of Figure 4.8. The main reason behind using these series of thresholds aimed at dump duration and strain jump is due to the fact that sometimes continuously rising or falling arm of a strain reading may be steep enough to have a differential strain jump of more than 25 $\mu\varepsilon$ in a 10-second window without having any dump event as shown in Figure 4.18, where the steeply rising strain in gauge C24 is falsely detected as a dump event. However, usually the dump duration in such cases will be much larger because the maximum and minimum in these cases occur at the extremities of the ten-second window, whereas a real dump event should have much narrower dump duration. The earlier threshold of 6 seconds of dump duration should have been able to close this episode, however due to complex operating conditions, sometimes a double dump leads to the maximum and minimum values occurring much farther apart as shown in Figure 4.18 for an elongated event that would be wrongly rejected. This leads to a longer dump duration being calculated that is in violation of the 6 second duration requirement, so gets rejected as a non-event. In order to safeguard against such wrong rejections, this composite threshold has been devised. Basically it gives the event a little bit of leverage in terms of dump duration by rising the allowable dump duration to 8 seconds, but at the same time, it also raises the bar for requirement of magnitude of strain jump from 25 to 35 micro-strains. Thus, if an event is able to satisfy both these thresholds simultaneously, it is quite justified to accept it as a major event for the time being.

Having a false major event detected or a real major event rejected are the two situations that should be avoided at all costs. Hence, the last check is introduced for the events that fail the composite threshold criterion mentioned above. These are targeted specifically at small events that occur on a steeply rising or falling arm of another event that had occurred immediately before it. What it does is it breaks the ten-second window into two equal parts of 5 seconds each and evaluates and compares the strain jump in each of these 5-second windows. If the ratio of the smaller strain jump to the bigger strain jump calculated in the two 5-second windows is less than 0.5, then it is an indication that one of the windows is seeing a sharp rise/fall in strain compared to the other window. Such sharp change in strain is indicative of occurrence of a dump event, and hence, the event is passed on as a major event. On the other hand, if the ratio of the two strain jumps in the 5-second windows were bigger than 0.5, it would mean that the strain jumps encountered in the two divided windows were quite close to each other. Such a situation is expected in the case of a continuously rising/falling arm of strain with a steep slope, where both the 5-second parts of the 10-second window experience almost the same strain change. These events are rejected as non-events and the processing is moved on to the next 10 second window. With the help of this check, both the errors shown in Figures 4.17 and 4.18 are automatically eliminated that would have otherwise occurred. Once all the dump events in each of the critical channels have been identified, they are stored into the dump event array with their time stamps in another time stamps array, which is used for event verification and database entry module later, as shown in Figure 4.10.

Now with a list of events tagged as major (or minor) and stored in a dump event array for each critical channel, it is time to look at the list of events and assess if what has been stored makes sense. Incorporating such assessments at each level of processing reduces the chances of error and imparts robustness to the program. As was discussed earlier that the data is processed in 10 second windows that move every five seconds, hence, there is always an overlap of 5 seconds between each consecutive window. So, there is always a chance that the same dump event can be seen by two consecutive windows, where one of them has a better view than the other. The window which gets full view of the dump event in its centre is able to capture the whole event and consequently, records a higher strain jump magnitude. On the other hand, the window getting a partial view of the event close to its boundaries records a partial dump event with relatively smaller strain jump magnitude. It may so happen that both of them get detected as major events, but in reality they are the same event because two events can not occur that quickly within 10 seconds. In worst cases, three consecutive windows are able to see the same event. Hence, this check is designed to look for overlapping dump events. Before entering an event into the array of dump events for a particular channel, the time stamp of the current potential event is matched with the time stamp of the events already recorded into the array before this. If the difference in the time stamps of any two events is less than or equal to 10 seconds, then the event with the larger magnitude of strain jump is stored and the one with smaller magnitude is purged out of the dump event array. Thus, the conflict of view between adjacent windows is taken care of and all the identified dump events are stored in an array of dump events for each critical channel along with their characteristics like strain jump magnitude, dump duration, major or minor tag, time stamp of the event, etc. Before closing and moving on to the dump event verification algorithm, the number of dump events in the array is counted and if the count exceeds five, then a warning is issued. By the experience of practical operating conditions, it is not possible or expected to have more than five dump events within a data file with five minutes of operation. After each dump event the dump truck needs to move away from the hopper and then another truck needs to back up to the hopper in its place to dump another load of oil sand. This moving out and backing up procedure requires a minute or two to complete each time. So, possibility of more than 5 dump events occurring in one data file is simply precluded.

4.7.3 Minor Event Identification Algorithm

The boundary line events detected in the 10 second moving windows for each critical channel, which pass the first threshold of 15 με but fail the second threshold of 25 με magnitude of strain jump, are processed further by the minor event detection algorithm shown in Figure 4.9. These events could be possible dump events of smaller magnitude, but at the same time, they also have the possibility of being due to larger noise amplitude. So, the goal here is to separate the grey area events from noise with reasonable level of confidence. Accordingly, appropriate thresholds have been selected to fulfill this goal. Possible drifts or changes in noise amplitudes are taken care of by setting a threshold of average value of past noise jump amplitudes for that critical channel plus 5 με. Gotman and Gloor (1976) describe background noise as the average amplitude of half-waves from the 5 second preceding the spike. This threshold ensures reliable event detection even with changing noise conditions. The 5 με margin used beyond the average noise jump amplitude makes sure that the peak noise condition has also been taken care of; hence, they are not falsely detected as minor events in the database. Figure 4.19 shows the strain signal in the vicinity of a dump event with noise greater than 18 Hz frequency range filtered out. The figure shows that the strain signal appears to be more stable with a clear peak strain amplitude and stationary static strain before and after the dump event. Figure 4.20 shows the noise that has been filtered out from Figure 4.19. The amplitude of worst case noise at some gauge locations varies from -5 to +5 micro-strains. Thus, the assumption of a 15 micro-strain as the first threshold was based on this clear amplitude of noise data.

Potential minor events that satisfied the threshold of noise magnitude were next subjected to the threshold of dump duration. As explained in the section on detection of major events, the normally expected dump duration is about 2 seconds; so threshold duration of 5 seconds is used for minor events. Obviously the algorithm is more stringent on the minor events than the major events that were allowed durations of 6 to 8 seconds under certain circumstances. However, those were events with much larger magnitudes of strain-jump, hence, it was necessary to allow leverage for other checks to be performed. But at this time, for the potential minor events, the magnitude of strain jump is much smaller and many tests have already been performed on the data, so it is not necessary to give too much room for variation in dump duration. Any potential event that fails this test is written into the noise queue data for the channel being processed. The events that pass this test are subjected to a couple of other simple tests, which are quite similar to those for the major events. The potential event is checked for any overlapping window in the past 10 seconds and the larger of the two is kept. The reason behind this test is the overlap of 5 seconds between two consecutive search windows, which has already been explained. Now, at this moment, an array of dump events identified in the critical channel and the array of its time stamps are available for further verification.

As the last line of defence against false counting of noise as events, time or inter-spike interval is used as a parameter to validate low magnitude strain jump as a minor event. From the knowledge of operation of the crusher and the structure there is a limit on how often a dump event can occur. Based on the assumed operation of the crusher at 70% of rated capacity, more than 500 single truck dumps are calculated everyday. This means the interval between two single dumps on an average should be close to 3 minutes. Add to this the fact that at many times the trucks are dumping together from both sides making it a double dump. This fact is further verified by video recordings taken during normal operation. A few minutes of time is taken in moving a truck that has finished dumping and arrival of a new truck for dumping. Hence, even normal operational constraints point towards more than one or two minutes of interval between dumps. This naturally makes it quite clear that for the 100% rated throughput capacity of the crusher to be achieved every component has to operate perfectly including the dump trucks. Even under the fastest of operating conditions, two events can not occur within one minute, most probably not even within 2 minutes. In a rather conservative way, a count of 5 windows or 30 seconds (25+5 sec) has been used as the threshold for inter spike interval between two minor events. It should be noted that minor events are mostly occurring in close to full hopper conditions, which is much slower and takes longer for all material to slide into the hopper. Hence, if the time stamp of a potential minor dump event happens to be within 30 seconds of any minor event already identified and saved in the dump event array, then the current potential minor event is rejected and its strain jump magnitude is written into the noise queue for the channel being processed. The flow chart for the algorithm is shown in Figure 4.9.

Any possible minor dump event must satisfy all these threshold criteria to emerge above noise, which has the potential to strike a balance between missed and false counted events. Considering for a moment that such margins of errors do exist, even then, with the low strain magnitudes involved, the cumulative influence of such few errors on remaining life prediction of the structure would remain negligible. Application of the software to the set of data with known dump events proved that all the minor and major events were successfully detected by the algorithm.

4.7.4 Event Verification and Database Entry

During the process of dump event verification, the time stamp of each dump event is compared across all the critical gauges and if a matching time stamp within a margin of 10 second duration is found in each of the critical channels, then the event is considered as verified in all the channels with a verification power of 100%. The 10 second margin is allowed due to the possibility of a dump event getting identified by two consecutive search windows. Failure to find a matching time stamp in the list of dump events identified in a particular critical channel leads to that channel being branded as not verified. If the number of unverified channels is more than half the size of critical channels (half of 6) for the event under consideration, then the event is not written into the database and a warning is issued to check the critical channels that have wrongly identified them as events. Upon manual verification, the event can be discarded and the algorithm adjusted to take into account such special situations in the future. Another potential dump event at another time stamp is taken up for verification thereafter and the same procedure is adopted. Flow chart in Figure 4.10 illustrates this procedure and Figures 4.11 to 4.18 show examples of dump events not verified at some of the channels and verified at most other gauges as well as some instances of false verification due to noise. For the dump events that are verified in more than 50% of critical channels, their time stamp and verification power are recorded into the database of events. Now, at that particular time stamp where a dump event has been identified and verified in the critical channels, strain jump is calculated for all the sixty strain channels and recorded into the database under appropriate columns. But this time around, the event detection algorithm does not need to run on each of the sixty channels, rather going directly to the time stamp of the window in which the dump event was verified and simply calculating the strain jump efficiently for each strain channel. One difference while calculating strain jump in all the sixty channels this time is that the strain jump is calculated in a processing window of 20 seconds duration instead of the earlier 10 sec window to take care of dump events occurring at the boundaries of the window. The boundaries of the 10 second window are widened at each end by 5 second, which eliminates errors due to discontinuous boundary at the events. There was no need to do this earlier during event identification because the focus then was to refine the search to be able to pin-point the exact time of occurrence of a dump event. Once an event has been identified and verified, then the exact magnitude of strain jump at each gauge location along with its appropriate sign is required, that is, whether it is compressive or tensile.

In addition to the strain jump magnitudes at each of the sixty strain gauges, the time stamp of the dump event, duration of dump, major or minor tag, average temperature at the time of the dump event, verification power for the dump event, and a comments column are also recorded into the database. Thus, each dump event is recorded as a new entry into the database, with time stamp of the dump event as its unique identification. The comments column clarifies about the channels unable to verify a particular dump event with verification power less than 1 but higher than 0.5, although majority of the channels did verify it and that is why the dump event was recorded into the database. An error checking mechanism also exists in the verification algorithm for those events that fail to meet the requirements of verification power being between 0.5 and 1. If those failed events happen to be minor events, then a simple warning is issued regarding the minor event that failed the verification test and the verification process proceeds to the dump event at next time stamp. However, if those events happen to be tagged as major events, then it is further checked if those events were identified by the critical channel gauges placed on bracing members. Due to their slenderness or noise effects, sometimes the bracing member gauges are over-sensitive and produce false events. If the falsely identifying gauges indeed happen to be the bracing member gauges C24 and C34, then a warning is issued again and processing continues. However, if the false verification was due to any other critical channel that are not over-sensitive like the pontoon gauges or vertical column gauges, which are generally very stable, then it could be sign of some trouble or a broken gauge. At this point of time, an option is provided to quit processing and manual intervention is required.

Once all the potential dump events found in the data file are passed through the verification algorithm (successfully or unsuccessfully), the total number of dump events actually verified in the file and recorded into the database is reported on the console and the data file is closed and moved to archive folder. The noise queue files are also saved for each of the critical channels and then a new data file is opened for processing. If repeated warnings are observed for a particular channel, it could be a sign that the gauge has broken down and due attention needs to be given to warnings until one is sure about the nature and reason of them. Over the years, in case some of the critical channels get broken, they will need to be replaced by suitable replacement channels. Thus, the event identification and data processing algorithm is able to successfully identify dump events, major or minor, verify them against a select group of critical channels, and record the events into a database of dump events. In the process, the size of data is immensely reduced by thousands of times, without losing any value in the vicinity of the dump.

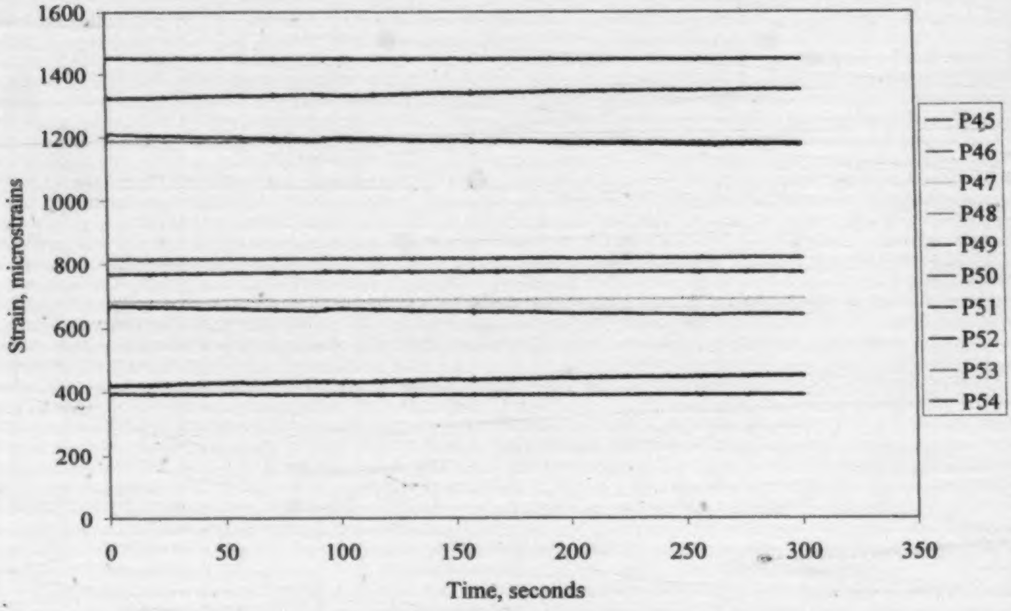

Fig. 4.11 Strain vs. time plot for the Pontoon gauges – a minor dump

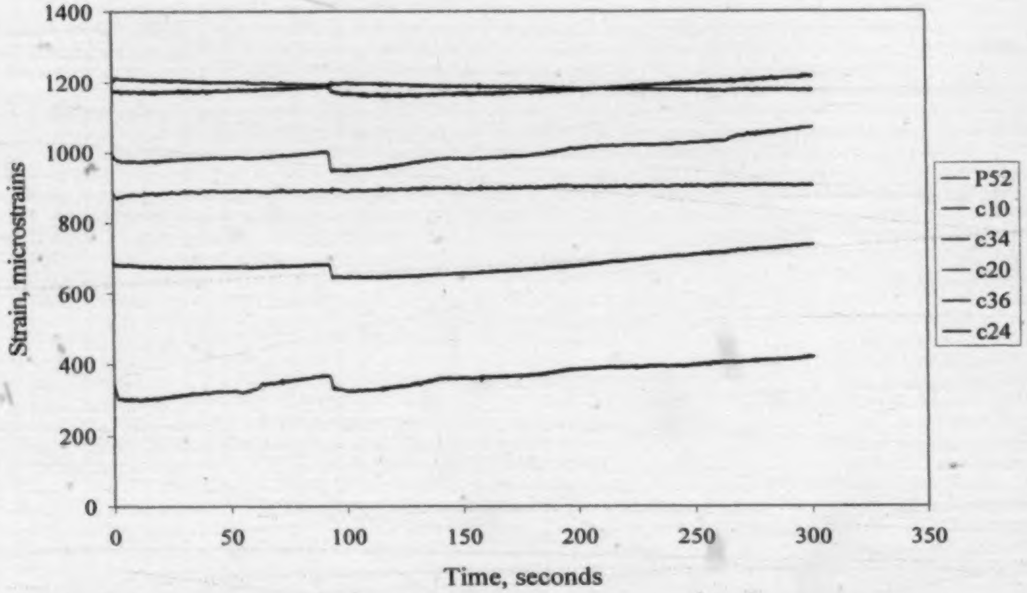

Fig. 4.12 Strain vs. time plot for the selected critical gauges – a minor dump

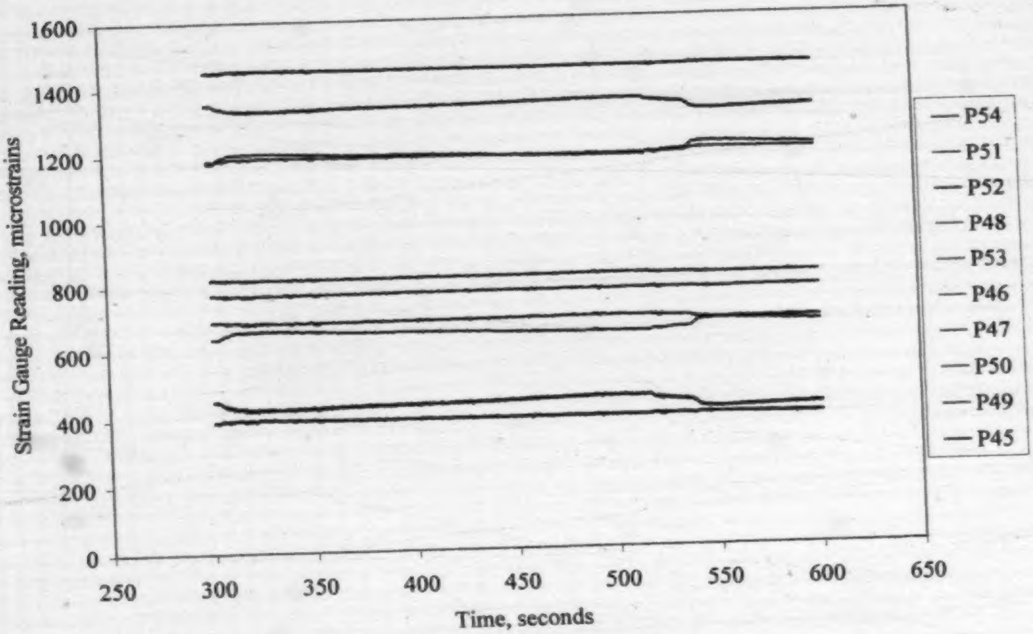

Fig. 4.13 Strain vs. time plot for the pontoon gauges – a major dump

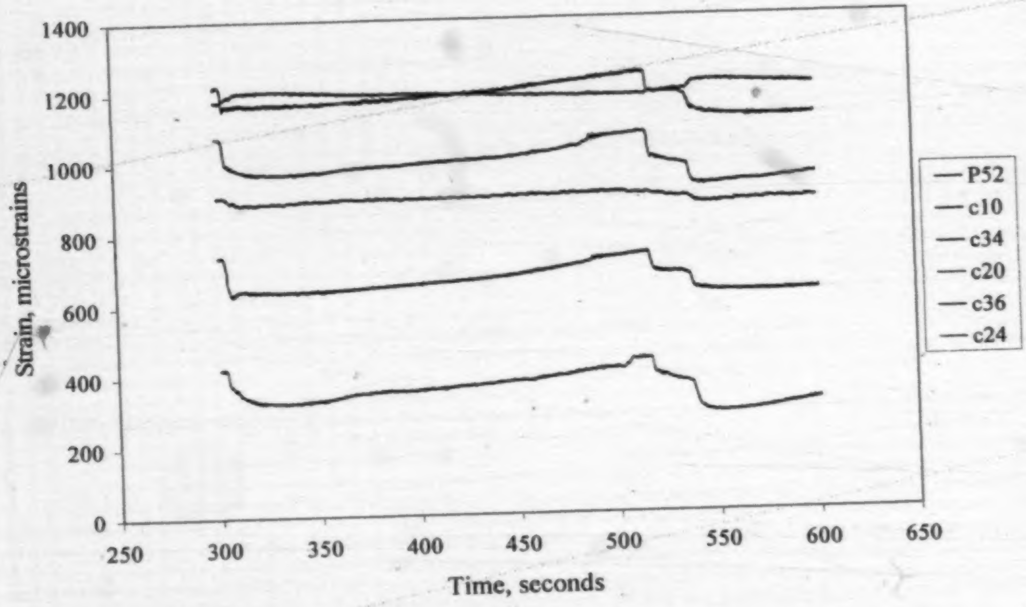

Fig. 4.14 Strain vs time plot for the selected critical gauges – a major dump

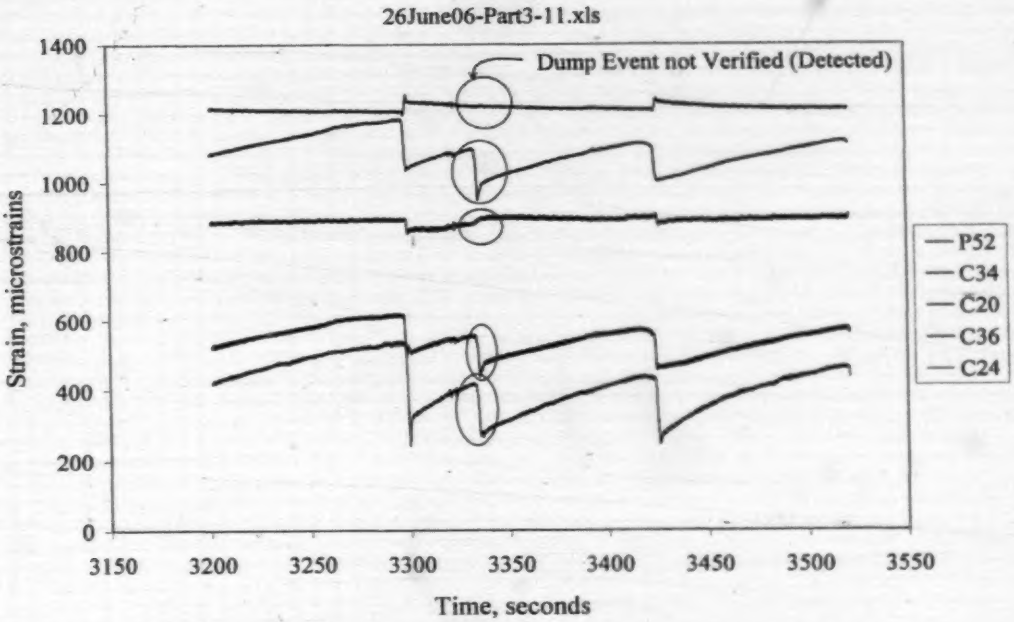

Fig. 4.15 Example of dump event not verified in one channel

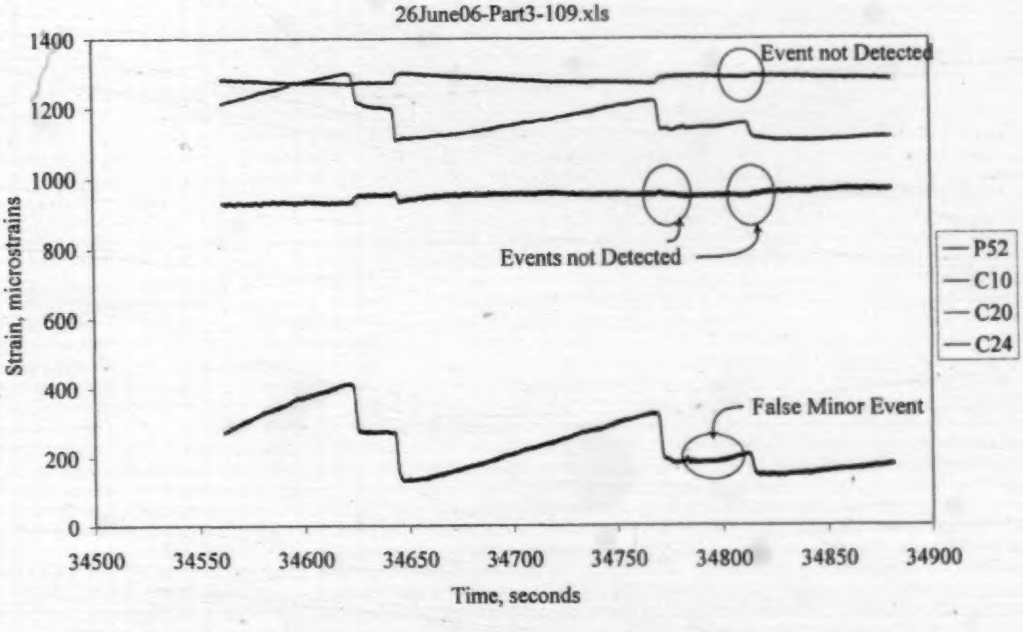

Fig. 4.16 Example of dump event not verified in more than one channels

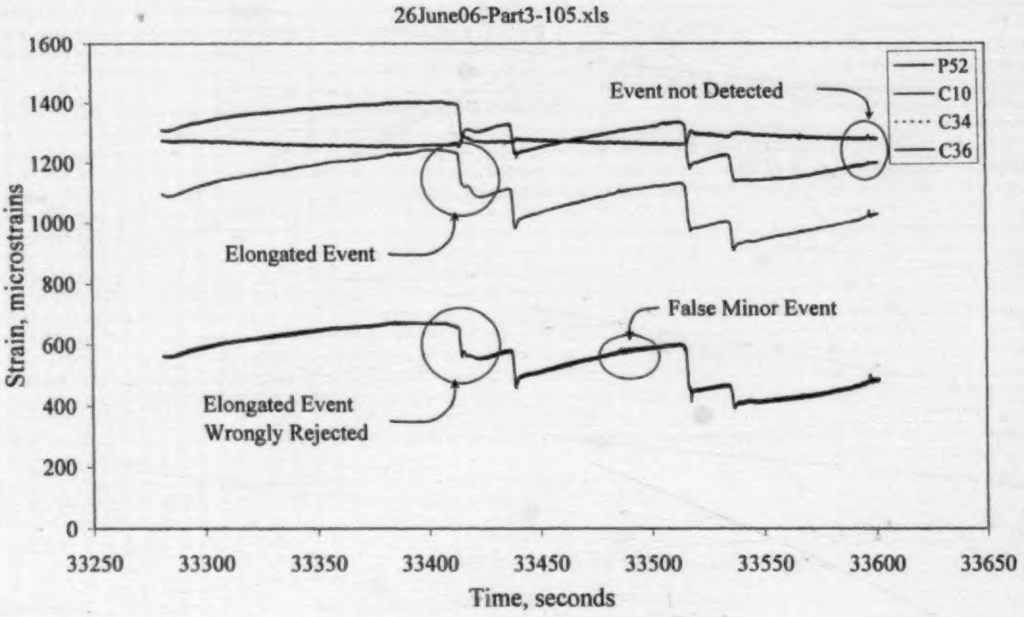

Fig. 4.17 Wrong rejection of a dump event

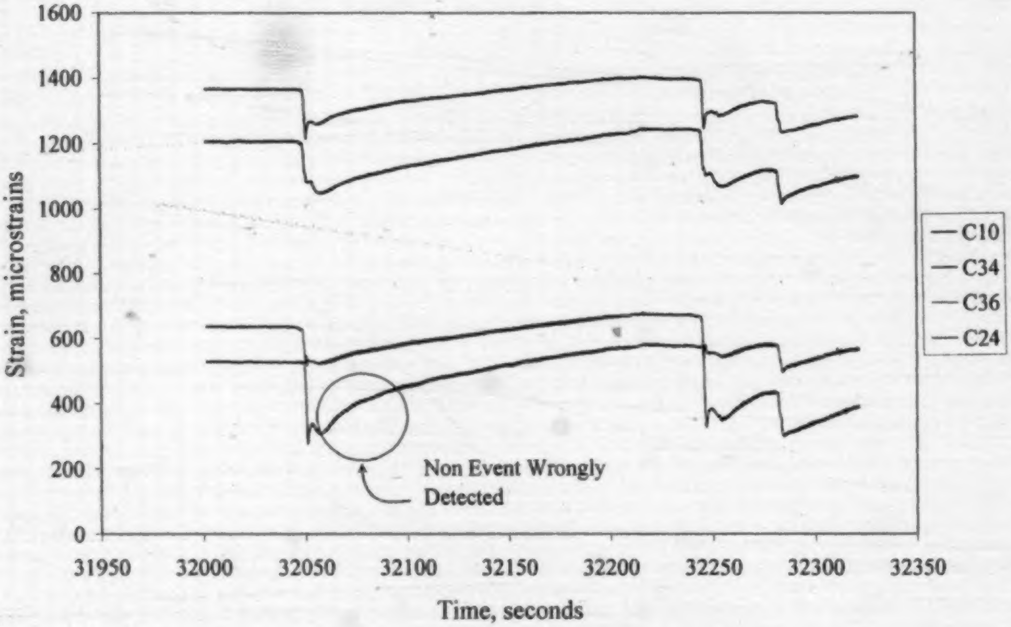

Fig. 4.18 Wrong detection of a dump event

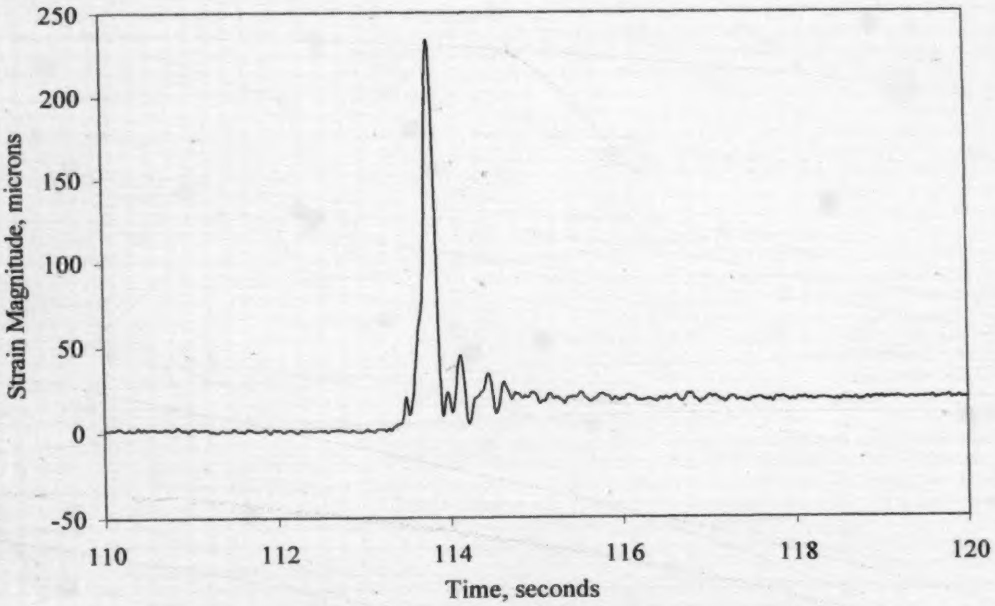

Fig. 4.19 Strain jump with noise greater than18 Hz filtered out

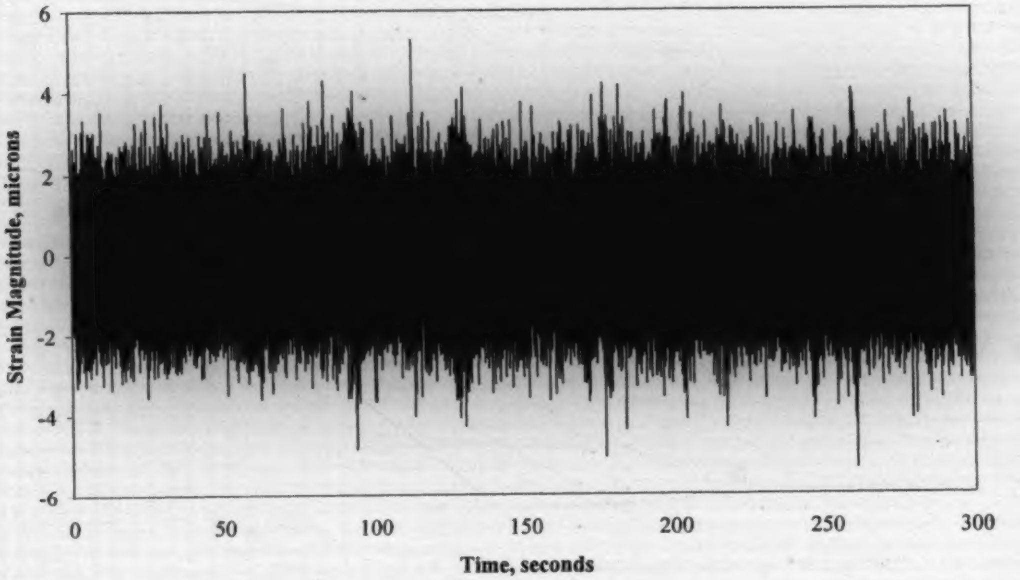

Fig. 4.20 Filtered out noise greater than 18 Hz frequency

4.8 Class Diagram

The job required to be done and the results desired by a user needs to be communicated to the programmer and vice versa. Much work has been done in standardizing the language of communication in the computer programming industry, of course not without their share of confusion created by everyone communicating in the way developed by themselves. Programmers worldwide got together to accept a Unified Modelling Language, popularly known as UML. Fowler and Scott (2000) aptly present it as "Natural language is too imprecise and gets tangled when it comes to more complex concepts. Code is precise but too detailed. UML has certain amount of precision without getting lost into details". Thus, UML is concise with just the right amount of details and is able to communicate clearly and quickly. Good communication and understanding of the user's world is the key to developing good software. There are many different types of diagrams available in the UML to present what a programmer intends to do as clearly as possible. Some of them are: Class Diagrams, Use Case Diagrams, Activity Diagrams, Interaction Diagrams and State Diagrams etc. UML is so powerful and diverse that sometimes even the standardized modelling language becomes too complex and rigid. It is not necessary to use each and every diagram or tool that is available with UML for every project; one can choose what suits one best. Still there are times when the official notations of UML could get into the way of a user's needs, in such scenario, Fowler and Scott suggest bending the language a little bit here and there is not taken as a taboo, as long as they don't cause any communication problems.

A Use Case Diagram gives a snap shot of one aspect of the software. So, the complete software would have a collection of Use Cases to communicate the user's needs. A Class Diagram is a concept in the user's mind and an Activity Diagram is useful where work flow processes are important. An Activity Diagram probes deeper than the Class Diagram. For a large software system, a package diagram is used, then for each package, a separate Class Diagram is presented. An Interaction Diagram is used for key interactions in the package or between different classes. It is important to understand here about all theses tools that UML is a communicating language not a method. The flow charts presented in the previous section are close to what the UML refers to as Activity Diagram, however, in a very simple manner without going into much complexities of the language. These flow charts or activity diagrams present the working details of the software planned for the desired output / goal of extracting useful information with reduced data size. Now in this section, an effort is made to present the conceptual frame work of implementation of the software through class diagrams and their interaction. Class diagrams are central to object oriented methods and widely used with great range of modelling concepts (Fowler and Scott, 2000).

Class diagrams are used at three levels of perspectives as per the authors, which are: conceptual, specification and implementation levels. They mainly present two types of static relationships, namely: associations and subtypes. A class diagram consists of attributes, operations and methods, along with some constraints applied. Generalization and association are the lines or arrows showing the relationship existing between various classes. There are advanced concepts like aggregation, composition and association class available for advanced users. These are so rich that it can be overwhelming to use, hence, it is not necessary to use all the notations available. Moreover, it is not necessary to show every feature of each class, only the most important ones can be shown and the rest hidden. Compact presentation of class diagrams lends much more clarity to it. Figure 4.13 below presents the conceptual level of various classes adopted in the programming of the Dump Event Filter for data processing and management.

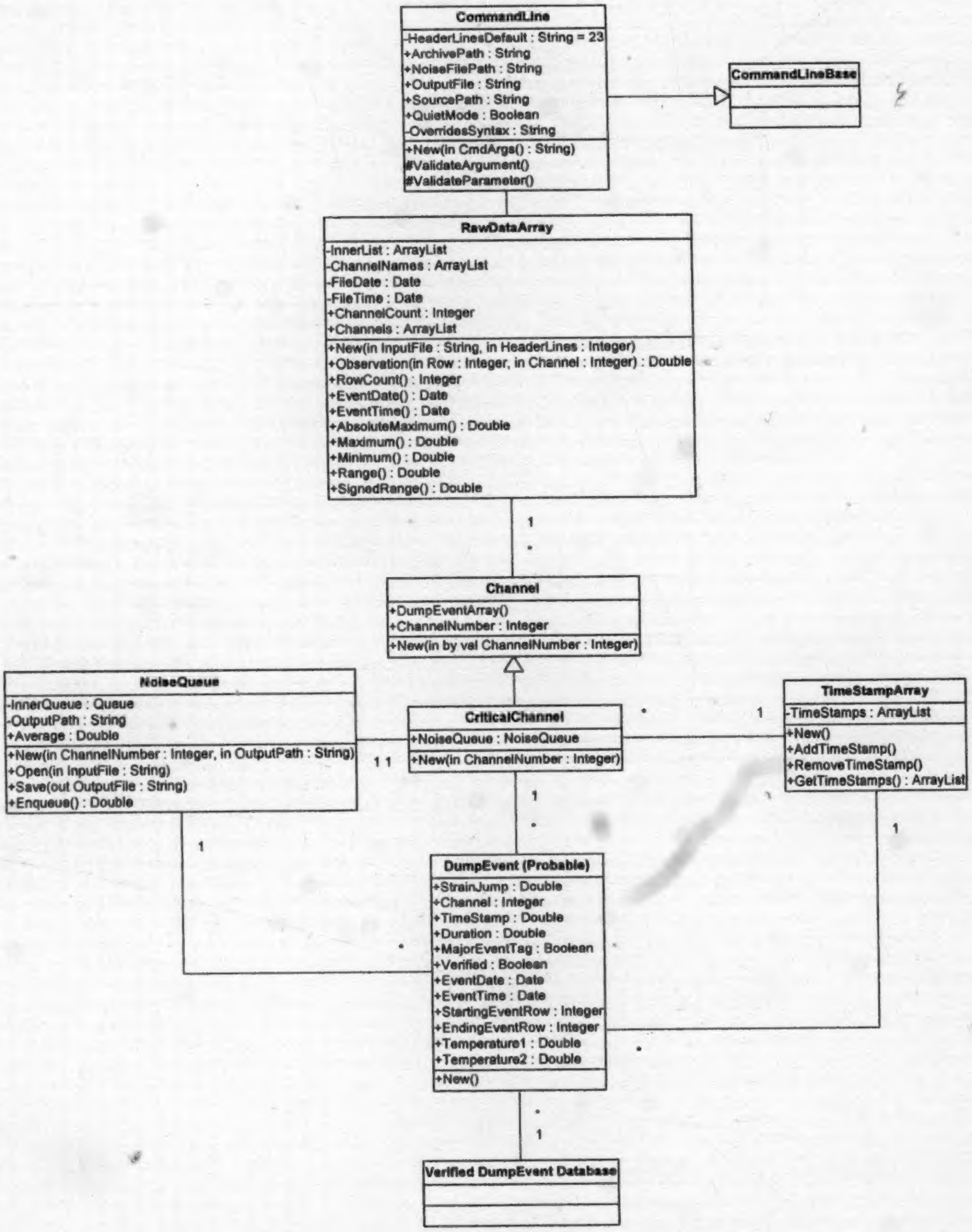
CommandLine
-HeaderLinesDefault : String = 23
+ArchivePath : String
+NoiseFilePath : String
+OutputFile : String
+SourcePath : String
+QuietMode : Boolean
-OverridesSyntax : String
+New(in CmdArgs() : String)
#ValidateArgument()
#ValidateParameter()
CommandLineBase
RawDataArray
-InnerList : ArrayList
-ChannelNames : ArrayList
-FileDate : Date
-FileTime : Date
+ChannelCount : Integer
+Channels : ArrayList
+New(in InputFile : String, in HeaderLines : Integer)
+Observation(in Row : Integer, in Channel : Integer) : Double
+RowCount() : Integer
+EventDate() : Date
+EventTime() : Date
+AbsoluteMaximum() : Double
+Maximum() : Double
+Minimum() : Double
+Range() : Double
+SignedRange() : Double
1
Channel
+DumpEventArray()
+ChannelNumber : Integer
+New(in by val ChannelNumber : Integer)
NoiseQueue
-InnerQueue : Queue
-OutputPath : String
+Average : Double
+New(in ChannelNumber : Integer, in OutputPath : String)
+Open(in InputFile : String)
+Save(out OutputFile : String)
+Enqueue() : Double
1 1
CriticalChannel
+NoiseQueue : NoiseQueue
+New(in ChannelNumber : Integer)
1
TimeStampArray
-TimeStamps : ArrayList
+New()
+AddTimeStamp()
+RemoveTimeStamp()
+GetTimeStamps() : ArrayList
1
1
1
DumpEvent (Probable)
+StrainJump : Double
+Channel : Integer
+TimeStamp : Double
+Duration : Double
+MajorEventTag : Boolean
+Verified : Boolean
+EventDate : Date
+EventTime : Date
+StartingEventRow : Integer
+EndingEventRow : Integer
+Temperature1 : Double
+Temperature2 : Double
+New()
1
Verified DumpEvent Database

Fig. 4.21 Class diagram for the data processing program

]

4.9 Database of Dump Events

The strain jump calculated for the dump events identified by the data processing algorithm is finally written into a database for permanent record and future access. Many different types of valuable statistical analyses can be performed on this reduced data with relative ease and efficiency compared to the original bulky and unprocessed data. Strain jump as a parameter adds much value and meaning to the stored data, which makes extraction of information and knowledge from the database quite effective. It is based on this premise of the database that the health monitoring system of the structure would stand on. On the basis of accumulated data and established structural signatures, the health of the structure can be monitored by comparing the statistical properties of the strain jump at various gauge locations over the years. Statistical analysis can be carried out on the data collected during different periods of time over the years, before and after damage has occurred, which should be able to show marked variation in its values. In addition to the statistical properties of strain jump at different gauge locations, inter-relation between various gauge locations will also be able to shed some light on such structural changes.

A database with effective structure is necessary for writing data into, getting data out of the database and its best utilization. A well designed model can be efficient, easy to work with, and easy to extract information from whenever required. Simplicity and performance of functional requirements has been the motto in deciding to go for a database model with a single data table for this project. For the type of work and type of data involved, it makes sense to keep them all together in one table for compact storage and easy access. Many different queries have been designed to extract information from the database without having to look into the big data table, which will be of value to the user and designer. One data column is assigned in the table for each attribute of the database that is sensors. Hence, each sensor reading corresponds to a separate identifiable data field that can be independently queried upon. Date and Time are compounded together into one field designated as the primary key such that no two records of data, that is dump events, can have the same date and time. This ensures unique identity of each data record (dump event) and eliminates duplicity. Apart from date and time, there are 60 other data fields to store strain jump data from sixty strain gauges all over the crusher structure for each dump event. The names of the fields in the database have been kept the same as the fields in the data acquisition system for uniformity and ease of data entry, for example data fields C1 to C40 store strain jumps from the forty column gauges. In addition to strain gauges, there were also some data from up to 10 transducers and 10 accelerometers. Similar to strain jump, displacement jump and acceleration jump can be calculated and recorded into the database. The displacement data will serve as a validation tool for data obtained by strain gauges. However, not all of them collect data at all times, hence, these additional 20 data fields may be null at many occasions. Further, acceleration readings are best used when conducting modal analysis for which a completely different set of instrumentation strategy will need to be adopted. The accelerometers and transducers placed on the structure did not last long, so any such tests in the future will need to be with short term instrumentation.

One extra Boolean field is added into the database to distinguish between Major Events and Minor Events. As mentioned earlier in the event identification algorithm that under certain circumstances the low magnitude strain jumps are classified as minor events and tagged accordingly by typing “Yes” into the Boolean field. The events that are clearly identified as major strain jumps are tagged as “No”. This will facilitate complete processing of the data as well as partial processing of the data that excludes the minor events, if so desired. Such statistical endeavours would be able to shed some light on operating design loads of some substance. The data under Temperature field and Acceleration field are obtained in a different way than the strain data, however, as far as the database is concerned, they are all numbers and are obtained at the same point in time. Temperature for each dump event is recorded as the average temperature in the five minutes of data file. So, more than one dump events occurring in the same file will have the same average temperature recorded. . Temperature data will help monitor the structure in the long term and help detect any changes in boundary conditions due to loosening of bolts or cracks at joints. A representative duration of dump is also calculated at the gauge P52 for each dump event and recorded into a separate field named Dump Duration. Verification power is another data field created for each dump event, which is calculated as mentioned in the earlier section. In general, verification power is expected between 0.5 and 1. A higher verification power would indicate a higher degree of confidence into the mutual operation of the critical gauges selected for dump event detection, whereas a consistently low verification power would signal the need to reassess the selected critical gauges. Finally, there is one text field for comments, which usually has the information about the critical channels that are not able to verify a particular dump event. If the verification power is 1, then the comments field is null.

Input masks and validation rules have been utilized for quality assurance of the database. For example, the date and time entered have to follow certain format and range, and so do the numeric data in other fields. The temperature data uses validation range of -60 to +40 degree Celsius, which are the extremes of temperature possible in Fort McMurray. All numeric data are double with two decimal places. The data coming from the sixty strain gauges are double and have to be within the range of -2000 to +2000, as this is the value in micro-strains at which steel starts to yield. Further, this data base only contains the strain jump due to dumping and does not include effects of superimposed dead loads. Hence, it is not practical to expect a strain jump going higher than this value. In case the strain gauge is broken or stops working, the differential strain jump for that gauge field will be calculated and stored as zero or close to zero. Any such anomaly in any gauge data will automatically alert the user of some inconsistent or aberrant behaviour that needs attention.

Thus, the database has one primary key data field of Date and Time, 60 strain gauge data fields (40 for columns C1 to C40, 10 for pontoons P45 to P54, 10 for hopper H55 to H64), 10 Displacement data fields, 10 Acceleration data fields, two Temperature data fields, one Boolean Minor Event data field, one Dump Duration data field, one verification power data field, and lastly, one Comments text field. There will be many different types of queries available at the disposal of the user to obtain further information about the collected data and interpret intelligently for an informed decision.

Such queries can generate, group, re-group, sort, and filter data for easy extraction of information. Queries are tools designed for information gathering and knowledge enhancement. Knowledge is the ability to act on decisions – it is actionable information. The user, manufacturer, and researcher would like to gain concise information about various aspects and at various locations of the structure. It is worth mentioning here that statistical queries are not magic tools, rather tools for information generation, human interpretation and validation of results remain of prime importance. Hence, further analysis of the data needs to be performed by suitable better statistical tools.

4.10 Summary

The proposed event identification and data processing algorithm integrated with the database system is able to effectively process, reduce, and archive the data for easy access and long term monitoring by about 10,000 times, without losing any valuable information. The algorithm is built upon multiple layers and varieties of thresholds derived from the operating conditions and response characteristics of the structure. Much has been drawn from the many similarities existing between the structural signal under impact of oil sand and the electrical signal generated by firing of neurons. Experience of detecting neural spikes in neuroscience has been applied into the structural domain in detecting strain jump. Strain jump has served as an excellent parameter in event detection and structural monitoring, with ability to predict remaining life of the structure. Magnitude of strain jump, dump duration, inter-spike interval, average noise amplitude and time stamp of the dump have been used as the parameters for signal processing and event detection. Moving search windows of 10 second and 20 second durations have been employed in event identification and feature extraction respectively. Two separate algorithms are used for major events with higher strain jump and minor events with strain jump magnitude very close to the ambient noise. Dump events identified over multiple channels are verified against each other to a satisfactory level of verification power before writing the characteristic features of the dump into the database for each gauge location. The algorithm is robust and is able to successfully process data collected under varying operating conditions to identify all dump events with remarkable accuracy. Many checks and balances exist in the algorithm to detect potential sources of error, which are communicated to the user for rectification or improvement in the future. Histogram of strain jump at each gauge location will able to predict the fatigue life of the structure to schedule appropriate inspection and maintenance interval. Hence, the proposed data processing and management algorithm has satisfactorily extracted all the pertinent information from the data and reduced it significantly to provide a platform for long term health monitoring of the structure.

4.11 References

Card, L. and McNeill, D.K. 2004. Novel Event Identification for SHM Systems using Unsupervised Neural Computation. Proceedings of SPIE 9th Annual International Symposium on NDE for Health Monitoring and Diagnostics, Conference vol. #5393, March 16-17, 2004.

Cheeseman, P. and Stutz, J. 1988. AutoClass: A Bayesian Classification System. Proc. 5th International Conf. on Machine Learning, Morgan Kaufmann, San Francisco, 54-64.

Eggermont, J. J. 1990. The Correlative Brain: Theory and Experiment in Neural Interaction. Berlin: Springer-Verlag.

Fowler, M. and Scott, K. 2000. A Brief Guide to the Standard Object Modelling Language. Addison-Wesley, 2nd Edition.

Garcia, P., Suarez, C. P., Rodriguez, J., and Rodriguez, M. 1998. Unsupervised Classification of Neural Spikes with a Hybrid Multilayer Artificial Neural Network. Journal of Neuroscience Methods, Elsevier Science, 82 (1998):59-73

Gloor, P. 1975. Contributions of Electroencephalography and Electrocorticography in the Neurosurgical Treatment of the Epilepsies. Journal of Advances in Neurology, 8 (1975):59-105.

Glaser, E. M. 1971. Separation of Neuronal Activity by Waveform Analysis. Advances in Biomedical Engineeering (ed. RM Kenedi) Academic Press, New York, vol 1:77-136.

Gotman, J. and Gloor, P. 1976. Automatic Recognition and Quantification of Interictal Epileptic Activity in the Human Scalp EEG. Journal of Electoencephalography and Clinical Neurophsiology, Elsevier Science, 41 (1976):513-529.

Hartigan, J.A. 1975. Clustering Algorithms. Wiley-Eastern, New York.

Hellman, G. 1999. Multifold Features Determine Linear Equation for Automatic Spike Detection Applying Neural nin Interictal ECoG. Journal of Clinical Neurophysiology, Elsevier Science, 110 (1999):887-894.

Lewicki, M.S. 1998. A Review of Methods for Spike Sorting: the Detection and Classification of Neural Action Potentials. Journal of Network: Computation in Neural Systems, IOP Publishing Ltd, U.K., Taylor and Francis. 9(1998):R53-R78.

Marion-Poll, F. and Tobin, T.R. 1991. Software Filter for Detecting Spikes Superimposed on a Fluctuating Baseline. Journal Neuroscience Methods, Elsevier Science, 37(1):1-6.

Wheeler, B.C. and Heetderks, W.J. 1982. A Comparison of Techniques for Classification of Multiple Neural Signals. IEEE Transactions on Biomedical Engineering, 29:752-759.

Wilson, S.B. and Emerson, R. 2002. Spike Detection: A Review and Comparison of Algorithms. Journal of Clinical Neurophysiology, Elsevier Science Ireland Ltd., 113 (2002): 1873-1881.

CHAPTER 5

STRUCTURAL BEHAVIOUR OF THE CRUSHER

5.1 General

The data collected at different times under different operating and testing conditions were analysed to investigate into the nature of structural response to loading under different situations. The Aurora II crusher is a complex industrial structure operating under severe and varying industrial environment. The strategy has been to focus on global behaviour of the structure as a whole without losing the significance of local data. Data obtained from each sensor has been analysed individually to obtain the structural response at that location. By testing under different conditions with sufficient amount of data from each sensor location, a response bandwidth of the sensor is established with the expected normal range of operation. Such statistical endeavour, however, requires considerable amount of data for establishing the response distribution function at each gauge location. Hence, the statistical side of the data will be dealt with in a separate chapter. This chapter is devoted to identifying typical behaviour patterns of the structure under different type of loading and testing conditions. As it turns out, it is convenient to express the behaviour patterns of the pontoon, columns and hopper as a group; with an attempt to determine the inter-relationship between various sensor readings establishing the local significance of each sensor in the global perspective. Response of the structure under temperature, control testing, normal operation, and different dumping conditions has been investigated. Since impact factor is used as an important design parameter in the industry, special attention has been given to discuss it in detail.

5.2 Understanding the Load

The first step towards understanding structural behaviour is to understand the load acting on the structure. The major load on the crusher comes from oil sand dumped by haul trucks into the hopper. Up to 400 ton of material can strike the hopper after falling through a distance of almost ten metres when the hopper is totally empty. The magnitude and location of the impact varies to some extent depending on many factors like the side of dump, level of material in the hopper, speed of dump, and grade of oil sand. Although the mass of material being dumped by trucks at each dump event is in the same range (between 300 to 400 T), its effect on the structure and the response generated can be vastly different from one another. Although information about the weight of oil sand being dumped and other dump parameters can be gathered, the actual force acting on the structure still remains unmeasured due to variations in each dump event. Hence, there is a need to correlate the load in terms of structural response that is measured. The most important parameter that can make a dump event severe is the fall distance, which is a function of the material level in the hopper. When the hopper is completely empty, it allows for the material to fall the greatest distance before hitting the hopper. And as force equals mass times acceleration, it is quite understandable why some dump events can produce the stresses (strains) they do. This leads to the need for characterizing various dump parameters that influence response. There are two components of response to each dump load, one is the dynamic part and the other is static component. The dynamic component of the response corresponds to the instantaneous rise in strain at the moment of dump to a peak and then immediate fall to a much lower value, and then follows the stable static component of the response (see Figure 4.1). The relative magnitudes of the dynamic and static components again depend on the aforementioned parameters. Impact Factor is defined as the ratio between dynamic and static components.

Impact or impulse loads are extremely short duration loads like drop-hammer hitting a pile, blasting of explosives, impact from a gun bullet, etc. Impact loads have two-pronged effect on a structure owing to its short duration of action, namely – high local impact on the area of contact, and relatively lower effect on the global behaviour of the structure. Even a small load, when dropped from a height, can cause an impact of several times the load. Naturally, the height of fall or the velocity of impact and impacting mass are the two key factors. The type of load acting on Aurora II crusher belongs to this category of dynamic load. The mass of oil sand impacting the hopper can be as high as 400 ton depending on the size of lumps. The height of fall into the hopper decreases with the rise in the level of oil sand in the hopper. Pre-existing material in the hopper has also a dampening effect and acts like a cushion to the falling load. Dump occurring on an empty hopper should naturally be the severest of all, whereas dump on the full hopper be producing minimum effect from impact.

In addition to the main and most frequent load coming from oil sand dumping, the Aurora II structure is subjected to other operational loads such as vibrations from machinery operation, dead load of equipment, loads during repair and maintenance, etc. However, the most significant other load can be identified as environmental load coming from temperature variation. Temperature in Fort McMurray, where the crusher is located, can vary anywhere from +30 in summer months to –50 in winter, a total of more than 80 degree Celsius variation over the year. Such huge temperature variations can elicit stresses / strains in the structure that can be much larger in magnitude than the response under normal dump operation. However, the fact that such variations are occurring over a period of one year and the daily variation would be limited to a much smaller temperature range of 10 to 20 degree Celsius, which is less critical to the structure from the aspect of fatigue life. At the maximum throughput of 15,000 ton per hour, one would expect about 40 dumps per hour assuming each dump truck carries an average of 375 ton of oil sand at a time. Thus, operating at the maximum design capacity would entail a total of 960 dump trucks dumping oil sand each day. However, it would be impractical to assume the crusher operating at maximum capacity all the time; hence, it can be assumed that on average the crusher operates at 70% of throughput capacity. Hence, a total of 670 dumps every day would be an expected affair, provided there are no production outages for maintenance or other reasons. Now, comparing 670 daily dump strain cycles to one cycle of strain due to a 10 degree Celsius temperature change, virtually makes the contribution of temperature to fatigue life calculations insignificant. Temperature, however, remains an important parameter defining the long-term behaviour of the structure and a structural signature of its unchanged boundary conditions. Any change in the structural stiffness, connections or boundary conditions would lead to some variation in the temperature response of the sensors located closest to such a structural change. Hence, influence of temperature on each sensor reading needs to be put on record prior to the structure coming into operation.

5.3 Zero Oil Sand Load Readings of Sensors

Prior to start using the data for analyses, it is important to verify the data for integrity and stability. Plots of strain against time for different sensors (Fig. 5.1) showed that data from all the working channels looked appropriate and coherent. Some of strain gauges and accelerometers were not working properly and hence, their data had to be excluded from analysis. Out of 60 strain gauges, 58 were working well and only two were broken. In order to make sure that the sensors were going back to their original position after each dump event, zero oil sand load readings were noted for each gauge before and after a dump event. The hopper was emptied completely at the beginning of the control test, which provided a base zero load reading. Thereafter, the hopper was emptied after each control dump. These readings after each dump event are plotted for the pontoon gauges in Fig. 5.1. The readings obtained from the data acquisition system were very stable and the structure did return back to its original zero state, as expected. This signifies that there isn't any short term drift in data due to temperature or other environmental or operating effects. There will definitely be drift in strain due to change in temperature over the long term. It is also expected and characteristic of electronic equipment to have a shift in their zero reading over time. Such long term drift in strain were one of the reasons behind selecting a differential entity like the strain jump as a monitoring parameter. However, it is of utmost importance to ensure that there is no short term drift, which would be a sign of the sensor's instability and unreliability.

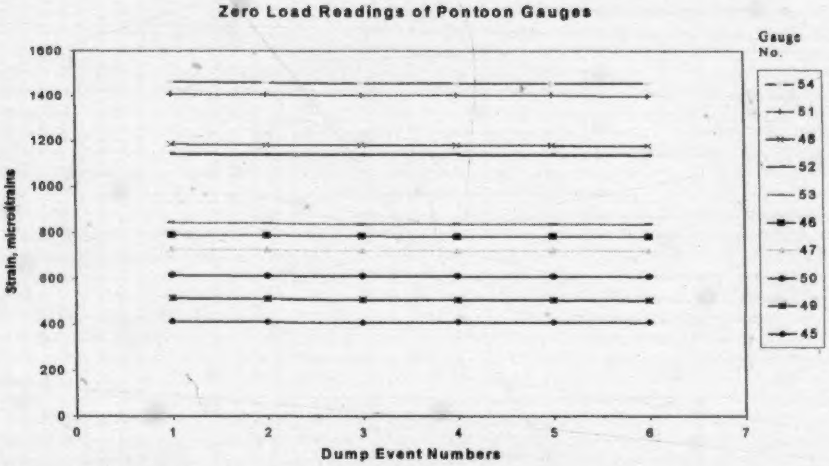

Fig. 5.1 Zero Load Strain Readings of Pontoon Gauges after each Dump

5.4 Adequacy of Rate of Data Acquisition

A decision was made to collect data at the sampling rate of 100 Hz (in section 3.3) based on past research experiences and information available through literature. For dynamic loads and ambient vibration tests, most researchers chose to record data between 100 Hz to 500 Hz. Acquiring data at a faster rate would provide better resolution and accuracy, albeit at a price of processing and storage costs. Hence, an investigation is carried out to determine the performance of sampling rate.

Higher the frequency content of interest, higher is the required sampling rate, as determined by the Nyquist rule. Most structural natural frequencies fall below a certain range, and beyond 50 Hz there isn't of much interest to civil engineers in general, unless complex dynamic analysis needs to be carried out with higher mode effects. Hence, 100 Hz sampling rate seems fine from the Nyquist point of view. In general, in order to accurately read a peak value in a sine wave, a minimum of 3 to 5 data points are needed to plot it in one rising or falling arm of the sine-wave. The strain changes (difference) between two consecutive readings were calculated for a typical data channel, which were then categorized into strain ranges of 0.05 micro-strains each. A statistical analysis with frequency of occurrence of each category was carried out and then normalized with the total sample size, i.e. the number of readings. Figure 5.2 shows the probability of occurrence of each strain change magnitude between two consecutive readings. It is clear from the probability curve that the most likely strain change magnitude between two consecutive readings is 0.1 micro-strains. And there is more than 90% probability that the strain change magnitude will be less than 0.2 micro-strains. Such small strain resolution when looking at strain changes of up to 800 micro-strains exudes sufficient confidence into the reliability of data and adequacy of sampling rate.

The same data is looked at from a slightly different perspective now. As discussed earlier, maximum number of data points would be desirable on each arm of the sine-wave for accurate representation of peaks. The strain data obtained from strain gauges contain some noise superimposed on actual data; hence, there will be many higher frequency sine-waves on top of the lower frequency ones. So, it is expected that there will be many higher frequency rising arms of imaginary sine waves that will have only one data point to plot them. However, it is also expected that such single data point rising arms will be of significantly low strain magnitude, as expected from noise. There will also be some lower frequency rising arms of imaginary sine-waves that will have many more data points to plot each rising arm to impart sufficient accuracy. Such multi-data-point rising arms should be of relatively higher strain magnitude, which is characteristic of a dump event. Figure 5.3 shows that these arguments here exactly hold true. The single riser data points almost invariably belong to noise and are of significantly low magnitude less than 0.1 micro-strains. The strain magnitude remains low for up to 3 or 4 data points per rising arm and then it starts picking up. A maximum of 23 data points were observed on one single rising arm in the vicinity of dump events. Notably, these are the regions with maximum observed strain change. This confirms the belief that the peak strain readings obtained are accurate and reliable. There are many other observations of 5 to 12 data points per rising arm in between, with moderate strain magnitudes. These are the regions in proximity of the dump event. In conclusion, this investigation has re-affirmed the sampling rate decision made earlier based on experience.

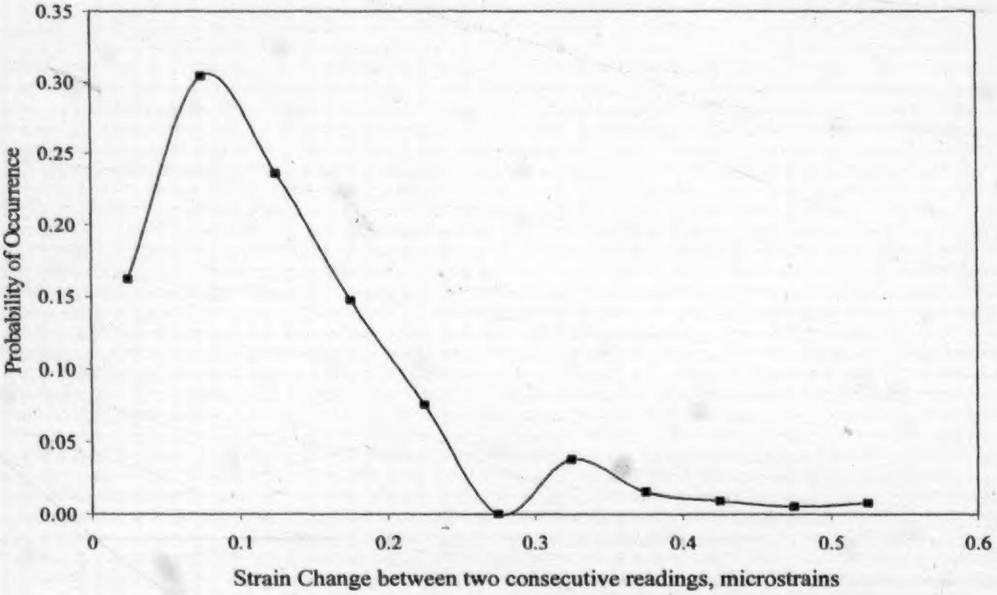

Fig. 5.2 Probability distribution of strain change between readings

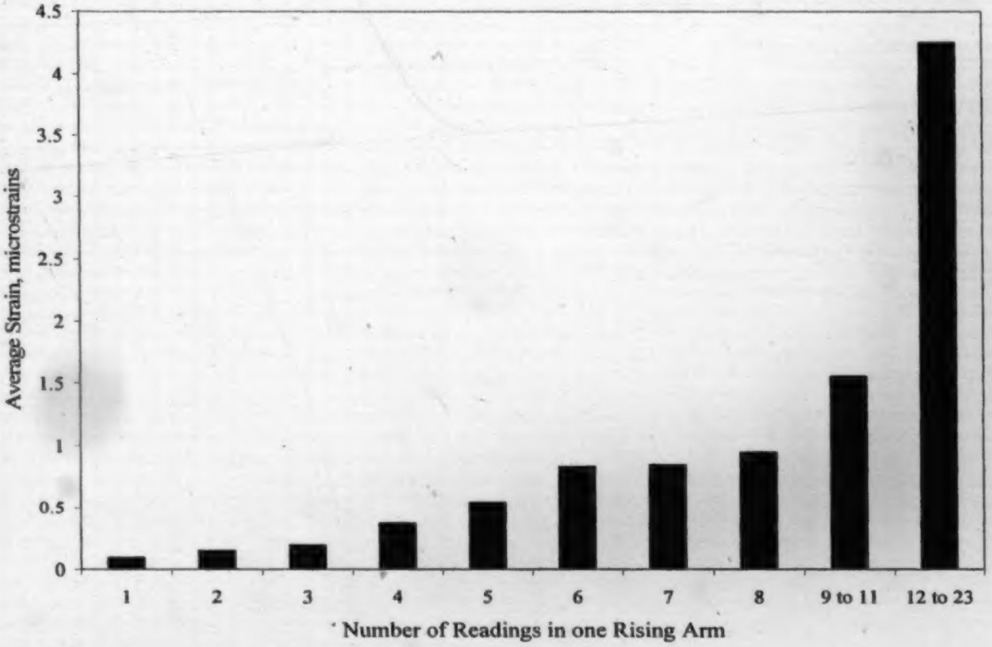

Fig. 5.3 Avg. strain change for different number of data points on a sinusoidal arm

5.5 Analysis of Thermal Data

The first set of data collected in October 2003 contained the base response of the structure under normal operating conditions, when the crusher was newly commissioned into operation. At the same time a second set of base data was collected under the influence of temperature alone for 24 hours, when no dumping was occurring. The reasons and motives behind these tests have been already explained in the section 3.6 on field testing. The temperature data is analysed with the aim of establishing a relationship between temperature and the strain readings observed at each gauge location for serving as a benchmark for future comparisons against changes in boundary conditions or damage. This approach augurs well for a multi-pronged structural health monitoring program.

The temperature data and corresponding strain data were collected every sixty seconds, which is equivalent to 0.017 Hz. It is worth reminding here that all other structural testing data under normal operation and control testing were collected at 100 Hz. This drastically reduced sampling rate for temperature related data is obvious because temperature and the strain induced by it are not expected to vary every micro-second as the strains under dynamic loads do. Collecting temperature data every minute was reasonable enough and convenient to process. A look into the data reveals that both strain and temperature readings do show some nominal variations over time. Such variations are the result of a couple of things combined such as noise and accuracy of measurement of the gauge. First and foremost is the influence of noise. As mentioned earlier in section 3.3, noise can significantly pollute data. The most plausible and immediate solution to errors due to noise is to filter the data. Averaging is the simplest yet effective technique for filtering noise, which has been used in the case of temperature data here. Generally, the variations in strain readings and temperature are both small. The second influencing parameter is the resolution of thermocouples in measuring temperature. There is always a possibility of an error equal to half the magnitude of resolution. Third and last, the change in temperature could be real over the course of a day. As was obvious from analysis, for time intervals of 10 to 60 minutes, temperature readings do genuinely change. Figure 5.4 shows the variation of strain with temperature every minute for gauge C4. Figure 5.5 shows the same variation averaged at 10 minute interval, which filters out the noise, resulting in a better view of the variation of strain with temperature.

The major difference between the two Figures 5.4 and 5.5 is the significantly reduced influence of noise by averaging every ten minutes. The general trend of the genuine component of strain variation with temperature is retained even after averaging, although the slope of variation is more well-defined and clearer post filtering. An interesting feature to note in these plots is that the path of strain rise with temperature is not the same as that for the falling temperature. When the temperature is rising from about 1 degree Celsius to about 5.5 degree Celsius, the strain in gauge C4 is also observed to rise following the upper line. Once the temperature hits the maximum and starts falling, the strain reading observes a sharp drop at the maximum temperature value and then starts decreasing gradually with temperature, along the lower line in the Figure 5.5. Both the upper and lower lines have the same slope, which defines the relationship between strain change and temperature for that gauge. This is an expected behaviour of steel to maintain constant rate of expansion and contraction as dictated by its coefficient of thermal expansion, and hence, the same linear slope for rising as well as falling temperatures. The sudden fall (change) in strain magnitude when temperature reversal occurs is also a known behaviour of steel. When temperature reversal occurs, readjustments and re-alignments of molecules and boundary conditions occur, which also has to overcome the initial frictional resistance to this changed situation. As the readjustment completes, the structure shows a new changed strain magnitude for the same (marginally lower) temperature. Sometimes, such strain reversal behaviour is also accompanied by a metallic panging sound, especially with thin-walled members. Once the initial frictional readjustment phase is over, it is again business as usual for steel to follow its coefficient of thermal expansion/contraction.

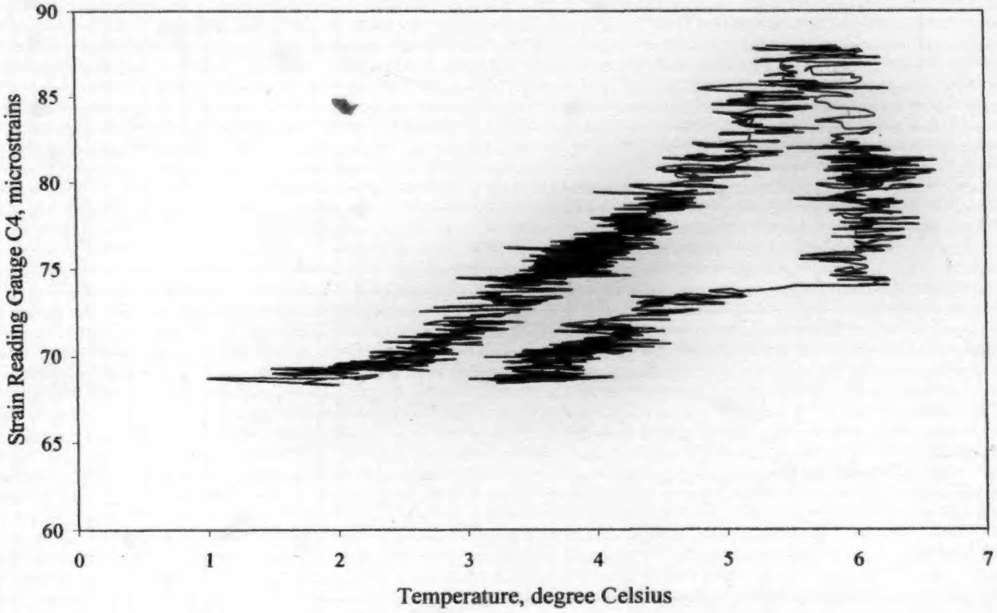

Fig. 5.4 Variation of strain with temperature per minute

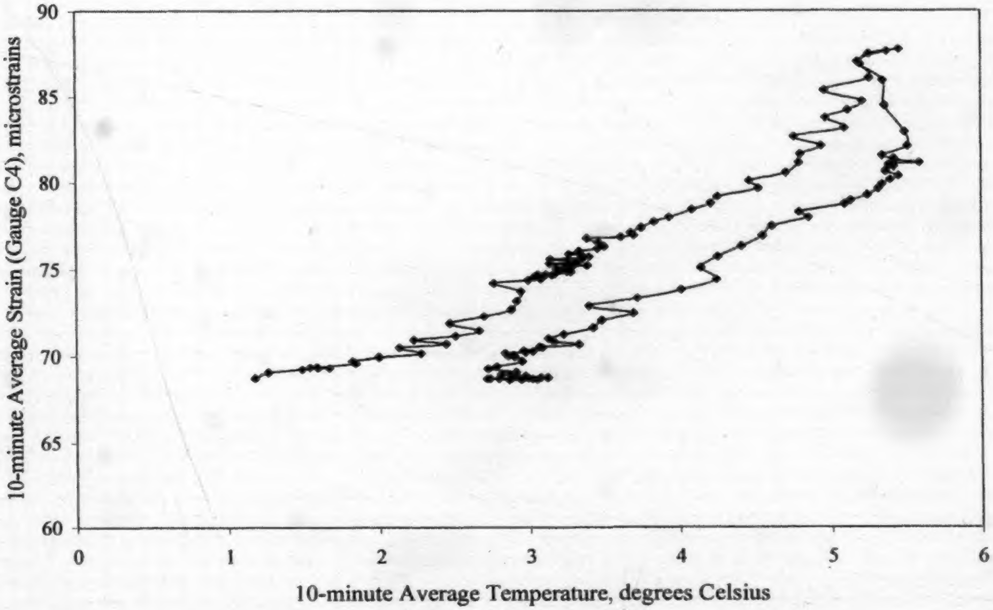

Fig. 5.5 Strain vs. Temperature averaged over every 10 minutes

The reason behind choosing the averaging interval of 10 minutes is explained in the following paragraphs. Averaging for 5 minutes or even 40 minutes should also be able to do the job of filtering out noise effectively, what is the difference then? Taking the example of pontoon gauge P52 this time, the standard deviation of strain over the period of 24 hours (1440 minutes) comes to 3.96 micro-strains, whereas in the same time period, the standard deviation of the two thermocouple readings are observed as 1.14 and 1.17 degree Celsius. The difference between maximum and minimum temperature readings in the 24 hour period was close to 6 degree Celsius, which was in the month of November. Now the real challenge of separating the influence of noise from genuine temperature data begins. To this end, an approach similar to dealing with wind related data was adopted for dealing with noise. In wind engineering, 10 minute to 60 minute averaging is used for calculating the mean wind speed. The 10 minute mean (or 60 minute) wind speed is then regarded as a random variable for the purpose of statistical analyses, which is governed by the theory of extremes. The concept of averaging is simply used to get a stable and reliable temperature reading based on a proven averaging interval. This serves dual purpose of filtering out noise and still having sufficient data available for plotting the temperature variation. In order to find the most optimum averaging interval for the temperature data, a statistical analysis is carried out with different averaging intervals, the optimization criteria being that of minimizing the variance of the mean.

Averaging intervals of 5, 10, 20, 40, and 80 minutes were selected for the purpose of statistical analysis. The procedure adopted for a 5 minute interval analysis is described here, which is repeated for the other intervals to generate the data for comparison. The average temperature reading for each 5 minutes is calculated and recorded as a random variable and called as Avg (5_rdg). Similarly, the standard deviation is also calculated for each 5 second interval and saved as another random variable called as SDev (5_rdg). The third and fourth columns of Table 5.1 show these calculations. Then, at the end of the table, the mean and standard deviation of the random variable in column three called Avg (5_rdg) is calculated. Similarly, the mean and standard deviation are also calculated for the random variable called SDev (5_rdg). A repetition of this procedure for 10-minutes to

80-minutes averaging interval leads to the rest of the columns in the table. At the end of the table, mean and standard deviation for each of these random variables named as Avg and SDev for different averaging intervals are calculated as shown in Table 5.1.

Table 5.1 Comparison of different averaging intervals for temperature readings

Time (Sec)	Temp (Deg)	Average (5 rdg)	SDev (5 rdg)	Avg (10)	SDev (10)	Avg (20)	SDev (20)	Avg (40)	SDev (40)	Avg (80)	SDev (80)
57600	3.621										
57660	3.523										
57720	3.758										
57780	3.530										
57840	3.491	3.584	0.109								
57900	3.517										
57960	3.739										
58020	3.667										
58080	3.268										
58140	3.379	3.514	0.195	3.549	0.153						
58200	4.045										
58260	3.673										
58320	3.634										
58380	3.876										
58440	3.530	3.752	0.207								
58500	3.549										
58560	3.223										
58620	3.836										
58680	3.660										
58740	3.575	3.569	0.224	3.660	0.225	3.605	0.196				
58800	3.392										
143340	1.736	1.849	0.287	1.827	0.207						
143400	1.658										
143460	1.723										
143520	1.979										
143580	2.163										
143640	2.300	1.964	0.276								
143700	1.940										
143760	0.995										
143820	1.979										
143880	1.730										
143940	1.920	1.713	0.413	1.839	0.356	1.833	0.284	1.981	0.304	2.108	0.277
Mean =			0.184		0.195		0.202		0.217		0.258
StdDev.=	1.172	1.160	0.070	1.160	0.052	1.162	0.050	1.166	0.074	1.169	0.134

The Standard Deviation of the Average (Avg.) for different averaging intervals is calculated in the table and plotted in Figure 5.6. It can be seen from the plot that the value of standard deviation remains more or less same with slight increase for higher averaging intervals. The averaging intervals of 5 and 10 minutes duration give the lowest standard deviation. A similar plot of the mean of standard deviation (SDev) for different averaging intervals is shown in Figure 5.7. The mean of SDev is higher for longer averaging intervals, with maximum value of 0.258 degrees recorded for 80-minute averaging, whereas the lowest value of 0.184 degrees is obtained for 5-minute averaging. The mean of SDev for 10-minute averaging is also sitting pretty close at 0.195 degrees. From the point of view of lowest standard deviation of the average (Avg) in Figure 5.6, both 5 and 10 minute averaging yield same results, hence there is no clear favourite. From Figure 5.7, 5-minute averaging slightly weighs over 10-minute averaging due to lower mean of SDev. However, they are both quite close. Now, having a look at the standard deviation of the standard deviation (SDev) plotted in Figure 5.8 for the different averaging intervals, the figure shows some interesting trend in its variation that now the shortest averaging interval of 5-minutes does not produce the most favourable result. Instead, 10-minute and 20-minute averaging produce the lowest standard deviation of SDev, which makes them more reliable and stable. From all this discussion a clear winner to emerge is the 10-minute averaging as the optimal interval, which stands out among all other averaging intervals in the comparisons of means and standard deviations.

Thus, all temperature related data were averaged every 10 minute interval to get rid of errors due to noise etc. Next, in order to establish a relationship between strain and temperature for each strain gauge, a rising or falling branch was selected to ascertain its slope. Figure 5.9 shows the slope of strain versus temperature plot for the column gauge C4, as given by the line of regression on the ten-minute averaged data. Care has to be taken to make sure that the data before and after temperature reversal occurred are not combined together. An R^2 value of 0.98 assures that a good curve-fitting has been obtained by the line of regression. The equation of the line of regression in Figure 5.9 gives the slope of the line as 4.439 micro-strains per degree Celsius, which then becomes the characteristic slope of the column gauge C4 for thermal variations in that temperature range. Correction has to be applied for the thermal non-linearity of the strain gauge over a large temperature variation. Any future change in this slope of strain with respect to temperature at a gauge location will be a sign of structural change, degradation or boundary change around it. A similar exercise at every gauge location yields a slope for each of the gauges. Table 5.2 shows the value of slopes for all Column gauges; and Tables 5.3 and 5.4 show those for the pontoon and hopper gauges respectively, which are reported by Denkhaus (2004). The slopes vary from 1.31 to 6.4 micro-strains per degree Celsius.

The variation of strain with temperature, i.e. the slopes obtained in the above tables are extrapolated and plotted in Figure 5.10 for all the pontoon gauges. A similar plot of thermal slopes for all the column gauges is shown in Figure 5.11. These figures render at a glance view of the thermal characteristic at each gauge location. It is apparent that a 20 degree rise in temperature can see a 50 to 90 micro-strains change in strain in the pontoon gauges, whereas the column gauges register between 20 to 100 micro-strains change. The true strain values may differ depending on the thermal correction for the gauge. However, within a particular temperature range over different seasons, the slope of the thermal lines should not change over the years, unless due to change in boundary conditions.

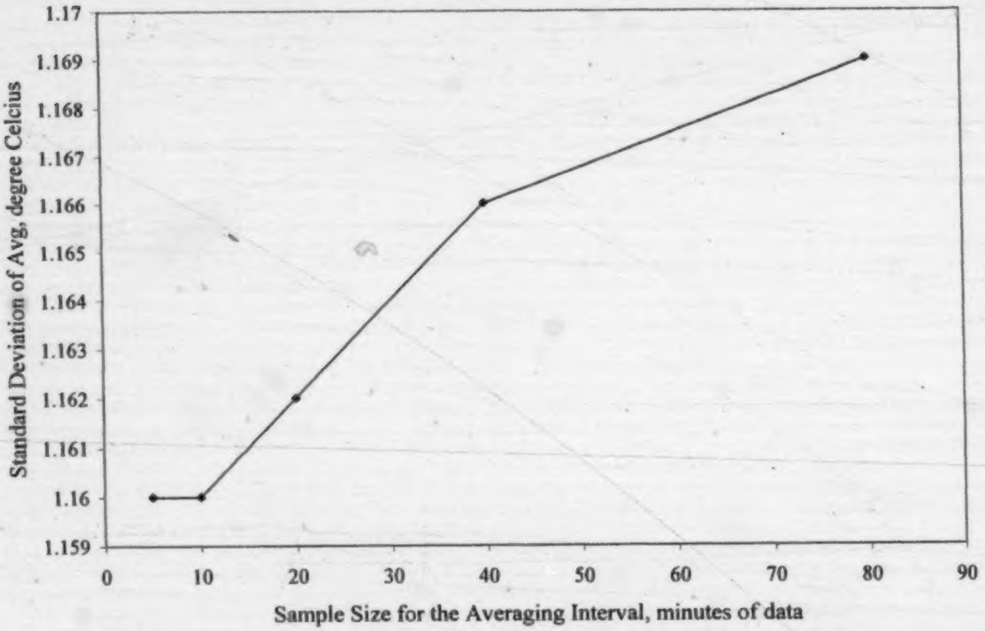

Fig. 5.6 Standard deviation of Average for different averaging intervals

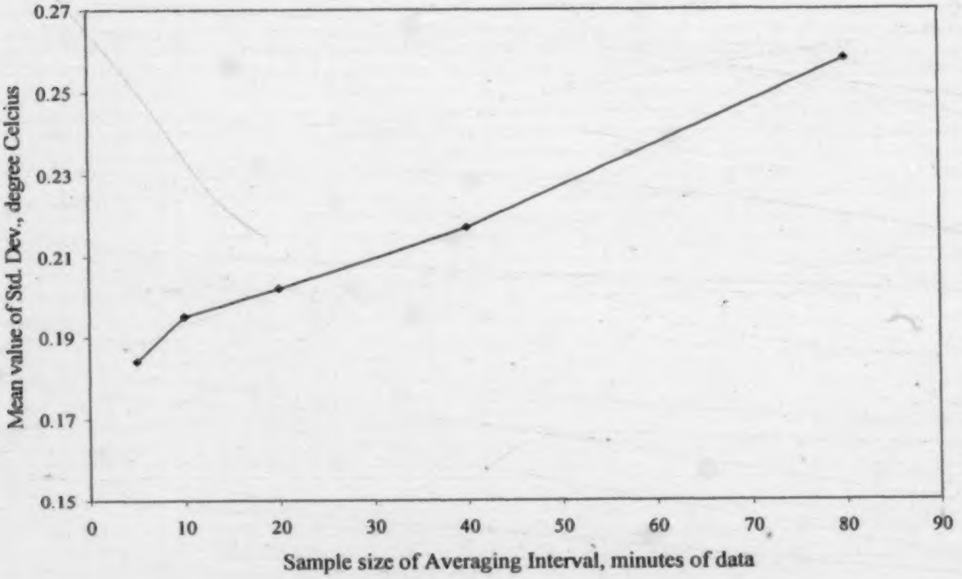

Fig. 5.7 Mean of SDev for different averaging intervals

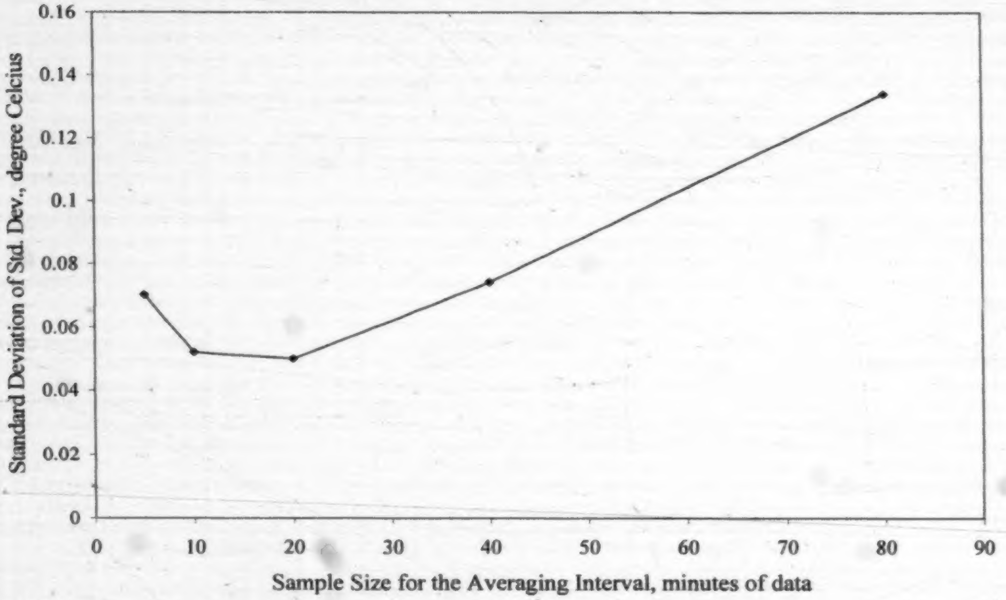

Fig. 5.8 Standard deviation of SDev for different averaging intervals

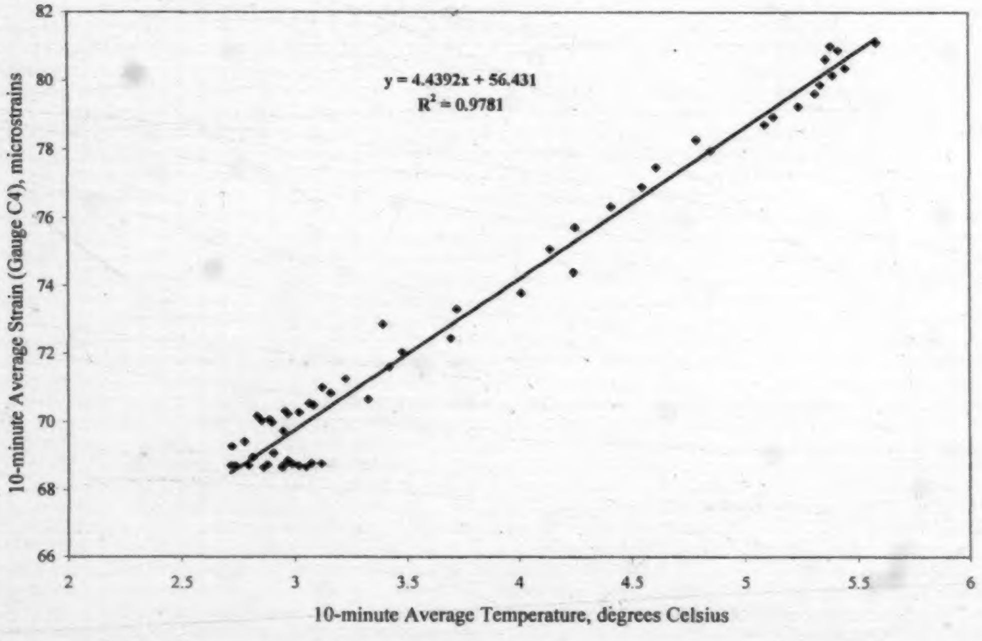

Fig. 5.9 Line of regression for strain variation with temperature

Table 5.2 Thermal strain slopes for different column gauges (Denkhaus, 2004)

Gauge	slope(με/°C)	R^2	Gauge	Slope(με/°C)	R^2
C1	2.95	0.955	C18	4.04	0.971
C2	4.37	0.982	C19	4.37	0.956
C3	4.53	0.989	C20	4.66	0.960
C4	4.58	0.988	C21	5.36	0.978
C5	3.96	0.966	C22	5.11	0.952
C6	4.44	0.963	C23	3.43	0.888
C7	4.00	0.983	C24	3.50	0.912
C8	4.89	0.988	C27	4.30	0.945
C9	4.25	0.975	C28	1.65	0.957
C10	5.47	0.987	C29	2.34	0.958
C11	4.99	0.969	C32	1.82	0.847
C12	4.63	0.973	C33	4.65	0.978
C13	3.69	0.967	C34	4.68	0.969
C14	4.20	0.939	C35	5.21	0.948
C15	4.14	0.932	C37	1.31	0.891
C16	4.30	0.916	C38	1.73	0.877
C17	4.55	0.988			

Table 5.3 Thermal strain slopes at different pontoon gauges (Denkhaus, 2004)

Gauge	slope(με/°C)	R^2	Gauge	slope(με/°C)	R^2
P45	3.61	0.963	P50	2.80	0.900
P46	2.43	0.887	P51	3.44	0.975
P47	4.23	0.966	P52	2.45	0.916
P48	2.81	0.916	P53	2.73	0.937
P49	4.26	0.971	P54	2.75	0.959

Table 5.4 Thermal strain slopes at different hopper gauges (Denkhaus, 2004)

Gauge	slope(με/°C)	R^2	Gauge	slope(με/°C)	R^2
H55	6.43	0.951	H61	5.99	0.928
H56	5.69	0.973	H62	5.28	0.951
H57	6.42	0.940	H63	5.22	0.940
H58	5.70	0.958	H64	5.48	0.945
H60	5.08	0.961			

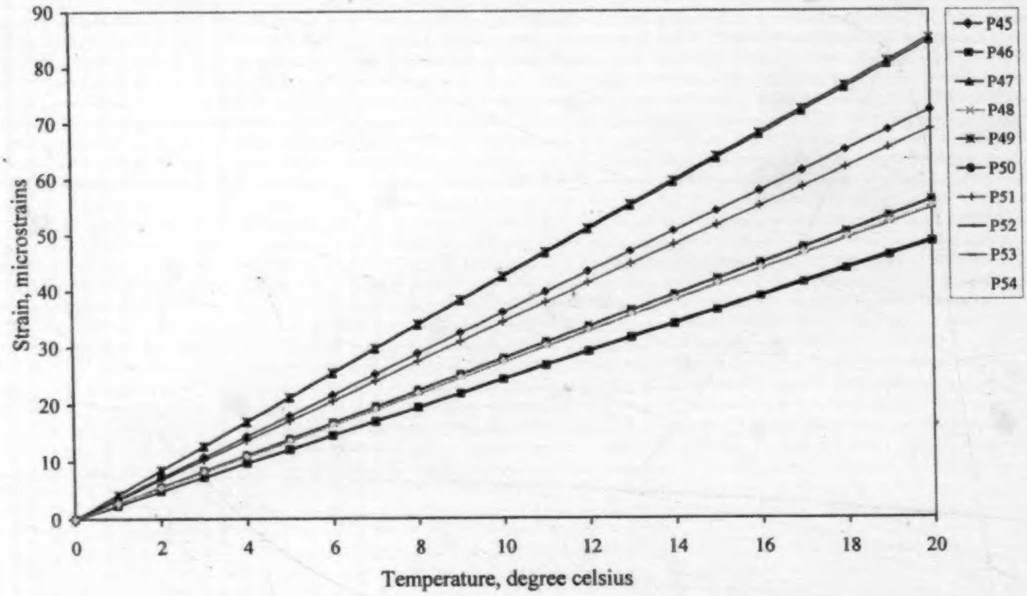

Fig. 5.10 Extrapolated strain variation with temperature at different pontoon gauges

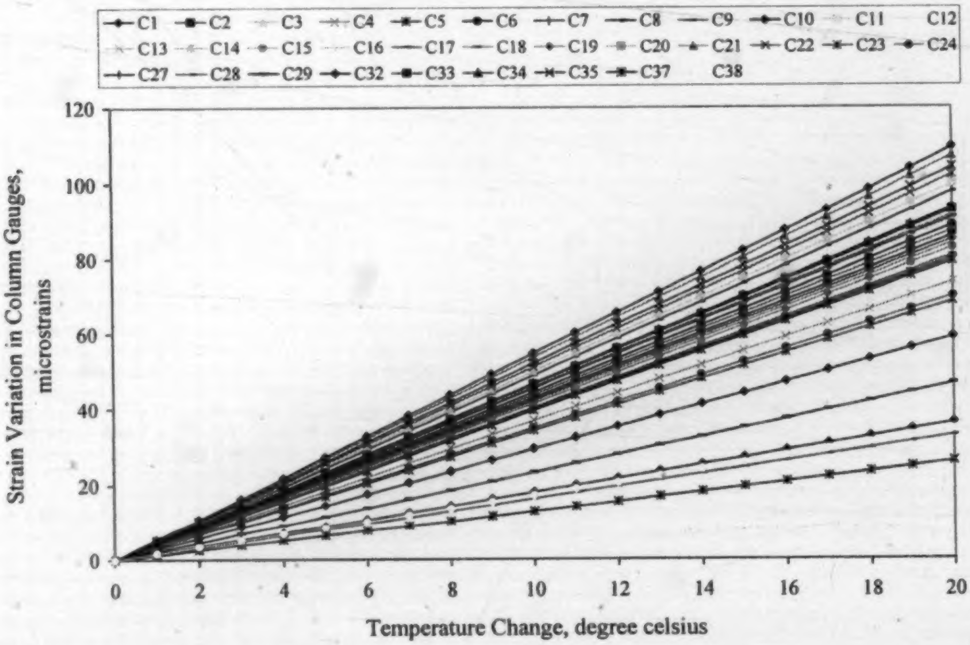

Fig. 5.11 Extrapolated strain variation with temperature at different column gauges

In the severe northern climate, temperature is a forceful player. With a total variation of more than 80 degree Celsius over summer and winter months, a structure will be subjected to many cycles of temperature induced stresses. However, as mentioned earlier, stresses due to the daily variation of about 10 degree Celsius in temperature sounds insignificant when compared to stresses due to more than 500 dumps occurring in a single day. Hence, the main objective of performing analysis on thermal data was to establish a benchmark slope of strain variation with temperature for each gauge. Thermal expansion and contraction in a member and the corresponding strain recorded in it are dependent on the structural boundary conditions. A cantilever beam fixed on one end and free on the other will record strain change under temperature variation, whereas, a beam fully fixed on both ends will record no strain change at all. Thus, lower the strain change recorded the more rigid boundary conditions the structure can be assumed to have. Each member in the crusher structure is a unique one, and hence, will have a unique slope of observed strain readings versus change in temperature depending on its connection (type and rigidity) with .the neighbouring members and the global boundary conditions. So, if there is any change in the connection strength (quality) or the global boundary condition or the structural stiffness of the member, its strain versus temperature slope will be altered from its original value. This is the concept behind collecting the base temperature readings for the structure under no load condition, so that its original slopes can be established. By monitoring these slopes over the years, an indication of changes in the structural system can be obtained by applying appropriate thermal corrections for the gauge. However, this methodology can only give an indication of change, it can not locate the position of such change; and it may not be very sensitive at all times. Hence, it can not be used as a stand alone system, but can be combined with other methods of damage detection for better reliability.

5.6 Parameters for Presentation of Field Testing Results

As mentioned earlier in section 3.6, three different field tests were conducted on the structure in October 2003, April 2004, and July 2006. The first field test in 2003 was when the thermal data and the base readings of the structure were collected under no load condition as well as under normal operation. During the second field test in 2004, data was collected under normal operation when normal production was in progress. And in addition, some data was also collected under a controlled testing condition when an effort was made to control some of the field variables. The third field test was conducted in July of 2006, which was entirely under normal operating conditions and no effort was made to control any parameter. Efforts in controlling operating conditions directly affect production and its cost, hence, the automatic choice of data collection is under normal operation. The common thing between all the tests conducted at different times was that they were all collecting data under similar type of oil sand dumping into the hopper. The primary differences between the tests were that – firstly they were collecting data at different times and secondly the dumping parameters could vary between each dump event. The influencing parameters have been identified as dump speed, hopper material level, and side of dump. During control testing these parameters were known, but during normal operation they were not known.

When presenting data in a statistical sense, although the data were collected at different times, no effort is made to discriminate them based on difference of a year or two between them; hence, all the data constitute the same population for statistical purposes. As discussed earlier in sections 4.2 and 4.3 of data processing, each dump event records a sudden increase in strain at each gauge location followed by a rapid fall and then a gradual decrease for gauges located in tensile zones. For gauges located in compressive zones, the same phenomenon is observed in the opposite sign sense. Thus, for each dump event and at each gauge location a strain jump is observed, which can be identified and stored by the data processing software. The only difference observed between different dump events and at different gauge locations is in the magnitudes of strain jump and static strain detected. For some dump events and at some gauge locations the strain jump is much higher, whereas at other locations it may be much lower. Hence, the strain jump at each gauge location can be treated like a random variable and the mean and standard deviation of strain jumps at each gauge location for various dump events can be calculated. The statistical analyses and distributions at each gauge location are discussed in detail later on in chapter 7. In this section, the focus is to discuss about the general structural behaviour of the crusher under a typical load and under different loading conditions.

5.7 Behaviour under Controlled Empty Hopper Dumping

As discussed earlier in section 5.2 regarding understanding the load, a million dump events occur every five years on the structure, however, the empty hopper dumps are the ones that produce the severest response from the structure. The simplest reason for high strain readings observed during such dumps is due to the greatest height of fall for the oil sand before hitting the hopper, which is close to 10 metres when empty. The force of impact is high and at the same time there is no cushion of existing oil sand available to dampen the impact a little because the hopper is empty. This section presents the strain jump magnitudes recorded at each gauge location for the most severe empty hopper dump from the left (north) side recorded during control testing in April 2004 in a graphical way. The dump event is identified as C1-L, where C stands for control testing and L for left side dumps. The response due to any other dump event would be similar, but much lower in magnitude. The pattern of strain distribution along different gauges might change with change in dump parameters though. More discussion into strain patterns would be conducted later on in the chapter. A similar behaviour would be expected for the dumping from right (south) side, but in a mirror image fashion because the crusher structure is symmetric.

5.7.1 Strain Jump along Column Gridlines

The strain jump magnitudes observed at different gauge locations are grouped together by their location for clarity of presentation and comparison. For example, all the forty column gauges from gauge number 1 to 40 are grouped and presented with respect to the column gridline they fall on. The cross sections of columns at various gridlines of the structure are identified and explained in chapter 3 section 3.5.2. Figure 5.12 shows the strain jump distribution at gauges along gridline 2. Negative strain jump means reduction in strain gauge reading occurring under compressive forces. Thus, compressive strains are negative and tensile strains are positive, which is exactly as obtained from the data acquisition system. Since the strain jump database is populated by the data processing software that operates on data recorded by the data acquisition system, the sign convention in this section is kept the same as that obtained from the sensors. However, later on when doing finite element modelling the sign convention would be reversed in order to conform to standard notations for tension and compression. Figure 5.12 shows, as expected, that the columns on the right side experience compressive stresses, where the left side dump hits with a trajectory. Some of the oil sand also falls on the left side of the hopper but the majority of it follows a trajectory motion to hit the right side of the hopper. The columns on the left side of the gridline 2 experience tensile stresses and the columns on the right side, where maximum impact force acts, experience compressive stresses. The maximum compressive strain observed and recorded with negative sign was at strain gauge C1 with a magnitude of 162 micro-strains. The maximum tensile strain on the left side columns of gridline 2 was observed to be 124 micro-strains (gauge C25). All the columns on the left side (gauge C25 to C28) exhibit tensile stresses whereas the columns on the right side do not all display compressive stresses. The outermost column on the right side (gauge C4) develops tensile stress compared to all others showing compressive stresses. Such behaviour can be attributed to presence of some local bending behaviour in addition to the compressive loads. The bending stresses can be a product of horizontal component of dumping forces or a second order effect combined with other factors.

A look at the strains on gridline 4 shown in Figure 5.13 reveals that the level of stresses experienced at gridline 4 is much higher than that at gridline 2. The maximum compressive strain of 757 micro-strains (gauge C8) is many times higher than the strains on grid2. It is worth noting here that the highest compressive stresses were detected in strain gauges C7 (657 με) and C8 (757 με) that are both placed on the flanges of a bracing member. The maximum compressive strain on any vertical member at grid4 happens to be 357 με at gauge C10. Even this value is two to three times higher than what was observed at grid2. However, the most important point here is that the bracing members are experiencing strains much bigger than any vertical columns. In addition, there also appears to be some bending occurring in the bracing member as depicted by the difference in strain jump between the gauges on either flange of the member (C7 and C8). Such large compressive stresses in bracing members and presence of bending suggest that the design of these elements need to be revisited in the near future. Relatively lower stiffness of these bracing members can also be a source of many other second order effects and excessive vibrations as experienced in the case of double roll crusher (DRC7) (Fowler and Gonzalez, 2000; Obaia and Gonzalez, 2001). Limited investigations conducted on the structure at that time was inconclusive in pin-pointing any particular reason behind such large vibrations. However, looking at the level of stresses in the bracing members and repetitive nature of loading, it could be a case of large displacements and vibrations occurring due to reduction in stiffness of braces over years of operation. The reduction in stiffness could be a result of combination of accumulated fatigue damage in the member and changes in boundary condition due to loosening of bolts. Such damage or changes make the already deficient braces more vulnerable to vibrations. Hence, an immediate observation at this time is to keep the lateral braces under watch list for strengthening in future designs.

The stresses in other columns at gridline 4 (Figure 5.13) are small for the level of impact associated with empty hopper dumps, though it would definitely serve the structure better to have lower strains in the vertical load bearing members than what has been observed. This again points to increasing the stiffness of some of the vertical members. At gridline 4 local bending is also observed in the interior columns as portrayed by the tensile and compressive stresses in strain gauge pairs C5-C6 and C32-C31. Interestingly, columns on both the left and right side of the hopper experience compressive stresses in general except for the local bending at the interior columns. This is primarily due to the fact that most part of the oil sand dump goes on to hit the right side, but some portion also falls on to the left side hopper in the vicinity of gridline 4 columns. The grid2 columns do not pick the compressive stresses due to the partial material on the left hopper, but the grid4 columns do, obviously because they are closer to the location of fall.

Figure 5.14 shows the column strains at gridline 5, wherein the inner gauges are on vertical members like gauge C13-C14 on the right side and gauges C37-C38 on the left side of the crusher centreline. The outermost gauges C15-C16 on the right side and C39-C40 on the left are placed on inclined struts that are supporting vertical columns on top of them. So, ideally the struts should be generating pure tension or pure compression, most of the time compression owing to their location and type of vertically downward loading. This indeed happens to be the case here with both the struts on the left and right sides displaying compressive strains. The strut on the left side seems to be in perfect compression without presence of any bending component. However, the strains on the right side strut (C15-C16) indicate significant bending with compressive strains in the range of 150 and 300 με. As discussed earlier that the right side of the hopper is more heavily loaded, it is only natural that the right side struts are subjected to higher compressive stresses. The vertical column on the right side with gauges C13 and C14 also shows local bending strains combined with axial compression varying from 81 με tensile to 146 με compressive. In general, the stress levels at column gridline 5 are lower compared to those at gridline 4. In fact, gridline 4 columns experience the most severe stress levels of all column groups.

The nature of stresses at column gridline 6 has a larger magnitude of almost double of those at gridline 5 (Figure 5.15). All the gauges shown in the figure are placed solely on the right side of the crusher and the columns on the left side at grid6 are not instrumented. So, conclusions can be drawn based on similarities with grid5. The gauges C23 and C24 belong to the strut on the right side supporting a column on top of it. Fortunately, this strut shows no sign of bending and a uniform compressive strain of about 435 micro-strains is observed. Gauges C 17 and C18 on the extreme left are placed on the inclined bracing, which is subjected to significant bending instead of axial stresses. Strains vary from a compressive 460 με to a tensile 450 με, behaving as a pure bending member. Owing to the higher magnitude of observed strain, this bracing member also falls into the list of elements suggested for review in the future. The vertical composite column has four gauges from C19 to C21 mounted on it and shows a uniform bending combined with axial compression with compressive strains varying from 100 με to 20 με.

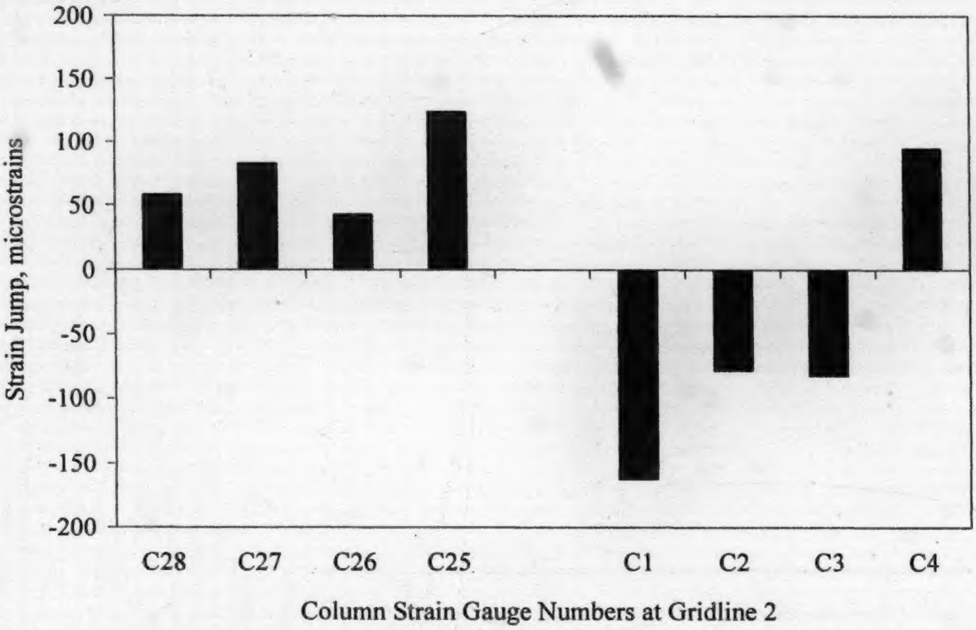

Fig. 5.12 Strain jump at column gauges on gridline 2 for dump C1-L

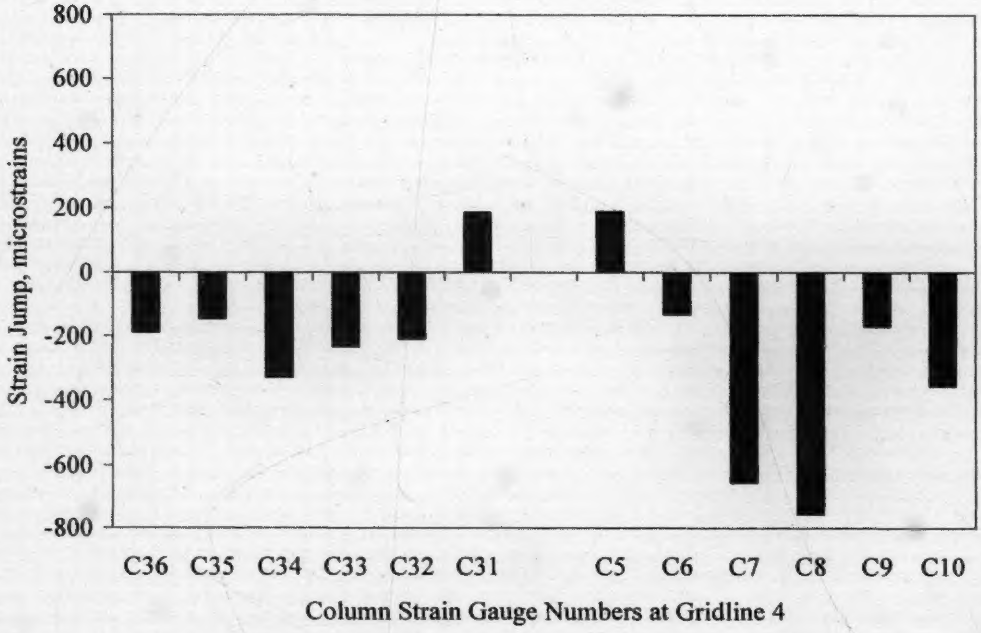

Fig. 5.13 Strain jump at column gauges on gridline 4 for dump C1-L

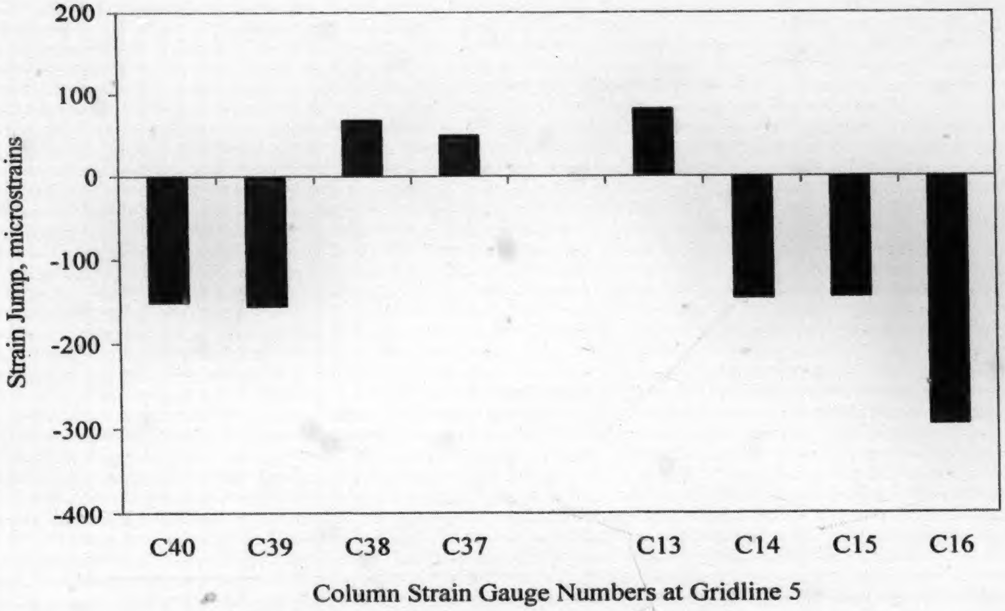

Fig. 5.14 Strain jump at column gauges on gridline 5 for dump C1-L

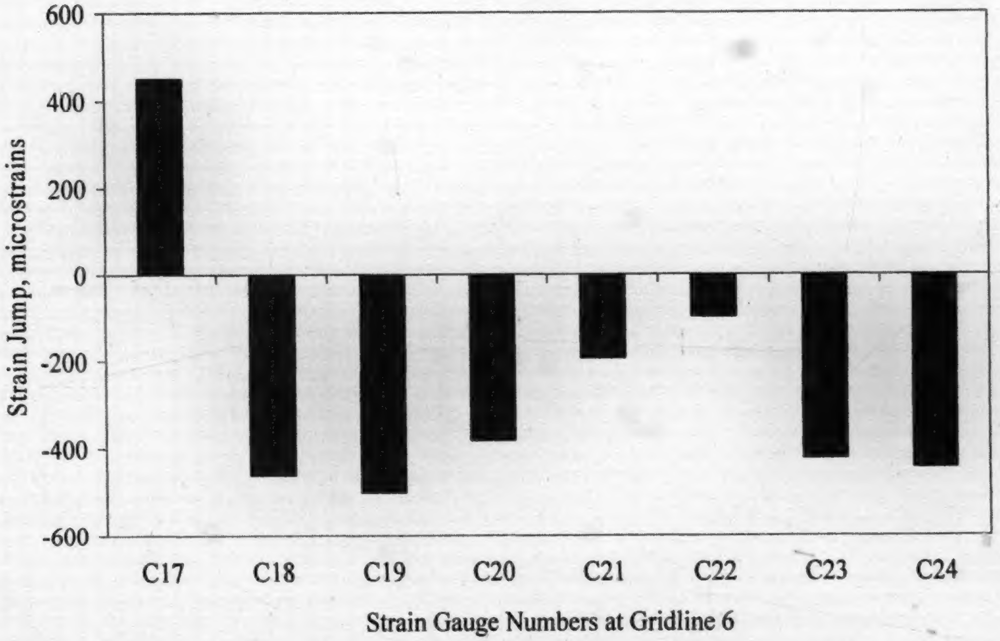

Fig. 5.15 Strain jump at column gauges on gridline 6 for dump C1-L

After discussing the stresses encountered in all the column gauges at all gridlines there have emerged three clear sets. The first set includes the vertical columns with low strains and minimal local bending. The second set includes those vertical columns with relatively higher compressive strains combined with some local bending. The third set is that of all inclined braces and struts that are supporting the vertical columns. This third set seems to be the most vulnerable under severe loading conditions, where high axial compression and sometimes large bending behaviour are also observed. The members falling into the second and third sets need to be re-evaluated for future designs. In order to further stress the effect of axial stresses combined with bending and to highlight the members where they are significantly high, the axial and pure bending components of strains have been separated and plotted in bar chart format in Figures 5.16 through 5.19. The average of strains on two flanges gives the pure axial component of strain, whereas half of the difference between the two strains gives the pure bending component of strain.

A quick look through the graphs (Fig. 5.16 to 5.19) reveals that the maximum bending stresses are occurring at the braces in gridline 6 (Figure 5.19) in the range of 450 micro-strains at gauges C17 and C18. A vertical column (gauges C19-C20) and another inclined strut (gauges C23-C24) at the same location also experience high axial strain of 450 micro-strains. The highest axial strain is however observed in the braces at gridline 4 (C7-C8) in the range of 750 micro-strains compressive (Figure 5.17). The bending strains at that location are 200 micro-strains in two of the inside vertical columns (C5-C6 and C31-C32 pairs). These high strains observed in pure bending and axial again suggest that the vertical load bearing system's performance under severest load condition is less than satisfactory because strains are reaching close to 40% of yield limits under live load alone, and these are real loads that can happen on the structure a couple of times in a month (or a year). Most importantly, these are the strains observed entirely under dumping or live load condition. There are other unaccounted stresses due to sustained load, operating machinery and temperature, which are significant in the oil sand industry. When taking all of them into account, there does not seem to be much factor of safety left to take care of other unforeseen circumstances. In addition, repetitive loading under high stresses will lead to fatigue, especially at joints that are always under complex high stresses.

A look into Figures 5.16 through 5.19 also reveals that the vertical columns are either subjected to high bending or high axial stresses, both bending and axial stress are seldom occurring together. This is not the case with the inclined braces and struts, which repeatedly face high axial strains in addition to high bending strains, except for C17-C18. At almost every gridline there is at least one vertical column that is subjected to high bending stresses. The only exception to this is gridline 6 where the vertical columns are not subjected to high bending, but the bracing is. This is an indication that significant lateral horizontal forces are acting at these gridlines. At all these gridlines 2 to 5, the axial component of strain in vertical column members is relatively much lower compared to the higher strained inclined bracing members. This again points towards the existence of significant lateral horizontal forces. All the vertical columns are moderately strained in pure axial compression at most times within a range of 100 to 200 micro-strains. The only location where the vertical columns are subjected to the highest axial compression of 450 micro-strains occurs at gridline 6 in Figure 5.19, as mentioned earlier. This leads to the conclusion that the vertical column members are moderately stressed in general, except at gridline 6.

Another important feature worth noting in the figures is that the axial component of strain is mostly compressive in nature, which is as expected. Except for some vertical columns on gridlines 2 and 5, where axial tensile components of about 50 micro-strains were observed, all other vertical columns were carrying axial compression with minimal bending. The bracing members and struts at all gridlines were always subjected to axially compressive forces in addition to bending. The inclined struts and bracing members experienced generally significantly high axial component of strain in addition to some bending. In some extreme cases, the bending component of strain became much larger, examples of which are gauge pairs C7-C8 and C15-C16 at gridlines 4 and 5 respectively. It can be concluded in general that the bracing members and struts are stressed close to

40% of yield strain in either axial compression or bending or both under severe live load dumping alone. This is the problem area that needs to be addressed in future design.

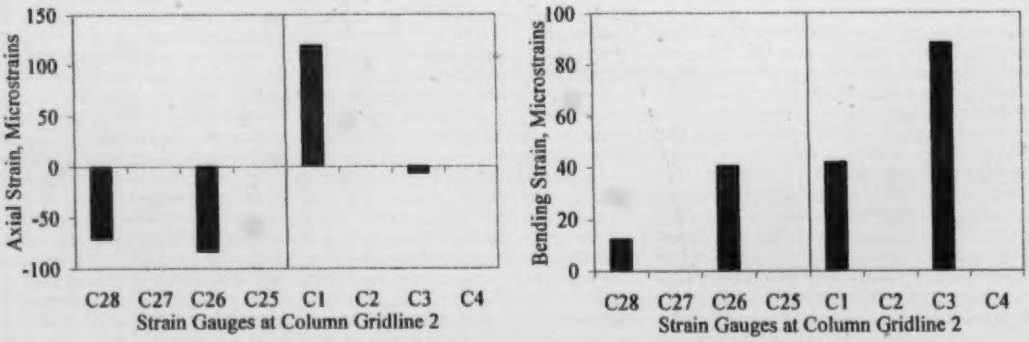

Fig. 5.16 Axial and bending strains separated at gridline 2 column gauges

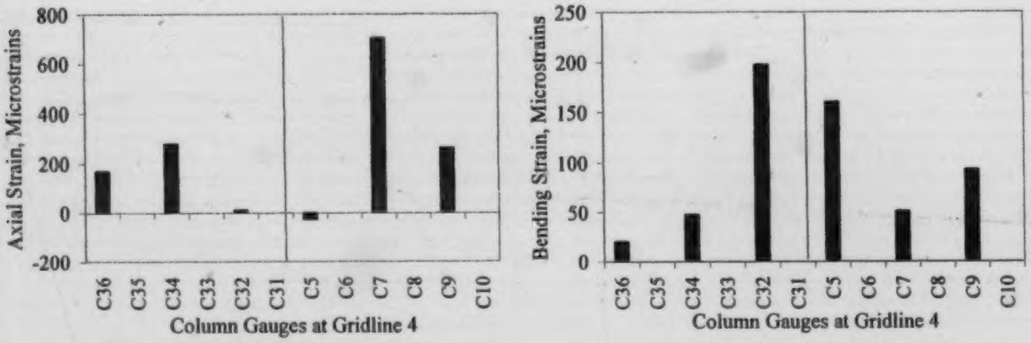

Fig. 5.17 Axial and bending strains separated at gridline 4 column gauges

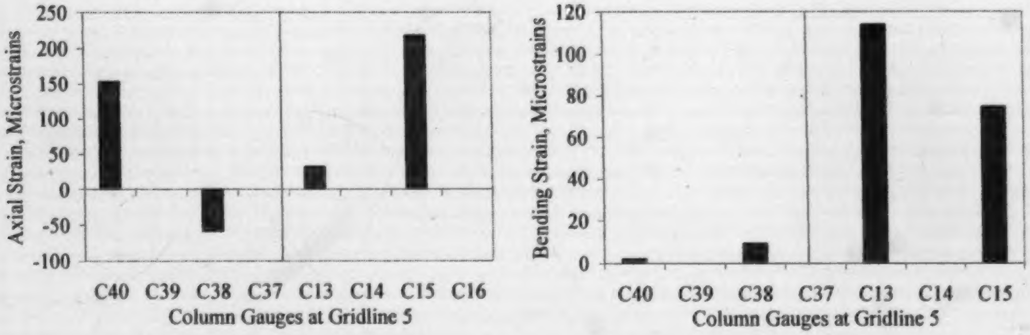

Fig. 5.18 Axial and bending strains separated at gridline 5 column gauges

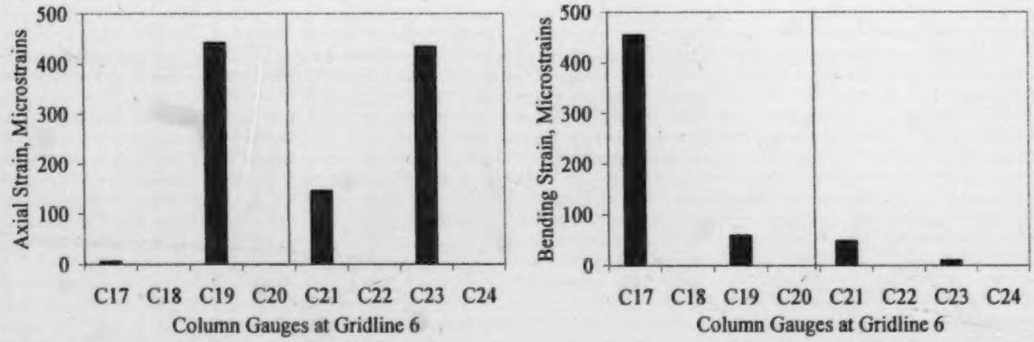

Fig. 5.19 Axial and bending strains separated at gridline 6 column gauges

5.7.2 Pontoon Behaviour under Empty Hopper Dumping

The pontoons are basically plate box girders (beams). Hence, the maximum strains were obtained near the mid span. The odd numbered gauges such as P45, P47 to P53 are located in the compressive zone, whereas the even numbered gauges such as P46 to P54 were placed in the tensile zone (Fig. 5.20. The gauges on either ends of the pontoon (beam) in shear span, P45-P46 and P53-P54, are shown at either ends of the bar chart in Figure 5.20 with lowest strain readings. Similarly, the gauges at mid span with maximum bending stresses are shown in the central (mid) portion of the bar chart. Gauges P47 to P52 are located in the bending region with P51 and P52 being the compression-tension gauge pair closest to the mid-span. Maximum tensile strain of 230 με and compressive strain of about 130 με were observed in mid-span section of the south side pontoon for the north side dump C1-L. Compared to the level of strains observed on the column gauges, the strains observed at the pontoon are of much smaller magnitude, which indicates a more sturdy design of the pontoon. However, it has to be borne in mind that the pontoon gauges are not located exactly at the extreme compression or tension fibre of the beam due to practical reasons. Hence, the actual strains there would be marginally higher than those observed at the gauge locations. It is also worth mentioning here that these are the strains associated with the severe empty hopper dump event, which is supposed to be limited in occurrence to 4 to5 times a year. Most of the time the hopper is more than 50% full, hence the strains jumps are much lower under normal operation. Figure 5.21 shows the absolute value of strains due to the same dump C1-L plotted on the positive side of the axis and Figure 5.22 shows the comparison of these strains to strains from other dump events under normal operation. The strains under severe empty hopper dumps are the highest compared to other dump events.

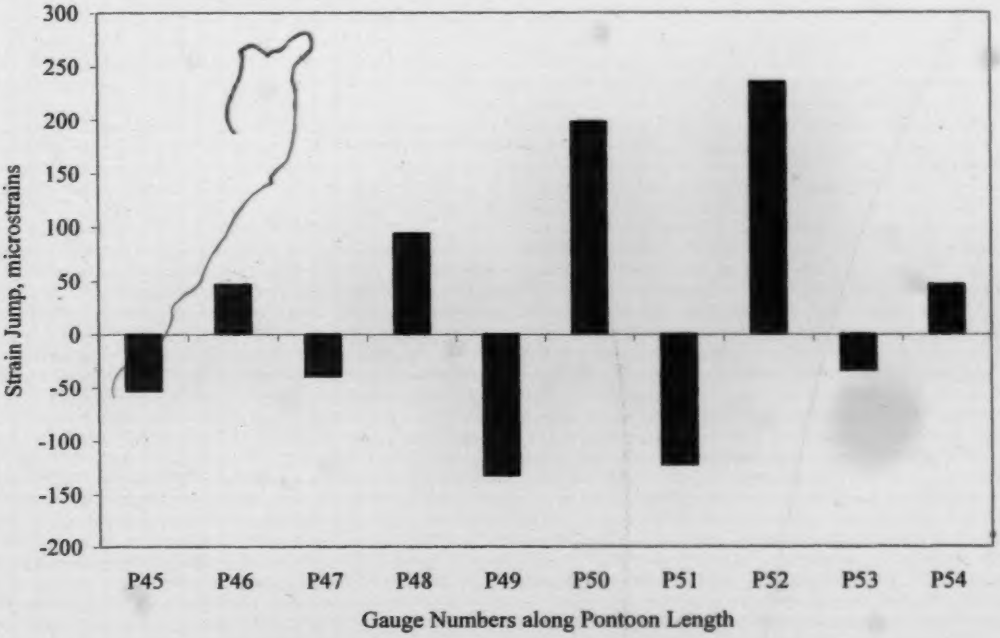

Fig. 5.20 Strain jump recorded at pontoon gauges for dump C1-L

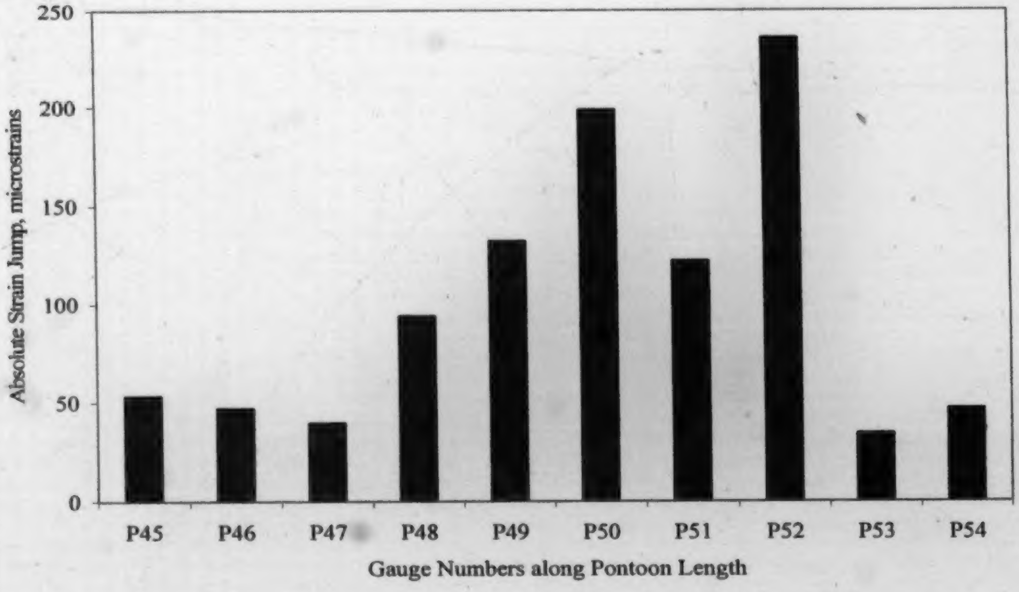

Fig. 5.21 Absolute strain jump recorded at Pontoon gauges for dump C1-L

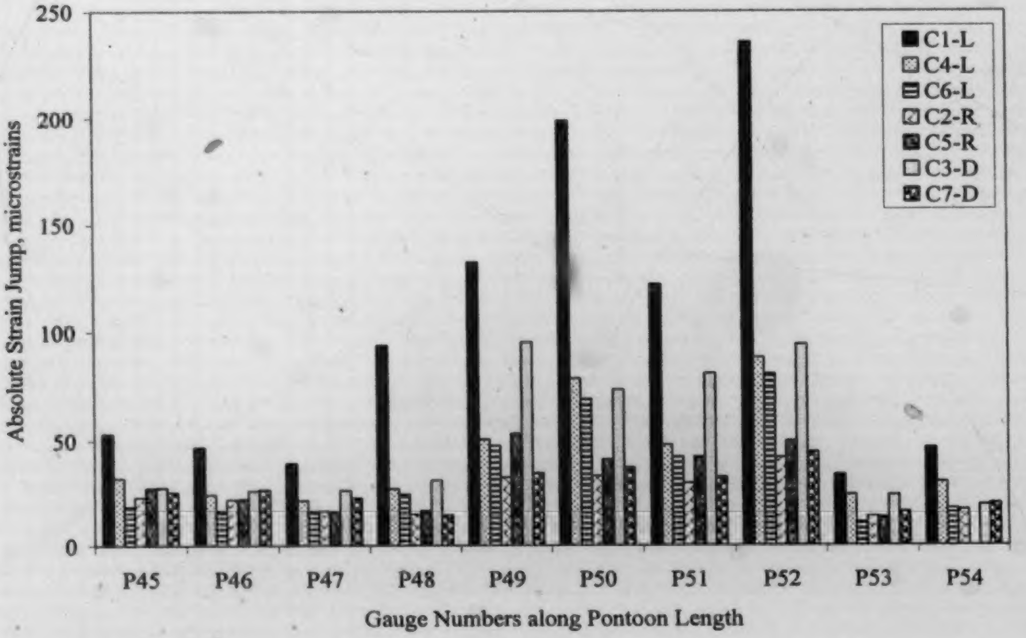

Fig. 5.22 Absolute strain jump recorded at pontoon gauges for various dump events

5.7.3 Hopper Behaviour under Empty Hopper Dumping

Out of the ten strain gauges placed on the hopper and shown in Figure 5.23, only two gauges H59 and H60 are located directly on the hopper plate in mutually perpendicular directions. The rest of the eight gauges are all placed on the horizontal and vertical stiffeners below the hopper plate. Interestingly, all the hopper gauges on the stiffeners produced compressive stresses under the dump C1-L, with maximum strain jump values of 200 micro-strains (Figure 5.23). This indicated that the hopper was bending as a cantilever and the tension face lay on the inside of the hopper and compressive on the bottom outside where the gauges have been placed. The gauges on the plate showed tensile strain in one direction and compressive in the other signalling some complex bending behaviour in the hopper plates. The strain jump recorded at the hopper gauges are much smaller in magnitude than those recorded at the column gauges, which is a good indication to the fact that the hopper gauges were probably not placed in the zone of maximum impact under the dump C1-L. Intuitively, hopper gauges should be most influenced by impact due to their proximity to the impact source.

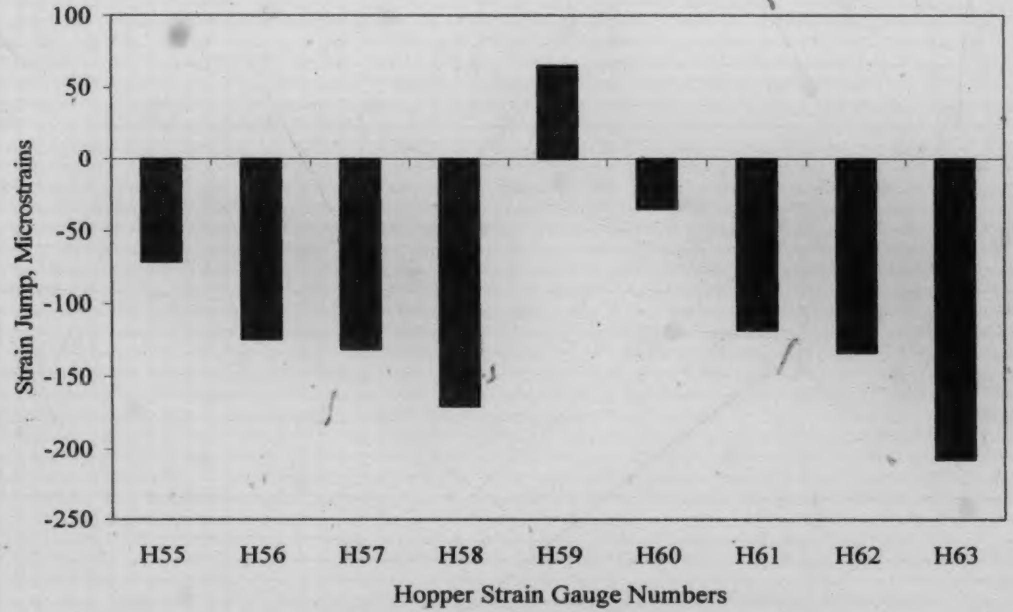

Fig. 5.23 Strain jump recorded at hopper gauges for dump C1-L

5.8 Impact Factor

Impact factors have been traditionally used in the design of industrial and civil structures. Modern computing technology does make dynamic analysis possible for design of important long span / slender structures, which are susceptible to wind and earthquakes. However, in industrial designs, impact factor based methods remain dominant. The major reasons for this being traditionally available design methods, satisfactory performance over the years, and unpredictability of loads. More often than not, industrial designs are relatively heavy making the structure stiff enough to nullify the effects of dynamics and vibrations, simply by assuming relatively high impact factors in design. Certain impact factors were assumed for design of the Aurora II Crusher based on past experience and now it is imperative for the SHM system to be able to shed some light on the real life impact factors for future designs.

5.8.1 Definition of Impact Factor

Different definitions of the impact factor are used by different researchers. However, most of the definitions lead to values that are quite close to each other. Hence, no attempt is made to go into any lengthy discussion on the right definition; rather an informed choice is made and consistently used for the purpose of this project. Impact factor is defined here as the simple ratio of maximum dynamic strain change observed during a dump to the static strain change due to the same dump. The dynamic strain change is obtained by the difference between peak and trough of strain curve during a dump event. This is nothing but the strain jump parameter discussed before, which includes the influence of both static and dynamic effect. Now, the static strain change associated with each dump is calculated by taking the difference of the average strains just before and after the dump. Care has to be taken to make sure that the average strain is not biased by its proximity to dynamic vibrations as well as it is not too far from the dump event to be affected by emptying of the hopper due to crusher operation. Fig. 5.24 illustrates the definitions of static and dynamic components of strain pictorially.

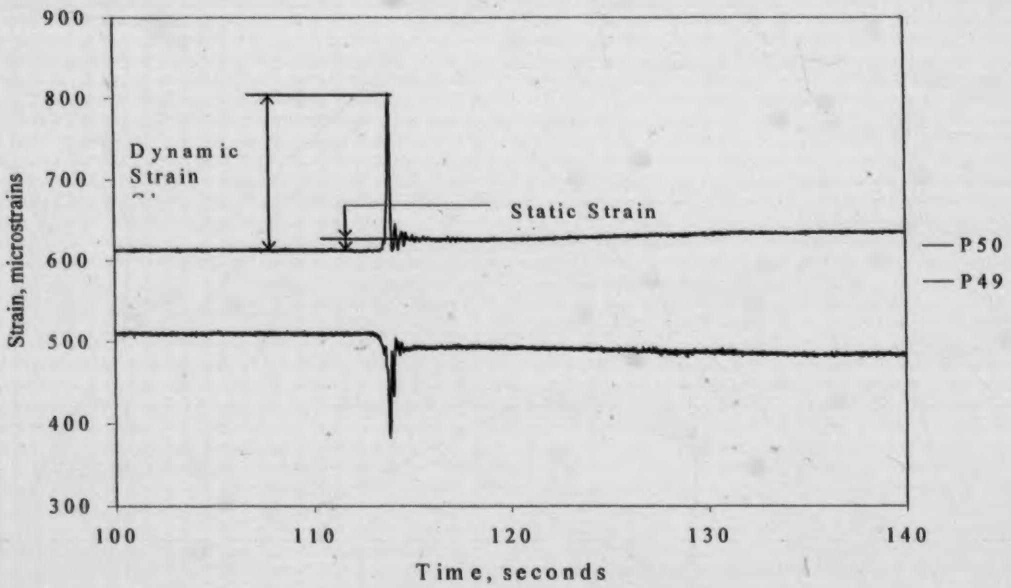

Fig. 5.24 Definition of impact factor

Figure 5.25 shows the static component of strain at the columns of gridline 6 for the empty hopper dump C1-L, where a maximum static compressive strain of 55 micro-strains is observed in the inclined strut gauge C24. The magnitude of static strains across different dump events would not vary by much from one event to another because in static sense they are caused by a similar static load of one truck load of oil sand. However, sliding of material in the hopper and the level of oil sand already existing in it will play a role in causing some variations in static strain. Such variations will be comparatively low for all practical purposes. The static strain associated with a double dump is larger because of the static weight of material coming from two trucks. However, the dynamic component from a single truck dump can be larger than a double dump depending on many other factors. The dynamic component of strain has a much larger variability depending on the many dump parameters, most importantly the height of fall. The strain variation due to dynamic effect has been observed to vary up to 800 micro-strains depending on the dump type and gauge location. For an empty hopper dump it can be very large, whereas for full hopper dumps it will be much smaller in magnitude. Figure 5.26 shows the static components and dynamic components of strain for the same

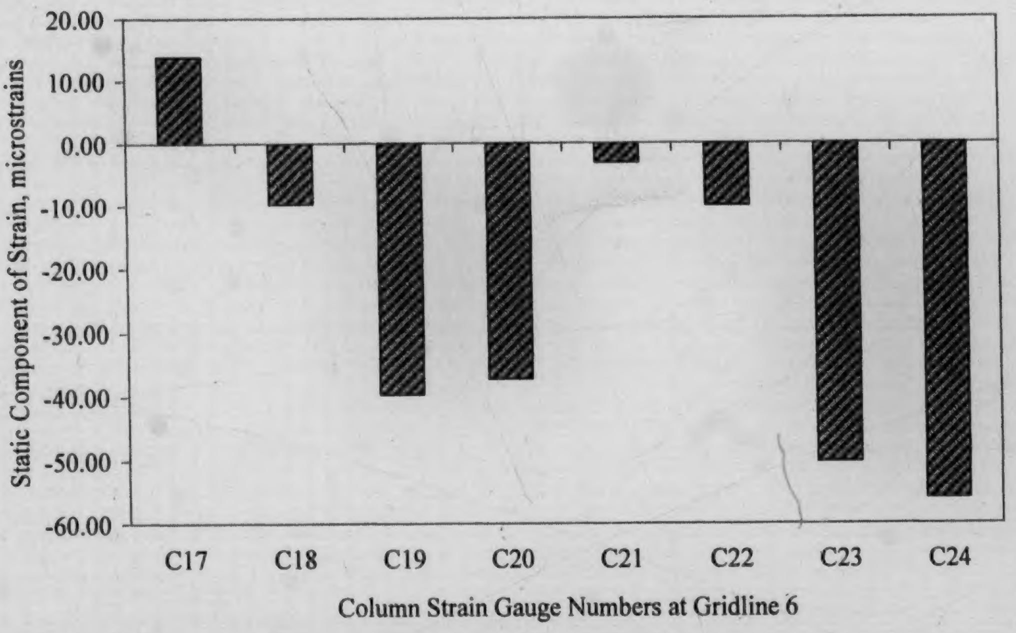

Fig. 5.25 Static component of strain at gridline 6 columns for dump C1-L

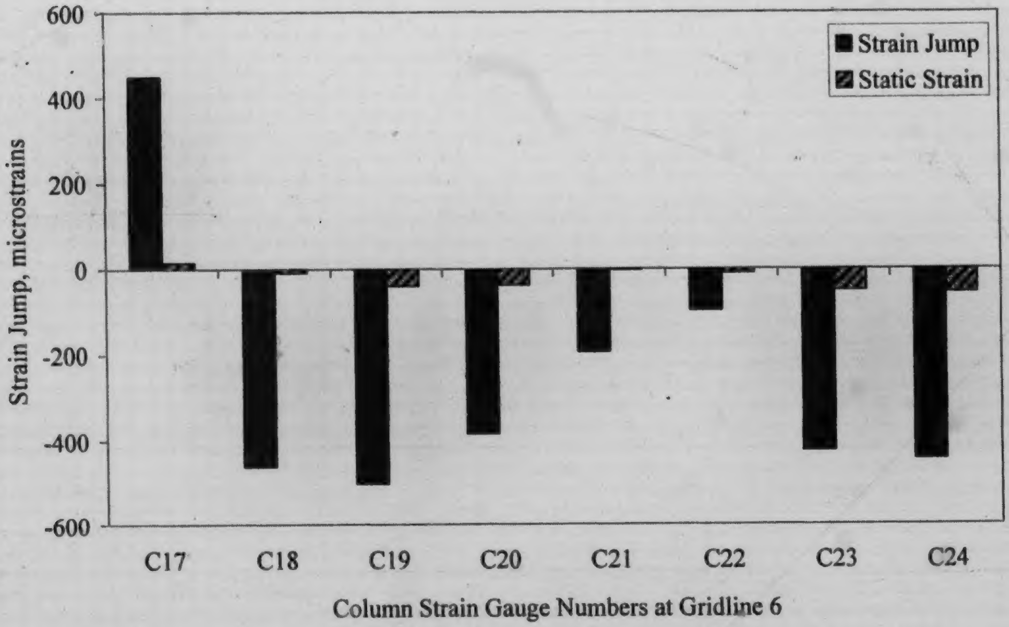

Fig. 5.26 Static and dynamic components of strain at grid 6 columns for dump C1-L

column gridline 6 for the same empty hopper dump event C1-L. It can be seen that the static strain looks so dwarf and almost negligible when compared to the dynamic component of strain. Taking the ratio of dynamic component with the static component, very large impact factors are obtained for this dump event. However, this will not be the case for all dump events, as is explained further in the following section.

5.8.2 Factors Affecting Impact Factor

The calculation of impact factor is quite sensitive to many factors. First and foremost, since it is a ratio against the static strain change, the magnitude of static strain change has critical influence on it. Particularly for low static strain change the impact factor calculation can be quite erroneously high. Hence, such extremely low data have to be identified and eliminated from consideration and for the most part, it can be seen that outliers single themselves out from normal data trends. On the same note, the impact factor value is also dependent on the location of the gauge being used in the calculation, depending on how sensitive it is to the global and local structural behaviour. An insensitive gauge to a particular load will produce little strain jump and hence, distorted impact factor. With careful consideration, unwanted effects due to magnitude of the numbers can be significantly reduced. The magnitude of strain jumps encountered in the case of severe dump events like controlled empty hopper dumps are quite high, hence, most of the values of impact factor calculated from such severe events are significantly high. Thus, the chances of distorted values in such dump cases are low compared to other normal operation dump events. However, there is still some chance of low static strain values at some less sensitive gauge locations and the influence of noise, which needs to be properly identified.

In the case of Aurora II crusher, other factors like the speed of dump, grade of oil sand, level of material in hopper, and weight of the dump significantly affect the strain jump magnitude; and consequently, the impact factor value calculated. In other words, the same truckload of oil sand dumped from the same height can produce completely different impact factor values depending on these factors. Obviously, the impact factor is especially high for rich ore dumped quickly on an empty hopper. On the contrary, lean oil sand dumped on a full hopper at a very slow rate would produce small impact factor.

5.8.3 Impact Factor Values for the Severe Empty Hopper Dump C1-L

Impact factor being a ratio, as already discussed, the low static strain values could be a source of highly distorted values. Hence, to avoid such errors and also to enable the designers a peek into the critical impact factor values while operating under severe dump conditions, this section presents the impact factors observed at all the sixty gauges under the empty hopper dump C1-L. Even with the most severe load in operation, there are still some gauges that record a much smaller static strain value compared to the strain jump value, which leads to extraordinarily high values for impact factor. Some of the gauges record low static strain component because of their location in low strain region, however, the dynamic component is still much bigger. This behaviour could be explained by the fact that after impacting the hopper, the dumped oil sand drops down to the bottom of hopper on the Apron feeder, thereby releasing the static strain to a negligible value at some locations. However, at most of the gauge locations, the impact factor values obtained were the true representation of the state of stresses occurring under impact.

Figure 5.27 shows the impact factor encountered at the ten strain gauges on the pontoon under the empty hopper dump C1-L. It is quite clear that at all times the impact factor remains below 25. In general, the values range between 10 and 15 at most gauges. A similar look into the impact factor values observed at the ten hopper gauges, as shown in Figure 5.28, reveals that in general the values varied between 10 and 40, except for one erroneous gauge with impact factor of 70. However, further investigation leads to the fact that four of the hopper gauges H55, H 60, H 61 and H63 were recording extremely small static strain of less than 5 $\mu\varepsilon$, hence the high impact factor values obtained at those gauge locations are unreliable. So, the maximum reliable impact factor on hopper is of the same order as those observed at the pontoon, about 10. However, when comparing this to the impact factor values obtained at column gauges in Figure 5.28, the hopper impact factors are comparatively quite small. Figure 5.28 shows the impact factor values at the column gridline 6 gauges, with values ranging between 10 and 60. This is the case at just one of the gridlines, a similar exercise at all the other gridlines would confirm the fact that the column impact factors (including braces and struts) are the largest of all. While the Strain Jumps observed at the pontoon and the hopper gauges were in a comparable range of 200 με, the Jump at column gauges were consistently stretching much higher up to 500 με and even 800 με. The highest strain jump on a vertical column was observed to be 500 micro-strains at gauge C19 on gridline 6, with an impact factor of 12.62. At another location on gridline 4, an impact factor of 8 was recorded for a strain jump of 400 micro-strains. The static strains in all these cases were also quite close to 40 and 50 micro-strains. Almost all of the forty gauges on columns experienced strain jumps higher than 50 micro-strains and many of them were cluttered around 100 micro-strains in average for vertical columns. The inclined struts and braces on the columns recorded the highest strain jump of all - close to 800 micro-strains. Most of the column braces registered strain jumps in the range of 500 micro-strains and impact factors between 20 and 50. As discussed earlier, this is a clear indication of vulnerability of bracing members under impact, whereas it seems the hopper gauges are not quite located in the region of hopper where the dumped oil sand is hitting, otherwise the values could be even higher due to local effects.

Figure 5.30 shows the impact factor values due to dump C1-L for all the sixty strain gauges across the structure plotted against their corresponding static strain values. It can be observed that as the magnitude of static strain increases, the value of impact factor decreases in general. Figure 5.31 shows the plot of impact factor values against strain jump. It shows the similar trend of decreasing impact factor with increase in strain jump, but with some randomness in the middle. The average impact factor is about 10, whereas for majority of the members (gauges) the impact factors are mostly under 20. There were only few countable exceptions to this rule and they pertained to either the gauges with very low static strains or column braces. Looking at the Figures 5.30 and 5.31 together, it can be noted that there are six gauges recording impact factors higher than 50, but they all have a moderate strain jump value between 50 to 100 με and a very small static strain value of 1 to 5 με. These are mostly column gauges at different gridlines with extremely low static strains, hence, these impact factors have to be simply disregarded from consideration as distorted. Such low static strains are occurring due to migration of the static load after impacting the hopper. The impact factors greater than 20 (but less than 50) are also severely affected by low static strain values. Out of the eight data points in the region in Figure 5.30, six of them were due to low static strains below 5 με occurring at three of the hopper gauges, two pontoon gauges and one column gauge. However, there were two data points with impact factor greater than 20 and static strain larger than 10 με. It can be seen in Figure 5.31 that these gauges also have a much higher strain jump close to 450 με, and they belonged to gauges C17-C18 on the column brace at gridline 6. Thus, except for these two values of impact factors, all other values higher than 20 can be neglected owing to error due to low static strain. The average impact factor at most gauge locations under empty hopper severe loading can be taken as 10, varying within the extremities of 1 to 20.

When looking into the data points with the largest values of static strain on Figure 5.30, it is found that the highest values of static strain to the range of 80 με belong to the braces at gridline 4, followed by braces and column gauges on gridline 6 and 5 with static strains from 40 to 60 με. These are the gauges which record the minimum impact factor in spite of having the maximum static strain, and probably also large strain jump. It can be observed on Figure 5.31 that the magnitudes of strain jump observed on all the sixty strain gauges were either close to or much higher than 50 με, the highest strain jump being close to 800 με. These maximum values of strain jump are occurring at the bracing members on gridlines 4 and 6 from 400 to 750 με, followed by other column and bracing members. The impact factor values for these high jump gauges are all 10 or higher, mostly less than 20 but two of them close to 50. These two are the gauges C17 and C18 at gridline 6, as discussed earlier.

This fact is further highlighted in Figure 5.32, which shows the variation of strain jump with static strain change for all strain gauges on the structure. It can be seen that most of the data fall along a linear relationship meaning that strain jump keeps increasing with increase in static strain values. The slope of this straight line is nothing but the Impact

Factor as per the definition adopted. Graphically, the average impact factor of 6.2 with 56% correlation is given by the straight line with slope of 6.2 in Figure 5.32. The only clear anomalies to this linear relationship are the circled data points lying far away from the straight line; and all of them belong to the inclined struts/braces. Thus, the relation between static component and dynamic component of strain for the column struts and braces appear to be markedly different compared with other parts of the crusher. On removing all the circled data points corresponding to the inclined struts and braces and redrawing the graph as shown in Figure 5.33, it can be seen the correlation coefficient of the strain jump and static strain data increases substantially from 56% to 75%. The new slope of the averaging trend line is about 7.2, but this line does not pass through the origin although it does have the best R^2 value. Setting the intercept of this line to zero forcing it to pass through the origin as shown in Figure 5.34, there is a slight drop in correlation coefficient and at the same time an increase in slope. The new slope is about 9.1, which is quite close to the average impact factor of 10 suggested earlier; hence, this is the minimum impact factor that must be adopted in the design of every component of the structure.

Thus, pontoons appear to be the most robust in terms of impact vulnerability, while the hopper and a few of the columns fall in the medium range, and the inclined bracing members and struts were the ones calling for attention. One of the major reasons behind this is the relatively small cross sectional areas of the struts that make them prone to vibration and bending in addition to axial compression under impact; hence, they should be reviewed in the future. Under normal operation, however, such high strains were not common.

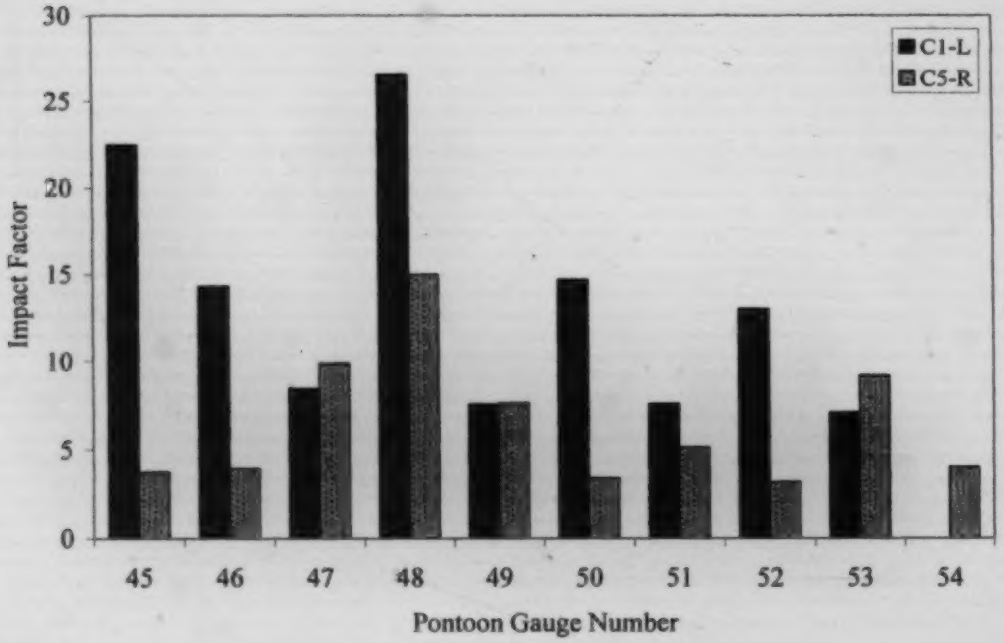

Fig. 5.27 Impact factors at pontoon gauges for dump C1-L

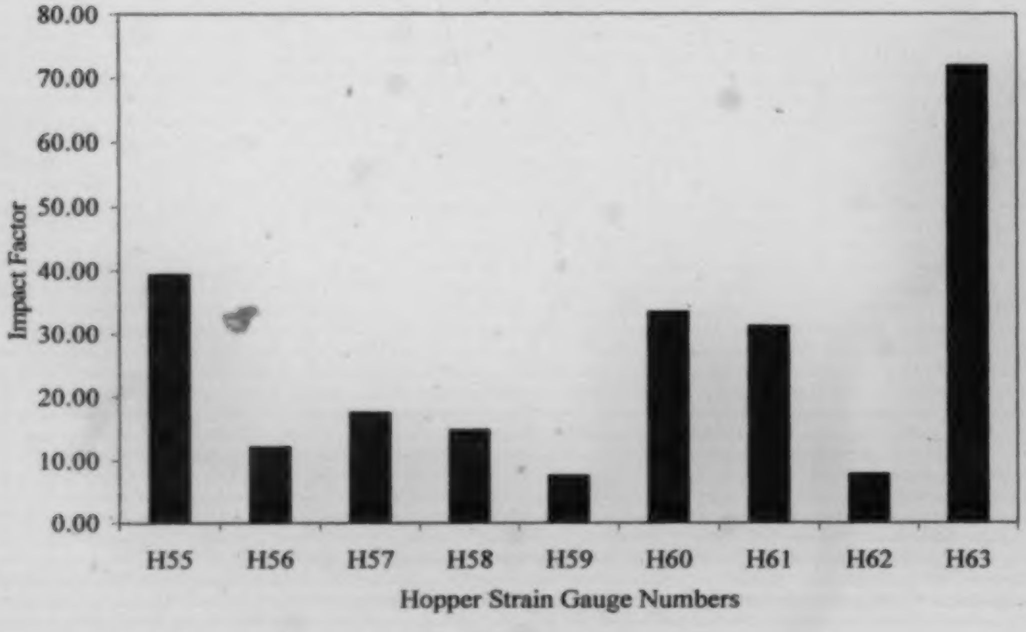

Fig. 5.28 Impact factors at hopper gauges for dump C1-L

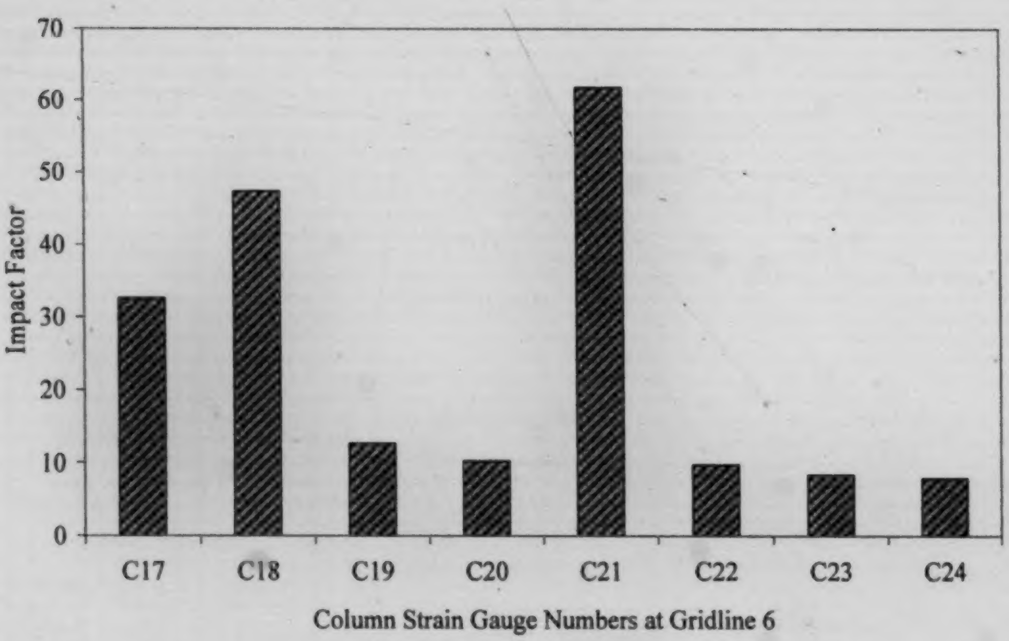

Fig. 5.29 Impact factors at column gridline 6 for control dump C1-L

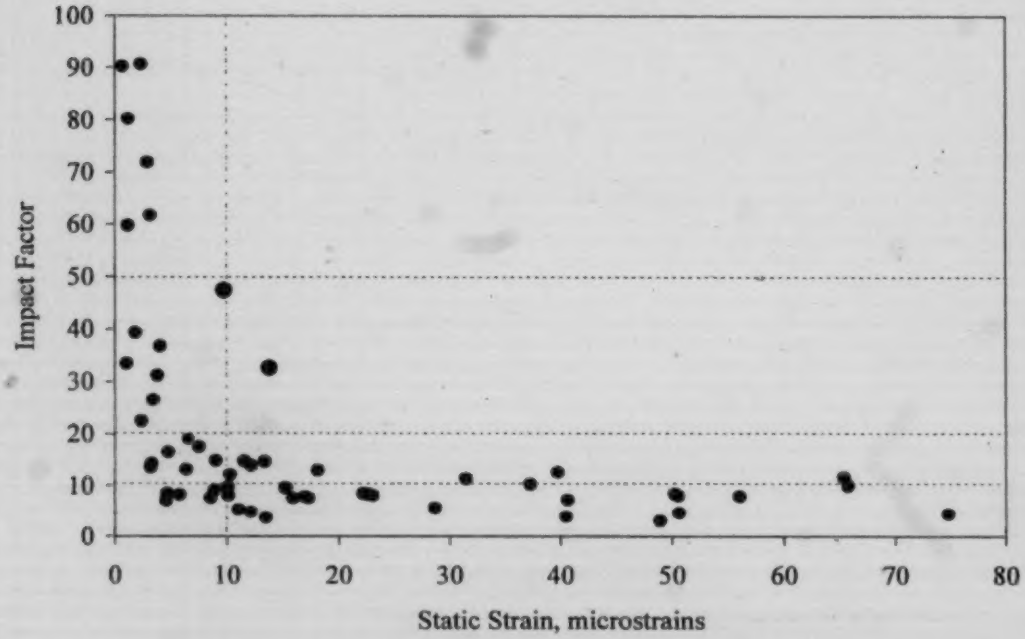

Fig. 5.30 Impact factor variation with static strain for dump C1-L

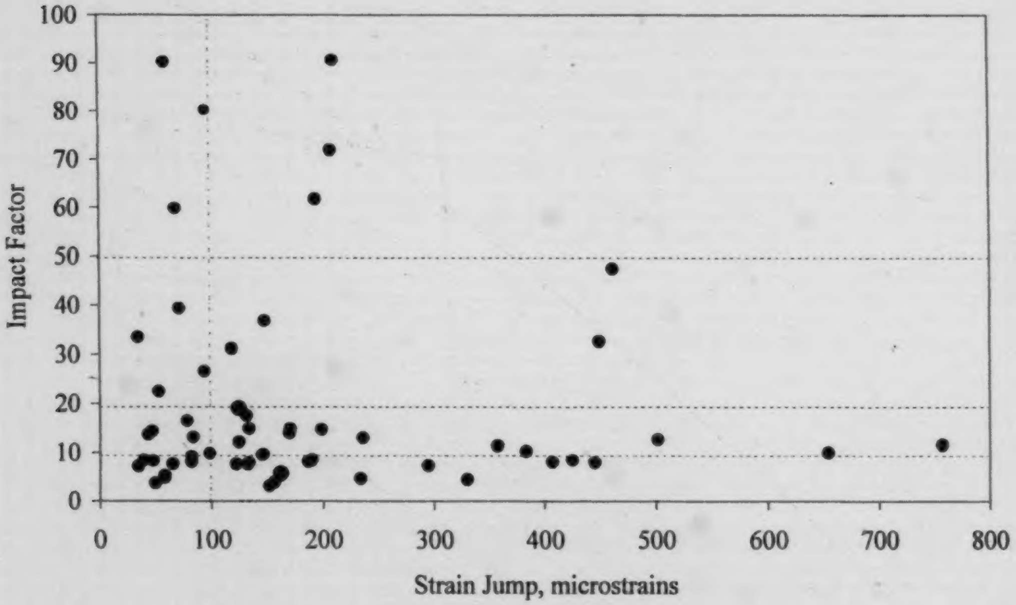

Fig. 5.31 Impact factor variation with strain jump for dump C1-L

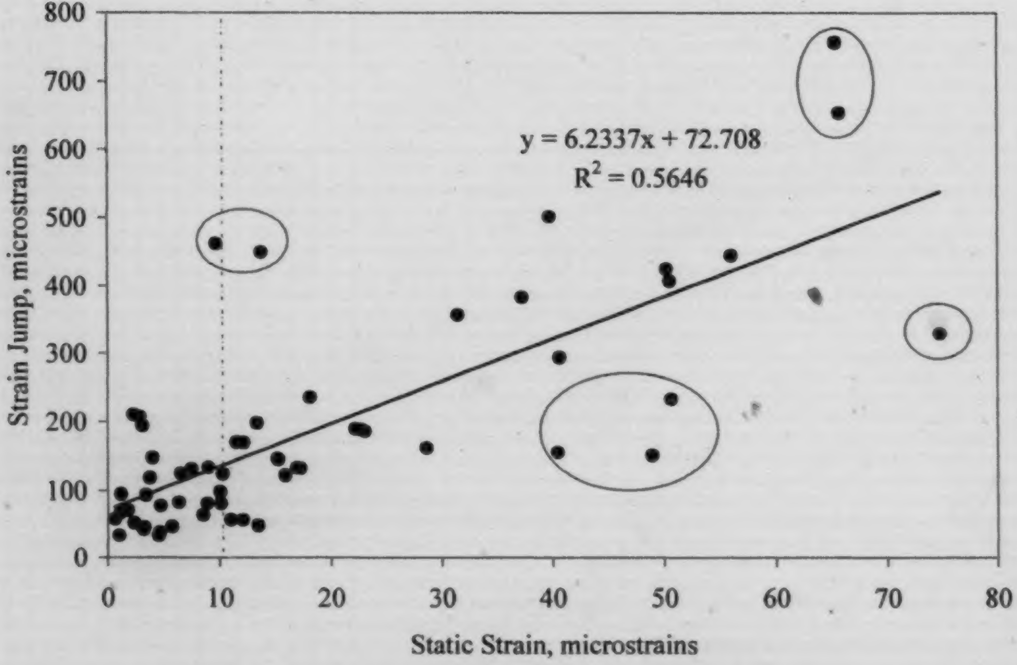

Fig. 5.32 Strain jump variation with static strain for dump C1-L

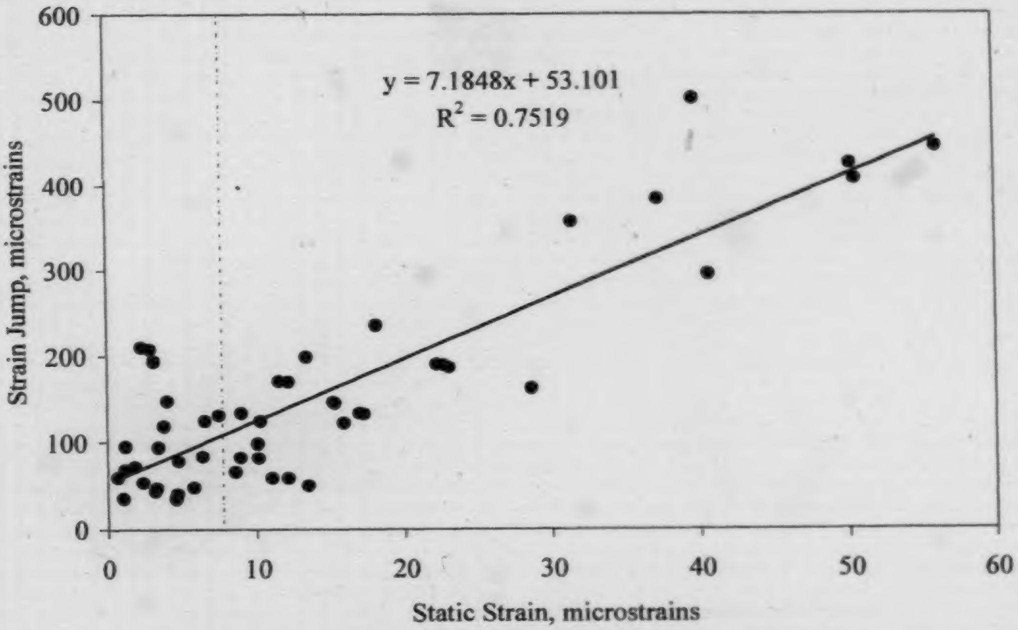

Fig. 5.33 Strain jump variation with static strain for dump C1-L

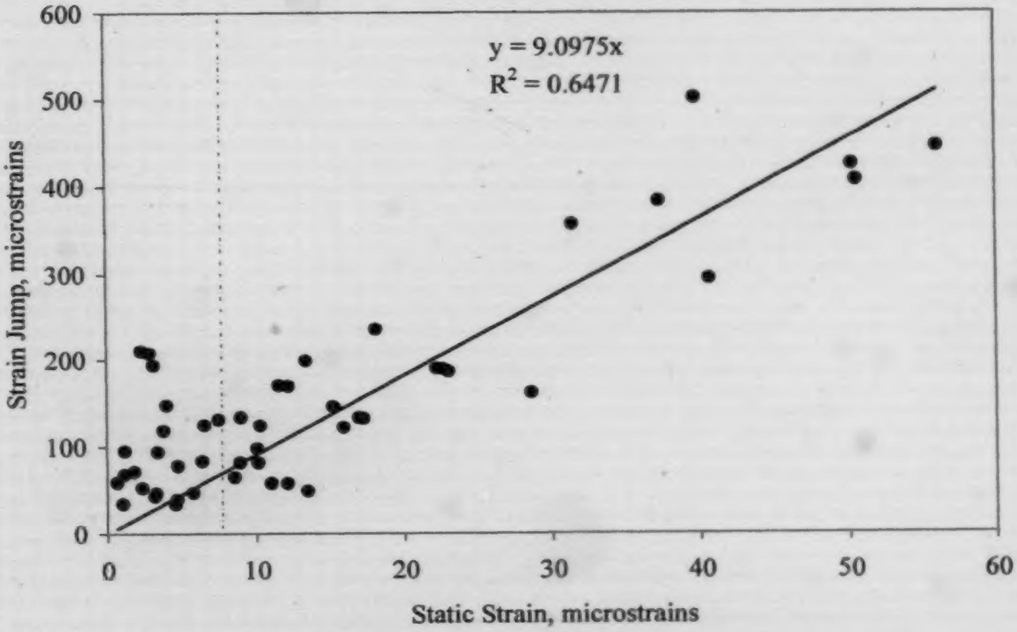

Fig. 5.34 Strain jump variation with static strain – new slope

5.8.4 Average Impact Factor on Pontoon during Normal Operation and Control Tests

The previous section dealt with the impact factors observed during the most severe single empty hopper dump event. This dump event brings to fore the maximum values of impact factor experienced by each structural member that should be kept in mind while designing. Now, this section deals with more than one dump event when the crusher is under normal operation along with controlled testing. The goal of this exercise is to get the usually occurring impact factors at different structural components under normal operation and to highlight a few other points about them. The values of impact factor were calculated for each dump event at each of the ten strain gauges on the pontoon. Data collected for 13 of the dump events during control testing produced 130 values of impact factor on the pontoon gauges ranging from 1 to 140 in magnitude, which is plotted against the static strain change values in Fig. 5.35 to Fig. 5.37. Obviously, the first task was to separate meaningful data from distorted data and outliers. As depicted by the averaging trend-line in Fig. 5.35 and Fig. 5.36 with a close up view, the value of impact factor is highly sensitive to change in static strain in the small magnitude range. The trend lines of logarithmic or exponential nature are found to closely match the data scatter. Impact factors calculated for associated static strain changes of smaller than 2 micro-strains are extremely high and unrealistic because such low strains can be categorized as noise, which is of the order of 5 to 10 micro-strains. Thus, too small a static strain mired in noise produce very high distorted impact factors like 80 or 140, which should be neglected from discussion for lack of sufficient evidence. In the same breath, impact factor values obtained for static strain changes of more than 5 micro-strains seem quite stable and repeatable at different gauge locations, whereas the accuracy of the transition region between 2 and 5 micro-strains remains questionable.

Between the static strain changes of 5 to 42 micro-strains, the impact factor values vary between 1 and 15 as shown in Figs. 5.35 to 5.36. Figures 5.37 and 5.38 plot the same data of impact factor with static strain, but they also specify which impact factor calculation is coming from which dump event. In Figures 5.35 and 5.36, all the data were mixed together and they lost their identity. The reason behind doing this exercise was to be able to distinguish which events were responsible for the high impact factors. Figure 5.38 plots the impact factor, static strain and dump type in a three dimensional surface diagram, which clearly shows which value of impact factor was associated with which dump event. Obviously, the maximum impact factor corresponded to the fast North dump of a rich ore on a completely empty hopper (C1-L) as shown in the figures. Another north side dump event on an empty hopper designated as C4-L, which is a lean ore dumped at much slower speed, produces much lower static strain change in the range of almost half that of C1-L. However, the corresponding impact factor values calculated for both dump events C1-L and C4-L are quite comparable at all gauge locations with the maximum being about 15 (Figures 5.37 and 5.38). All these discussions lead to the conclusion that maximum impact factor of 15 on the pontoons is well validated during the control test by different dump types. Figure 5.38 also shows that all the controlled dump events denoted by the letter C (C1-L to C9-L), which are primarily on an empty hopper, are producing consistently larger impact factor compared to all the other dump events under normal operation denoted by the letter N (N1-L to N5-D). The suffix L stands for left dumps, R for right, and D for double dumps. During normal operation the hopper is partially full. Hence, it verifies the fact that the heaviest impact loads are occurring when the hopper is totally empty.

In order to examine the locations on pontoon with low static strains, Fig.5.39 shows the variation of static strain change along the pontoon gauge locations for different dump events and Fig. 5.40 shows the impact factor at the same gauge locations. It is clear from Fig. 5.39 that gauges in the shear span at either end of the pontoon numbered 45 to 46 and 53 to 54, show the lowest change in static strain due to static component of the load, which is as expected for a beam. The static strain magnitudes for those four gauges are invariably less than 5 micro-strains for every dump event (Fig. 5.39). Not surprisingly, Fig. 5.40 shows that at those four gauges in the shear span of the pontoon the impact factor values shoot extraordinarily high compared to all other data, which is due to the effect of low static strain magnitude. Hence, it is reaffirmed that impact factors calculated for low static strain range are affected by many measurement and computational errors including noise and should be excluded from consideration.

Fig. 5.39 also shows that the static strain change associated with double dump events top the chart in magnitude, with the top three being double dump events. Thereafter, North dumps produce higher static strain change than the South side dumps in general, with a few exceptions occurring due to too slow or too fast dumping. The static strain change associated with a single North dump is about half of that for a double dump, which is exactly as it should be. Some variation does occur in the magnitude of static strain even for the same type and side of dump, the reason for which can be attributed to dump speed. For a fast dump with rich ore, all material falls into the hopper at once producing higher static strain as well as impact factor. Alternatively, for a slow dump as in the case of a lean ore, the material falls in smaller lumps at a certain time lag, thus breaking a single dump event into smaller sub-dumps. For the purpose of calculating impact factor, only portion of the sub-dump that produces the highest impact is considered. As static strain is calculated by taking difference of averaged strain just after and before the highest impacting lump, the strain change doesn't correspond to the whole truck-load, rather to a smaller portion of it. Slower dumps produce lower static strain changes as well as lower strain jumps and impact factors.

So far, the maximum impact factors occurring on the pontoon and the dump events responsible for those have been looked into. The maximum impact factor observed being 15 at the pontoon mid span for empty hopper dumping (Figures 5.37 and 5.38). The variation of static strain and impact factors along the length of the pontoon have also been plotted along with the reasoning that the values of impact factor in the shear span are erroneously high and the values calculated closer to the mid span give more reliable values for impact factor (Figures 5.39 and 5.40). These figures also showed that double dump events cause maximum magnitude of static strain change because of double amount of static load. The general variation of impact factor with static strain has also been plotted and approximated the variation by logarithmic and exponential curves (Figures 5.35 and 5.36). In the static strain change range of 20 to 42 micro-strains, which are mostly due to double dumps and few of the faster north side dumps (Fig. 5.35 and 5.39), the impact factor values are much lower between 1.5 and 3. Thus double dumps

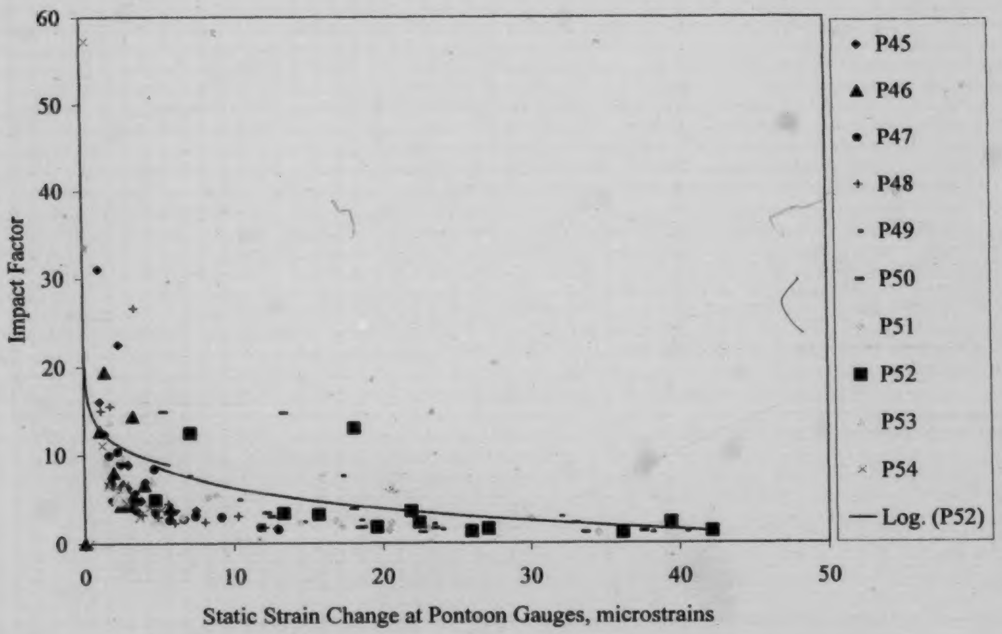

Fig. 5.35 Impact factor distribution at different static strain levels

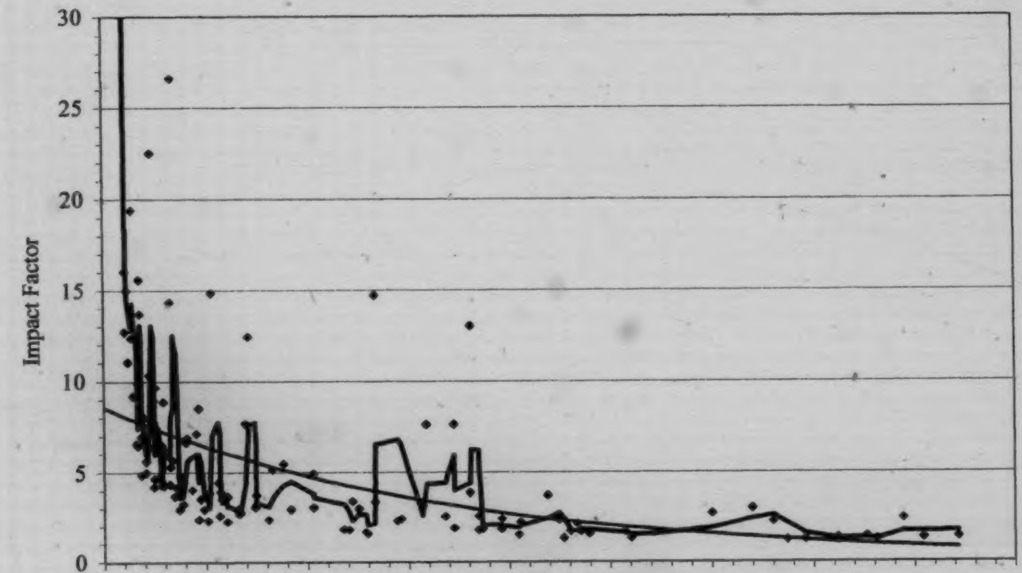

Fig. 5.36 Impact Factor at different static strain levels – a close up view

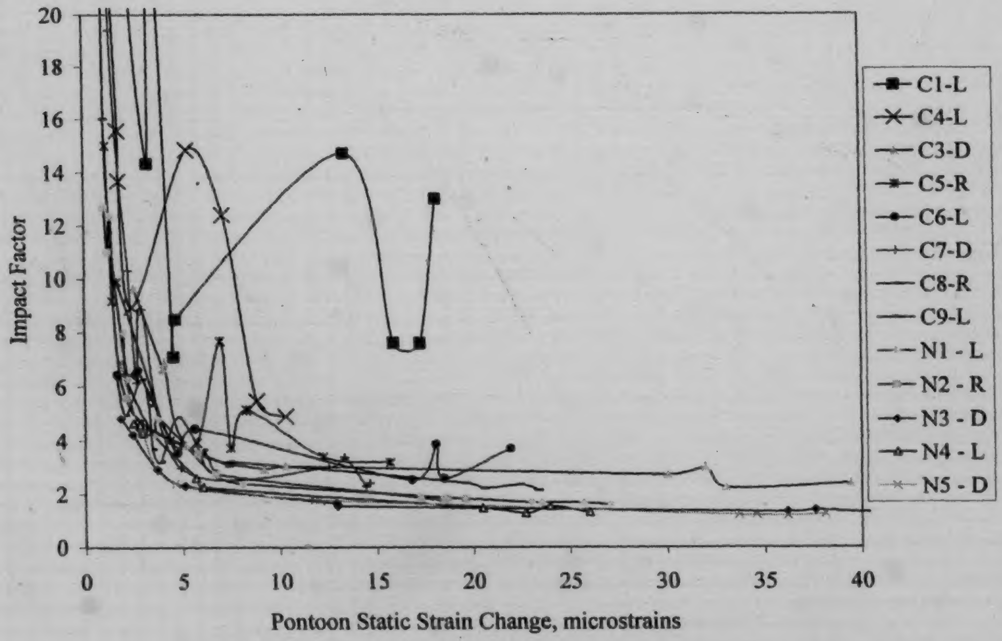

Fig. 5.37 Impact factor at different static strain levels for different dump events

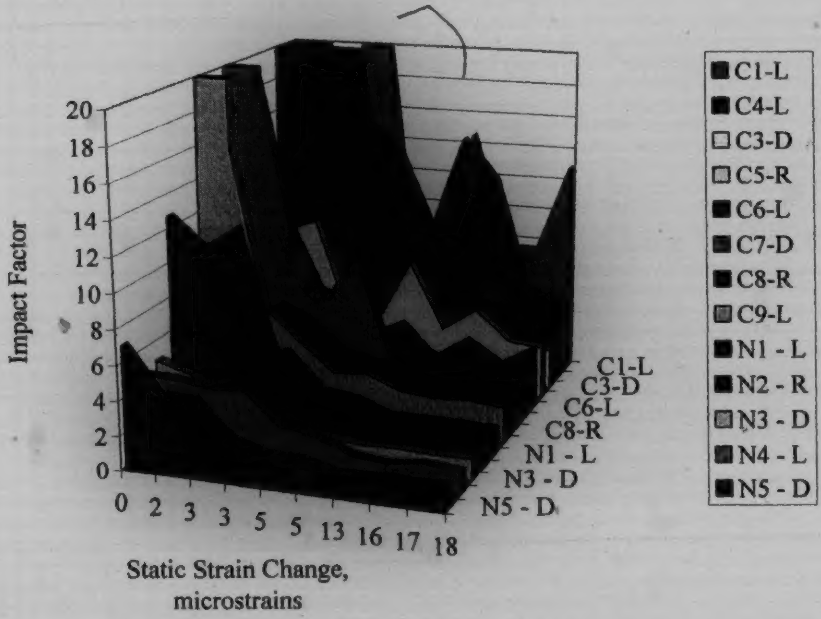

Fig. 5.38 Impact factor at different static strain levels for different dump events – 3D

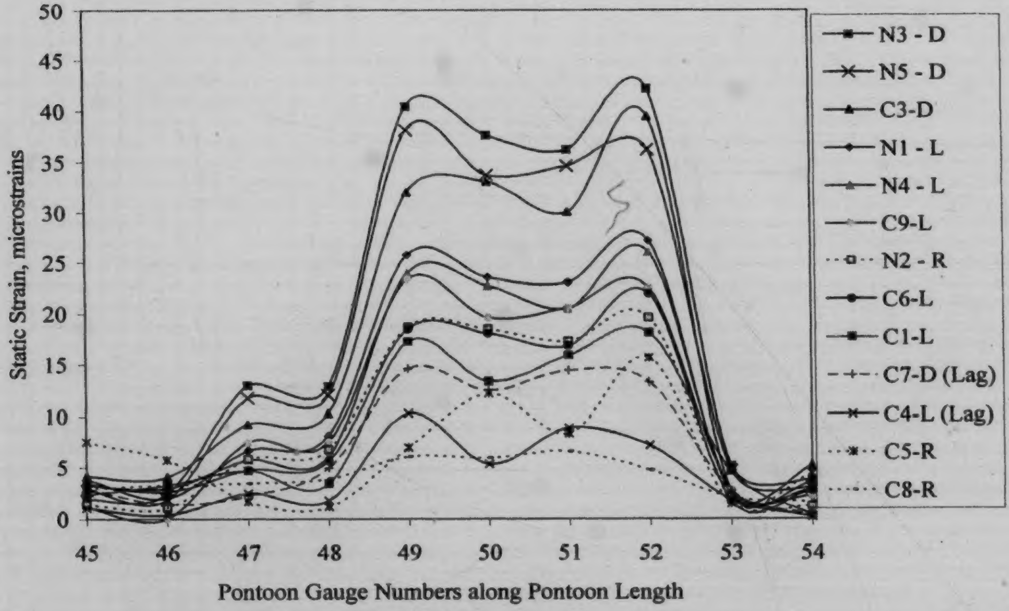

Fig. 5.39 Static strain change along the pontoon for different dump events

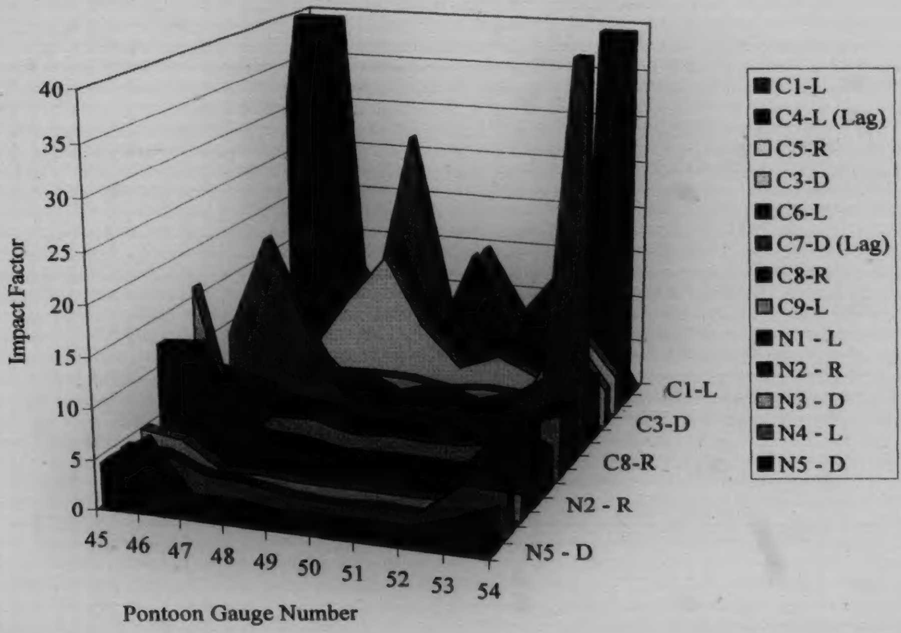

Fig. 5.40 Impact factor distribution along the pontoon gauges for different dump events

with higher static strain change give lower impact factors. Even in the range of 5 to 20 micro-strains of static strain change, which correspond to the single dumps, the only cases with high impact factor of 15 were due to the north side empty hopper dumps. Other than those two dumps, in all the rest of the dumps under normal operation, no matter whether dumped from north, south, or both sides, the impact factors always remained less than 5. In general it can be concluded that the impact factor values for pontoons vary between 1 and 15 depending mainly on the level of material in the hopper and the side of dump. The average impact factor under normal operating condition usually ranges from 1.5 to 5 at most times, with the average being about 3.

5.8.5 Average Impact Factors for Columns and Hopper

Statistical analysis on impact factor data of over one hundred dump events from the base data in 2003 was conducted by Denkhaus (2004). The study indicated that impact factors for pontoon varied from 1.25 to 2.5 during normal operation, with the exception of dumps occurring on an empty hopper where impact factor rose to the range of 5 to 12. Thus the findings from the control tests in April 2004 compare well with the impact factor from normal operation in 2003. During the 2004 tests, the impact factor on pontoons varied between 1.5 and 3 when the hopper was full and between 1 and 15 when the hopper was empty.

Along similar lines, the impact factor on column gauges under normal operation varied between 1.2 and 4. However, in some cases of higher impact dumps possibly due to empty hopper, the impact factors were peaking up to 25 and averaging consistently high in the range of 2.5 to 8. A few of the gauges recorded impact factors that were higher than that, but are neglected because they were associated with static strain less than 5 micro-strains (1 MPa stress) which made them severely affected by noise and other sources of error. Impact factor calculations on the ten hopper gauges revealed that under normal operation the average value of impact factor varied from 1.2 to 3.6. In the case of a few extreme dump events, on the other hand, the impact factor varied between 4 and 10. Intuitively, the closer the strain gauge is to the impact source, the higher the impact factor should be. However, the maximum impact factor recorded for hopper gauges, 10, is much lower than that for the column gauges, 25, braces 50, and the pontoon, 15. The relatively smaller values for the hopper gauges suggest that the regions of maximum impact on hopper are not instrumented.

5.9 Influence of various Dump Parameters on Strain Jump

Thus far, the structural behaviour of the crusher have been looked into under different operating conditions such as thermal, controlled testing, and normal operating condition. Strain jump parameter and impact factor have been defined and analysed at each gauge location. Response of the structure under empty hopper severe dump condition and associated maximum values of strain jump and impact factors at each gauge location have been presented. Individual strain response at each gauge location as well as response of groups of gauges have also been analysed together. Column gauges at each gridline have been grouped together, whereas the pontoon gauges and hopper gauges are grouped in two separate groups. Influence of bending and axial component of stresses in columns have been separated and scrutinized. Finally, the maximum impact factor for each structural component under heavy loading and also the average impact factor for the components under normal daily operation have analysed and presented. Now in this section, the main goal is to compare across different gauges, different dump event types, and different operating conditions with a view to establish certain behaviour patterns and explore further into the structural response. Strain jump has been used as the parameter for such comparisons for reasons well established. For the purpose of such comparison, the responses at pontoon gauges have been used as the benchmark in most cases to allow a common ground. Different operating parameters like: empty hopper, full hopper, dump speed, side and type of dump have been investigated.

5.9.1 Empty Hopper Strain Jump vs. Full Hopper Static Strain

The response of the structure to a dump under an empty hopper condition is compared with that under full hopper condition to start with. Strain jump for empty hopper dump

C1-L was the most severe of all. Now, the strain jump at all tensile gauge locations on the pontoon are calculated and plotted in Figure 5.41. The figure only shows the strain jump values for the tensile gauges (P46, P48, P50, P52, and P54) located on the bottom flange of the pontoon for clarity of presentation because all these gauges are located at the same distance from the extreme fibre. The figure also shows another curve below the strain jump curve for dump C1-L. This curve is the plot of strain change from empty hopper (no load condition) to hopper completely full, observed at the same tensile gauge locations. The most important point here is that this is the strain change due to static loading when an empty hopper is completely filled with oil sand. There is no dynamic component here, but the hopper is statically loaded to the maximum extent possible. Thus, this graph is a comparison of the worst dynamic component of loading to the worst case scenario of static loading when the hopper is full.

The maximum strain increase at the pontoon mid-span for the severest case of North dump (C1-L) on an empty hopper encountered was 229 micro-strains. The maximum static strain, on the other hand, for a 100% full hopper was 70 micro-strains at the same location (Figure 5.41). Thus, with respect to a full design load of static material on the hopper, the maximum strain due to impact on an empty hopper is higher by a factor of 3.26. At other gauge locations along the pontoon, this factor reaches as high as 3.40. As a result, impact load case on an empty hopper governs the maximum strain value, and consequently, the design load. Since manufacturer's recommended operating parameters prohibits dumping material on empty hopper, this severe load case can be regarded as rare one with a low probability of occurrence. However, every time the structure is emptied for scheduled maintenance and repair operations, when production resumes, dumping has to begin from an empty hopper condition. So, based on a very reasonable and minimum maintenance requirement of once every three months, such loads can be expected at least once every four months and probably 4 to 8 times every year.

The response of the structure can be different even for the same type of dump event when the material level in the hopper varies from one dump to another. The variation of strain jump with hopper material level is discussed in the sections to follow. Figure 5.42 shows

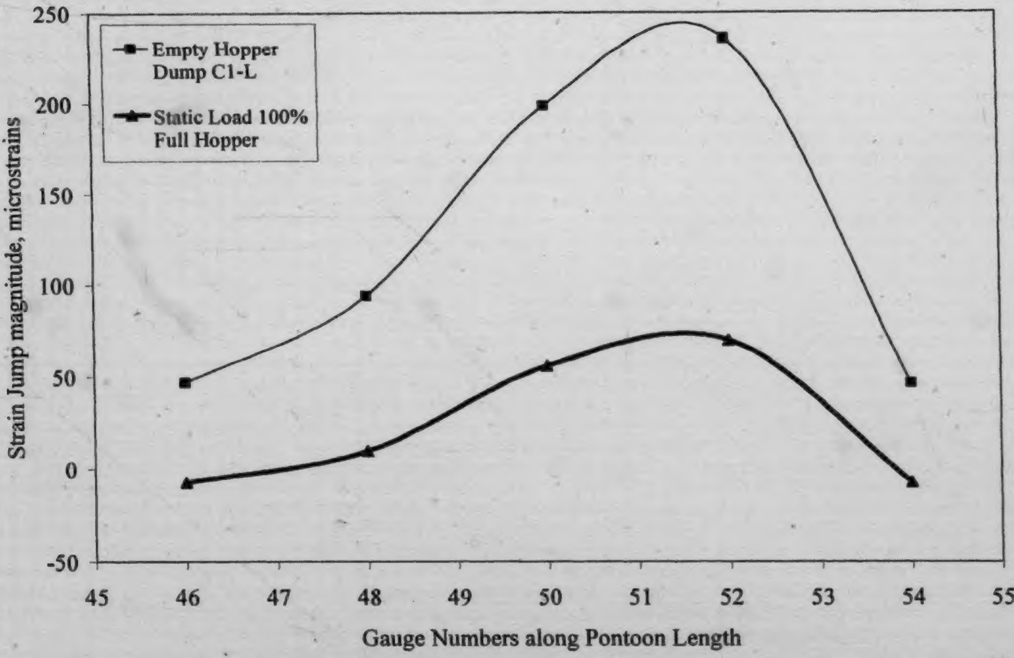

Fig. 5.41 Empty hopper strain jump vs. full hopper static strain

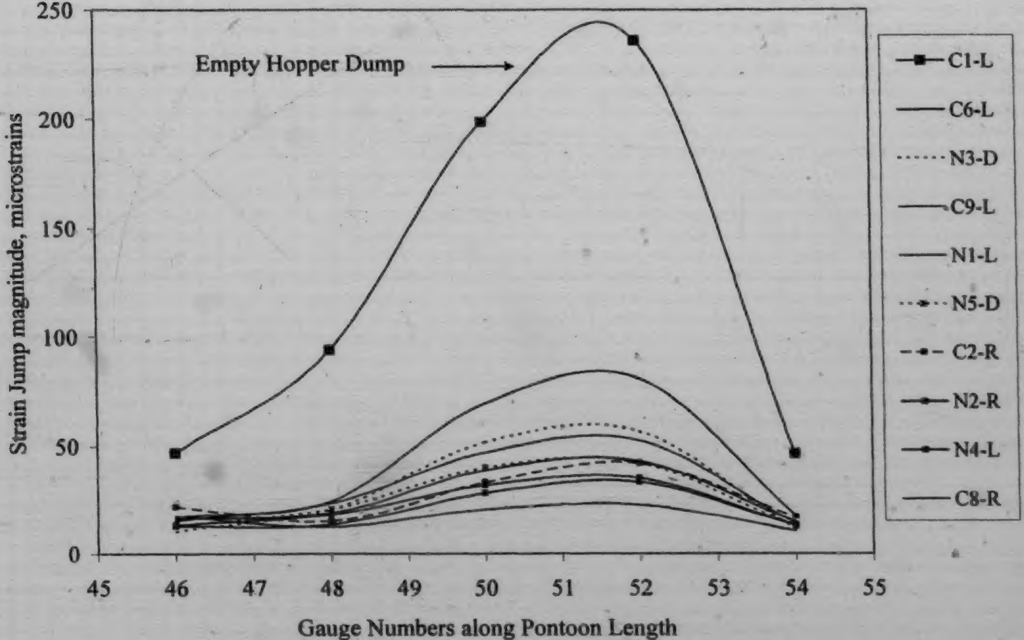

Fig. 5.42 Comparison of various dump events along pontoon gauges

that strain jump profile for empty hopper dump is much larger than all the other curves for dump events under normal operation with varying level of material in hopper, which is quite close to the static strain with hopper 100% full. Thus, the dynamic component of dumps under normal operation is comparable to the static component of totally full hopper.

5.9.2 Influence of Side of Dump on Strain Jump

As already mentioned, the crusher hopper is able to take dumps from left, right, or both sides simultaneously. The responses of the structure to these different types of dump events are different from one another as is evident by the magnitudes of the strain jump parameter. In order to monitor the structure, it becomes important to recognize the similarities and differences between these different types of dump events. Although it may be difficult to pin-point any such differences by taking a solitary gauge at a time, it becomes quite obvious when a group of gauges and their inter-relation are considered. Such inter-relation patterns can be a subject of further research in making use of artificial neural network based methods for classification, monitoring and damage detection. Figure 5.43 is a plot of strain jump at all tensile gauge locations (P46 to P54) along the pontoon for different dump events. It is evident from the figure that the influence of North side (left) dump is far more critical than south side (right) dump as shown by dump C1-L and all the other left side dumps that produce clearly larger magnitudes of strain jump compared to the right side dumps. The reason being that the material dumped from North side strikes the South side of the hopper, where most of the strain gauges are installed including the south side pontoon. Similarly, the south (right) side dump has lower effect on the south side pontoon because most of the dumped ore hits on the north side of the hopper first. In Fig. 5.43, all higher strain curves belong to left side dump, whereas all the lower strain curves belong to the right side dump events. Double dump events have characteristics of both left and right dumps depending on the sequence of dumping; hence, they are naturally in between the two. It can also be observed that side of dump is not the only defining criterion that determines the magnitude of strain jump due to the event. Other factors like speed of dump and the hopper level come into picture to determine how much the strain jump should be. These effects are further discussed in the next few sections.

It appears from Fig. 5.43 that the relative magnitude of strain jump could be used to determine the side of a particular dump to a certain extent, thereby dumping from the left side will produce a certain strain profile along the pontoon that is different from the profile for a right side dump. However, as the crusher operates at higher hopper levels, the difference between the left, right, and double dumps diminishes. A left dump on a relatively full hopper will produce a strain profile very close to that due to a right dump on a relatively empty hopper. Thus, the advantage of magnitude of strain jump in classifying dump events is lost. Figure 5.44 below shows the plot of normalized strain jump for the same control dump events 1 to 9 along the length of the pontoon. All the strain jump readings on the pontoon gauges have been normalized with respect to the maximum strain jump reading, which occurs at gauge P52. The right half of the graph sees normalized strain jump falling quite on top of each other, whereas the left half shows some distinction between dumps from different sides. The pontoon gauges directly under the hopper, P46 and P48 (left half on graph), show higher relative normalized strain (with respect to mid span strain) for right dumps than for left dumps. Left side dumps have higher effect on the mid span strain of the South pontoon but relatively lesser high effect near supports, whereas right dumps have lower effect on mid span strain of the South pontoon and relatively higher local effect near the supports because of direct load coming from the columns supporting the hopper above. When saying high and low effects here, it is in relative terms with respect to the change at mid-span. The absolute magnitude of strain jump at pontoon mid-span is always the highest of all, but relative to the shear span gauges, the increase ratio is higher for the left side dumps. Hence, the difference in normalized strain between the pontoon mid span and supports is clearly visible for the left and right side dumps. The double dump gets mixed up with either the left or right dump behaviour depending on which side of the double dump is dictating the behaviour. For example, dump C7-D is following the profile of right side dumps, which is an indication that the right side dump is more influential in this double dumping. On the contrary, in the case of C3-D, the left side dump is governing, so it follows the behaviour

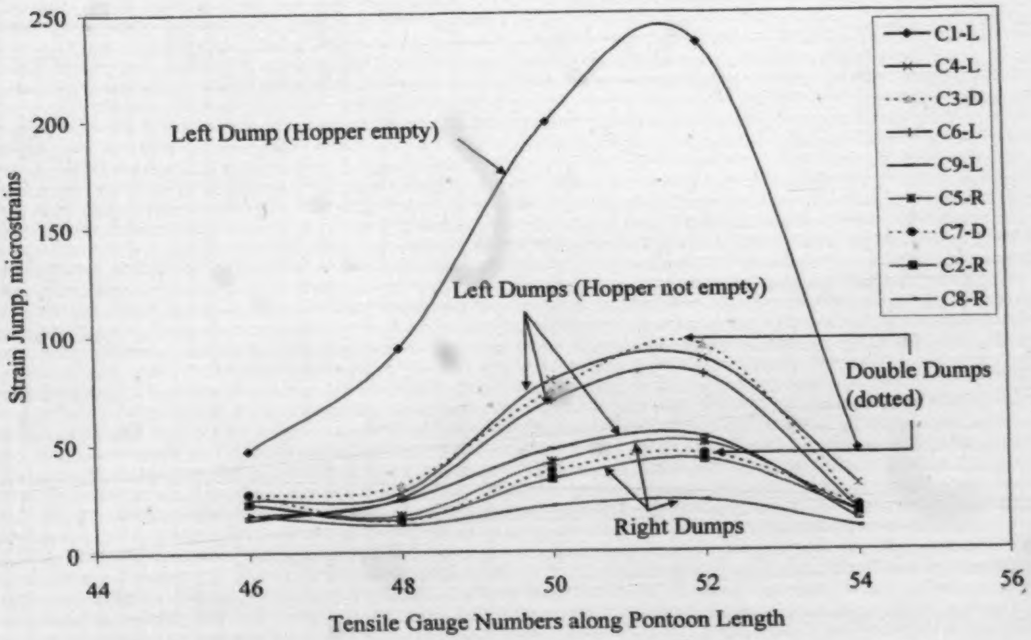

Fig. 5.43 Strain jump along the pontoon for different control dump events

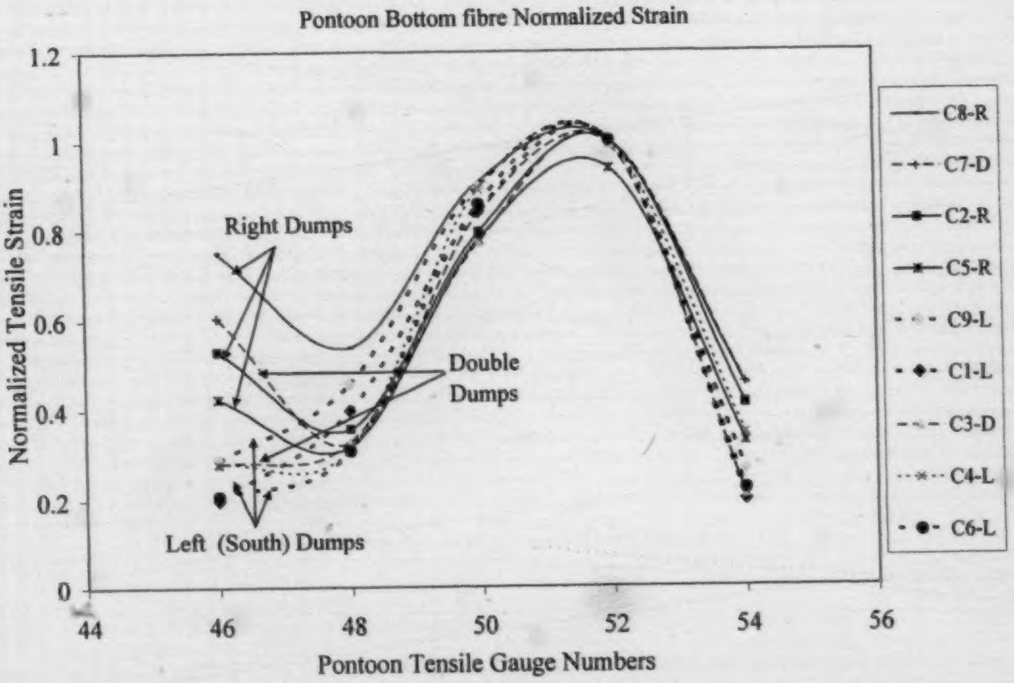

Fig. 5.44 Normalized strain jump along the pontoon for different dump types

pattern of left dumps. Such pattern recognition can be used in ultimately classifying dump events based on strain patterns in long term monitoring of the crusher.

It can be seen in Figure 5.44 that the strain jump at gauge P46 in the shear span for the right side dumps varied between 50% and 75% of the mid-span strain jump, whereas for the left side dumps, it was about 20% of mid-span strain jump. At all other locations the normalized strain jump were quite comparable, the distinguishing feature for right dumps being the sharp rise beyond gauge P48 towards gauge P46 that is nearer to the supports.

5.9.3 Influence of Duration of Dump on Strain Jump

As mentioned earlier, the speed or duration of dump is an influential parameter in determining the strain jump associated with each dump event. The material available to be dumped into the hopper for each dump event is almost the same about 350 to 400 ton. However, if the dump event takes a long time to drop that volume of oil sand into the hopper, the material falls in smaller chunks thereby sub-dividing a single dump event into a number of smaller sub-dumps. Since the magnitude of dynamic component or impact is directly proportional to the mass of material and distance of fall, smaller chunks (masses) of material falling into the hopper will produce smaller strain jump. Further, once there is some material available in the hopper, the chunk falling last will always get some cushion to dampen the impact due to fall. Hence, it is expected that slower dumps with longer dump duration will produce smaller strain jump.

Based on the data obtained during control test, an effort was made to assess and verify the nature and extent of such an influence. Again the pontoon gauges were used for this purpose, but it is understandable that the behaviour will be similar for any other gauge location. While comparing the influence of dump duration (speed), it is important to maintain all other operating parameters constant. However, controlling every parameter perfectly for a long time was not possible in the field due to practical reasons, so the best or closest match is taken for comparison. Figure 5.45 shows the plot of strain jump variation for each tensile pontoon gauge with respect to different dump durations occurring from the North side on a totally empty to 20% full hopper. Thus in this figure, the side of dump is held constant to left side dumps but the hopper was not totally empty in all cases, though it was close to empty. Hence, the hopper level is varying between 0% and 20%; and slight aberration due to this is expected in the graph. In general, faster dump produces higher strain. However, when the hopper is 20% full, the strain jump magnitude drops a little from the expected value. Dump duration of about 15 seconds seems to be a critical speed below which strain jump due to the dump event rises exponentially. This could serve as a guide for dump truck operators to minimize impact load on the crusher.

Similar observations are noticed when plotting the normalized strain variation with dump duration for each pontoon gauge as shown in Figure 5.46. The strain jump magnitudes are normalized with respect to the maximum strain jump observed at that gauge location. Normalization reveals that each of the strain gauges along the length of the pontoon experiences similar relationship of strain jump variation with the duration of dump. The normalized strain jump increases with decrease in dump duration and shoots up exponentially beyond the critical duration of about 15 seconds. The other factor that affects the trend lines is the material level in the hopper. In Figures 5.45 and 5.46, the strain jump is reduced slightly when the hopper is 20% full compared to when it is totally empty; and that is why the curve seems to be rising in the latter part instead of falling continuously. Similar trend of decreasing strain jump with increase in dump duration is observed for right side dumps but with relatively lower magnitudes of strain jump. Needless to mention, similar trends are also followed for all other strain gauge locations on columns and hoppers.

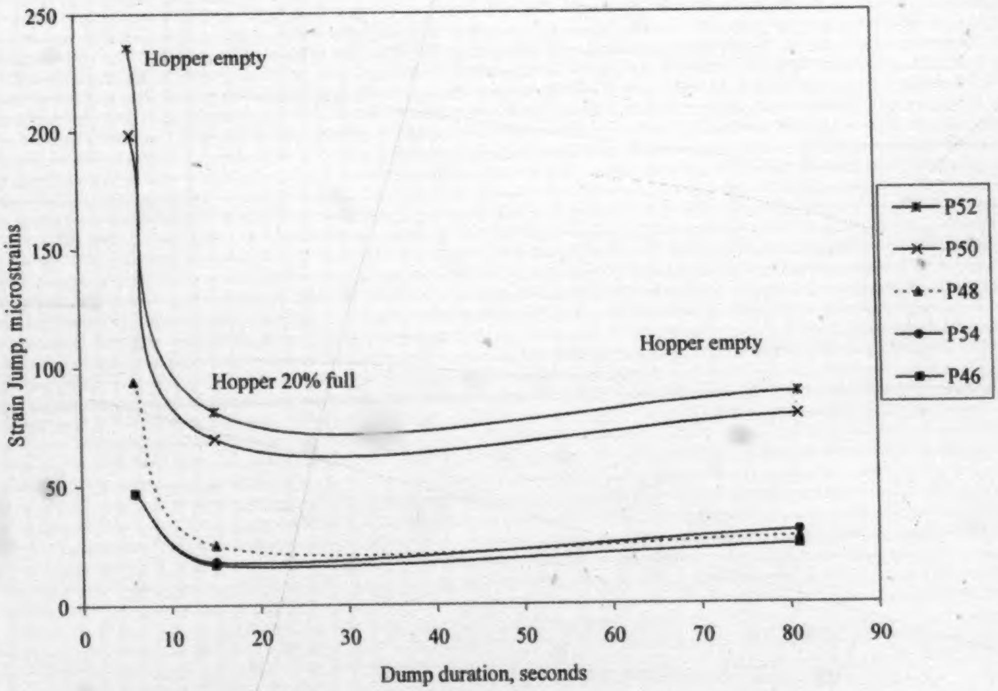

Fig. 5.45 Strain jump variation with dump duration for pontoon gauges

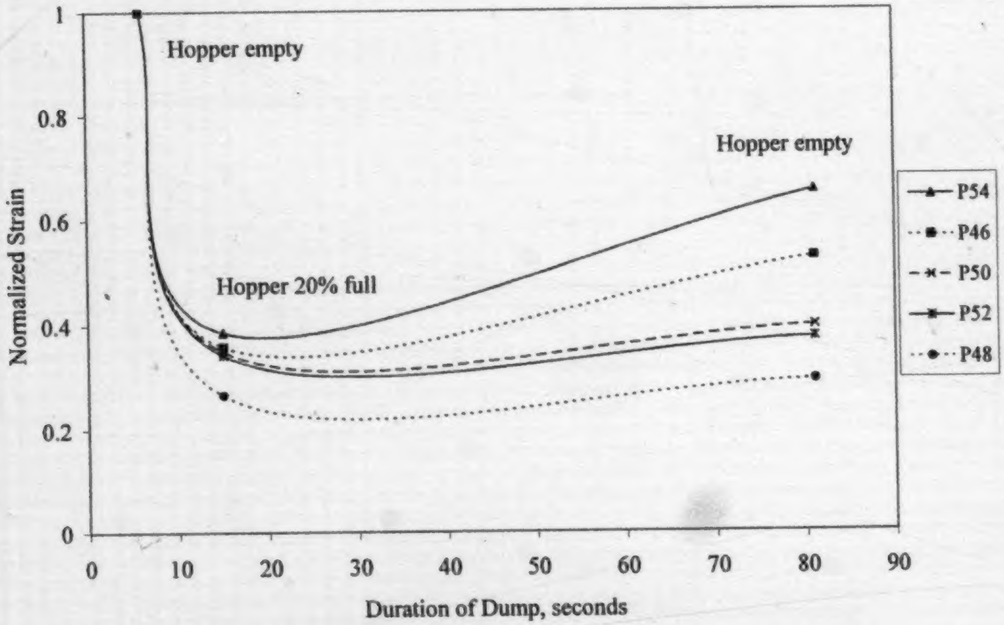

Fig. 5.46 Normalized strain jump plot with duration of left dumps

5.9.4 Influence of Hopper Material Level on Strain Jump

Material level in hopper influences strain jump magnitude due to a dump event, as indicated previously. It is only natural that as the level of material in the hopper increases, the pre-existing cushion of material acts as a damper to the impact of new material. Furthermore, as the hopper material level rises, the height that the dumped material has to fall through before falling into the cushion of material gets shorter and shorter. The strain jump and dynamic component are directly related to the height of fall, which generates the maximum inertial force. Effect of impact is at its highest when material is dumped into a totally empty hopper, which is not good for the long-term health of the hopper. That is why manufacturer's specification advises to avoid such dumps by programming the feeder to stop when material level is reduced below a set point.

Strain jump due to left dump events of comparable durations have been plotted in Fig. 5.47 for two of the pontoon gauges P52 and P54. In keeping with the above discussion, the magnitude of strain jump is seen to be consistently dropping with the increase in material level in the hopper. When the material level in the hopper is 80% that is the hopper is full, the strain jump magnitude is the lowest, whereas for empty hopper it is the largest. When the strain jump magnitude drops below about 20%, the strain jump rises sharply. This observed 20% mark will be designated as the critical hopper level for operation purposes, which is consistent with Aurora II operation practices in the field. However, at the time of scheduled maintenance the hopper has to be emptied and when the production resumes, dumping has to occur into an empty hopper, which is unavoidable. Figure 5.47 also shows that for extremely slow dump events like the one with 81 second dump duration (dump C4-L), the strain jump magnitude is quite small in spite of being dumped into an empty hopper. The reasons for this behaviour have already been explained. Such slow dumps are possible when the ore is rather lean in bitumen content. The effect of dump duration is mixed with effect of hopper level in this case. Thus, the rise in strain jump for dumps into the hopper with less than 20% material level is exponential for short duration dumps, whereas for long duration dumps it is still rising but rather linearly.

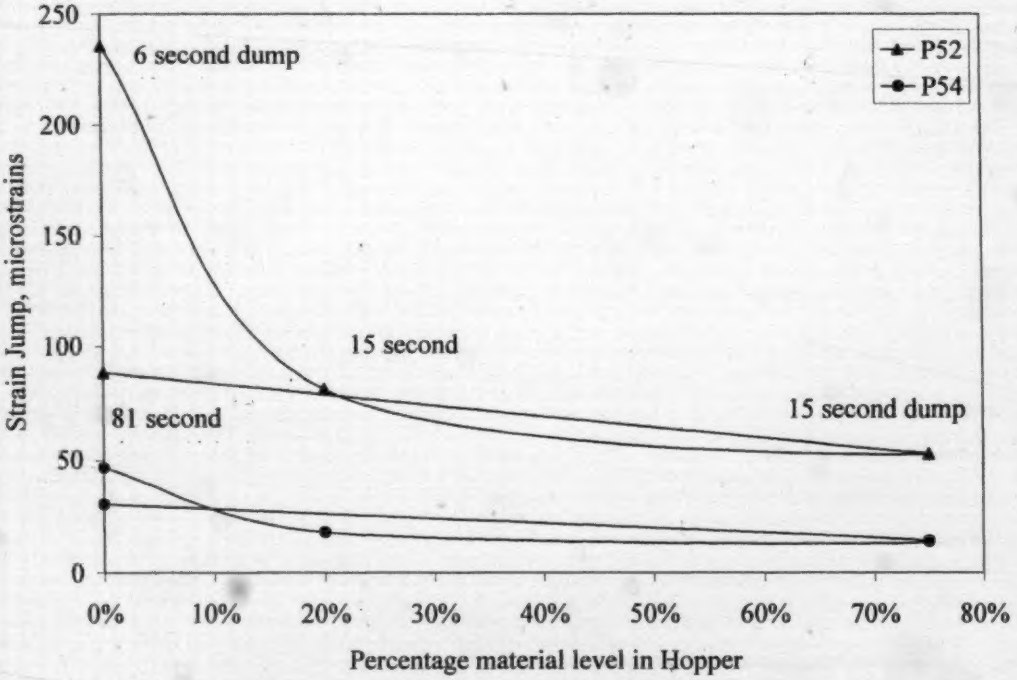

Fig. 5.47 Variation of Strain Jump with Hopper Material Level

5.10 Displacement and Acceleration Readings

There were ten displacement transducers and ten accelerometers placed on the crusher as shown in Chapter 3 on instrumentation. Data from these sensors were collected during the first field test in 2003, when the base data was collected. However, during the subsequent tests in 2004 and 2006, it was found that most of those transducers had already fallen off the structure and only a couple of accelerometers were properly working. During the first field testing, all the transducers and accelerometers placed lower down on the structure near the foundation recorded very low level of signal indicating small displacement and acceleration. However, the displacements recorded on the LVDT (transducers) at the top of the columns were comparatively larger. The maximum displacement at the top of the column in vertical direction was 10.32 mm. The displacements in the vertical direction were less than 1 mm for 60% of dumps and those in the horizontal were less than 1 mm for 90% of the time. Detailed analysis of these displacement readings has been reported by Denkhaus (2004). Displacements at the bottom of the column where they connected with the pontoons were less than 0.5 mm for 99% of the dumps, as expected of a well-designed industrial structure.

Since all of the LVDT placed on the structure to measure the column displacements at the top and bottom fell off in a couple of months after the first field testing, it was not possible to replace those gauges back in their original positions without interfering with the production of the crusher. Hence, it was decided to do away with those sensors for the subsequent tests because stopped production would cost significant amount of money. Most of the accelerometers had also either fallen off or stopped working properly, leaving only a few that were working. Going by this reliability track record, it seems these sensors are not the best suited for long term monitoring projects. Since there were sufficient number of strain gauges and only two out of sixty had broken down, they performed much more reliably over the years.

5.11 Summary and Conclusions

Aurora II Double Roll crusher is a complex combination of hopper plates, beams, bracings, columns and supporting pontoon. It is subjected to impact loads of two 400 ton heavy haulers as continuous normal operating condition. Although, no substantial structural maintenance problems have occurred in the past on the four crusher of this category, there is little work or knowledge regarding the margin of safety in the design specifically in the impact factor estimation. This issue may become crucial in the near future when At-face slurry system demands a fully mobile crusher. Detailed investigations of the crusher behaviour under temperature, normal operation, and control testing have been carried out and the results presented.

1. Linear relationships exist between temperature and strain gauge readings at different locations within small temperature variations. Slopes of this relationship for each gauge have been plotted and they vary from 1.31 to 6.4 micro-strains per degree Celsius, which can be corrected for thermal coefficient of the gauge for larger

temperature variations. Ten minute averaging interval has been adopted for eliminating noise in the thermal data.

2. The adequacy of rate of data acquisition during operation has been explored and found to be quite satisfactory by good number of data points captured in every rising arm of strain in a strain jump due to a dump event.
3. North side (left) dump has much higher influence on South pontoon than South side dump. Empty hopper dump C1-L is the most severe dump event.
4. The maximum measured absolute strain value at pontoon mid-span is 229 micro-strains. At column gauges the maximum strain observed was 450 micro-strains for vertical members and 757 micro-strains for struts and braces; whereas the maximum strain observed in hopper gauges was 200 micro-strains.
5. The strain readings measured at all column gauges were broken into bending and axial strain components. Presence of some local bending was observed in some vertical column gauges and most of the inclined struts and braces. The bracing at gridline 6 recorded bending and axial strain components of 450 micro-strains each.
6. Maximum impact factor of 15 was measured for pontoon, 25 for columns, and 10 for hopper based on the readings of sixty strain gauges during tests in October 2003 and April 2004. These values correspond to empty hopper. For dumps on partially full hopper during normal operation, average observed impact factor were 3 for pontoon, 4 for columns and 3.6 for hopper.
7. Maximum dynamic strain due to a single dump on empty hopper is 3.3 times higher than maximum static strain due to a completely full hopper.
8. Normalized strain jump pattern along the pontoon is a good indicator of the side and type of dump. The strain jump magnitude increases rapidly with decreased dump duration below 15 seconds. It also increases rapidly with decreased hopper level below 20%. It is therefore recommended that normal operating conditions sustain these impact-reducing limits.

5.12 References

Sharma V.P., Cheng J.J.R. and Obaia K. 2006. "Structural Health Monitoring of Aurora II Crusher". Research Department Progress Report 35 (09), Syncrude Canada Ltd., Edmonton, Alberta.

Sharma V.P, Denkhaus C.L., Obaia K. and Cheng J.J.R. 2006. "Structural Behaviour of Syncrude's Aurora II Crusher". First International Structural Specialty Conference, Canadian Society for Civil Engineering (CSCE), May 23-26, Calgary, Alberta, Canada. ST-120--1:11.

Sharma V.P., Cheng J.J.R., Denkhaus C., and Obaia K. 2005. "Structural Health Monitoring of Syncrude's Aurora II crusher in the Canadian oil sands". Second International Conference on SHM of Intelligent Infrastructure, SHMII-2 2005, Nov. 16-18, Shenzhen, China.

Sharma V. P., Obaia K., Cheng J.J.R., and Neudorf J. October 2004. "Smart Structures: Controlled Field Test of Aurora II Crusher". Syncrude Research Department Progress Report 33 (10), 1.2. Syncrude Canada Ltd., Edmonton, Alberta.

Denkhaus C. 2004. Structural Behaviour of Syncrude's Aurora II Crusher. Master's Thesis, University of Alberta.

ISIS Canada. Spring 2001. "Guidelines for Structural Health Monitoring". A Design Manual published by ISIS Canada, a Network of Centres of Excellence.

Fowler, C.G. and Gonzalez, S., 2000 a. Assessment of Aurora Crusher Structural Displacement. Syncrude Canada Ltd., Research Department Progress Report, 29 (09), pp.026-034.

Obaia, K. and Gonzalez, S., 2001. Investigation of Support Displacement of DRC7. Syncrude Canada Ltd., Research Department Progress Report, 30 (09), pp. 1-13.

CHAPTER 6

DYNAMIC PROPERTIES OF AURORA II CRUSHER

6.1 Introduction

Dynamic characteristics like natural frequencies and mode shapes are unique properties of a structure, which can easily be considered as its thumbprint. As a human thumbprint or signature is unique to the individual, so is the structural thumb print/signature. Two structures can have same natural frequencies and mode shapes only when the structure is an imitation of it or is very much like the original structure, the equivalent of a clone in medical parlance. Structural properties, however change/shift with time as the structure ages or deteriorates. Any change in operating environment or boundary conditions can also lead to the changes in its structural properties. Such evolution or change in structural properties is a source of concern to structural engineers. Any change in structural properties or operating environment can lead to altered structural response in a way significantly different from what it was designed for, with possibilities of failure in performance or structure. Vibration based damage detection techniques are being developed in the lab and its performance experimented on simple structures. Although not anywhere near perfect, utility value of such techniques cannot be negated. An effort to integrate the inherent value of these dynamic techniques with static indicators may hold the key to successful damage detection on real life structures.

This report analyses the key theories involved in the understanding and investigation of the dynamic properties of Aurora II crusher; and presents the results with appropriate discussion. A glimpse of issues related with dynamic data acquisition and signal processing is also provided.

6.2 Scope of Work

The Aurora II crusher is a highly complex industrial structure with its dynamic properties not investigated and unknown thus far. Economy in design, crunch for materials, and tough market competition being the direction of the future, accurate knowledge of structure and the loads acting on it is necessary. Field measurement of vibration characteristics of the crusher and its response to the acting loads provides a valuable input for the design of future generation of fully mobile crushers. With knowledge of structural dynamics, structures can be designed to withstand dynamic forces in a better and more efficient manner. On the contrary, complete ignorance of these effects can lead to unsatisfactory service or even a complete disaster, examples of which are abundantly available in history like the Tacoma Narrows Bridge. Determination of a complete set of natural frequencies and mode shapes of the structure poses a bigger task that requires a completely different set of instrumentation and test methodology. Given the complexity of the structure and its interaction with many other interfering components like the retaining walls, the apron feeders, and the crusher machinery, the task itself will not be a simple one. There are too many variables involved and modes that are closely spaced, hence determination of complete modal frequencies and mode shapes for the crusher is beyond the scope of current work. The main focus is to be able to capture the few fundamental frequencies of the structure and associated damping without going into details of the mode shape at this juncture. A more detailed study on the dynamic aspects of the crusher can be done in the future, if necessary. Hence, though incomplete, a significant number of modal frequencies can be determined from experimental field data. Once these properties are established and known, they can be used as one of the indicators in the integrated SHM system.

In general terms, the vibration modes of the crusher can be classified as vertical, lateral, torsional, and longitudinal. Determination of the true mode shapes will be a bigger challenge than determining the modal frequencies. Modal damping values associated with each mode can be estimated from the exponential decay curve of free vibration after impact.

6.3 Dynamics of the Load on Aurora II

Dynamic properties of a structure assume importance whenever it is faced against a dynamic load like earthquake, wind, traffic, impact, etc. Each type of dynamic load in itself has certain characteristics like frequency content and amplitude. Wind loads have more sort of a widely distributed frequency content modelled by white noise, whereas earthquakes vary greatly in frequency as well as magnitude. The frequency content of the soil through which the earthquake ground motion propagates can interact with the frequency content of the earthquake at its source and produce a modified earthquake ground motion at each site. Thus, a single earthquake can have different ground motions and thereby different effects on structures at different locations depending on the geology of the area. Once an earthquake or wind comes in contact with (hits) a structure, the structure responds based on its own natural frequencies and its interaction with the frequency content of the event. Such interaction and response are obtained by superimposing (multiplying) the admittance function of a structure over the spectral density function of the load. Vehicular traffic, on the other hand, can have different load patterns on a structure depending on many factors like speed of the vehicle, its size, weight, axle distances, stiffness of the shock absorbers, etc.

Impact or impulse loads are a different category of extremely short duration dynamic loads, like drop-hammer hitting a pile, blasting of explosives, impact from a gun bullet, etc. Impact loads have two-pronged effect on a structure owing to its short duration of action, viz – high local impact on the area of contact, and relatively lower effect on the global behaviour of the structure. Even a small load, when dropped from a height, can cause an impact of several times the load. Naturally, the height of fall or the velocity of impact and impacting mass are the two key factors. The type of load acting on Aurora II crusher belongs to this category of dynamic load – impulse. The mass of the oilsand dumped into the hopper can be as high as 400 ton depending on the size of lumps. The height of fall into the hopper decreases with the rise in the level of oilsand in the hopper. Pre-existing material in the hopper has also a dampening effect and acts like a cushion to the falling load. Dump occurring on an empty hopper is the severest of all, whereas dumps on the full hopper produce little effect from impact.

A vital characteristic of impact load is that the structure is sent into free vibration, governed only by its own structural natural frequencies and has no interaction whatsoever with the loading frequencies as in the case of other dynamic loads. The mass of the structure is increased though in the process due to the added material from the dump. This leads to some migration in the natural frequencies of the structure from the values obtained for empty hopper condition. The bigger the dump, the higher is the magnitude of vibration. Eventually, the free vibration comes to an end owing to structural and other sources of damping. There is significant presence of other interfering frequencies like operating machinery and electromagnetic effects; however, they are small in magnitude and periodic in nature to be attributed as noise. The modal damping can be calculated from the free vibration decay curve, which could be higher when the hopper is full. There isn't a way to measure the exact nature of the load and the nature of impact, which varies with climate and speed of dump, other than that the oil sand weight is known and the response of the structure under impact is known at 60 strain gauge locations. The side of dump and material level in the hopper can excite selected modes more than others and thereby, produce different structural response signatures. Also different gauges at different locations could capture some vibration frequencies better than others.

6.4 Vibration Based Damage Detection

Dynamic signatures have been abundantly used in research to characterize structural health. Various methods of frequency identification are available Fourier transform being the most popular of them. When there is a damage or deterioration, the signature dynamic properties will change / shift, which can be tracked by various available damage detection techniques like frequency based methods, mode shape changes, matrix update methods etc. (Los Alamos, 1994 and 1996; Khattak and Cheng, 2003). Although the determination of natural frequencies and other dynamic properties and the theories behind them are quite reliable and accurate, the detection of change in such properties due to damage or deterioration is not obvious unless and until the damage is quite substantial (Khattak and Cheng, 2003; Bagchi et al., 2004). Such anomalies make these vibration based damage detection techniques reliable only on simple laboratory models, but not on real life complicated structures with thousands of degrees of freedom and hundreds of variables. Having said this, dynamic properties remain to be the unique foot prints of the structure.

Although the vibration based detection techniques are far from being perfect, the utility value of such techniques cannot be negated. Examples of dedicated damage detection exercises on different structural problems can be found in Los Alamos (1996), which are tailor made systems for the particular problems in question. These techniques being less than reliable for low damage levels and for complicated structures, they are yet to be used in combination with other static indicators of damage. Integrating the inherent value of these dynamic techniques with static indicators may hold the key to successful damage detection on real life structures. Many authors conclude that mode shape and frequency determination estimate can only be made accurately if the natural frequencies are well separated and lightly damped, such that the response at a particular frequency is dominated by the corresponding mode shape. Further, with low intensity vibrations like in ambient vibration testing, it is difficult to obtain a good vibration record when the ambient vibration is small and the damping estimate is not very reliable (Khattak and Cheng, 2003, Afhami et al., 1998).

6.5 Signal Processing Tools for Dynamic Analysis

The signals that are generated by the sensors attached to the structure due to physical change from deformations (stress/strain) in the structure have to be conditioned before being read (digitized) by the data acquisition system. Signal conditioning is the first step in modifying signals, electrical voltage in this case, with a purpose for better data accuracy/reliability and ease of interpretations. Signals generated by each type of sensors are different in nature and magnitude, and hence, require different type of conditioning, which is appropriately done by the signal conditioning modules included in the data acquisition system. However, signal modification or processing does not end after data acquisition. In fact, the real challenge of processing begins from there.

In order to make sense out of the thousands of numbers blurred by noise and obscured by structural complexities or limitations of data, the data has to be appropriately processed to make things look brighter and clearer. Signal processing can be as simple as using a spreadsheet to get rid of unwanted information and highlighting the data or graph that presents a trend which can be explained by a theory. On the other hand, a dedicated processor and software can be used to process and analyse the data for the same purpose with a much more organized and repetitive system. For example, separating the static component from the dynamic component of a structural response is a goal that requires specific processes to modify the signal before it is achieved. In the same way, finding structural frequencies and mode shapes of the structure requires the operation of Fourier Transform to be applied on the data. Discrete time signals or data sequence processing employ filters to smooth out noisy data or to enhance certain patterns of interest. This section presents a brief foray on this aspect of SHM system, which is related to digital signal processing for dynamic properties.

Digital Filters are the most widely used tools in signal processing to rid the data of the most common problem in data acquisition, namely noise. Digital signal processing (DSP), growing phenomenally since the mid ninety-sixties, can be implemented either through hardware or software. It can also be classified as analog filter and digital filter. Analog filter designs are mostly reserved for specialist uses due to its advanced mathematical involvement. Modern sampling and digital processing tools on the other hand make digital filters the ideal choice owing to its programming flexibility, ease of building and implementation, and superior cost to performance ratio. Digital signal processors and frequency analyzers are fast replacing the analogue systems due to their high performance, versatility, and integration of computer aided data acquisition (McConnell, 1995). The author identifies two broad areas of interest in DSP as Digital Filters and Spectrum Analysis, with many points of overlap between them. It also makes one strong point, that most of the important signal processing activities take place in the frequency domain, which signifies the value of faster sampling rate in data acquisition. Spectrum Analysis leads to Discrete Fourier Transform (DFT) and Fast Fourier Transform (FFT).

An excellent example of use of a hardware filter is demonstrated in dealing with aliasing in the frequency domain. A series of N discrete points to represent the original signal may not give an adequate representation if the sampling rate is too slow. On the contrary, a fast sampling rate can give an excellent digital representation, but with a larger data file. The sampling function multiplication or convolution in the frequency domain gives rise to an error called as aliasing. Thus, a much higher frequency component may be represented as a lower alias frequency, one tenth of the original, to produce a false frequency spectrum. A digitized signal recorded by a data acquisition system will therefore be already infected with an alias as soon as the signal is converted from analog to digital, if the sampling rate is not fast enough. The Nyquist frequency governs the minimum required rate of data sampling, which says that the sampling rate must be twice as fast as the desired frequency range of interest to avoid aliasing errors. Hence, anti-aliasing becomes important in frequency analysis unless extremely high scan rate than required is used. Aliasing cannot be handled digitally after capturing the data. It has to be taken care of while the data is still in the analog form. Hence, an electronic (hardware) filter with a sharp roll-off is applied to the electrical analog signal before it is digitized, so that the high frequency components above the Nyquist frequency are removed from the measurements (McConnell, 1995). In most data acquisition systems today the DAQ hardware is designed to cut off all frequencies higher than 1 KHz, where for structural purposes the frequencies of interest mostly lie between 0 to 50 Hz. This was exactly the case with the data collected on Aurora II crusher. Anti aliasing filter produces a modified signal, which can be represented mathematically as follows, where F (w) is the output frequency, H (w) is the frequency response function of the anti-aliasing filter, and X (w) is the input frequency.

$$F(w) = H(w) \cdot X(w), \qquad [6.1]$$

Filtering alters the frequency content of a signal with the assumption that the signal content of interest is separable from the raw signal. Depending on the frequency range that the filters pass or attenuate, they can be classified as – low pass, high pass, band pass, or band stop filters (National Instruments, 1998; 2000). In essence, the anti-aliasing filters mentioned earlier are low pass filters of analog type. Other than the functional classification, the filters are also classified based on the value upon which they operate, into Finite Impulse Response (FIR) filters and Infinite Impulse Response (IIR) filters. The FIR filters operate on input values alone, whereas the IIR filters operate on current and previous input and output values. The FIR filters are simple whereas the IIR filters can be significantly faster and more efficient and reliable. Different types of IIR filter transfer functions are available to do the job namely – Butterworth, Chebyshev, inverse Chebyshev, Elliptic, and Bessel filters. Each filter has certain characteristic feature suited for a particular purpose. The governing selection parameters are ripples in the pass band, roll-off (attenuation) from pass band to the stop band, phase linearity or shift, and error in the stop band. An ideal filter should have unit gain (0 decibel) in the pass band, and a gain of zero (-inf dB) in the stop band. However, in practice, there is always a finite transition region between the pass band and stop band with a gradual decrease, which is called as the transition or attenuation zone. Passing signal through a filter causes ripples in the pass band as a source of error. All these terms are illustrated in Figure 6.1 (National Instruments, 2000). For filtering out noise the Butterworth filter has been used in this project for its low ripple error in the pass band, a smooth monotonic decrease in the transition region, and a zero magnitude in the stop band as shown by its performance plot in Figure 6.2. The higher order Butterworth filter greater than 5 approaches the ideal low pass filter response.

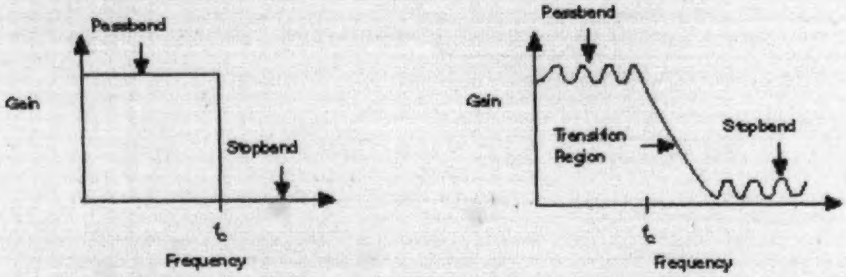

Ideal Filter

Real Filter

Fig. 6.1 Ideal and real Filter Transfer Functions (Source: National Instruments, 2000)

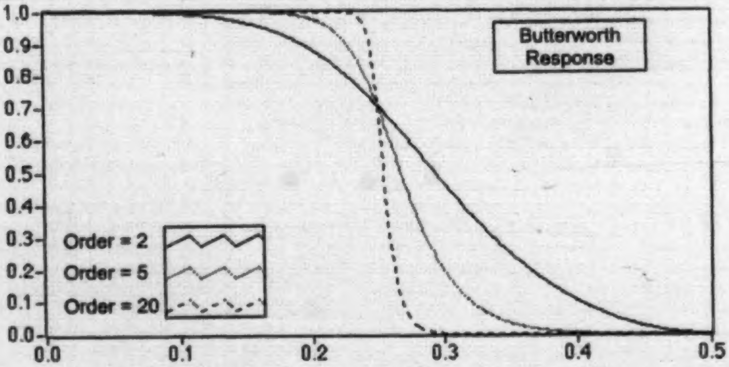

Fig. 6.2 Butterworth Filter response (Source: National Instruments, 2000)

6.6 Frequency Analysis

Most signal analyses go through the frequency domain and are a very popular and effective tool for data processing. Right from digital filtering to spectral analysis or dynamic response of a structure, concepts of frequency domain of analysis are valuable. Fourier's theorem states that any waveform in the time domain can be represented by a sum of sine and cosine terms with appropriate magnitudes or weights in the frequency domain. In the frequency domain it can be represented by a pair of amplitude and phase values at integer multiples of the fundamental frequency. Thus, there is a pair of equations for Fourier Transform (FT) and Inverse Fourier Transform (IFT). When the component amplitudes of the frequencies are plotted as a function of frequency, it gives what is called as the frequency spectrum for discrete time functions or spectral density for continuous time functions.

There is a subtle difference in the FT equation for signals that are periodic, transient, or random in nature. The digital frequency analyzer (or DAQ) samples a signal over time period T at a certain scan rate. It assumes that the captured signal is periodic with fundamental period T and that only frequency components of integer multiples of the fundamental frequency are present in the signal. When talking in terms of discrete time functions, the original analogue periodic time signals are digitized by taking N digital data points over the time period T. Rectangular window functions at increments of T/N seconds are used to scan the N data points. Hence, the amplitude of each frequency component X, which is a multiple of the fundamental frequency, is given by the following Discrete Fourier Transform (DFT), where X_p is the amplitude of frequency component for the p^{th} mode in the frequency domain and *f(n)* is the magnitude of the nth data point in the time domain (McConnel, 1995).

[6.2] $$Xp = \frac{1}{N} \sum_{n=0}^{N-1} f(n)\, e^{-ipn(2\pi/N)}$$

We also have the following relationships for the maximum frequency range of interest and the frequency resolution of measurement dF.

[6.3] $$F_{max} = f_s / 2 \qquad \text{and} \qquad dF = 1/T = f_s/N$$

Wherein, the maximum frequency is F_{max}, sampling frequency is f_s, and dF is the resolution of frequency measurement. In this case, for a 100 Hz sampling rate, the frequency resolution was dependent on the total number of data points N taken in the frequency analysis. The key elements in the development of the digital frequency analysis were the invention of FFT algorithm by Cooley and Tukey (1965), developments in digital computing and processing technology. The FFT is a fast version of the DFT transforming digital time domain signals into digital frequency domain. The FFT spectrum output produces complex numbers with every frequency component having a magnitude and phase given by the real and imaginary parts of the number. In order to retrace the signal in time domain, both magnitude and phase information of the signal has to be stored. In most cases, however, only the magnitude is plotted as a function of frequency called as the power spectrum, which is always real.

The basic assumption involved with digital frequency analysis is that the signal is periodic with fundamental period T regardless of the facts involved. Now, depending on the file size and time length of data being analyzed, this fundamental period keeps changing. The signal is stationary and present before, during, and after the sampling for analysis. Thus, it cannot be guaranteed that always an integral number of cycles of the fundamental frequency are being sampled. Consequently, there is a discontinuity in slope and magnitude at the ends of the sample signal when it is assumed to be periodically repeating in the time T, causing spectral leakage to occur. Spectral leakage distorts the measurement in such a way that the energy from certain frequency content is spread over adjacent frequency lines or bins. When the sample signal is perfectly periodic, the spectrum has energy contained in exact frequency bins without any smearing. However, when leakage occurs for imperfectly periodic signals, a single large peak of the actual frequency in the power spectrum plot may be smeared off into two or three smaller peaks leading to confusion as to the correct frequency and magnitude to be interpreted. The amount of leakage is dependent on the amplitude of the discontinuity at the boundaries, a larger discontinuity producing bigger leakage (McConnell, 1995; National Instruments, 2000).

Windowing is a tool used to reduce the size of the discontinuity, and consequently, the amount of smearing. The time domain signal is multiplied by another time domain waveform known as a window, whose amplitude tapers gradually and smoothly towards zero at edges, resulting in a windowed signal with very small or no discontinuity May different types of window functions are available for different applications like the uniform (rectangular), Hanning, Hamming, Flat top, Force, Exponential window, etc. In general, Hanning window is satisfactory in 95% of cases; hence if nothing is known, this is the automatic choice. If analysing transient signals such as impact and response signals, it is better not to use the spectral windows; instead use the Force and Exponential windows. There is also a trade off between spectral leakage suppression and spectral resolution. As the main lobe (the main peak) narrows with higher frequency resolution, the ability to distinguish between two closely spaced frequency components increases. As the spectral resolution improves, the window energy spreads into its side lobes and the leakage worsens, which is also called as the picket fence effect (McConnell, 1995).

6.7 Natural Frequencies of the Aurora II Crusher

Fast Fourier Transform tool available in Labview program was utilized to convert data collected at 100 Hz in time domain into frequency domain data with phase and amplitude information. Figure 6.3 shows a power spectrum plot for a typical data file of 200 second long that was collected at 100 Hz. Thus, T = 200 sec, and N = 200*100, which gives a frequency resolution of dF = 0.005 Hz and maximum possible frequency F_{max} of 50 Hz. Thus, the frequency content of the structure could be anywhere between 0 to 50 Hz based on the data collected. For a more detailed dynamic test a faster data acquisition rate of 500 to 1000 Hz could be used for a wider frequency spectrum. The power spectrum is nothing but a plot of amplitude (or power) associated with each frequency between 0 and 50 Hz. The peaks represent higher amplitudes at those particular frequencies, indicating that either the structural natural frequencies are close to those frequencies with high amplitude or there are some other electromagnetic or mechanical sources of noise operating at that frequency range. It is important to distinguish between structural frequencies and noise frequencies. Further, not all natural frequencies of the structure are seen and captured at every gauge location. Some gauges are located in such a way that some modes of vibration just don't produce any displacement at that location, and consequently, do not record peak amplitude at that modal frequency in spite of the fact that it is a genuine structural frequency. Similarly, the load pattern and frequency also have influence on the frequencies identified by Fourier analysis. Some loads are applied at such locations and frequencies that it would excite certain mode shapes highly and be indifferent to others. Hence, the point is that data from gauges located at different places on the structure and collected during different loading conditions need to be looked into, including no load condition, in order to identify as many modal frequencies as possible.

Having a closer look at Figure 6.3 it can be observed that there are many peaks in the power spectrum and the first task at hand is to separate noise frequencies from genuine structural frequencies. This objective is fulfilled by trial and error. The time domain data is passed through a high pass filter to gain insight into the frequencies of influence for noise. Mostly noise occurs at higher frequencies and at certain frequencies of operation of machinery or near the frequencies of electromagnetic interference. They are all usually high, hence, the high pass filter brings out all the noise in the data. Figures 6.4 through 6.7 present the noise filtered out by high pass filters with different cut-off frequencies for the data file with dump event C1-L. The results are presented only for the pontoon gauge P52 in particular and a few others but are similarly applicable on all data. In Figure 6.4 the cut-off frequency is kept at 5 Hz. As expected, this high pass filter with such a low cut-off frequency intrudes into more than what is noise. Hence, if everything beyond 5 Hz were assumed to be due to noise, then more than 60 micro-strains of combined strain with positive and negative signs would be lost as noise. Therefore the notion that everything beyond 5 Hz is noise is rejected. Similar trial and error approach is adopted for cut-off frequencies of 10 Hz in Figure 6.5 and 15 Hz in Figure 6.6. In both the cases, the magnitude of strain lost as noise would be more than 14 and 11 micro-strains respectively. This magnitude of noise already sounds much better when compared with the previous magnitude of 60 micro-strains, however, a look at the Figures 6.5 and 6.6 would reveal that there is still some magnitude of peak being lost in the region of the dump event. Whereas the effective noise magnitude in the region away from the dump event stands much lower at about 6 micro-strains. Hence, a higher cut-off frequency of 18 Hz is selected in Figure 6.7, wherein combined noise magnitude is reduced to between 8 and 10 micro-strains. Notably, the noise magnitude observed is uniform across the full length of the data file, including the region of dump event. Hence, in all future analysis, contribution of frequency components higher than 18 Hz is filtered out as noise without significant influence on the magnitude of peak strain during dump.

With a view to check the influence of filtering out noise on the overall magnitude of peak strain, the signal from pontoon gauge P52 for the dump event C1-L is passed through different low pass filters and the results presented in Figures 6.8 to 6.10. Figure 6.8 presents the case with the best cut-off frequency of 18 Hz, wherein a magnitude of 233.77 micro-strains was obtained for strain jump parameter compared to the magnitude of 235 micro-strains observed in the unfiltered raw state. The zoomed in view of the same figure is presented in Figure 6.9. Next, Figure 6.10 shows the magnitude of strain jump obtained after using a cut-off frequency of 5 Hz in the low pass filter. In the first glance both the figures for cut-off frequencies of 18 Hz and 5 Hz look quite similar. However, when comparing Figures 6.9 and 6.10 closely, it is realized that the magnitude of strain jump has dropped by 16 micro-strains from 233 to 216.5 micro-strains. Thus, a drop of about 2 micro-strains in magnitude of peak strain when filtering out noise beyond 18 Hz for frequency analysis is readily acceptable and the best. So, the structural frequencies are below 18 Hz.

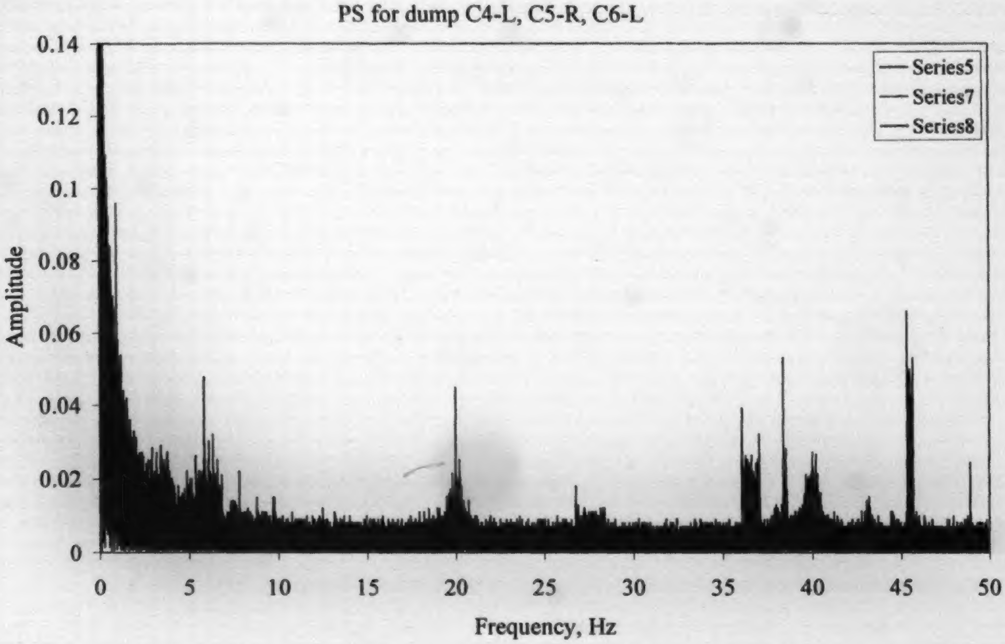

Fig. 6.3 Power spectrum plot for data collected on pontoon gauges during a dump

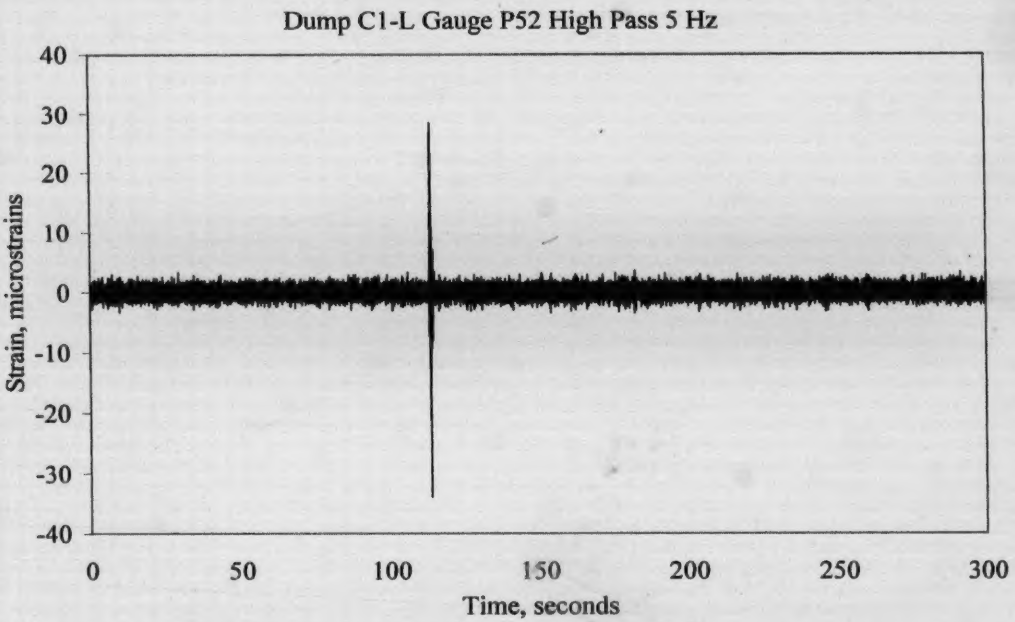

Fig. 6.4 Signal at gauge P52 passed through a high pass 5 Hz cut-off filter

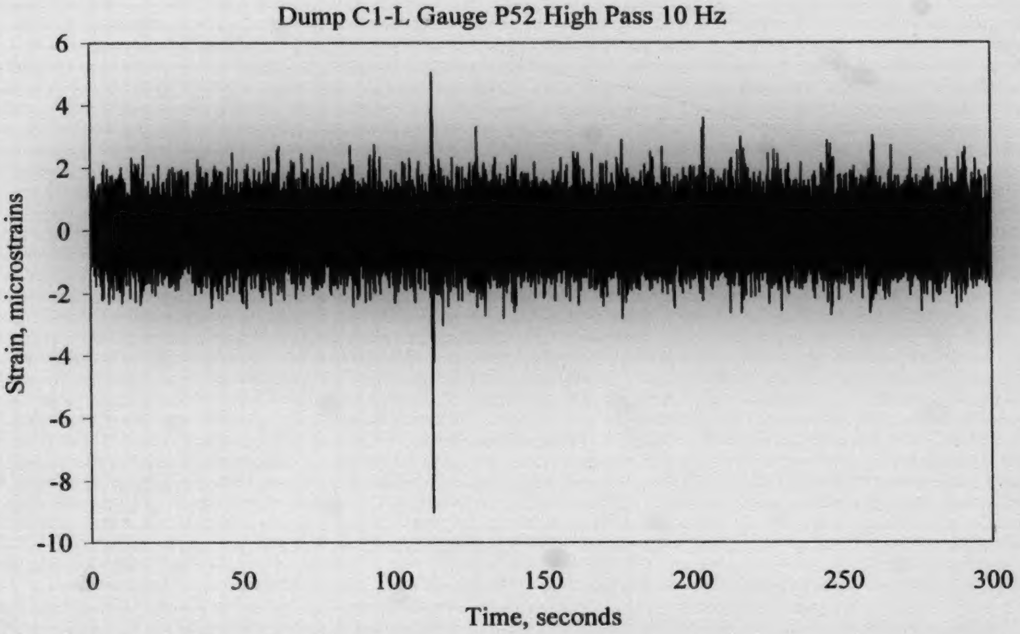

Fig. 6.5 Signal at gauge P52 passed through a high pass 10 Hz cut-off filter

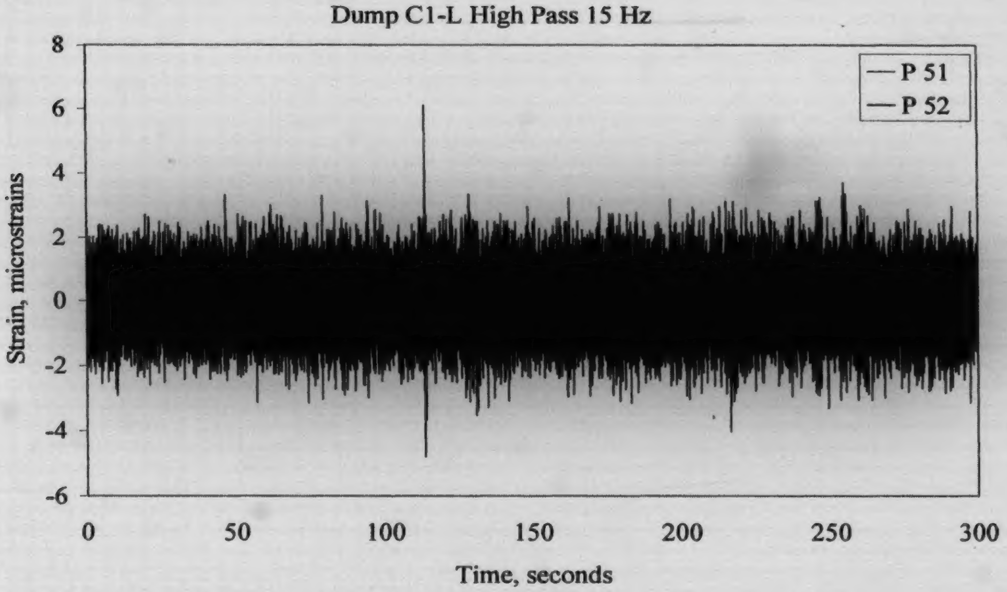

Fig. 6.6 Signal at gauge P52 passed through a high pass 15 Hz cut-off filter

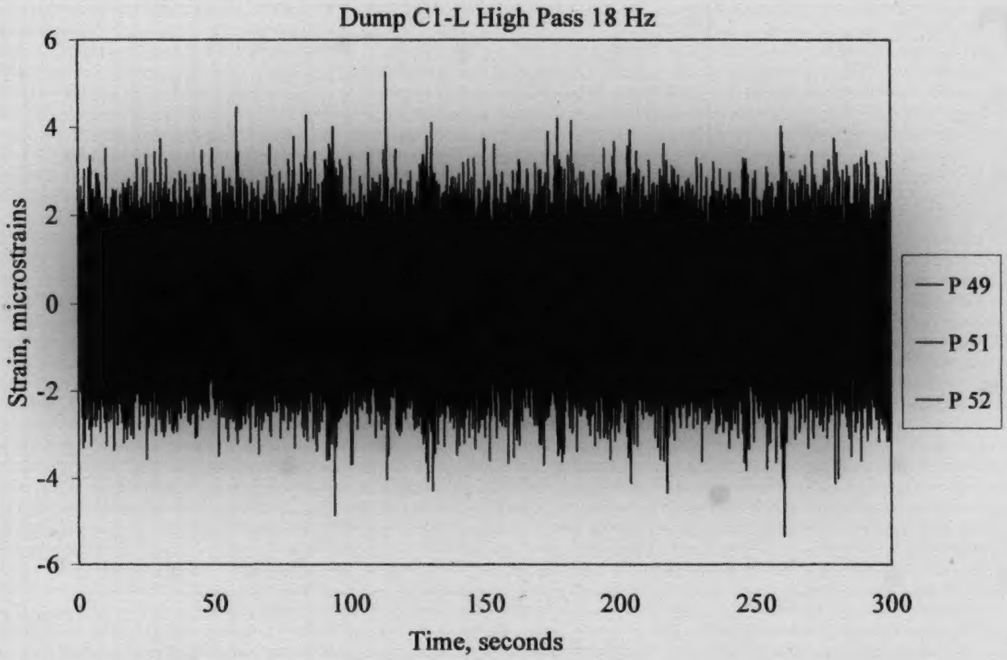

Fig. 6.7 Signal at gauge P52 passed through a high pass 18 Hz cut-off filter

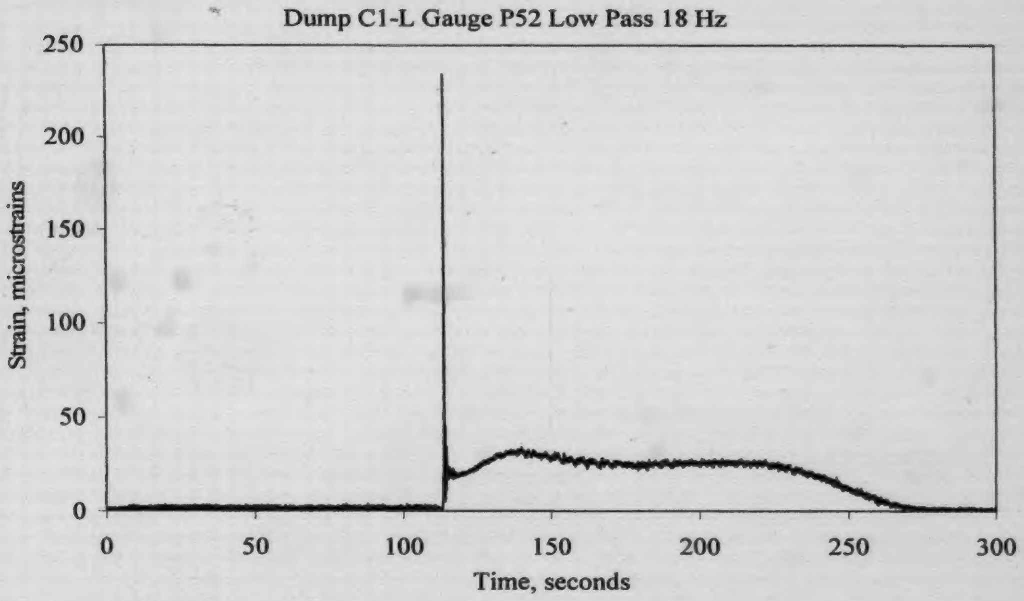

Fig. 6.8 Signal at gauge P52 passed through a low pass 18 Hz cut-off filter

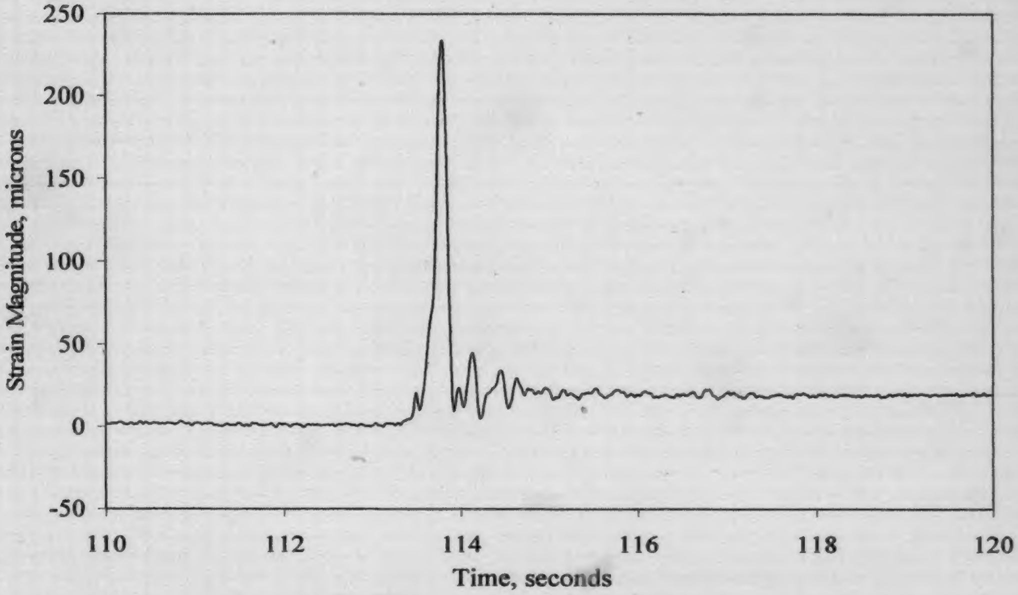

Fig. 6.9 Signal at gauge P52 after passing through an 18 Hz low pass filter

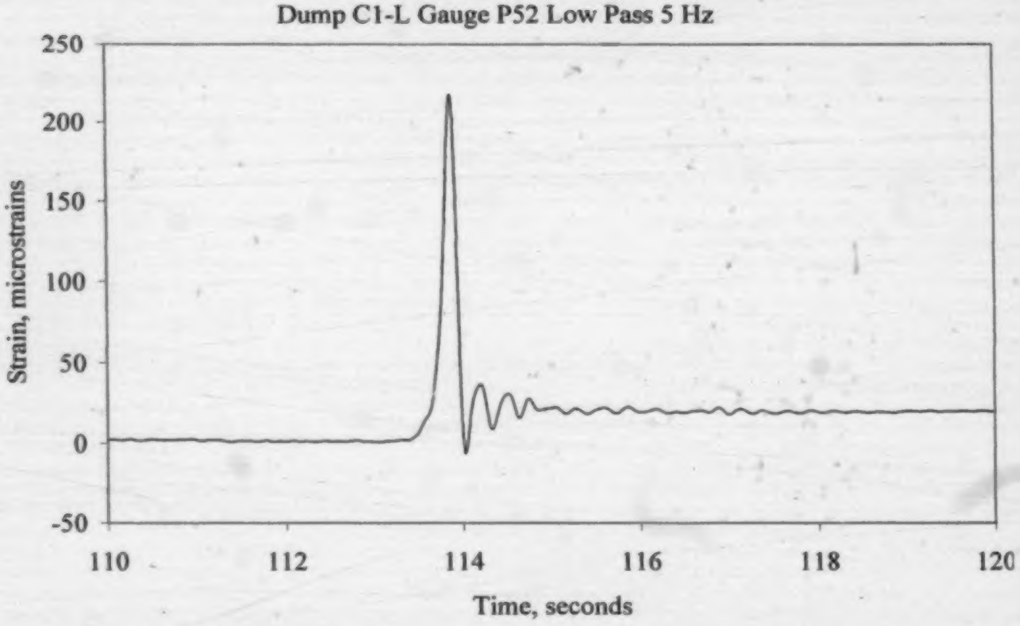

Fig. 6.10 Signal at gauge P52 passed through a low pass 5 Hz cut-off filter

Now that the upper limit for natural frequencies of the structure is known to be 18 Hz, it is also important to know the lower limit. Figure 6.11 below shows the static component of the strain during a dump event, which is obtained by passing the signal through a low pass filter with 0.1 Hz cut-off frequency. It can be seen in the figure that the peak and all the ripples have been almost totally cut off leaving out only gradual rise and fall associated with static filling and emptying of the crusher hopper, without any influence of impact. The magnitude of peak static strain is just above 30 micro-strains as compared to 233 micro-strains obtained by including the effect of impact or dynamic component. The magnitude of static strain is quite reasonable and same as obtained by other methods, although significantly smaller than the dynamic component. Hence, it could be concluded that the natural frequencies of the structure lie between 0.1 to 18 Hz; where everything above 18 Hz frequency is noise and everything below 0.1 Hz is due to static loading. To be more precise, the natural frequencies of the structure would lie between 0.1 Hz and 10 Hz, because a wider frequency window is chosen to reduce errors due to the window boundaries when filtering. A look at Figure 6.3 would confirm the fact that there isn't even a single peak of significance in the power spectrum plot between 10 Hz and 20 Hz. So, it can be concluded that all structural frequencies are between 0.1 Hz and 10 Hz.

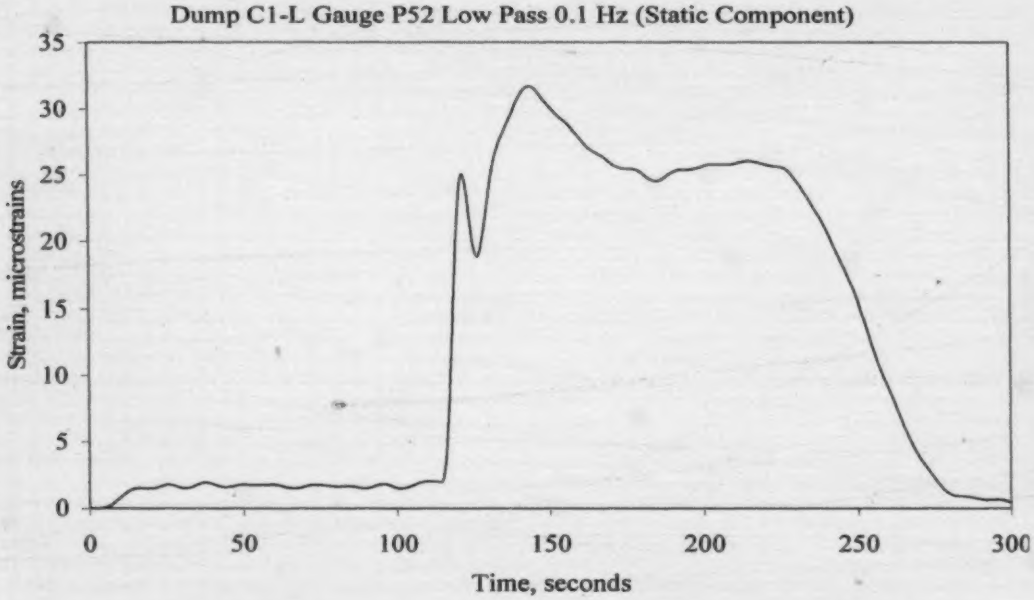

Fig. 6.11 Signal at gauge P52 passed through a low pass 0.1 Hz cut-off filter

After establishing a range to look into for finding the natural frequencies of vibration for the Aurora II crusher, the task now is to focus deeper in the 0.1 to 10 Hz region for data at different gauge locations and under different loading scenarios to gather similarities and dissimilarities in peak values in each case. Since a detailed modal analysis is not being conducted, the complete mode shapes would not be revealed, however, the dominating frequencies of importance would be known. The natural frequencies determined here are grossly incomplete owing to type and location of instrumentation, which is not primarily designed for frequency analysis. Most of the data collected are coming from strain gauges. Strain gauges put on columns can only record vertical compressive or tensile strain, and hence, the majority of the lateral or transverse modes of vibration of the columns are missing. Before going into the details of natural frequencies of importance, the length of data file (time: T) and its effect on the spectral density is investigated. Figure 6.12 shows the power spectrum plot for the signal collected at gauges

P51 and P52. The sampling rate for the data remains at 100 Hz, but instead of taking the complete data file for Fourier analysis, only 10 seconds of data is used. Thus, with a time period T of 10 second assigned to the first fundamental frequency of the Fourier frequencies, the frequency resolution obtained is 0.1 Hz. Figure 6.12 shows that there does not seem to be any clear winners in terms of the Fourier amplitudes. The two peaks at 5.86 and 6.83 Hz are only marginally above other noise peaks. It seems that 10 seconds of data is not enough to clearly discriminate between different frequency contents and assign the magnitudes to the right frequencies.

The frequency resolution in the power spectrum plot of Figure 6.13, which is for the same data but for a bit longer time of 50 seconds, comes up as 0.02 Hz. The figure reveals some interesting clear peaks at 0.96, 3.91, 5.871 and 7.80 Hz. There are some other smaller peaks in the neighbourhood of larger peaks, which are due to some spectral leakage and noise. The result clearly seems to be getting better than the previous graph for 10 seconds of data. A similar power spectrum plot for a still longer data file is presented in Figure 6.14 – for a length of 100 seconds of data. This time around the clear peaks are observed at 0.96, 2.93, 3.417, 3.904, 5.852, 6.834 and 7.808 Hz. Thus, the number of peaks is increasing with the increase in length of data file. Compared to the previous case of 50 seconds of data with four clear frequency peaks, for the 100 second length of data the number of peaks has grown to 7. Thus, a higher frequency resolution is leading towards a higher number of clearly identified natural frequencies. However, along with more number of peaks, there is also more influence of spectral leakage on the power spectrum plot in the vicinity of peak frequencies. Now the point is how far the number of identified frequencies could go on increasing by using a longer data file. This question is answered by the next graph in Figure 6.15, which is for a file length of 200 seconds. There is no further increase in the number of clearly identified frequencies of dominance. The same seven frequencies that were identified earlier for 100 second long files are identified for the 200 second long files. There would still be ambiguity among closely spaced frequencies as to whether they are all independent frequencies of the structure or are a product of the spectral leakage phenomenon. This would require further analysis in the time domain as well as frequency domain.

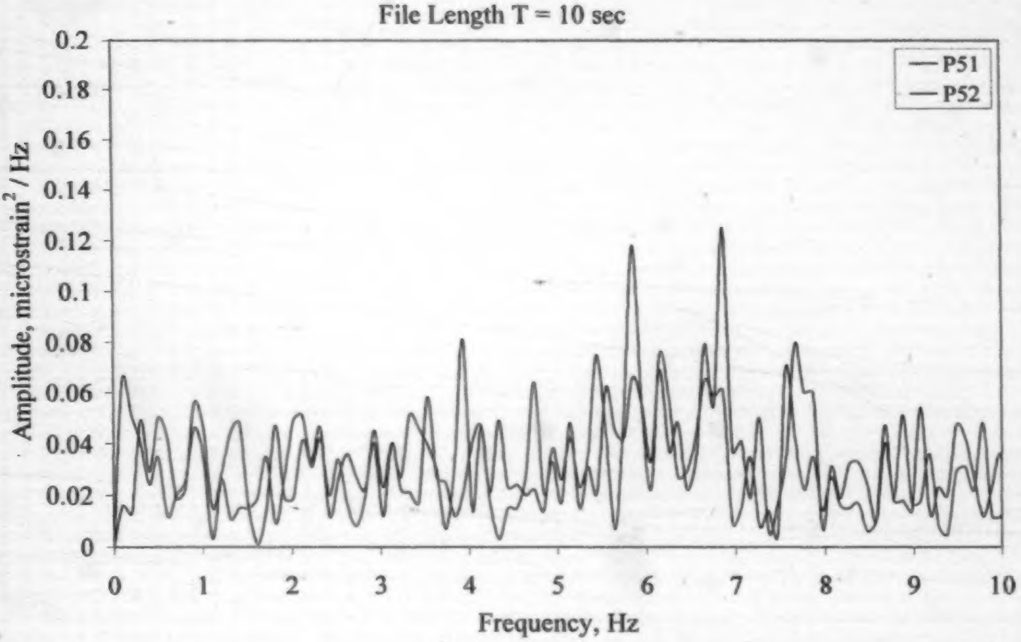

Fig. 6.12 Power spectrum for 10 sec long data at gauges P51 and P52

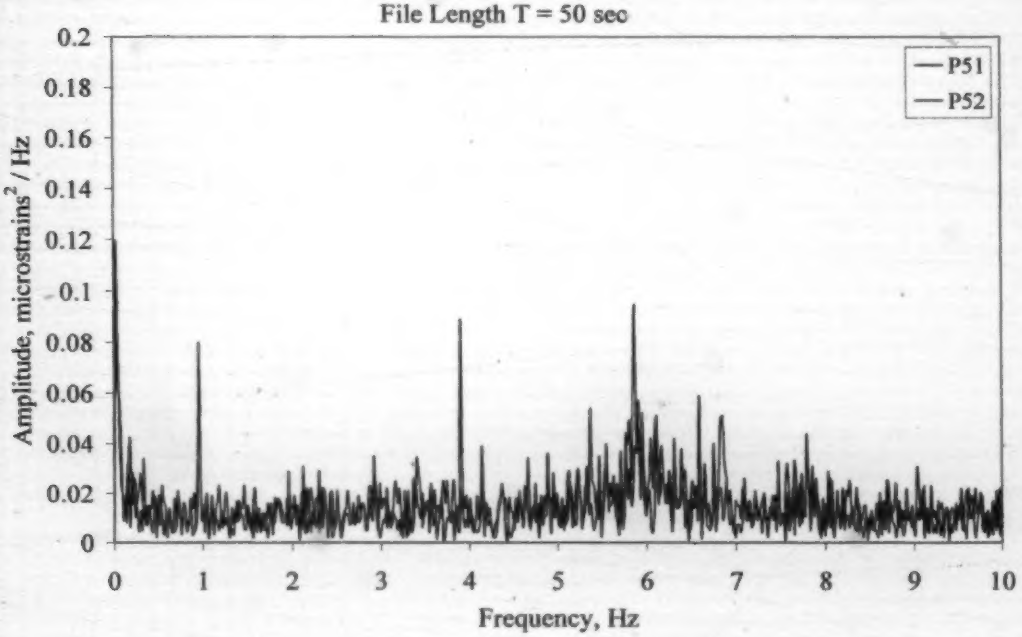

Fig. 6.13 Power spectrum for 50 sec long data at gauges P51 and P52

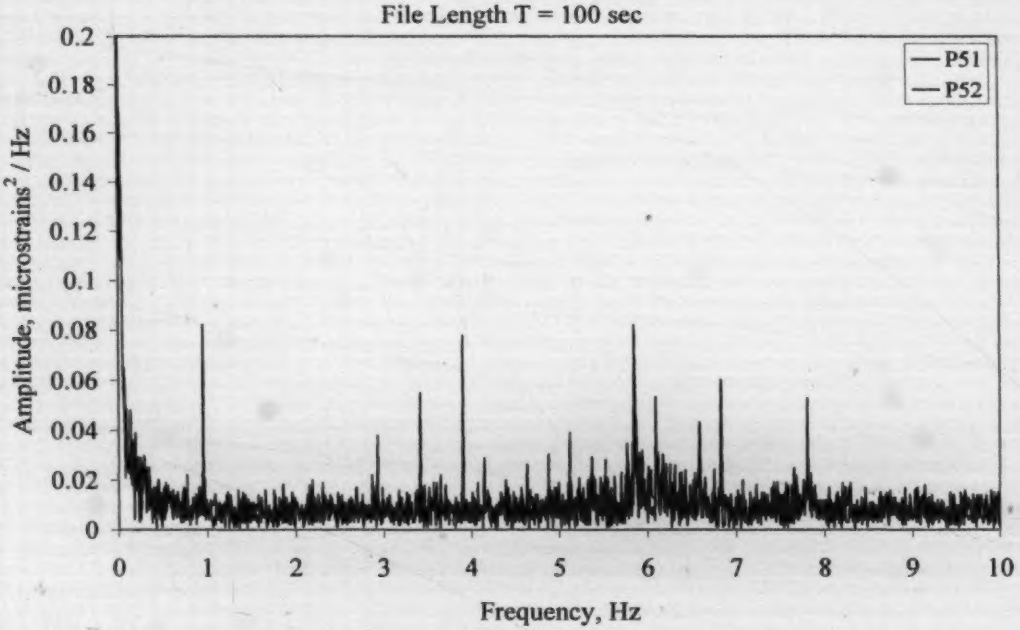

Fig. 6.14 Power spectrum for 100 sec long data at gauges P51 and P52

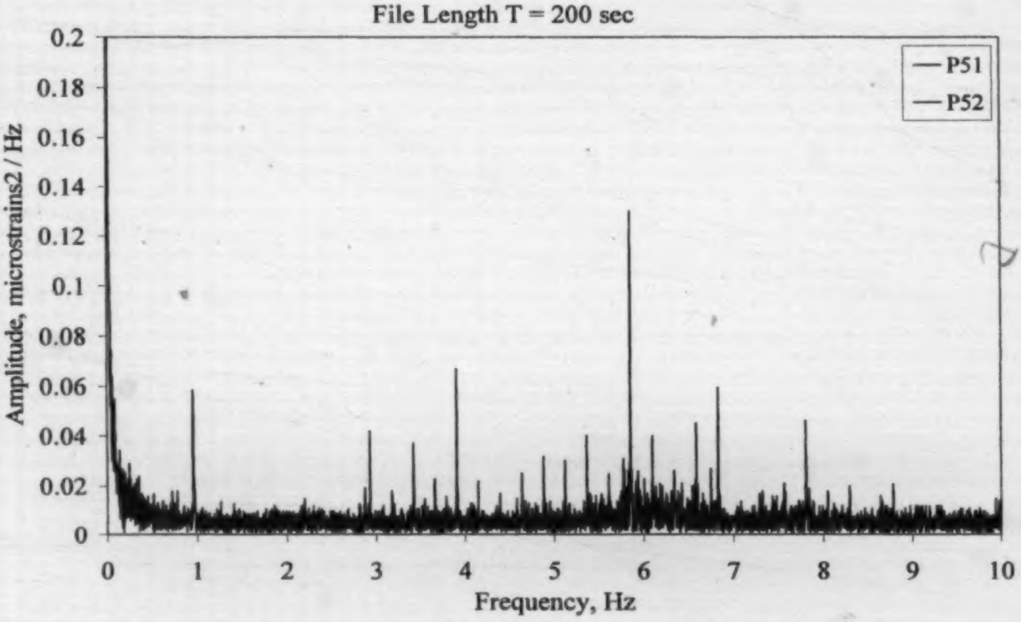

Fig. 6.15 Power spectrum for 200 sec long data at gauges P51 and P52

Having established the range of noise frequencies and frequencies of dominance from structural point of view, data files of 200 seconds are used for better spectral resolution and clear identification of structural frequencies. There are other factors like the side of dump and location of the gauge that influences the shape of the power spectrum. However, there is one factor that affects it the most and that is the influence of change in mass due to dumping of oil sand into the hopper. Natural frequency of a structure depends on its mass and stiffness. So, when the mass of the structure is changed by adding oil sand into it, its natural frequency will migrate towards smaller values because frequency is inversely proportional to mass. This trend is evident in Figure 6.16, which shows the power spectrum for data with dump event C5-R. Similar plot is obtained in Figure 6.17 for the data containing dump events C4-L, C5-R and C6-L happening in quick succession. The frequencies clearly identified earlier are no longer clear and many peaks are mired together close to each other. This is an indication of shifting natural frequencies due to significant change in mass. Frequency identification is still possible but much more difficult with this changing noise like scenario of frequencies. Another important observation to be made from Figures 6.16 and 6.17 is that the amplitude of more number of frequencies smaller than 1 Hz is increasing in the power spectrum. Going back to Figures 6.12 to 6.15, which plot the power spectrum for the base data without any dump events occurring, it can be noticed that the smallest frequency of significance identified was at 0.96 Hz. Below this frequency the amplitudes in power spectrum remained pretty low to be identified, except for the static component in the spectrum at close to zero Hz. However, in Figures 6.16 and 6.17, the magnitudes of the peaks below 1 Hz frequency are significantly higher, though difficult to clearly identify due to their shifting nature.

Having a look at the power spectrums plotted for data from some other dump events the observations previously made can be verified and clear trends can be identified. Figure 6.18 presents the power spectrum for data collected during the critical dump event C1-L in April of 2004. As expected during a dump event, migration of frequencies and spectral leakage can be easily observed. However, in spite of all these changing masses and errors of leakage, there are some clear peaks at the frequencies of 0.24, 0.49, 0.96, 2.93, 5.873, and 7.82 Hz. Many of these frequencies are the same as observed earlier for the base data when no dumps were happening. However, 0.24 Hz and 0.49 Hz were not prominently visible in the base data that are now appearing as clear peaks for the dump C1-L data. A similar trend is observed in Figure 6.19 for the data collected in June 2006 during normal operation of the crusher with hopper partially full, the peak frequencies occurring at 0.24, 0.49, 0.96, 2.93, 3.91, 4.89, 5.86 and 7.81 Hz. Thus, it is clear that the frequencies below 1 Hz are identified for higher mass of material in the hopper, when there is a dump or the hopper is full. In addition, there are other frequencies between 1 Hz and 10 Hz that are repeatedly identified in different power spectrums. An example of similar power spectrum obtained for data collected at the column gauges is presented in Figure 6.20. Due to the orientation of gauges on the columns only limited modal frequencies are captured, which are same as some of the values obtained earlier. There is also influence of frequency shift due to dumping.

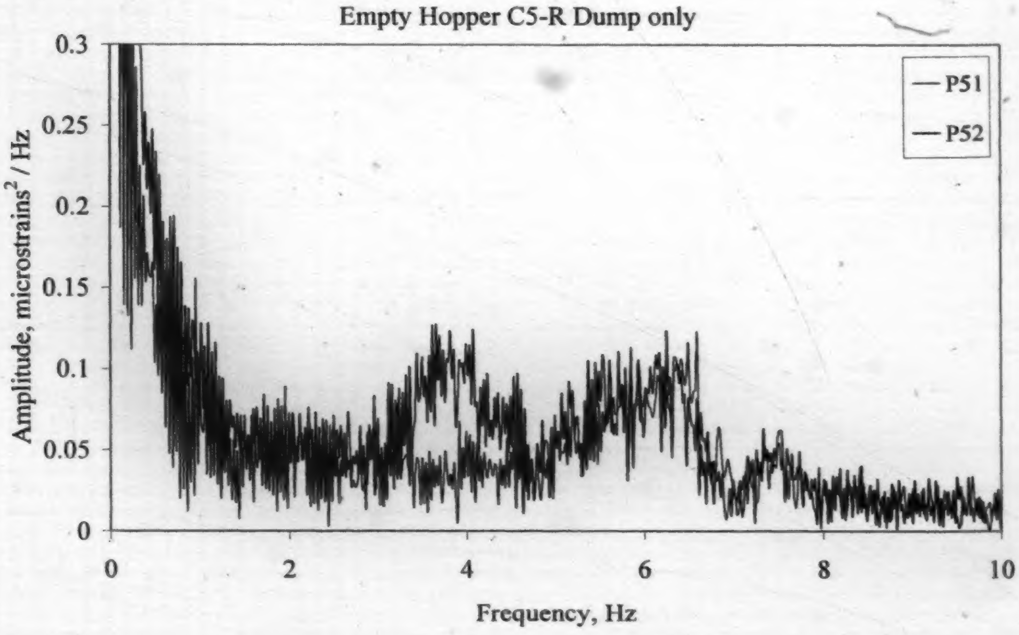

Fig. 6.16 Power spectrum during dump C5-R at gauges P51 and P52

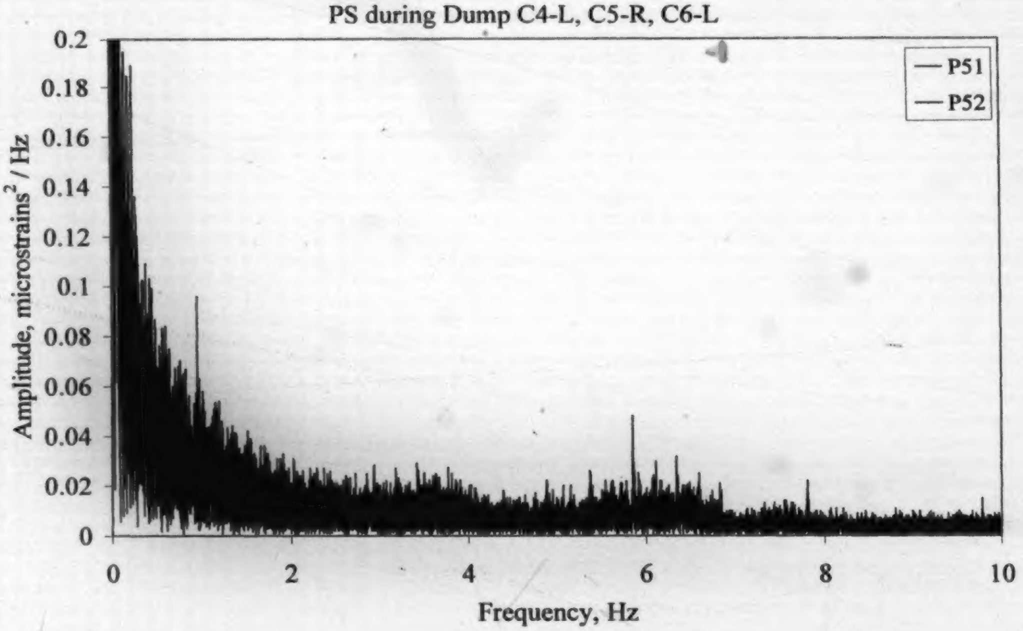

Fig. 6.17 Power spectrum during multiple dumps at gauges P51 and P52

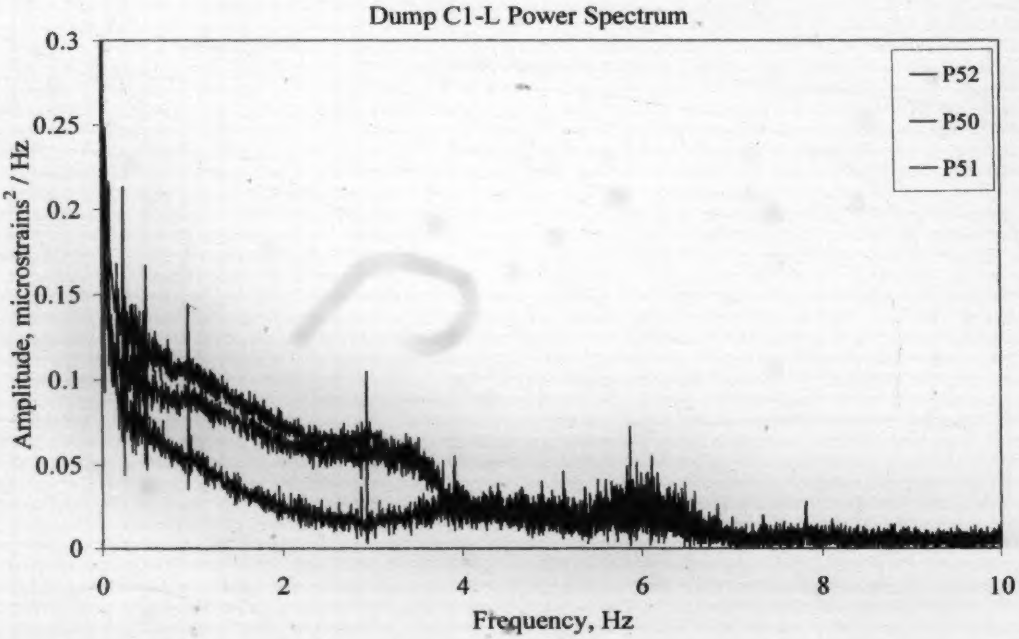

Fig. 6.18 Power spectrum for data during severe dump event C1-L in April 2004

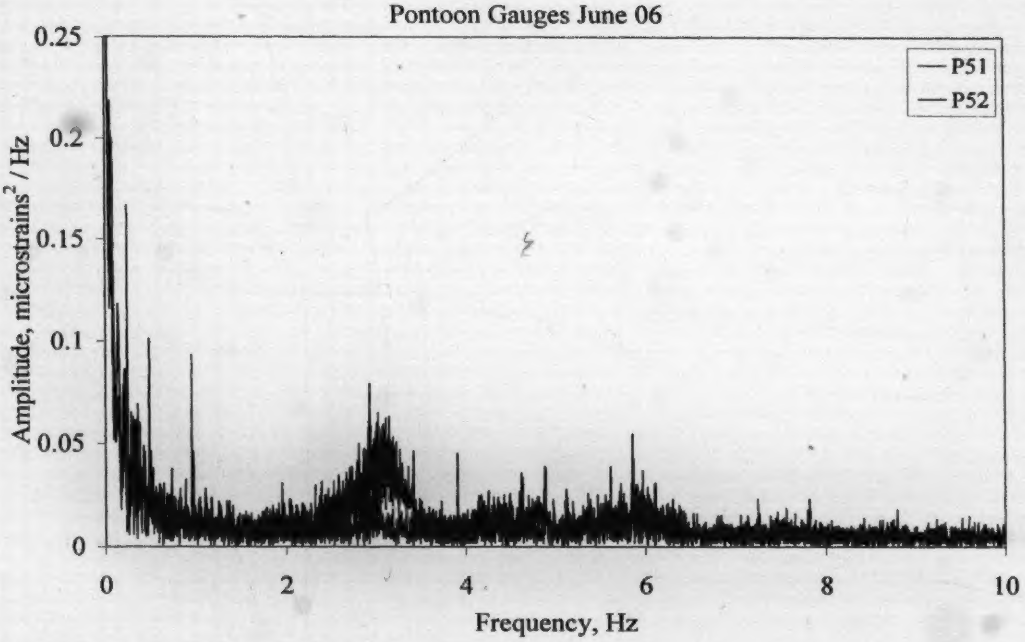

Fig. 6.19 Power spectrum for data collected at pontoon gauges during June 2006

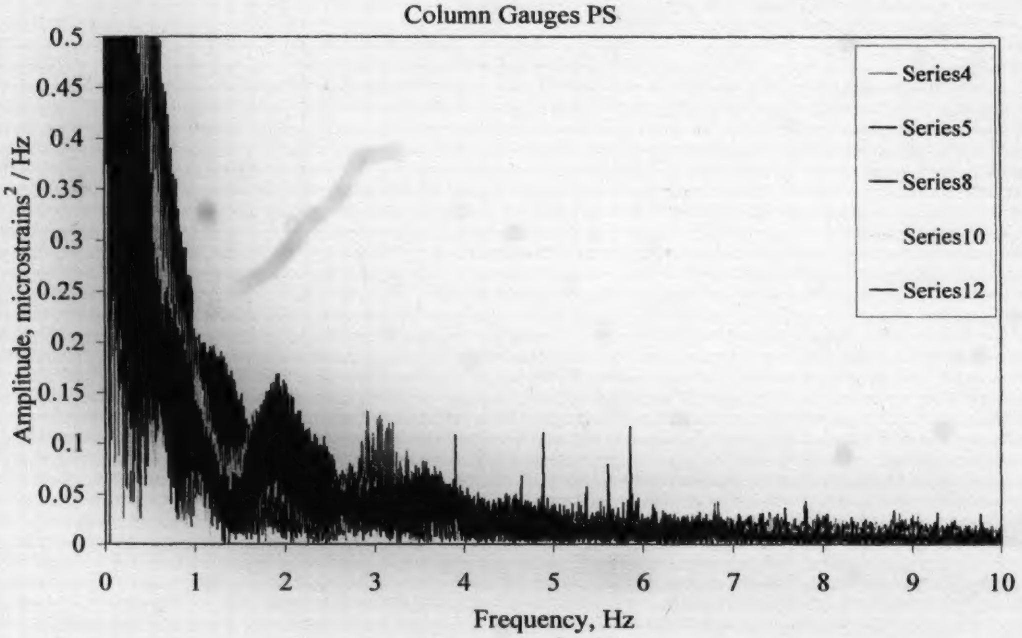

Fig. 6.20 Power spectrum for data collected at column gauges during June 2006

6.8 Band Filtering for Modal Amplitude and Damping

In the previous section noise was separated from structural response and a range of frequencies that were dominant in the power spectrum plot were picked with a frequency resolution of about 0.005 Hz. A number of peaks were obtained at particular frequencies for different gauges and loading conditions. Now, in this section each of those dominant frequency zones are looked into separately. This task is achieved by using band filtering using Butterworth filter of order five (Afhami et al., 1998, Khattak and Cheng, 2003). The frequency bands are selected in such a manner that each band is able to encompass and filter out the effect of at least one dominant frequency in the power spectrum. The filtered frequencies are then converted back into the time domain by using the Fourier amplitude and phase information for the frequencies of interest. Thus, strain amplitude vs. time plot is obtained for each dominant frequency that is filtered out, though with some phase lag due to filtering. Such a plot is able to give an insight into the strength of the particular mode of vibration on the overall response of the structure as well as the damping factor in action for that mode. Each of these pseudo-modal responses has certain amplitude of vibration and a rate of decay for the vibration, which are discussed in more detail further. The strain time histories are blown up in the region the dump event is occurring and the structure going into free vibration due to the impulse. Depending on whether the time domain plots are for higher frequency content or lower frequency content, the decay curves are usually plotted for a period of 1 to 40 seconds, in such a manner that a nice decay is obtained with sufficient number of peaks to enable the calculation of damping ratio. The logarithmic amplitude decay formula is used for calculating damping ratios associated with each dominant frequency of vibration. Such damping ratio calculations have their own sources of error and can not be assumed to be perfectly filtered from effects of other nearby frequencies. However, they definitely provide a reasonable estimate for design purposes and response prediction. The following formula is used for the calculation, where ξ is the damping ratio for the mode in question, u_o is the magnitude of starting peak and u_{o+m} is the magnitude of the m^{th} peak after that starting peak (Chopra, 1995).

[6.4] $$\xi = \frac{1}{(2 * \pi * m)} * \ln\left(\frac{u_0}{u_{0+m}}\right)$$

In the reverse order beginning from higher frequencies to the lower, Figure 6.21 and 6.22 present the time domain plot of strain for 1 second duration, with frequency content earlier identified as noise. Figure 6.21 is the strain-time plot for frequency band between 42 Hz and 48 Hz, the region where some noise peaks were observed in the power spectrum. As expected, the magnitude of strain remains pretty low between +1 and -1, which is desirable for noise frequencies. A similar plot for the frequencies between 15 to 25 Hz is shown in Figure 6.22, which again happens to be of low amplitude. Both these plots reinforce the conviction that these frequency bands only represent noise and not any structural frequencies of interest.

Going further down, the next Figure 6.23 presents the time domain response of the frequencies between 7.5 Hz and 10 Hz. There is a larger peak observed along with gradual decaying of the free vibration response. As observed earlier in this range of 7.5 to 10 Hz in Figure 6.15, there is one single peak of significance observed at around 7.808 Hz. Hence, it could be assumed that the response in Figure 6.23 must be due to this particular structural frequency of interest. The damping ratio for the response history is calculated by the logarithmic decrement method after 7 peaks as 2.6%. A similar plot for the frequency range of 6.5 to 7.5 Hz gives the time history in Figure 6.24 that is targeting the peak structural frequency perceived at 6.834 Hz. The damping ratio calculated for the eleventh logarithmic decrement is 2.73%. One common feature that should be mentioned about these two graphs is that the magnitude of strain obtained is still very low, only marginally beyond the noise amplitudes. The time history for a frequency range that includes both of the above ranges, which is from 6.5 to 10 Hz, is plotted as shown in Figure 6.25. It can be immediately observed that the amplitude of strain in this case is nothing but the sum of the amplitudes in the previous two cases. The overall damping pattern remains same, but due to mixing of amplitudes of different frequencies, the amplitude of vibration is not following the smooth logarithmic decrement pattern in this combined frequency range (Figure 6.25).

Figure 6.26 presents the free vibration decay curve for duration of 2.5 seconds for the frequency range between 4.8 Hz to 6.5 Hz in the time domain, with damping ratio calculated for the tenth logarithmic decrement as 5.3%, whereas for the fifth logarithmic decrement, the damping ratio is obtained as 3.87%. The maximum amplitude of strain in this frequency range is quite significantly between +25 and -25 micro-strains, eventually reducing to almost zero under free vibration decay. This response phenomenon in the said frequency range pertains to the dominating frequency of interest 5.852 Hz in particular (Figure 6.15), which is definitely one of the structural natural frequencies. Similarly, Figure 6.27 presents the time domain plot with frequency components between 3.5 Hz to 4.8 Hz, the dominant frequency in this range being 3.904 Hz. The amplitude of maximum strain observed during dump is again significantly high for this frequency component, which indicates its contribution in the overall response of the structure. Naturally, this confirms it as one of the natural frequencies of the structure. The damping ratio obtained for the tenth logarithmic decrement is 3.8% for this mode of vibration.

Now, in the lowest frequency zone of 0.1 Hz to 3.5 Hz, many peaks were observed at close spacing in the power spectrum (Figure 6.15 etc.) that also varied with the dump load. Hence, separation of contribution from each of those frequency components would be quite difficult with the limitations of data type. The matter is further complicated by the fact that there is presence of spectral leakage in the region and filtering is never ideal due to the presence of transition zone and some rolling. Since the lowest frequency zone is closest to the static component, chances of spectral leakage are even higher. Figure 6.28 shows the response time history component with the frequency content of 0.1 Hz to 3.5 Hz. In spite of all the possibilities of error in this zone, it can easily be deduced from the graph that there is more than one frequency of dominance in this range by the higher frequency rolling combined with relatively lower frequency decay. It can also be concluded that the component of strain response in this frequency range is substantial between +150 and -100 micro-strains; hence, some of the natural frequencies do fall in this range.

Since two peaks were observed in the power spectrum at 2.93 and 3.417 Hz that are too close to each other to be effectively filtered, a frequency band of 1.5 Hz to 3.5 Hz is selected to separate out some of the influence of these two frequencies (Figure 6.29). The maximum strain values in the vicinity of the dump vary between +60 and -80 micro-strains, magnitudes of some significance to justify the presence of natural frequencies of interest in the range. Since this is a mixed mode plot due to the presence of more than one structural frequency in the range, some irregularity can be observed in the otherwise smooth sine waves. The damping ratio calculated for the fourth logarithmic decrement of this mixed vibration mode comes to 11.3%, which is much higher than the earlier calculations for the higher vibration modes.

Figure 6.30 shows the strain time history for contributions from the frequencies lower than 1.5 Hz. The figure clearly indicates presence of more than one frequency of dominance due to some high frequency rolling on top of a lower frequency vibration. Hence, this frequency zone between 0.1 to 1.5 Hz is further broken down into three smaller regions. The vibration associated with the first region of 0.7 Hz to 1.5 Hz is shown in Figure 6.31, with damping ratio calculated for the fourth peak as 13.96%. The peak frequency of dominance in this region in the power spectrum happens to be 0.96 Hz, with amplitude of strain varying between +30 and -30 micro-strains. In the second zone of 0.4 Hz to 0.7 Hz frequency band, Figure 6.32 shows its influence on the structural strain response, with the maximum amplitude varying between +25 and -20 micro-strains and the damping ratio at 10.32%. The peak frequency in this zone occurs at 0.49 Hz, which can be credited for this response. On similar grounds, Figure 6.33 shows the response due to frequency band of 0.1 Hz to 0.4 Hz, which has the maximum amplitude varying between +20 and -25 micro-strains. The damping ratio calculated for this zone was erroneously high at 27%, which could be due to spectral leakage from the static component. However, the peak frequency responsible for this response can be identified as 0.24 Hz from the power spectrum.

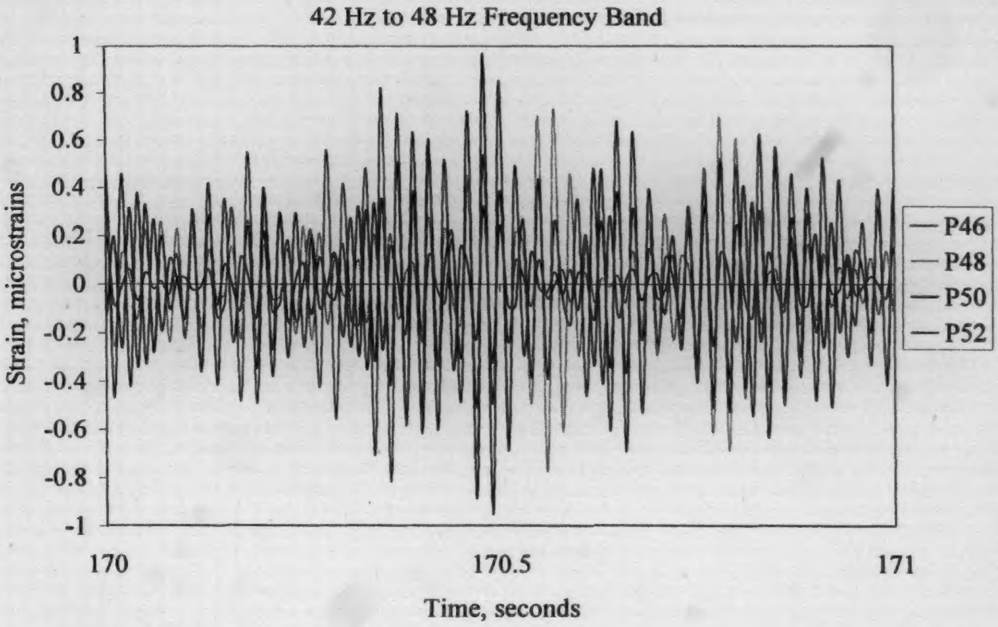

Fig. 6.21 Contribution of noise frequencies between 42 and 48 Hz to response

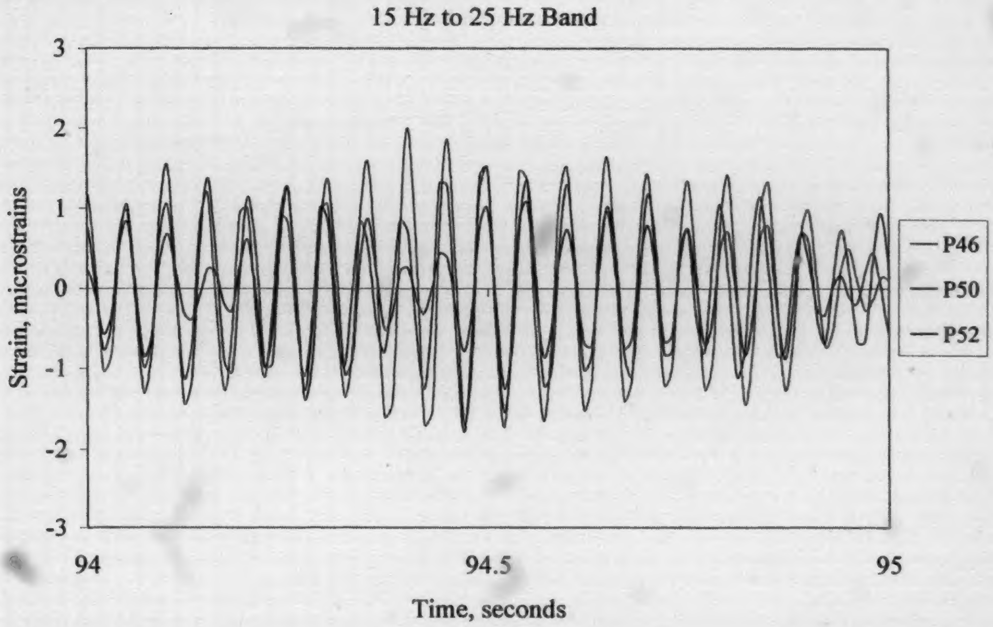

Fig. 6.22 Contribution of noise frequencies between 15 and 25 Hz to response

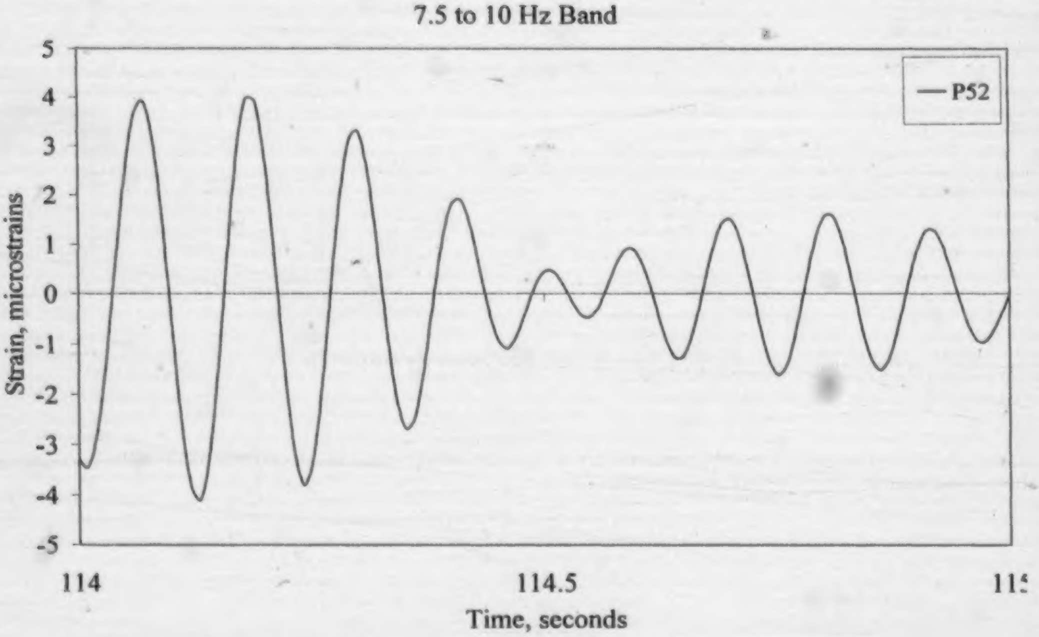

Fig. 6.23 Contribution of 7.81 Hz modal frequency to structural response

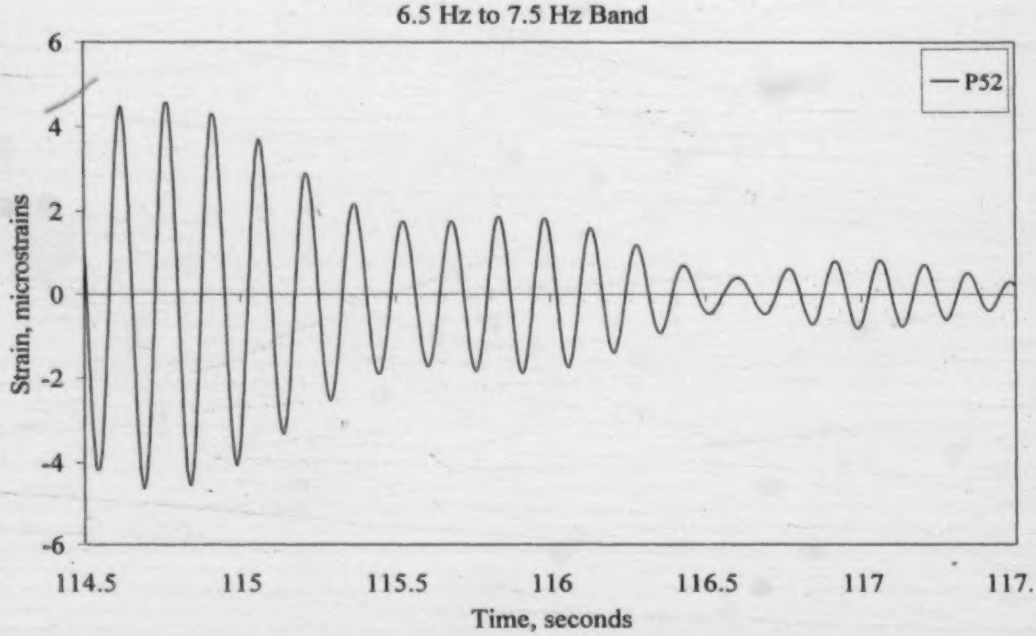

Fig. 6.24 Contribution of 6.834 Hz modal frequency to structural response

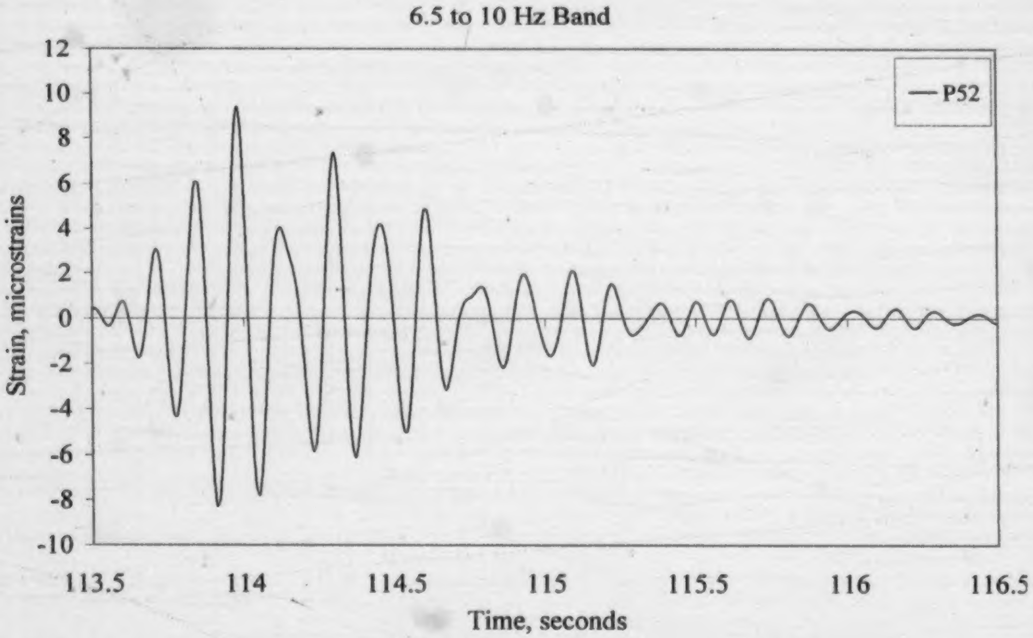

Fig. 6.25 Contribution of 6.834 Hz and 7.81 Hz modal frequencies to response

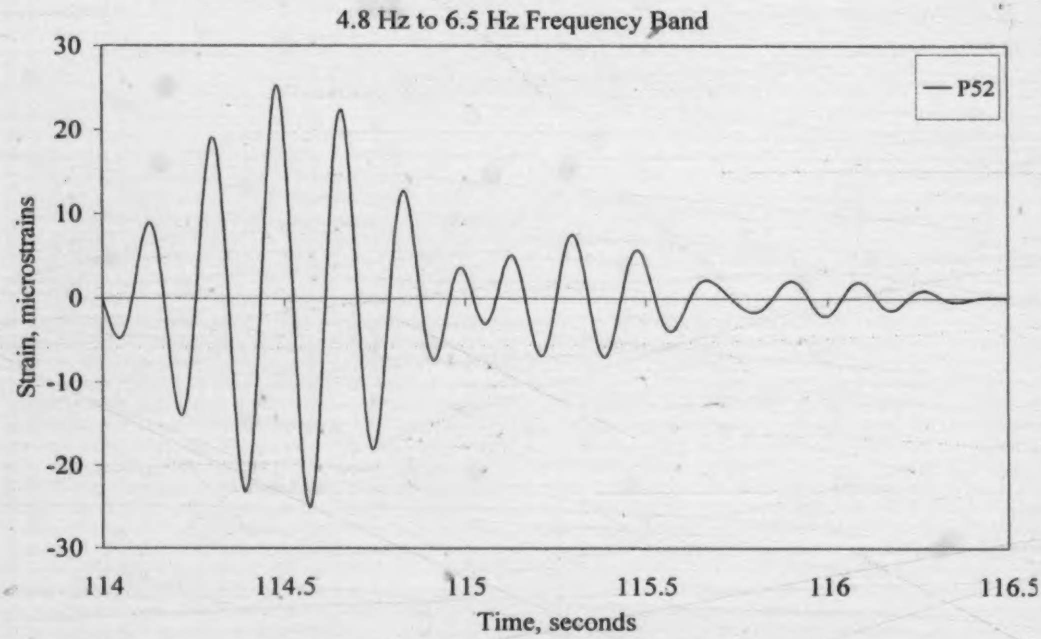

Fig. 6.26 Contribution of 5.86 Hz modal frequency to structural response

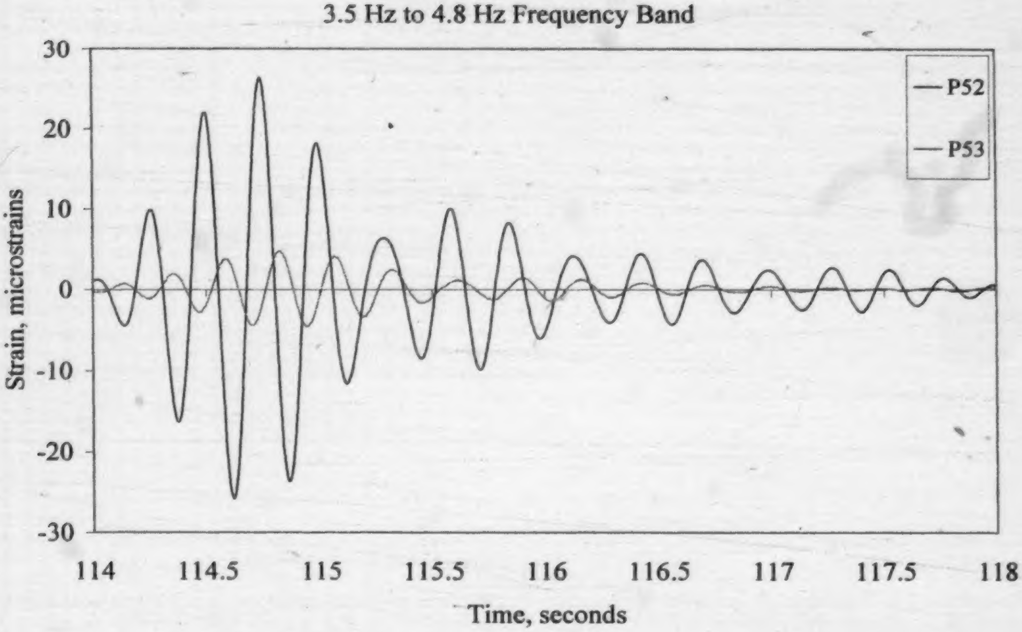

Fig. 6.27 Contribution of 3.91 Hz modal frequency to structural response

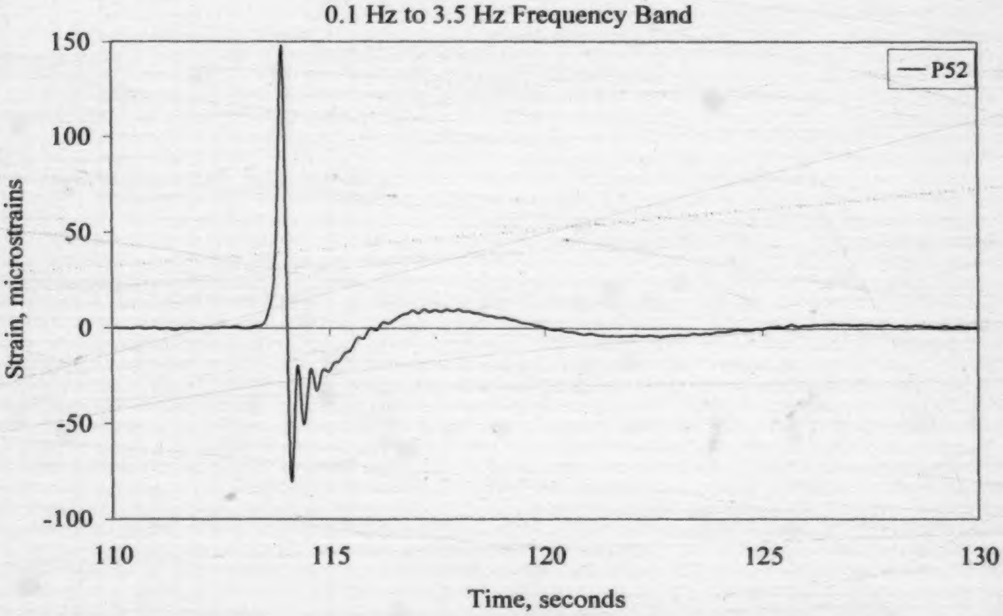

Fig. 6.28 Contribution of mixed frequencies lower than 3.5 Hz to response

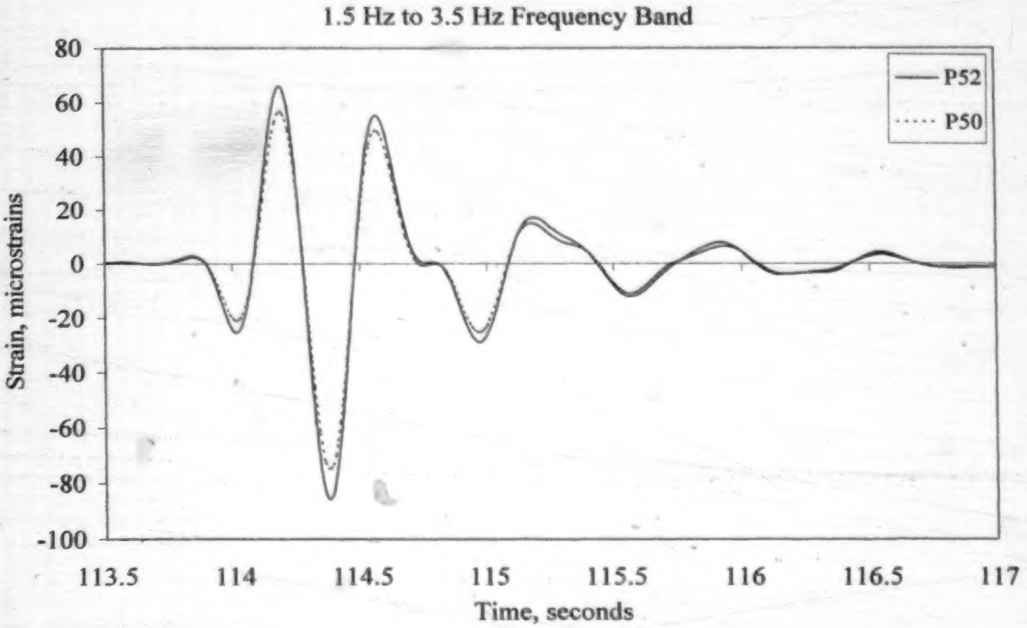

Fig. 6.29 Contribution of 2.93 Hz and 3.417 Hz modal frequencies to response

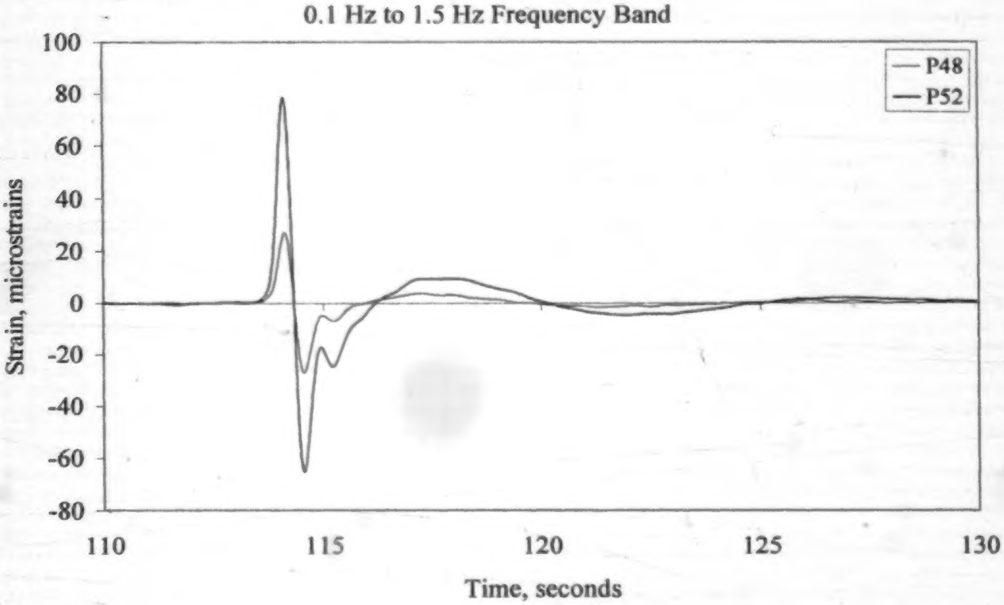

Fig. 6.30 Contribution of modal frequencies lower than 1.5 Hz to response

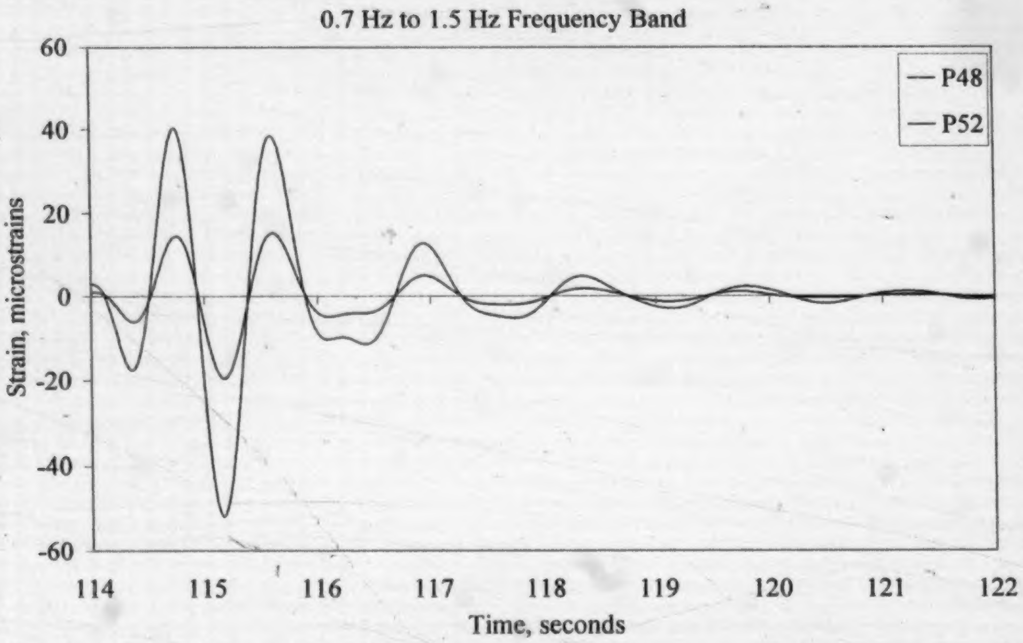

Fig. 6.31 Contribution of 0.96 Hz modal frequency to structural response

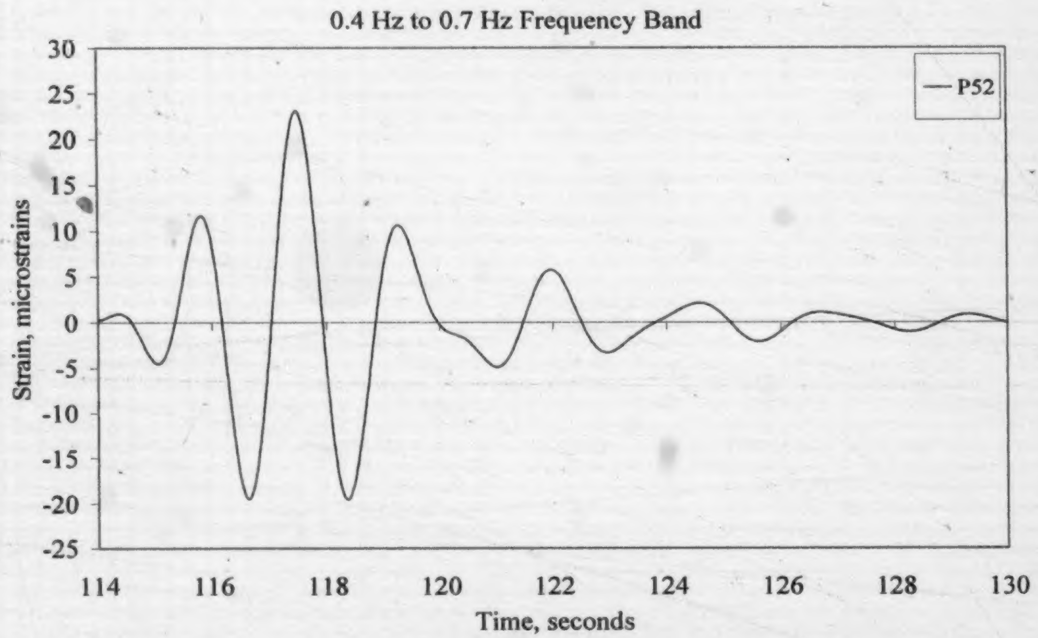

Fig. 6.32 Contribution of 0.49 Hz modal frequency to structural response

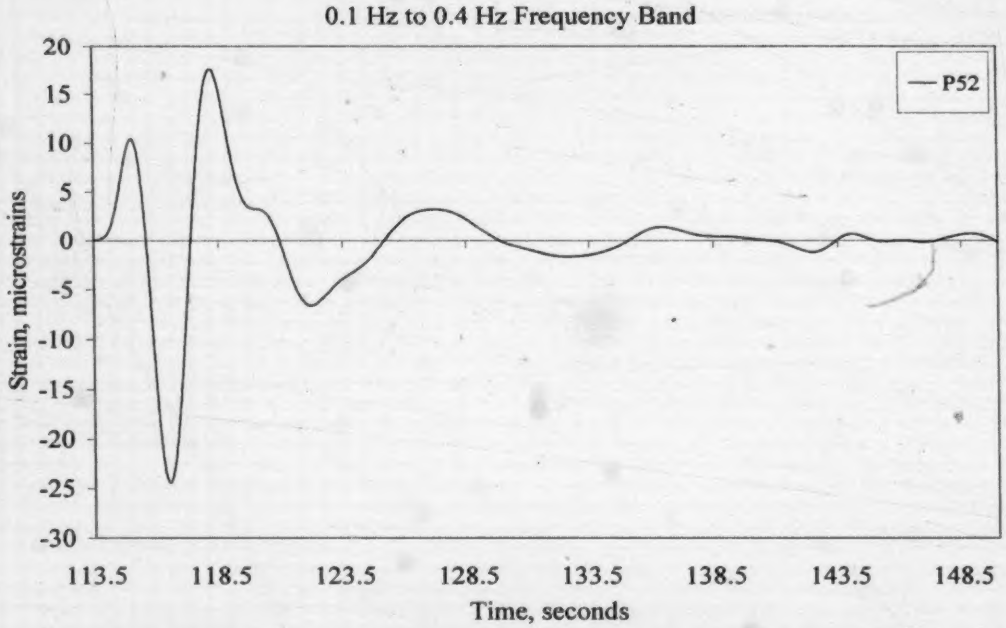

Fig. 6.33 Contribution of 0.24 Hz modal frequency to structural response

6.9 Summary

The nature of the load and structural response under it has been dealt with in a dynamic sense. By using Fourier transform and digital filtering tools, the natural frequencies and damping characteristics of the structure has been analysed. Power spectrum and filtering techniques re-affirmed that frequencies above 10 Hz were all noise and the structural frequencies were between 0 to 10 Hz. By trial and error with different periods of data files, data between 100 to 200 seconds long gave the best results in power spectrum, which amounted to frequency resolution of between 0.01 Hz to 0.005 Hz. The static component of the response is obtained by passing the signal through a low pass filter with cut off frequency of 0.1 Hz. The major frequency peaks identified by various power spectrum plots are: 0.24 Hz, 0.49 Hz, 0.96 Hz, 2.93 Hz, 3.417 Hz, 3.91 Hz, 5.86 Hz, and 7.81 Hz. The peak frequencies start shifting and getting blurred under dumping of oil sand into the hopper. An increase in the mass of the structure due to the added mass is the reason behind such shift and blur due to spectral leakage. Some of the low frequency modes become more prominent under dumping of oil sand, such as the frequencies of 0.24 and 0.49 Hz. Not all frequencies are captured at all gauge locations and under all loading conditions due to obvious reasons. Band filtering in the frequency bands of importance gives the amplitude of vibration due to various frequencies and their modal damping, which usually varies between 3% and 5% for the higher vibration modes. For the first three or four fundamental modes of vibration, the modal damping ratio was obtained between 11% and 15%, which indicates high damping due to many mechanical and functional components.

6.10 References

Afhami, S., Alexander, S.D.B., and Cheng, J.J.R. July 1998. "Field Instrumentation and Monitoring of Crowchild Bridge in Calgary, Alberta. SMSB V Conference in Calgary, Alberta, July 13-16.

Bagchi, A., Humar, J. L., and Xu, H. 2004. "Vibration Based Damage Identification for the Crowchild Bridge, an Innovative Steel Free Deck Bridge located in Canada". Structural Health Monitoring Journal.

Chopra, A. K. 1995. "Dynamics of Structures: Theory and Applications to Earthquake Engineering". Prentice Hall, New Jersey, U.S.A.

Khattak, N. A. and Cheng, J. J. R. April 2003. "Assessment and Rehabilitation of FC Girder Bridges". Structural Engineering Report No. 253, Department of Civil and Environmental Engineering, University of Alberta.

Los Alamos. June 1994. "Damage Characterization and Damage Detection in the I-40 Bridge Over the Rio Grande". LA-12767-MS, Los Alamos National Laboratory, New Mexico.

Los Alamos. May 1996. "Damage Identification and Health Monitoring of Structural and Mechanical Systems from Changes in Their Vibration Characteristics: A Literature Review". LA-13070-MS, Los Alamos National Laboratory, Los Alamos, New Mexico.

McConnell, K. G. 1995. "Vibration Testing: Theory and Practice". John Wiley and Sons Inc.

National Instruments Corporation. January 1998. “Labview User Manual”. National Instruments Corporation, Austin, Texas.

National Instruments Corporation. 2000. “Labview Measurements Manual”. National Instruments Corporation, Austin, Texas.

CHAPTER 7

STATISTICAL ANALYSIS AND FATIGUE LIFE

7.1 Introduction

Strain jump associated with each dump event identified by the data processing and management system is stored in a database, which can be used for a myriad of statistical analyses to gain knowledge about the structure and the loads acting on it. The reduced volume of data makes post processing relatively convenient and efficient compared to the original bulky and unprocessed data. Ways to extract useful information from the data in order to gain knowledge for decision-making is necessary. Many data processing and damage detection techniques have been used lately into SHM, statistical pattern recognition being one of them. From engineering point of view it is much more practical to store and analyze data such as a strain jump associated with each dump event rather than some numbers in the frequency domain. Thus, a set of statistical parameters is calculated at each strain gauge location based on strain jump recorded during a large number of dump events, which would serve as a monitoring benchmark over the years. This chapter is dedicated to presenting the statistical patterns and parameters observed from such statistical analyses on the database of dump events.

7.2 Strain Jump Stats at the Critical Gauges

Statistical properties such as mean, median, standard deviation, maximum and minimum values, etc. are considered of much value to this SHM project. Based on 1300 dump events encountered in April 2004 and June 2006, a certain pattern and values have been generated for each of the statistical parameter in consideration. When monitored over a long period of time, each of these statistical parameters has the potential to monitor and detect changes in performance to a certain extent. Clear and categorical damage detection is an independent and complete research area in itself, which however is not the main goal of this research, rather to develop and facilitate the platform for such damage detection that can be built upon in the future. Statistical properties of dump event data collected at 82 sensors have the potential to successfully monitor the structure in the long term. For the purpose of discussion and presentation in this chapter, only the selected 10 to 12 most critical gauges are shown. Similar results can be obtained for each of the remaining gauges as well.

Table 7.1 shows the statistics of data for 1300 dump events at the selected twelve gauges with gauge numbers as shown. The mean of strain jump values and the mean of absolute of the strain jump are both tabulated. In many cases the magnitudes are quite comparable in both cases, whereas in some they are significantly different. It basically depends on the type of member the strain gauge is put on. If the member is usually in tension or in compression most of the time, then the mean or mean of absolute will have similar magnitudes. However, if the member fluctuates between tension and compression depending on the type of loading, then the magnitudes of the two means are different from one another. Gauges placed on vertical columns are found to exhibit such fluctuating behaviour depending on whether the horizontal component of the load is acting to the right or to the left of the column, for example gauge C1 and gauge C20. Standard error of the mean is usually quite low between 1 to 3 micro-strains. The 95% confidence interval for the mean is also within a range of 1 to 4 micro-strains, which is excellent for the magnitudes of the mean concerned.

In addition to the mean and standard deviation of strain jump at a gauge location, the maximum (positive, tensile) and minimum (negative, compressive) values are also of importance in monitoring the health of a structure. The difference between the positive and negative values of strain jump is defined as the Range, which is another useful parameter worth monitoring. Thus, any significant variation in these statistical parameters at a gauge location would signal some major change in the structural stiffness or boundary conditions. Such changes if found at more than one gauge locations, would reinforce the belief that the structure has seen some major event or damage. The strength of such changes on different gauges might help pin-point the location of damage as well.

Table 7.1 Statistical properties of Dump Events at the critical gauges (unit: micro-strains)

Gauge No.	Mean	Mean of Absolute values	Median	Std. Dev.	Std. Error	95% C. I.	Minima	Maxima	Range
C1	6.62	29.58	25.29	18.63	0.52	1.01	-246.35	111.71	358.06
C7	-95.01	97.84	89.81	45.70	1.27	2.49	-655.63	85.67	741.30
C10	-98.87	101.35	93.03	52.92	1.47	2.88	-438.00	65.43	503.43
C13	42.57	44.04	41.42	19.61	0.54	1.07	-52.86	117.42	170.28
C16	-164.12	168.47	153.48	87.84	2.44	4.78	-507.49	137.48	644.97
C20	-6.71	33.77	28.94	20.48	0.57	1.11	-384.12	110.71	494.83
C24	-158.32	162.30	145.89	85.39	2.37	4.65	-495.63	139.66	635.29
C34	-113.94	116.88	108.31	55.69	1.54	3.03	-596.92	92.64	689.56
C36	-105.75	109.06	103.08	54.00	1.50	2.94	-512.22	64.77	576.99
C40	-120.60	125.49	117.37	61.29	1.70	3.33	-373.95	102.29	476.24
P52	25.85	29.41	23.34	18.59	0.52	1.01	-43.32	235.28	278.60

Figure 7.1 shows the bar chart of maximum (positive or negative) values and the mean values of strain jump encountered at various strain gauges on the structure. Such plots can be made daily, weekly, monthly and annually. Such a break up of statistical information allows accounting for effects of climate and temperature on such data, if any. Thus, a daily, monthly or annual maximum, minimum and mean strain jump values can be calculated. Any shift in the values can be monitored and recognized gradually over time.

It can be gathered from Figure 7.1 and Table 7.1 that the extreme values of strain jump encountered at various strain gauges could be in the range of more than 700 micro-strains. A better view of the extreme values and the mean values is shown in Figure 7.2. It can be observed that the extreme values are many times larger than the mean values, which signifies that the extremes are less frequently occurring. The largest magnitudes of strain jump observed are occurring on the bracing members, like C7, C8, C16, C17, C23, C24, C34, C36, C40, etc. Figure 7.3, which shows only the mean strain jump across many gauges, confirms that the same members also happen to have the highest magnitude of mean strain jump. Thus, those members are regularly under high stress and it is not one secluded case of high stress loading. The absolute mean strain jumps at most of the gauges happen to be less than 100 micro-strains, except for a few gauges that inadvertently happen to be on the bracing members. The mean strain jumps on the rest of the gauges are varying between 20 and 100 micro-strains. These first values for the statistical parameters at each gauge location would serve as the benchmark for monitoring of the structure that can be adjusted later as per future needs and behaviour. These statistical observations also help identify the structural members that are consistently under comparatively higher stresses, which would be of much help in making appropriate modifications in future designs.

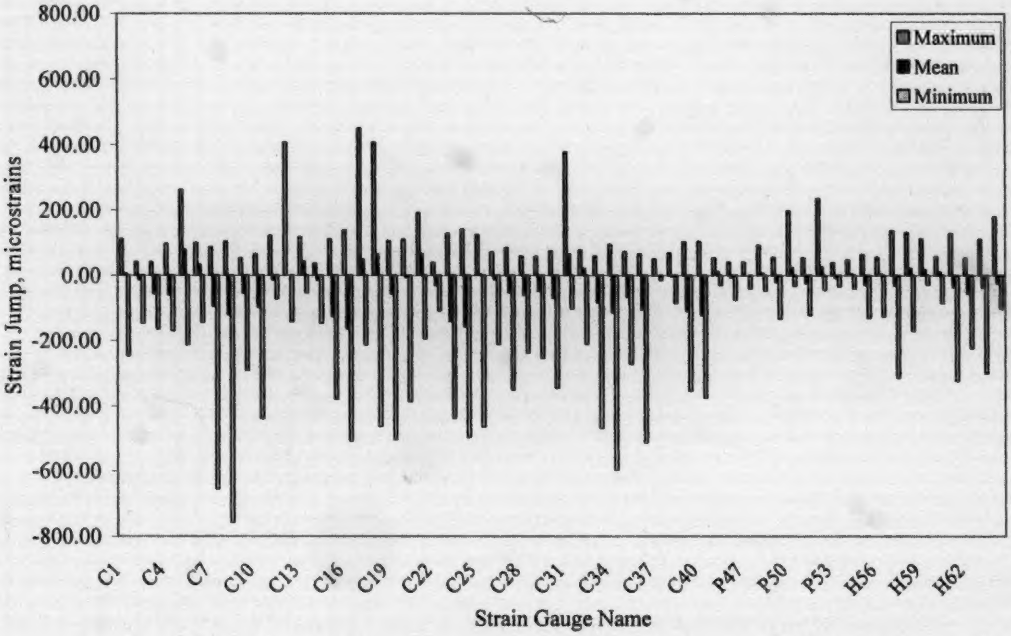

Fig. 7.1 Mean and extreme (max/min) values of strain jump at different gauges

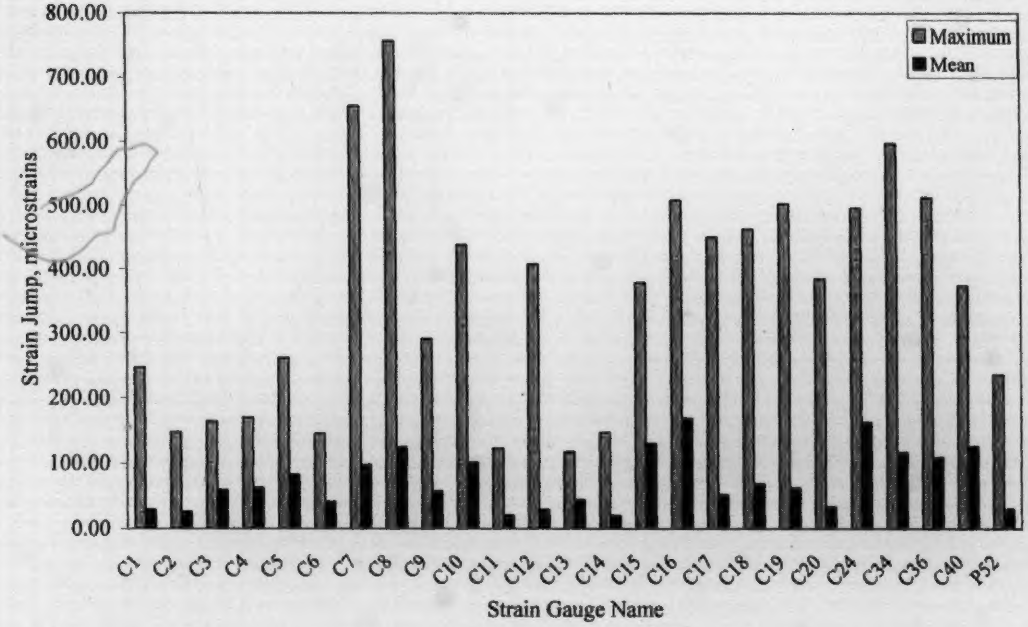

Fig. 7.2 Mean and maximum values of strain jump at different gauge locations

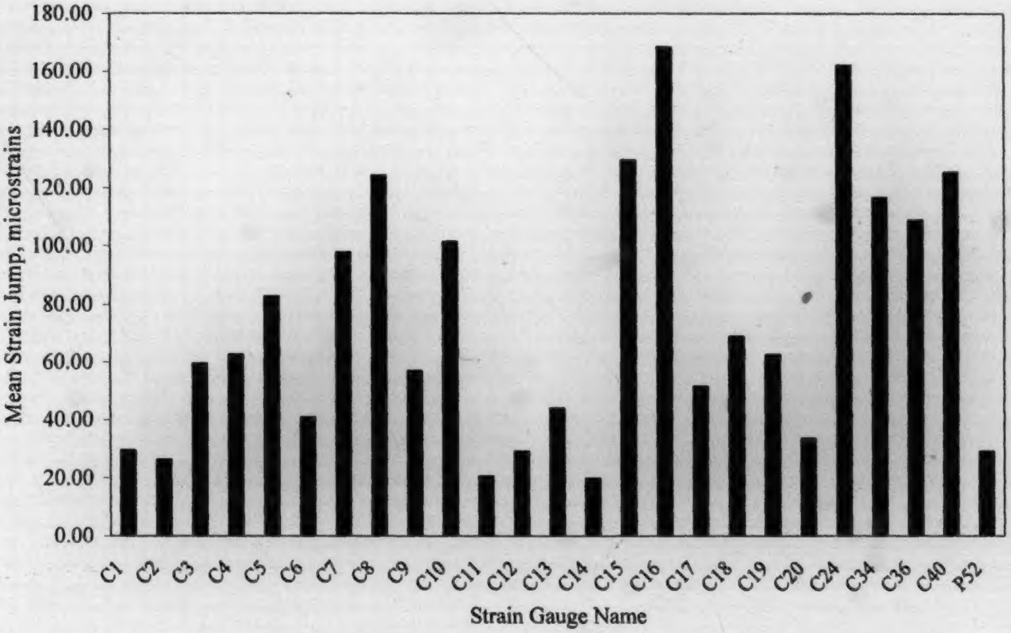

Fig. 7.3 Mean values of strain jump at different gauge locations

7.3 Histogram of Strain Jump at the Critical Gauges

Histogram is a great statistical tool that lends meaning to large numerical data set by grouping some data together into a suitable number of groups or bins and presenting it graphically in a more organized way. Histograms are eventually able to represent the probability distribution functions for a random variable, which in this case happens to be the strain jump recorded during dump events. Thus, the frequency of occurrence of a particular strain magnitude at a particular gauge location, and consequently, its corresponding probability of occurrence can be viewed in a glance on histograms. In a statistical sense, assuming that a sufficiently large sample population has been considered, it can be argued with confidence that the sample mean would approach population mean. Hence, assuming that whatever loading or dumping pattern has been observed in a day or in a week of operation of the crusher, a similar loading pattern can be expected to repeat every time. And by the same argument, the same response pattern repeated at each gauge location. So, the histogram at each gauge location would represent the characteristic property of structural response at that gauge location and its distribution shape and sample mean would remain similar over time. This would be taken as the statistical property of the population of response at that gauge, which does not change with time and remains statistically constant, except when damage occurs. Thus, histogram shape and its spread over time can be monitored for any significant change, which would be a sign of structural change due to damage. Sigma Stat and Sigma Plot software have been used to generate and plot the histograms.

Figures 7.4 to 7.15 show histograms of strain jump response at selected critical strain gauges experiencing typically high strains plotted from a database populated by 1300 dump events occurring during tests conducted in April 2004 and June 2006. The histograms are able to show the response of the structure at the gauge locations under different loading conditions over the course of the day. Knowledge of number of dump events and their strain magnitudes every year makes it possible to predict the remaining fatigue life of the structure and recommend a maintenance schedule. In addition, strain patterns among different groups of sensors are also established to complement the monitoring process. Significant variation in the mean value and extreme values of strain jump or its pattern would serve as the wake up call to conduct more in depth analysis and inspection of the structure.

It is quite obvious from the histograms that the column gauges experience much higher strain levels more frequently than the gauges on pontoon or hopper. Figure 7.14 shows the histogram of dump response at the pontoon mid span as captured by gauge P52. Strain jump associated with most of the dump events at the gauge location P52 are centered around 25 to 50 micro-strains, which could be considered as the mean range. However, there are a few occasions when the strain varies from -50 to 230 micro-strains, their occurrences being few and far though. It can also be observed that two separate distributions are obtained for positive strain values and negative strain values, as depicted by the two peaks on either side of the zero strain. Similarly, Figure 7.15 shows the dump response of critical gauge H61 placed on the underside of the hopper. Again the magnitude of strain jump is mostly between 0 and -100 micro-strains, with rare cases going close to -300 micro-strains. However, when comparing these strain jump magnitudes to the ones recorded by column gauges as shown in Figures 7.4 to 7. 13, it can be immediately observed that the strain jump magnitudes at hopper and pontoon are lower in comparison.

Now that it is established column gauges experience higher stresses repeatedly, a little more is investigated into them. Not all column gauges experience equally high stresses. Gauges placed on the columns in Gridline-2 experience typically low strains, which is evident by the fact that none of the gauges on Gridline-2 feature in the list of critical gauges, simply because they are smaller in magnitude. As can be seen in Figures 7.4 to 7.13, all of these gauges are placed on columns in Gridlines-4, 5 and 6. Among all column gauges, the strain jump recorded on the column bracing members are the highest encountered on the structure. Figures 7.9 to 7.13 present the histogram of strain response under dumping at the gauges on bracing members like gauge C7, C34, C16, C40, and C24. It can be observed that these gauges frequently observe strain jump in the range of

200 to 400 micro-strains, and on many occasions even up to 500 and 600 micro-strains. Thus, even the average (or mean) strain jump magnitudes for these bracing gauges are higher than 100 micro-strains. It can also be noticed that most of the bracing members are subjected to compressive stresses (negative strain jump) due to most of the dumping. However, on some occasions they do as well experience tensile stresses in the range of up to 100 micro-strains. As explained earlier, these histograms for the bracing members also show two different distributions for the strain jump with positive sign and negative sign, as evidenced by one large peak and one smaller peak on either side of the zero strain. Thus, these distributions of tensile and compressive strains together can constitute a useful monitoring tool in the long run.

On the contrary, the strain jump at the gauges on the vertical column members appear to be significantly lower in magnitude as shown in Figures 7.4 to 7.8 for gauges C10, C5, C36, C13, and C20. These gauges are taken at least one from columns on each of the column gridlines 4, 5, and 6. Strain jump in the range of 100 to 200 micro-strains are found most frequently occurring, whereas a few rare occurrences of up to 400 micro-strains. Thus, the pontoon is expected to have the longest fatigue life, the vertical column members to have relatively shorter life, and the inclined column bracings to have the shortest fatigue life based on the frequency of high stress cycles they are subjected to. The strains on hopper gauges are also relatively lower in comparison to columns and bracings. However, since all parts of the hopper have not been instrumented, its fatigue life can not be predicted with accuracy. In the next section the fatigue life calculations for typical structural members of the crusher is carried out based on the histograms plotted here.

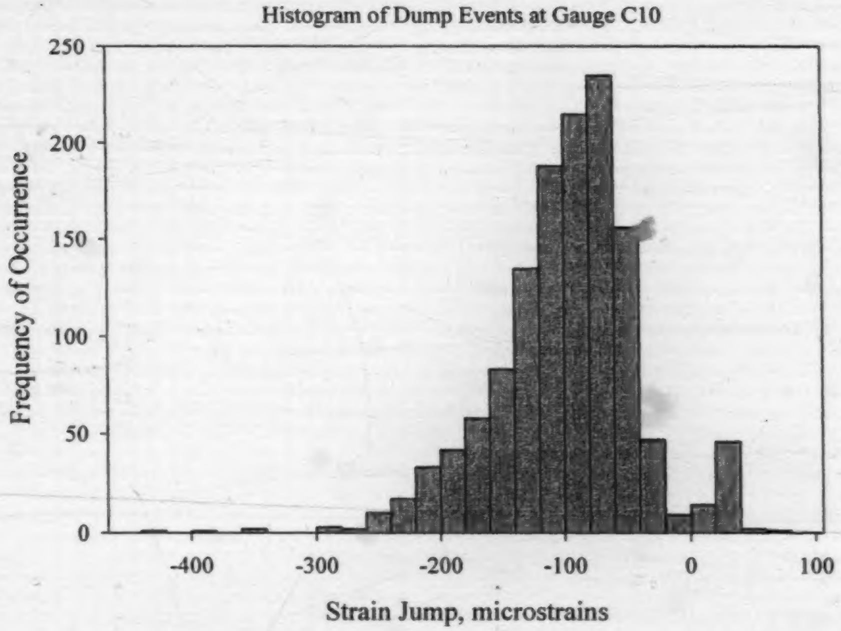

Fig. 7.4 Histogram of strain jump at column gauge C10 on Grid-4 Right side

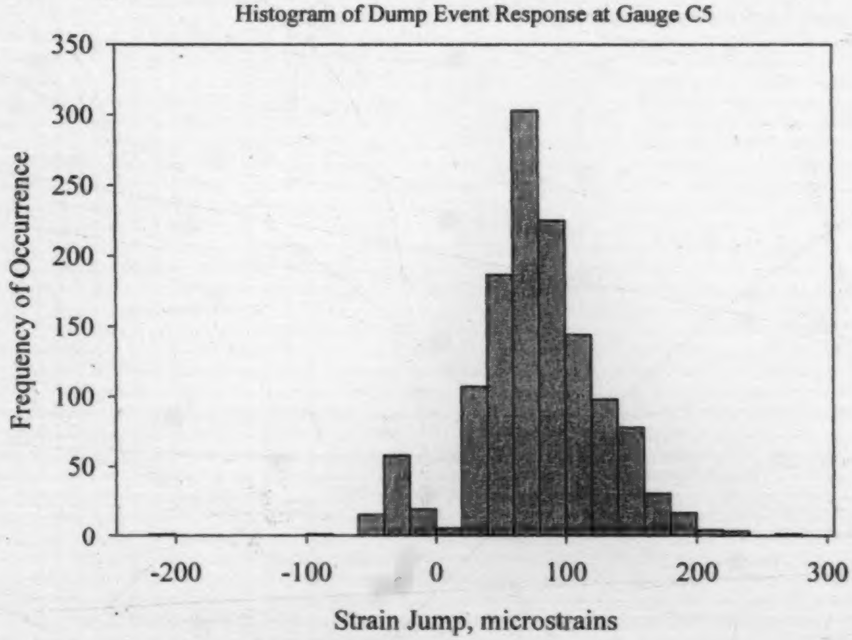

Fig. 7.5 Histogram of strain jump at column gauge C5 on Grid-4 Right side

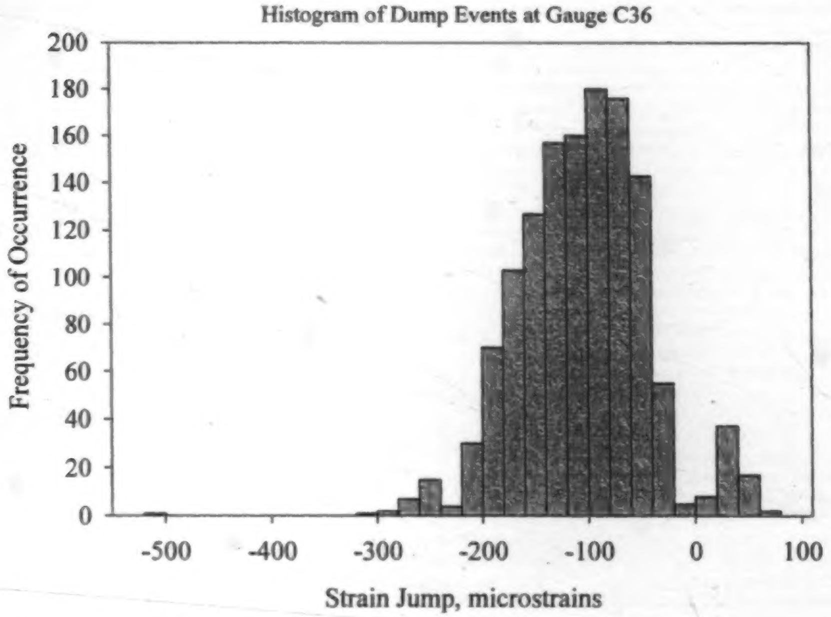

Fig. 7.6 Histogram of strain jump at column gauge C36 on Grid-4 Left side

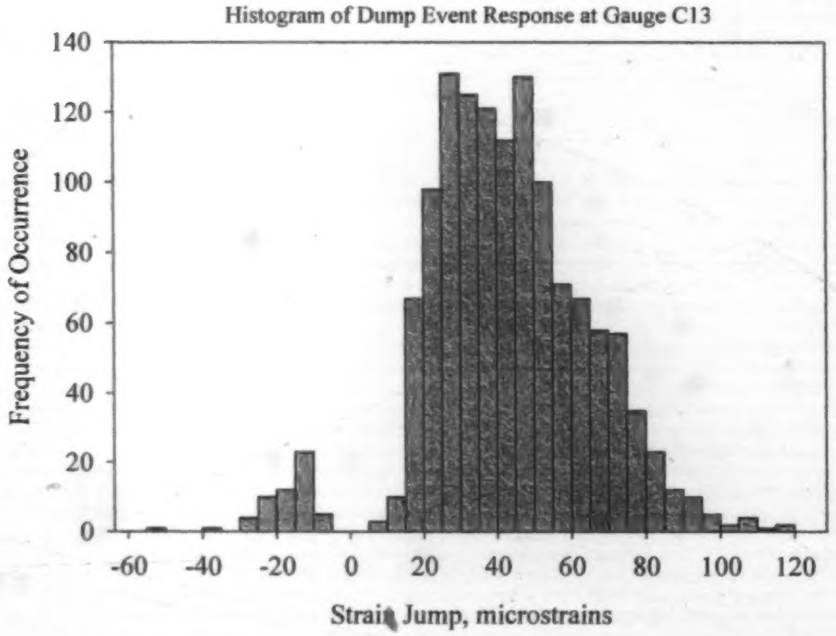

Fig. 7.7 Histogram of strain jump at column gauge C13 on Grid-5 Right side

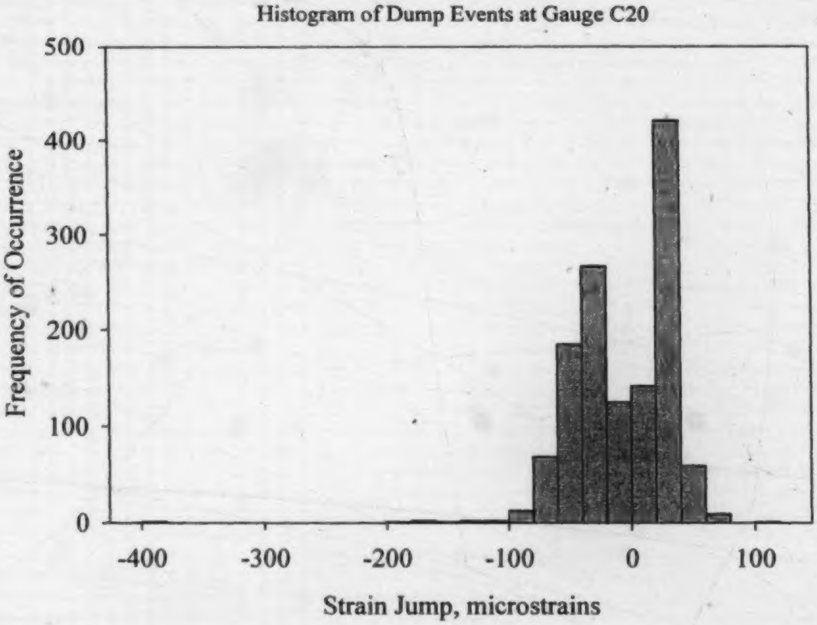

Fig. 7.8 Histogram of strain jump at column gauge C20 on Grid-6 Right side

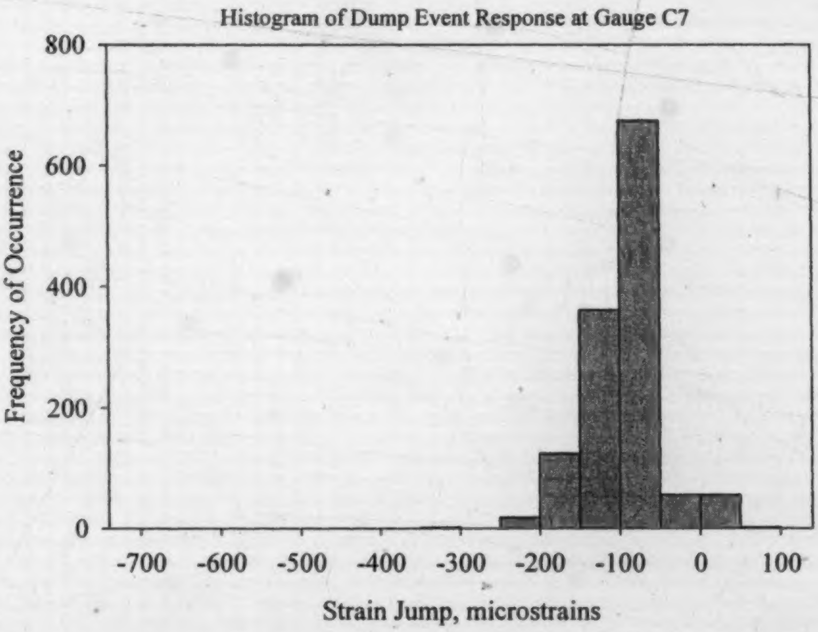

Fig. 7.9 Histogram of strain jump at bracing gauge C7 on Grid-4 Right side

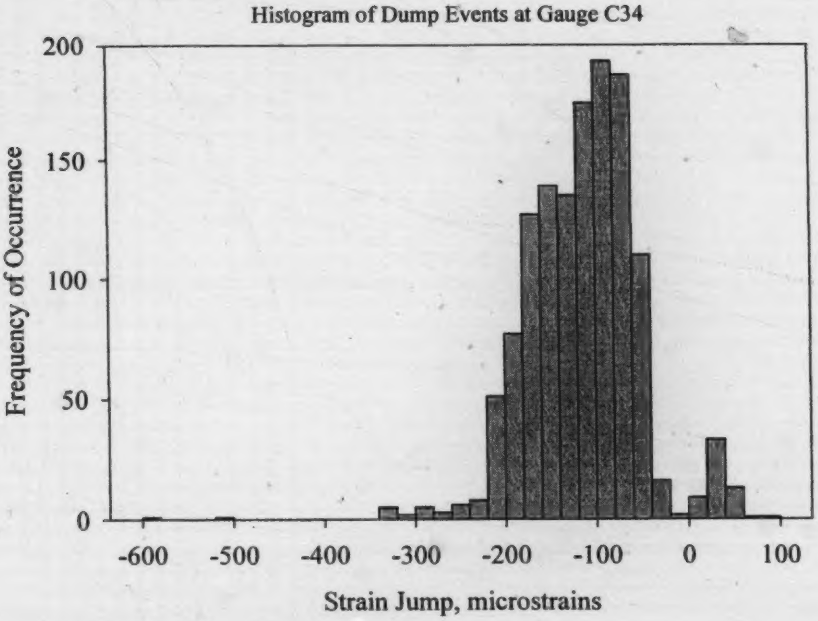

Fig. 7.10 Histogram of strain jump at bracing gauge C34 on Grid-4 Left side

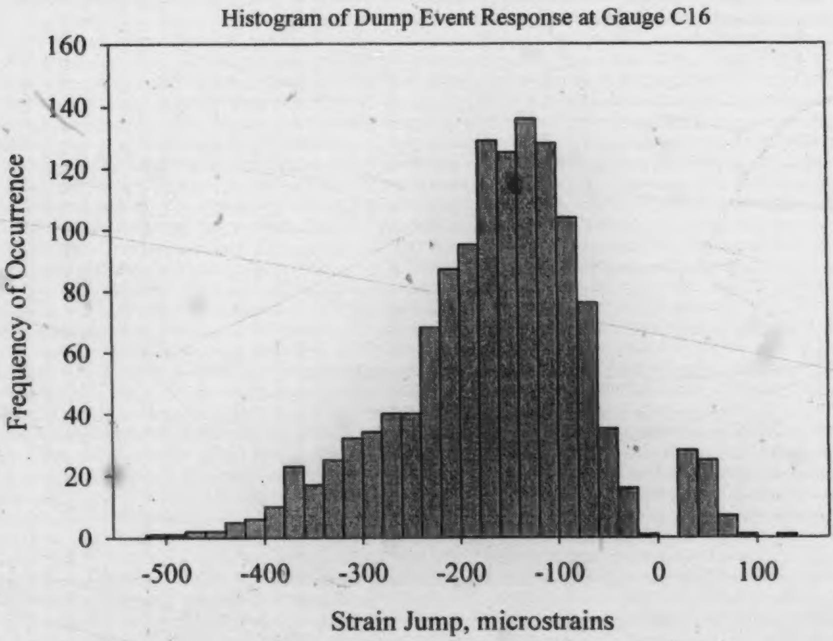

Fig. 7.11 Histogram of strain jump at bracing gauge C16 on Grid-5 Right side

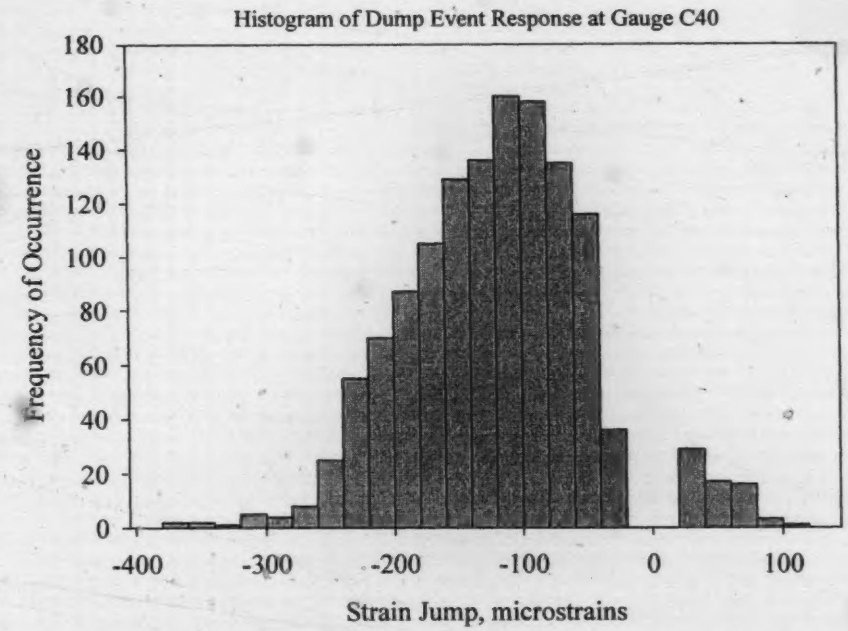

Fig. 7.12 Histogram of strain jump at bracing gauge C40 on Grid-5 Left side

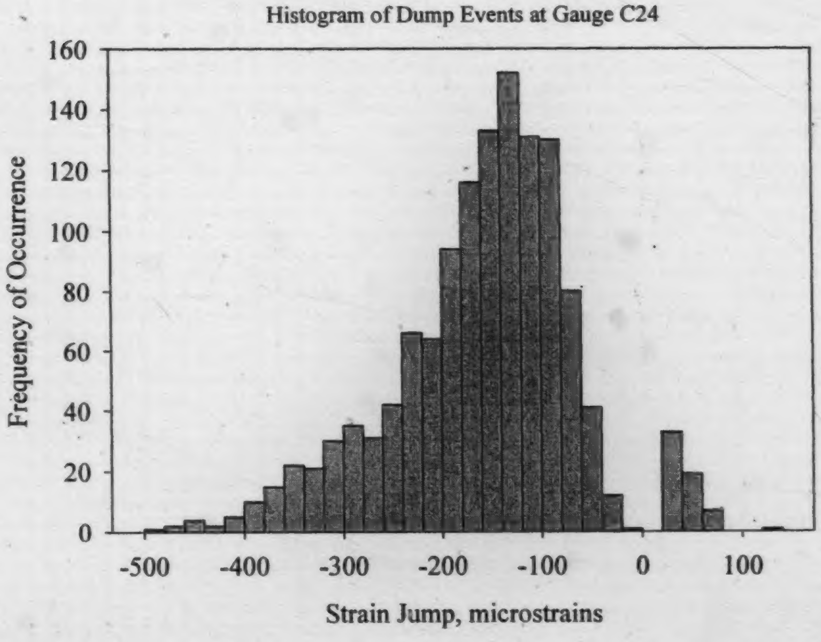

Fig. 7.13 Histogram of strain jump at bracing gauge C24 on Grid-6 Right side

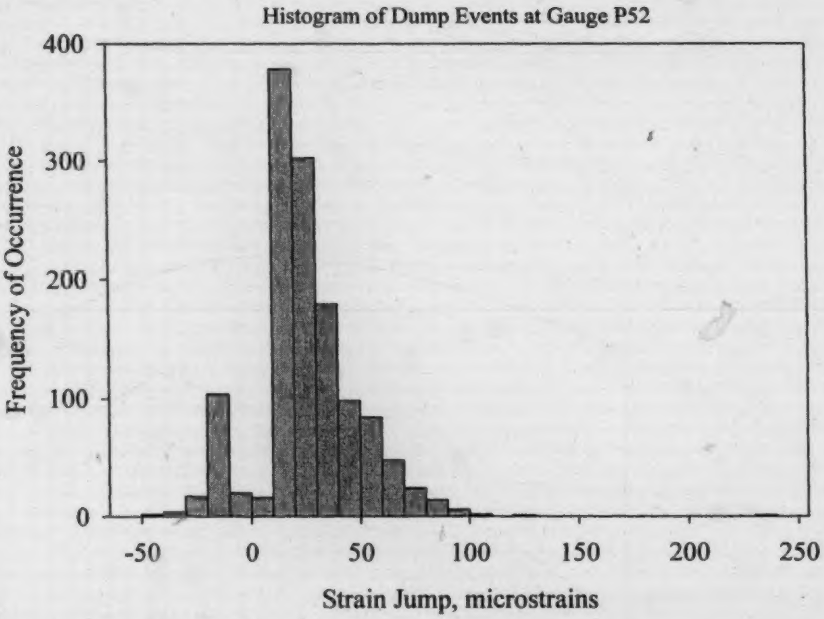

Fig. 7.14 Histogram of strain jump at gauge P52 on pontoon mid-span

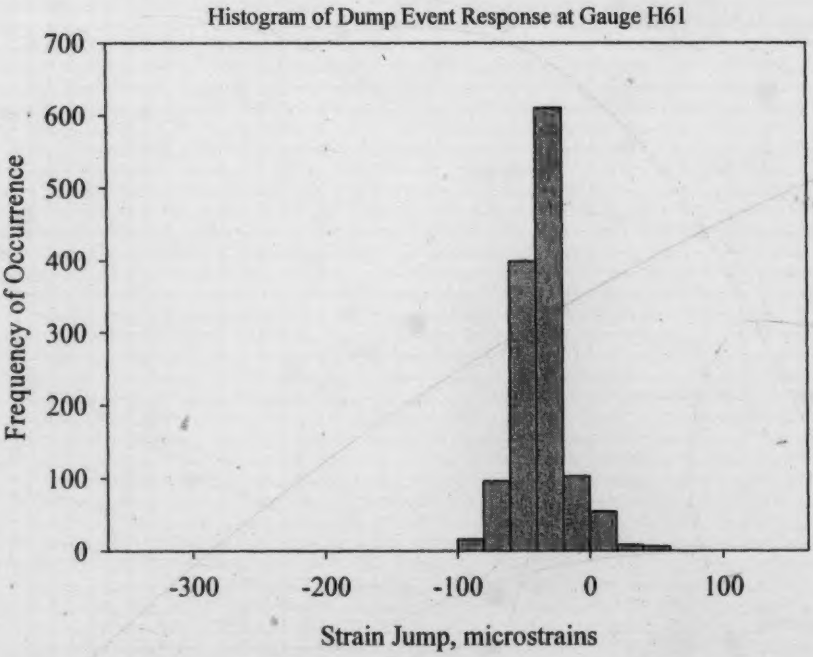

Fig. 7.15 Histogram of strain jump at gauge H61 on hopper

7.4 Fatigue Life Calculations

Fatigue and fatigue induced fracture are the leading causes of failure of steel structures. With the repetitive nature of loading experienced by the Aurora II crusher, calculation and assessment of its fatigue life assumes much significance. With the abundance of real field data provided by the SHM system that is permanently stored in the database system, it is possible to perform a very realistic fatigue check on the crusher structure. A typical sample of each component of the crusher that is under significant repeated loading has been selected for this purpose. The history of loading or strain is obtained from the histogram plotted from the database of strain jump at each of the typical critical gauge locations. Thus, one gauge each is presented for the pontoons, columns and the hopper. In order to apply the provisions of Limit States Design of Steel Structures S16-01 into fatigue life calculation of the crusher structure and its components, it is necessary to establish the nature of stress concentration or the Detail Category of connections as per the code.

The crusher structure is built by welding at most locations, with bolting at strategic locations to facilitate easy assembly and erection. Naturally, when there is presence of welding the connection has to be categorized as a welded detail in spite of the presence of comprehensive bolting, primarily because there is presence of a crack prone zone on the member. Most of the connection details are fillet welded with presence of both longitudinal and transverse welds, as well as web and flange stiffeners in the vicinity of the connection. There is also presence of some gusset plate connections. As per CSA S16-01, 2001 such connections are mostly categorized into Category E. Thus, at best some connection details can be a Category C and at worst Category E. Looking at the majority of the connection details and preferring to err on the conservative side, it is decided to treat them all as category E details for the purpose of fatigue life calculations. The fatigue life of a member is given in terms of the number of stress cycles by N in the following equation.

$$N = M\,(\Delta\sigma)^{-m} \qquad [7.1]$$

where, M is the constant specific to the category detail, m is the slope taken equal to 3 or 5, and Δσ is the strain jump or constant amplitude strain range in MPa.

Since the structure is not subjected to constant amplitude stress range at all times and the magnitude of stress can vary widely as shown by the histograms in the previous section, an equivalent stress range approach has been used for calculation of fatigue life. The equivalent stress range is calculated based on the strain histories depicted by the histograms using the following equation based on the Palmgren-Miner cumulative fatigue damage rule (Kulak and Grondin, 2002).

[7.2] $$\Delta\sigma_e = \left[\Sigma\alpha_i \cdot \Sigma\Delta\sigma_i^m\right]^{\frac{1}{m}}$$

where, $$\alpha_i = \frac{n_i}{\Sigma n_i}$$

n_i is the number of stress cycles suffered at stress range level $\Delta\sigma_i$ and $\Delta\sigma_e$ is the equivalent stress range for constant stress fatigue life calculation.

Based on these equations, the equivalent stresses for the column bracing members are obtained as the highest of all. The equivalent stress at gauge C24 on a bracing member is obtained as 40.71 MPa for the stress history encountered and recorded at that location. For this equivalent constant stress assuming a category E connection detail, the fatigue life of the bracing member is obtained as 5.34 million cycles. Since the crusher structure is subjected to an average of 0.203 million cycles per annum, the life of the bracing member in simple terms is obtained as 26 years. This fatigue life calculation is not based on theoretical assumptions, rather on actual field operating stresses. This life of 26 years is calculated for one of the worst affected bracing members and a connection detail category E.

A similar exercise for the strain jump at critical gauge C10 on vertical column member yields an equivalent stress range of 25.41 MPa, which leads to a fatigue life of 24.48 million cycles or 120 years of operation. Similarly, the equivalent stress range for the hopper gauge H62 is obtained as 15 MPa and that at pontoon gauge P52 is obtained as 8.27 MPa. Both the stress ranges are representative of the field equivalent stress range faced by pontoon and hopper. However, their relative magnitudes when compared to the equivalent stress range at the columns and bracings are quite low. Consequently, the fatigue life of those members under these constant equivalent stress cycles for category E detail are calculated as infinity. Hence, in general, the structure as a whole and the bracing members in particular happen to be acceptable from fatigue point of view based on field test results. The equivalent stress ranges presented here are for the most critical gauge locations representative of the hopper, columns, and pontoon, and hence, present a conservative estimate of the structure as a whole. Based on the weakest link in a chain philosophy, the bracing members govern the fatigue life of the structure and hence, they are the ones that will need repair or maintenance most frequently. Hence, in worst case scenario based on the field observations, the fatigue life of the crusher structure is 26 years.

Once the fatigue life of the structure in a healthy condition has been established, it is now necessary to investigate the ability of the structure to withstand fatigue in a slightly damaged condition. As mentioned earlier in Chapter 2 that one of the main problems encountered on similar crusher structures in the past has been due to loss of bolts at connections leading to cracking. Hence, assuming a similar loss of bolt condition at the connection of a critical member would mean significant rise in the critical stress at that location. It is assumed that two thirds of the bolts are lost in a critical member, which entails into the remaining one third bolts carrying the full load leading to further stress concentration at the connections. Since the stress factor for critical stress would be 3 for the assumed loss of bolt condition, the worst case of equivalent constant stress range of 40.71 MPa at gauge C24 on the bracing member is multiplied by this factor. Thus, for a new equivalent stress range of 122 MPa, the fatigue life is obtained as just below one year (0.98 years) for category E detail. For a better connection detail of category B, the fatigue life for the same stress would be obtained as more than five years. Hence, in order to avoid failure of any member or connection due to fatigue or cracking, it is important to inspect and monitor the structure on a regular basis. A minimum inspection interval of one year should be maintained for detecting and correcting any loose bolts or total loss of bolts condition. On the other hand, if the connections with lost bolts are not repaired or maintained for one to five years continuously, then even the connections with the best detail category are under threat of fatigue cracking. Hence, the focus of such annual inspections would be the connection zone, especially the bolts that are loose or go missing. A more detailed and major structural inspection of the crusher structure and all its connections should be conducted at least every five years. The critical components such as the hopper, columns and braces should be inspected annually and loose or missing bolts replaced.

7.5 Summary

1. The dump events identified and verified by the processing algorithm are written into the database of dump events, which can be used to plot histograms for each gauge and conduct statistical analyses. Fatigue life of the main structural components is estimated based on the strength of statistical information. Statistical patterns and values for parameters like mean, median, standard deviation, error of the mean, maximum and minimum values have been generated at each gauge location on the structure, which can be monitored over a long run to identify shift in those values due to structural changes or damage. The 95% confidence interval for the mean is obtained between 1 to 4 micro-strains, which are excellent for the strain magnitudes concerned. Strain Range is defined as the difference between maximum and minimum strain values recorded, which also serves as a good monitoring parameter.

2. The bracing members were found to be consistently experiencing both the largest peak strain values and also largest mean strain values, indicating that they were consistently under high strain averaging more than 100 micro-strains. The histogram of strain jump distribution at each gauge location and its shape represents the characteristic property of structural response at that

gauge, which could change over time due to structural changes or damage when monitored. Gridline 2 columns were the least stressed whereas gridline 4 columns and bracing members were found most heavily stressed by statistical analysis. The pontoon gauges showed quite stable behaviour under continued loading.

3. Fatigue life calculation based on equivalent stress range by Palmgren-Miner cumulative fatigue damage rule yielded an equivalent stress of 40.71 MPa for one of the bracing members. Assuming a category E detail based on drawing details provided and the pictures taken, a fatigue life of 5.34 million cycles or 26 years is obtained. It seems satisfactory in normal condition of the structure, however, when some bolts were assumed missing, which is not an uncommon occurrence under heavy impact and vibrating machinery, the fatigue life would drop down to one year by including the effect of additional stress concentration in unfavourable circumstances. Hence, an annual inspection of all joins and bolts, tightening if necessary, is recommended for ensuring satisfactory performance and long life of the structure.

7.6 References

Kulak, G. L. and Grondin G. Y. Limit States Design in Structural Steel, seventh edition. Canadian Institute of Steel Construction, Toronto, Ontario, 2002

Canadian Standards Association, CSA S16-01. Limit States Design of Steel Structures. Toronto, Ontario, 2001.

Systat Software, Inc. Sigma Stat and Sigma Plot Reference Manuals, 2006.

CHAPTER 8

MODELLING AND SIMULATION

8.1 Introduction

More than eighty different types of sensors were used on the Aurora II crusher to collect data continuously under field operating conditions. Although continuous data collection was not immediately started due to constraints posed by processing and managing of the data produced by the sensors, sufficient data was collected over the years under different operating conditions. Since it is not possible to instrument every member and every location on the crusher structure, finite element modelling is a tool used to fill in the gaps left by instrumentation and experimental data. A good model based on sound assumptions of material properties and boundary conditions is able to reproduce numerical results that closely represent the field behaviour of the structure. Such a model calibration exercise also gives rise to a typical load case that represents the severe field loading condition, which the designer should be taking into account in all future designs. Finite element analysis is also a convenient and cost-effective way of conducting various analyses under different scenarios of damage without actually damaging the structure physically. All these aspects and benefits of finite element modelling and simulation of the Aurora II crusher are presented in this chapter.

8.2 Krupp's STAAD Pro Model

Krupp Canada Inc. used two different 3-dimensinal models for the purpose of structural design on STAAD Pro 2003 (Research Engineers International, 2003) commercial finite element analysis and design software. One model incorporated the hopper and columns, whereas the second model was solely for the box girder pontoon resting on concrete foundations. Many different design load cases were used for the hopper and column model; and corresponding loads were transferred to the pontoon model at the points of contact between the columns and pontoons. However, this design model was inconvenient to work with and calibrate with field observations. Hence, a unified model was built by joining the two independent models together and applying appropriate boundary conditions. All the supports provided to the columns were removed and they were instead connected to the nearest nodes on the pontoon model. In locations where nodes were not present exactly under the beam/column elements, rigid elements were used to connect the beam columns to the nearest nodes on the plate elements of the pontoon for full compatibility between beam and plate elements. Some beam elements and bracing members or struts were added where required by the geometry of the structure. The two models were connected keeping in view symmetry along the longitudinal (X) axis. Due to this combining of models, all the node numbers and member numbers as well as their property names and numbers have changed from what was originally supplied by Krupp Canada Inc. Hence, all load applications, load cases, results and observations should be viewed with respect to the new combined 3-dimensional model instead of the earlier separate ones. The member property values like stiffness etc. were kept the same as provided by the designer.

The STAAD Pro 2003 software is able to perform linear static analysis, second order static analysis, non-linear analysis, and dynamic time history or response spectrum analyses. It is able to model the most common truss, beam, plate, and shell elements along with appropriate end release facilities. Surface elements as well as solid elements are also available. Full displacement compatibility exists between plane and space frame members when connected together and no additional constraints are required. The plate/shell elements are able to handle both thick and thin plates with four nodes specified and a fifth node generated automatically at the centre of the element, when quadrilateral plate elements are chosen. Triangular elements can also be used in the similar way, with all nodes numbered either clockwise or anticlockwise. All basic protocols of shape, size, etc. of the elements (Cook et al., 1989) are applicable to this software like any other software. Post analysis, the element force outputs are available at the four nodes and the central node, however, not along any of the element edges. Loads can be nodal or applied on members, with appropriate load factors for different load cases. Material properties for standard steel members have been used in analysis with the pontoon supported on foundation by multiple pinned supports. The cross sectional properties of the beam and plate elements are retained as originally provided by the manufacturer/designer. The combined model has a total of 4024 nodes with 6748 beam elements and 6645 plate elements.

8.3 Model Calibration and New Field Design Load Case

8.3.1 Calibration by Trial and Error

A full view of the model in a typical STAAD Pro window with a typical Krupp design load case applied on it is shown in Fig. 8.1. The shaded portion on the hopper implies the points of load application on the nodes and members. Since the point of application of load and its magnitude varies widely depending on the material pre-existing in the hopper and the height of fall, many different load cases can be imagined for analysis purpose. The designers have used an extensive list of many different types of load cases with different impact scenarios and impact factors. However, all these design load cases are based on experience, assumptions and limited experimental data. Hence, it is necessary to develop a design load case that is based on actual field observations under severe impact loading, since empty hopper loading is the most severe loading condition. The purpose of model calibration was to calibrate the finite element model and establish a load case that was able to reproduce results close enough to the field observations. The primary assumption is that the model geometric and material properties are of acceptable standard in representing the true likeness of the structure, as provided by the crusher manufacturer.

The load acting on the structure is a direct function of the type and size of truck used for dumping oil sand into the hopper and the level of material existing inside it that determines the height of fall. Figure 8.2 shows a picture of the 400 ton Caterpillar haul truck and its characteristic dimensions. Based on those dimensions, a certain width and height distribution of loading was assumed on the hopper with different load factors in such a manner that the 400 ton load was uniformly distributed along all the nodes in the region. The loaded are on the hopper was taken as equal to the width and depth of the truck body with uniform distribution of 300 ton of weight. Different levels and locations of load application were considered in the analysis as shown in Figures 8.3 and 8.4. Analyses with many different trial load cases were carried out and the results were matched with field observations. As it turned out, the results would match with the field observations at one column grid quite well, but then they would vary significantly at other column gauges. Having too many nodes or points of load application made the task of calibration quite challenging because there were so many variables. The three components of load, i.e. vertical, horizontal, and lateral, could be applied at each node with different magnitudes. Hence, in order to make the task of calibration more accurate and realistic, a simplified approach was taken to reduce the number of variables.

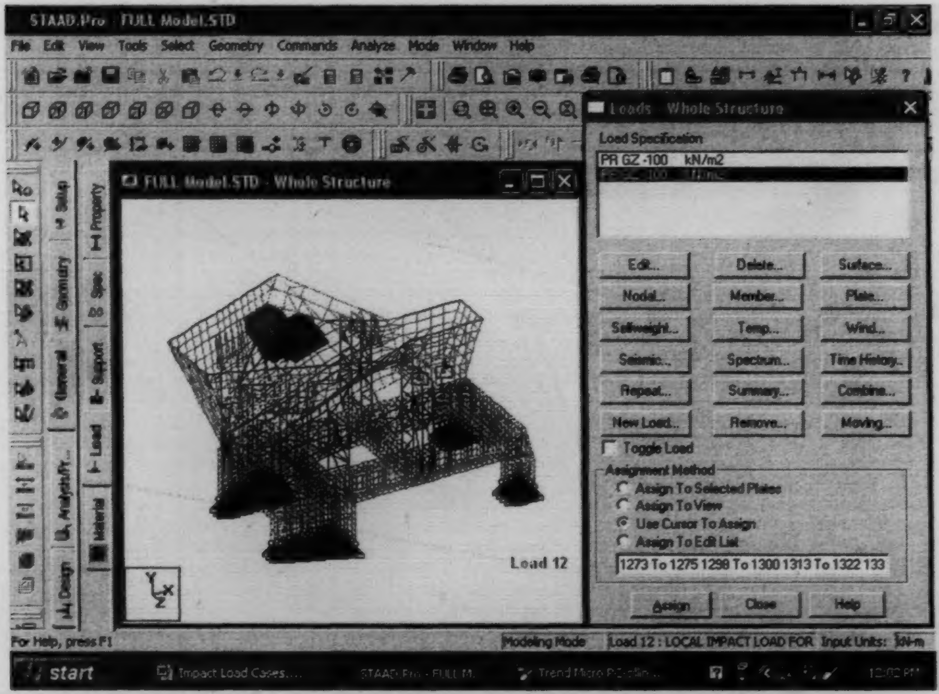
STAAD.Pro FULL Model.STD
File Edit View Tools Select Geometry Commands Analyze Mode Window Help
FULL Model.STD - Whole Structure
Setup
Geometry
General
Property
Spec
Support
Load
Material
Analysis/Pr...
Design
Load 12
Loads Whole Structure
Load Specification
Edit...
Delete...
Surface...
Nodal...
Member...
Plate...
Selfweight...
Temp...
Wind...
Seismic...
Spectrum...
Time History...
Repeat...
Summary...
Combine...
New Load...
Remove...
Moving...
Toggle Load
Assignment Method
Assign
Close
Help
For Help, press F1
Modeling Mode
start
Impact Load Cases....
STAAD.Pro - FULL M...
Trend Micro PC-cillin...
12:02 PM

Load Specification:
PR GZ -100 kN/m2

☐ Toggle Load

Assignment Method
○ Assign To Selected Plates
○ Assign To View
● Use Cursor To Assign
○ Assign To Edit List

1273 To 1275 1298 To 1300 1313 To 1322 133

Load 12 : LOCAL IMPACT LOAD FOR Input Units: kN-m

Fig. 8.1 Krupp's impact design load case

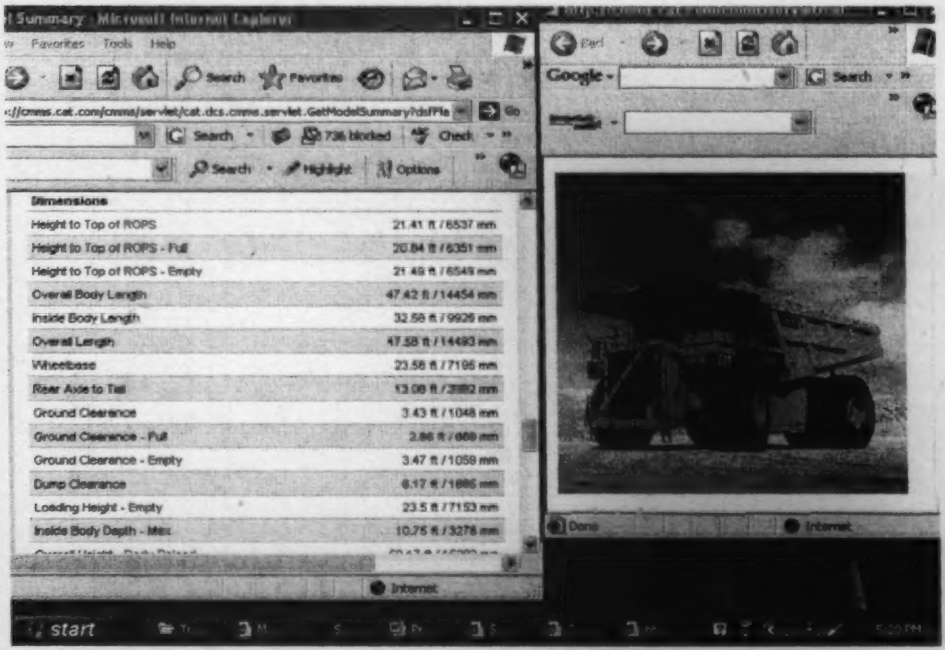

Dimensions	
Height to Top of ROPS	21.41 ft / 6537 mm
Height to Top of ROPS - Full	20.84 ft / 6351 mm
Height to Top of ROPS - Empty	21.49 ft / 6549 mm
Overall Body Length	47.42 ft / 14454 mm
Inside Body Length	32.58 ft / 9926 mm
Overall Length	47.58 ft / 14493 mm
Wheelbase	23.58 ft / 7196 mm
Rear Axle to Tail	13.08 ft / 3982 mm
Ground Clearance	3.43 ft / 1048 mm
Ground Clearance - Full	2.86 ft / 869 mm
Ground Clearance - Empty	3.47 ft / 1059 mm
Dump Clearance	6.17 ft / 1886 mm
Loading Height - Empty	23.5 ft / 7153 mm
Inside Body Depth - Max	10.75 ft / 3276 mm

Summary - Microsoft Internet Explorer
Favorites
Tools
Help
Search
Favorites
://cmms.cat.com/cmms/servlet/cat.dcs.cmms.servlet.GetModelSummary?dsfFla
Go
Search
736 blocked
Check
Highlight
Options
Internet
Google
Search
Done
Internet
start

Fig. 8.2 The oil sand dumping haul truck

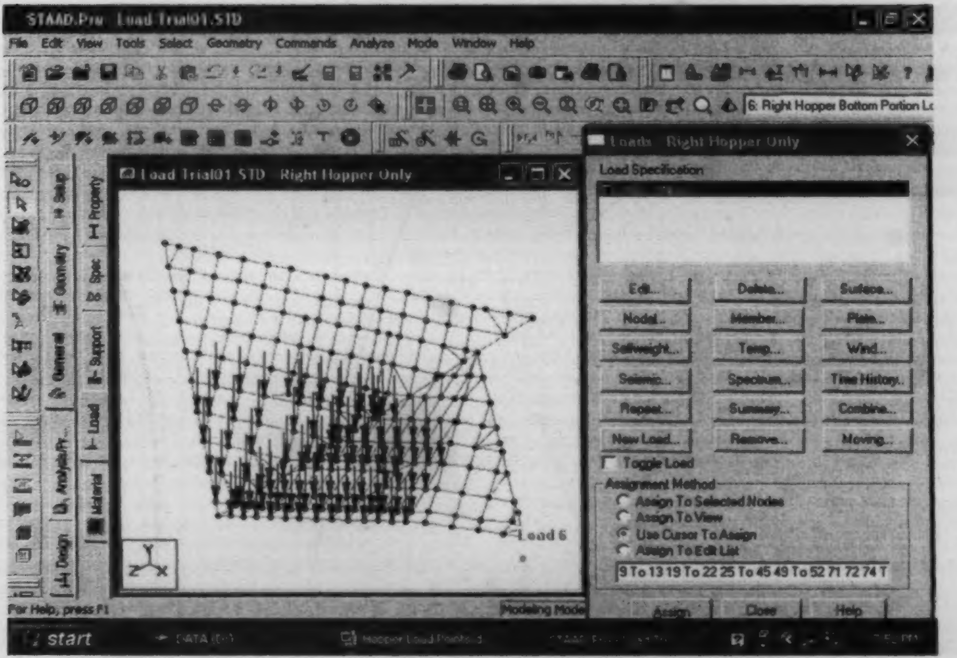

Load 6

Assignment Method
○ Assign To Selected Nodes
○ Assign To View
● Use Cursor To Assign
○ Assign To Edit List

9 To 13 19 To 22 25 To 45 49 To 52 71 72 74 T

STAAD.Pro - Load Trial01.STD
File
Edit
View
Tools
Select
Geometry
Commands
Analyze
Mode
Window
Help
6: Right Hopper Bottom Portion Lo
Load Trial01.STD - Right Hopper Only
Loads - Right Hopper Only
Load Specification
Edit...
Delete...
Surface...
Nodal...
Member...
Plate...
Selfweight...
Temp...
Wind...
Seismic...
Spectrum...
Time History...
Repeat...
Summary...
Combine...
New Load...
Remove...
Moving...
Toggle Load
Assign
Close
Help
Setup
Property
Geometry
Spec
General
Support
Load
Analysis/Pr...
Material
Design
For Help, press F1
Modeling Mode
start
DATA (D:)
Hopper Load Position

Fig. 8.3 Trial uniform load case at bottom of hopper

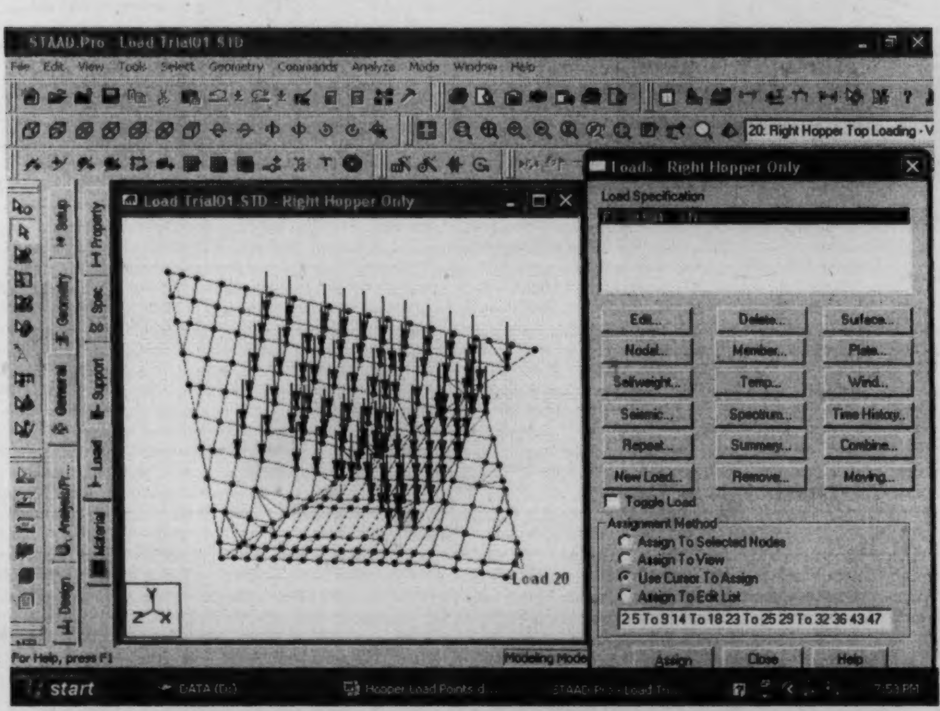
STAAD.Pro - Load Trial01.STD
File Edit View Tools Select Geometry Commands Analyze Mode Window Help
Load Trial01.STD - Right Hopper Only
Load 20
Loads - Right Hopper Only
Load Specification
Edit...
Delete...
Surface...
Nodal...
Member...
Plate...
Selfweight...
Temp...
Wind...
Seismic...
Spectrum...
Time History...
Repeat...
Summary...
Combine...
New Load...
Remove...
Moving...
Toggle Load
Assign
Close
Help
For Help, press F1
Modeling Mode
start
7:53 PM

20: Right Hopper Top Loading - V

☐ Toggle Load

Assignment Method
○ Assign To Selected Nodes
○ Assign To View
● Use Cursor To Assign
○ Assign To Edit List

2 5 To 9 14 To 18 23 To 25 29 To 32 36 43 47

Fig. 8.4 Trial uniform load case at top of hopper

Instead of having a uniformly distributed load at the point of contact between the oil sand and the hopper body, the load is applied on the structure at the column top at each gridline. Thus, there are two components of load, i.e. vertical and horizontal, at gridlines 2,3,4,5, and 6. That would limit the number of load points and load magnitudes to 12 in total. The gridlines and column locations are explained clearly in Chapter 3. Not all loads are necessary to act at all gridlines, but there are some additional load points due to twisting of the structure along the axis of symmetry. Thus, there could be some difference between loading on the left and right side of the hopper for the same load case. So, the approach taken was that of unit load method. A unit load was applied at each of the column gridlines on each side of the axis of symmetry in both vertical and horizontal directions and the corresponding stresses obtained from analysis of the structural model were recorded. Thus, a set of readings at each of the forty strain gauge locations in field was taken from the finite element analysis for each of the unit load cases. Based on the performance of the structure against each of the unit loads, some of the unit loads were accepted and some were rejected, some were also given a larger load factor for a better match with field results. Thus, after about thirty different trial analyses of load combinations with different load factors, the closest matching finite element analysis result was selected to be proposed as the new design load case for all future designs under severe empty hopper loading. Table 8.1 shows the stresses recorded at each of the column gauges due to each 1000 KN load acting at columns on each of the gridlines in vertical or horizontal direction, or on left or right side of the hopper. Different combinations and load factors were used for each of the unit load case by trial and error to get results as close as possible to the field observations at most of the gauges. The table also shows the actual stresses observed in the field at those gauge locations as well as the stresses under the combined load case numbered as 24, which was deemed closest match to the field observations. The load combination and factors were reached at by trial and error. As can be seen in the table, the numerical results of load case 24 were quite close in value to the field observations at most of the gauge locations. It is virtually impossible to match the results at every gauge location perfectly; rather some compromise and qualitative judgement are required to be made for best overall performance. Some of the load-combinations gave near perfect match at one column gridline but wandered astray at other gridlines. Figures 8.5 and 8.6 show the load case 24 that matched best with overall field observations and the STAAD input file for the load case is shown in the Appendix.

8.3.2 The New Calibrated Design Load Case

Figure 8.5 shows the vertical components of the load combinations and factors associated with the closest matching Load Case 24, whereas Figure 8.6 shows its horizontal components. Many variations of load factors, magnitudes, and locations were tried before and after arriving at this load case. Based on the overall performance with respect to the field observations, the load case was deemed qualitatively as the best fit. The points of load application were chosen based on the best fit obtained with field observations, so in effect it was an exercise on optimization that was carried out by trial and error. The symbol A in the figure stands for 1000 KN of vertically downward load; and the symbol H represents 1000 KN of horizontal load. As can be seen, most of the vertical loads are acting downwards indicating a vertically downward impact due to the fall of oil sand into the hopper. A 400 Ton truck would cause about 4000 KN of static load if no impact were allowed. However, the total vertically downward load of 10,100 KN indicates presence of ample impact by a factor of more than 2.5 times the static truck load. Nevertheless, there is also presence of a small magnitude of vertically upward load, which is an indication of a couple acting on the hopper twisting it laterally. In the same vein, the total horizontal force acting in the negative Z (right) direction on the right side hopper was 4000 KN, whereas the load in the positive lateral (left) direction on the left side hopper was close to 2000 KN. Again, a total of 1.5 times the static standard truck load was acting in the horizontal direction due to impact.

Table 8.1 Unit load response for calibration by trial and error

Gauge Number	At Corner	At Length	Field Stresses	Model Stresses Load Case 24	Stress at Column Gauges due to Each 1000 KN Load Applied											
					Vertically on Right Side Columns of					Horizontally on Right Side Colm of				Vert / Hor On Left Side Columns		
					Grid 2	Grid 3	Grid 4	G 6 (in)	G-6 Out	Grid 2	Grid 3	Grid 4	Grid 5/6	Vert G2 (+)	Vert on G4	Hor G4 (+)
Grid-2									(300 KN)					(upward)	(downward)	
C1	1	50%	32.4	28	13.16	2.9	0.48	-0.01	-0.75	4.13	1.86	-1.64	-10.22	-0.94	0.316	-2.272
C2	3	50%	15.6	15.49	13.35	1.69	-0.48	-0.673	0.37	-2.47	-1.53	-1.9	6.36	-0.3	0.136	-1.184
C3	1	50%	16.4	23.3	5.75	2.29	-0.96	-0.975	0.53	4.85	4.33	2.3	10.95	-0.24	0.0524	-1.032
C4	3	50%	-19	-2.63	2.8	2.51	-1.46	-1.543	1.67	-7.08	-2.48	0.66	26.07	0.13	-0.236	0.128
C28	1	50%	-11.6	-12.4	0.25	-0.06	-0.16	-0.875	-0.5	2.74	1.39	-0.07	-3.65	-20.3	-1.092	2.264
C27	3	50%	-16.6	-17.3	0.62	0.25	-0.02	-0.783	-0.3	0.62	-0.18	-0.84	-1.7	-18.2	-1.352	0.8
C26	1	50%	-8.6	-10.18	0.86	0.42	0.1	-0.01	0	-0.08	-1.2	-1.29	0.66	-6.46	0.164	-1.088
C25	3	50%	-24.8	-15.2	0.92	0.75	0.34	0	0.2	-4.55	-3.61	-2.19	2.85	-1.93	-0.176	-2.432
Grid-4																
C5	1	50%	-37.8	-35.53	-0.51	4.8	23.78	0.51	-3.75	-12.66	-17.06	-30.33	-49.47	-0.17	-0.476	1.32
C6	3	50%	26.6	11.44	0.43	2.27	11.64	1.67	-0.92	-0.99	-3.59	-7.23	-16.78	0.03	0.148	-0.448
C7	0 (3-4)	50%	130.8	66	-0.855	0.075	4.85	0.648	2.05	2.275	9.5	21.435	24.22	0.1	0.038	0.172
C8	0 (1-2)	50%	151.4	90	-1.21	-0.54	3.66	0.575	2.86	5.16	14.45	30.745	35.42	0.245	0.07	0.372
C9	1	50%	34	66.88	-2.05	-0.56	6.22	0.783	0.81	9.63	12.3	15.83	8.85	0.96	0.188	1.136
C10	3	50%	71.4	98.62	-0.7	-0.91	1.5	0.2	2.5	9.33	16.79	32.93	31.54	0.89	-0.028	1.664
C36	0 (1-2)	50%	38	62.4	-1.36	-0.485	0.06	-0.524	-0.185	-0.735	0.65	1.62	-0.85	1.135	2.73	30.592
C35	0 (3-4)	50%	29.6	45	-1.16	-0.41	0.09	-0.065	-0.045	-0.515	0.54	1.23	-0.75	1.255	5.04	18.064
C34	1	50%	65.8	67.6	-0.2	0	0	-1.075	-0.35	0.5	0.56	0.55	-1.55	0.97	3.956	31.816
C33	3	50%	46.6	47.21	-0.03	0	0	-0.408	-0.11	-0.6	-0.29	0.02	-0.05	0.39	4.824	20.704
C32	1	50%	42	22.82	-0.07	-0.17	-0.1	0.693	0.2	1.69	1.15	0.58	0.31	2.36	18.844	-11.808
C31	3	50%	-37.2	-10	0.17	-0.08	-0.24	1.35	0.39	1.46	0.83	0.28	0.91	0.05	16.432	-25.888
Grid-5																
C13	1	50%	-16.36	-4.2	-0.07	1.3	3.4	10.06	-0.8	-0.55	-5.43	-13.23	-52.79	-0.2	-0.052	-0.032
C14	3	50%	29.25	22.4	0.98	-0.1	-0.72	7.11	0.61	1.85	1.89	2	12.02	-0.2	-0.18	0.12
C15	2	25%	29.02	55.7	0.6	-1.85	-5.6	2.7	9.95	-0.96	8.24	23.3	121.8	0.24	-0.084	0.064
C16	4	25%	58.91	72.4	-0.03	-2.08	-6.22	4.71	16.07	-1.16	9.44	27.16	135.51	0.36	-0.024	0.392
C40	0	75%	30.29	36	-0.03	-0.22	-0.06	2.142	0.458	2.9	1.64	0.21	-3.065	-3.46	-5.358	22.456
C39	0	75%	31.2	38	-0.03	-0.22	-0.06	2.142	0.458	2.82	1.64	0.21	-3.065	-3.46	-5.358	22.456
C38	4	50%	-13.65	-22.35	0.13	0.14	0	-1.893	-0.4	-1.08	-0.6	-0.04	1.17	2	3.452	-13.576
C37	2	50%	-9.89	3.34	0.13	0.14	-0.22	-0.028	0.06	-0.07	-0.02	0.14	1.08	-1.5	-1.032	3.656
Grid-6																
C17	2	50%	-89.8	-26.63	0.15	2.12	6.37	37.25	0.97	1.96	-9.03	-27.2	-126.68	-0.35	0.144	-1.064
C18	4	50%	92.2	-13.49	-0.05	1.32	4	26.6	1.73	1.15	-5.6	-16.68	-78.41	-0.175	0.13	-0.731
C19	0 (3-4)	0%	100.2	56.5	-0.465	-1.02	-2.44	16.13	4.06	-2.195	3.455	12.685	68.02	0.16	-0.115	0.76
C20	0 (3-4)	0%	76.6	56.5	-0.465	-1.02	-2.44	16.13	4.06	-2.195	3.455	12.685	68.02	0.16	-0.115	0.76
C21	0 (1-2)	0%	38.8	24.5	-0.4	1.5	5.21	28.204	2.85	-1.05	-7.315	-19.565	-84.46	-0.24	0.044	-0.424
C22	0 (1-2)	0%	19.6	24.5	-0.4	1.5	5.21	28.204	2.85	-1.05	-7.315	-19.565	-84.46	-0.24	0.044	-0.424
C23	0	25%	84.8	75.75	-0.7	-1.66	-3.67	8.54	22.15	-0.235	7.61	20.973	99.062	0.365	0.039	0.536
C24	0	25%	88.8	77.75	-0.7	-1.66	-3.67	8.54	22.15	-0.235	7.61	20.973	99.062	0.365	0.039	0.536
Note: Stresses are in MPa calculated for a unit load of 1000 KN at each gridline																
Compressive Stresses are positive and Tensile are negative.																

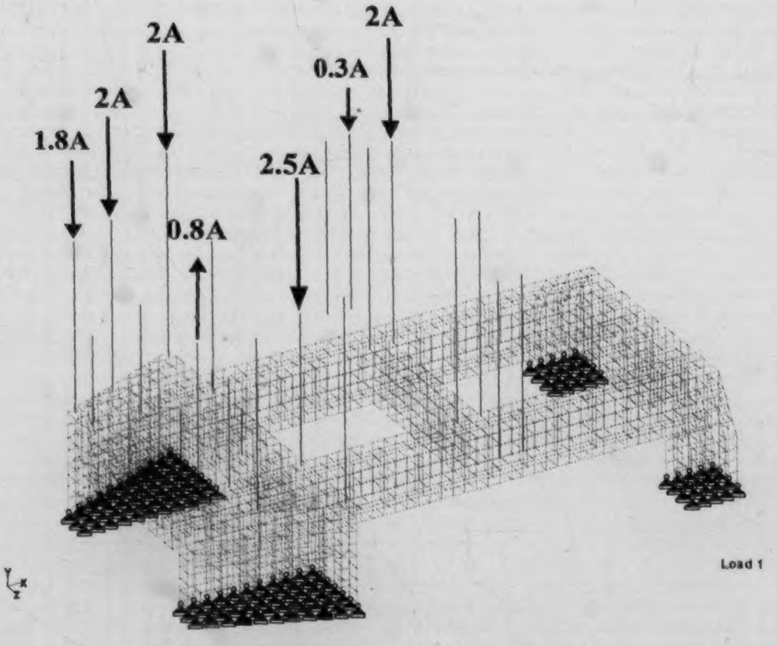
2A
2A
0.3A
2A
1.8A
2.5A
0.8A
Load 1

Fig. 8.5 Vertical components of new design load case

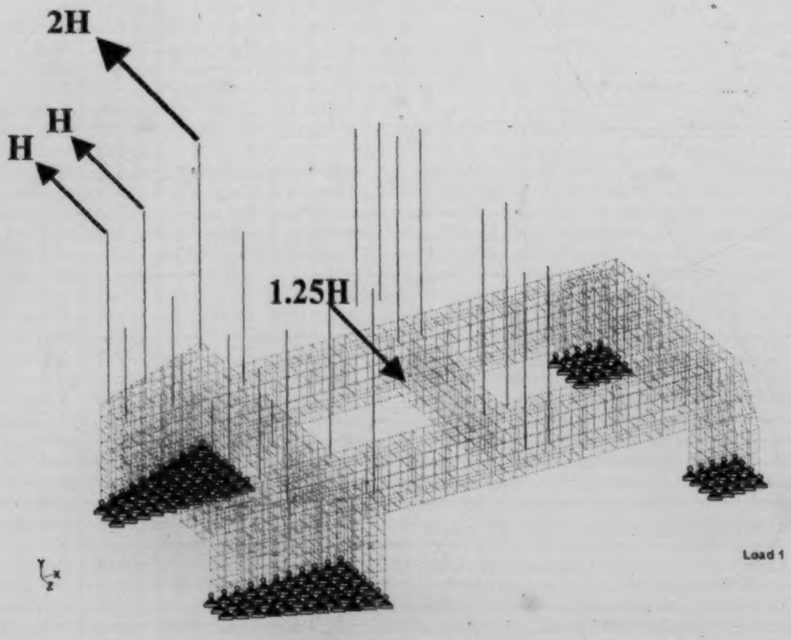
2H
H
H
1.25H
Load 1

Fig. 8.6 Horizontal component of new design load case

Basically, the oil sand dumping translates into a combination of horizontal and vertical impact loads on the hopper that are transferred on to the columns. This is the most severe load case acting under empty hopper condition wherein the fall distance is the largest. Under normal operating conditions where some material is pre-existing in the hopper, the fall distance will be smaller and hence, the magnitudes of the horizontal and vertical forces will be smaller. The point of application of load can move up or down depending on how full or empty the hopper is. However, the loads can not move to the left or right much because the haul trucks have a fixed location of dumping and only minor shifts are possible. Considering all these arguments, it can be safely assumed that this empty hopper dumping remains the most severe operating load for all column gridlines and the pontoons.

Looking into the new design load case grid by grid one at a time will give a clear picture of what is happening at each gridline and help see the mechanism of action. Figures 8.7 to 8.9 show the cross sections of the crusher at gridlines 2 to 6 along with the loads acting on them. As seen, horizontal or vertical loads were not applied at every column on each gridline. The locations and magnitudes of the load were strategically varied to match the stresses caused in the field. Gridline 2 shown in Figure 8.7 is moderately loaded with a total of close to 2000 KN of vertical load and 1000 KN of horizontal load. The vertically upward force acting on the left side of the hopper is due to the twisting couple that occurs because the columns on the right side pull those on the left side in a rigid body like fashion. The twisting couple is of 800 KN in magnitude whereas the rest are vertical and horizontal loads of 1000 KN each transferred to the columns through the hopper.

Gridline 4 columns are the most heavily loaded under impact as most of the dumping takes place on either side of this grid. Figure 8.8 shows a total vertical load of 4500 KN and combined horizontal load of 3250 KN. The vertical loads are almost equally transferred among the columns on the left and right side of the hopper. However, it is the horizontal loading that is occurring differently from gridline 2. The horizontal loads at gridline 4 are occurring in opposite directions on either side of the hopper, which is due to the fact that portions of the dumped oil sand fall onto both sides of the hopper. Due to the inclination of the hopper the vertical loads on both sides are downward, but the horizontal loads are in opposite sense. It is also clear from the figure that the portion of the load falling on to the right side hopper as the oil sand is dumped from the left side has a longer trajectory, hence the larger horizontal force magnitude. Much of the material rebounds back on to the left side hopper along with the portion that falls directly on to the left hopper, hence the vertical force is larger and the horizontal force is smaller in comparison on the left side hopper.

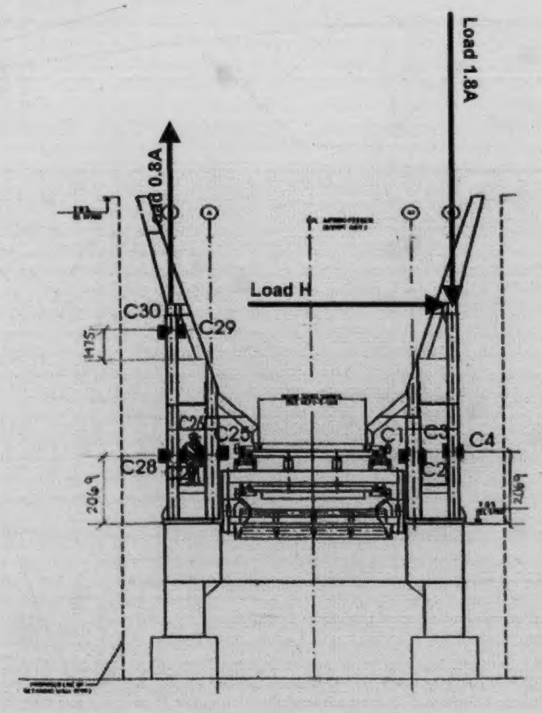

Fig. 8.7 Load distribution at gridline 2

Finally, Figure 8.9 shows the loads acting on gridline 6 columns due to the severe empty hopper dumping. Gridline 6 columns are the farthest located from the scene of action, that is, the hopper. However, they are still connected to the hopper and columns at other gridlines through trussed longitudinal stiffeners. These stiffeners are able to provide ample resistance to movements in the vertical and longitudinal direction, and hence, transfer some of the vertical dump load to act on gridline 6 columns. However, not much

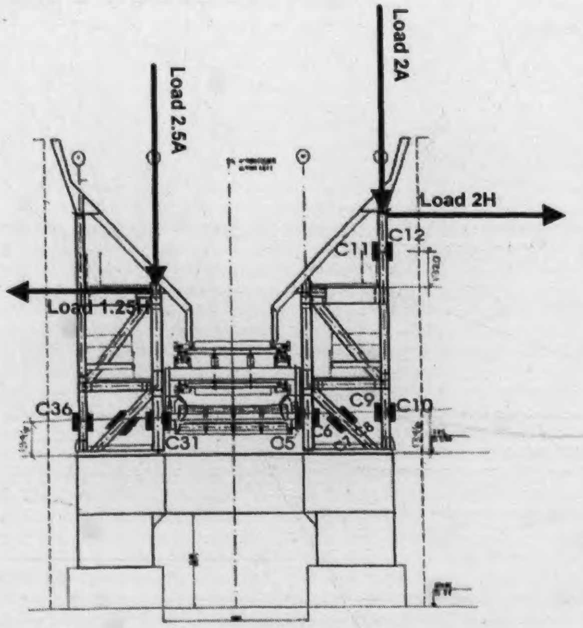
Load 2.5A
Load 2A
Load 2H
Load 1.25H
C12
C11
C36
C31
C5
C6
C7
C8
C9
C10

Fig. 8.8 Load distribution at gridline 4

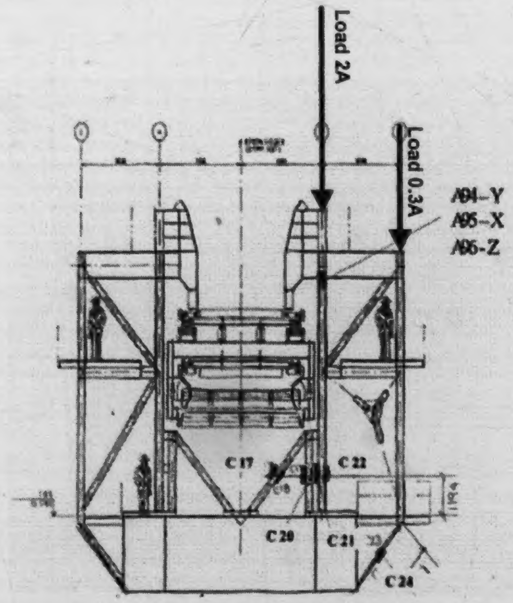
Load 2A
Load 0.3A
A94-Y
A95-X
A96-Z
C 17
C 22
C 20
C 21
C 24

Fig. 8.9 Load distribution at gridline 6

stiffness exists between columns at grid 6 and those at grid 4 in the lateral direction because they are not moment braces, so no horizontal forces are transferred. All the horizontal force impact is limited and absorbed by the column gridlines around the hopper, but some vertical force does get transferred to the gridline 6 columns.

8.3.3 Model Calibration Results

Sufficient information has been provided in the preceding sections about the calibration exercise, its methodology, and the actual field load case devised for calibration. Calibration results and performance of the numerical model in comparison to the field observations at each of the gridline is investigated in this section. Figures 8.10 to 8.13 show the comparison between the model analysis results and field observations at different column gridlines. The comparison in general reveals a very good match between field observations and numerical analysis at all column gridlines. There are a few exceptions that can be termed as a poor match and each of those instances categorically pertain to the inclined struts or braces about which much has been discussed in the previous chapters.

Most of the gauges on column gridline 2 in Figure 8.10 show a good match between model analysis and field. This fact is further strengthened by the error plot between field and model analysis shown in Figure 8.14. The error or difference between field and analysis is mostly very low in comparison to the largest stresses. The worst error is smaller than 20 MPa at all locations. Comparatively, the relative error magnitudes on gridline 4 gauges are larger, but the overall match is still very good. Figure 8.11 shows the comparative bar chart between field and model stresses at each gauge location on column gridline 4. In the first glance a good match can be seen at each gauge location except for gauges C7 and C8, both of which are placed on the bracing member that is subjected to excessive vibration and bending under severe loading. Looking into the error plot for the gridline 4 gauges in Figure 8.15, the errors are a little higher than grid 2, but still around 20 to 30 MPa. The only exception being the matching error for the two gauges on the bracing member that have 60 MPa in error, which is poor and unacceptable. However, keeping in view the overall match and the bracing member being the only exception whose performance has been a reason of concern or attention, the match could still be rated as very good.

The match obtained at gridline 5 gauges in Figure 8.12 is also very close at most gauges, even at the inclined struts having the gauges C15, C16, C39 and C40. Figure 8.16 shows the error between analysis and field at those gauges of gridline 5, which are quite low. Errors at most gauge locations are less than 10 MPa; and only at the inclined struts the error rises in the vicinity of 20 MPa. The comparison between field and analysis results at gridline 6 gauges is shown in Figure 8.13. Overall, a reasonable match is obtained at many gauge locations. However the match at gauges C17 and C18, which are again located on bracing members, is very poor. The error at these two gauges rises as high as 80 MPa, as shown in Figure 8.17. However, except for the bracing member, other gauges show pretty good match with error being limited to less than 20 MPa in magnitude. Thus, the overall quality of match between analysis and field observations on all column gridlines has been quite good, the only exceptions being at the inclined struts and bracing members.

Having discussed the overall match and error between field observations and model analysis results, a closer look is now taken into the stresses at each gauge location by breaking them into axial and bending components. Since the gauges are located mostly in pairs on the flanges of the columns, it is possible to reasonably break the stress at each column into equivalent axial stress and bending stress components. By doing this exercise on both the analysis and field observations, separate comparisons are now made between the axial components of the stresses and the bending components. Figure 8.18 shows the comparison of axial stresses at gridline 2 gauges and Figure 8.19 shows the comparison for bending stresses at the same gridline. The comparisons in both these figures are quite close for the level of stress acting, however, the axial stress comparison matches better than the bending in general. Similarly, Figures 8.20 and 8.21 show the comparisons for axial and bending stresses respectively at gridline 4 gauges. Except for the aberrant bracing member having gauge C7 and C8, the quality of match is excellent for the axial stress component in Figure 8.20. The match obtained for the bending stress component in Figure 8.21 is also of acceptable standard, but the bending stresses are showing more error than the axial components.

Comparisons at gridline 5 gauges in Figures 8.22 and 8.23 also show similar aspects, wherein the overall quality of match is quite good but the bending components show relatively larger mismatch or error. However, the glaring example of biggest mismatch can be found in the bending component at gridline 6 gauges C17/C18 as shown in Figure 8.25. The axial components shown in Figure 8.24 on the other hand are of quite acceptable standard. The larger error on the bracing members and struts are arising due to their lower stiffness and presence of local bending.

8.3.4 Plate Stresses on Pontoon Girder

After satisfactory viewing of the beam stresses in the vicinity of column gauges at different gridlines, now it is the turn of pontoon stresses to be scrutinized for match-up between field observations and model analysis. A good match obtained at the pontoon gauges would be able to reaffirm the validity of the field load case presented earlier, as well as the reasonable performance of the finite element model as a whole, especially stress transfer between columns and pontoons. As depicted in Figure 8.26, the match between field strains and model analysis strains at the ten pontoon gauges show that half of the gauges provide a good match, whereas the other half not so good.. At a couple of gauges, like P48 and P52, the match is not as good as expected, however, in general the match obtained is acceptable at most gauge locations. One of the reasons for some mismatch to an extent can be attributed to the relatively coarse finite element modelling of pontoon plates. Each element is of size 0.5 m X 0.5 m, which allows for only four elements along the depth of the pontoon girder. Thus, with a finer mesh a relatively better match could be expected but at the cost of considerable computing time for the complex structure. Hence, it goes on to convey the message that the field load case is equally applicable from the point of view of pontoon stresses and the unified finite element model of the crusher structure is performing well but could be refined for better results.

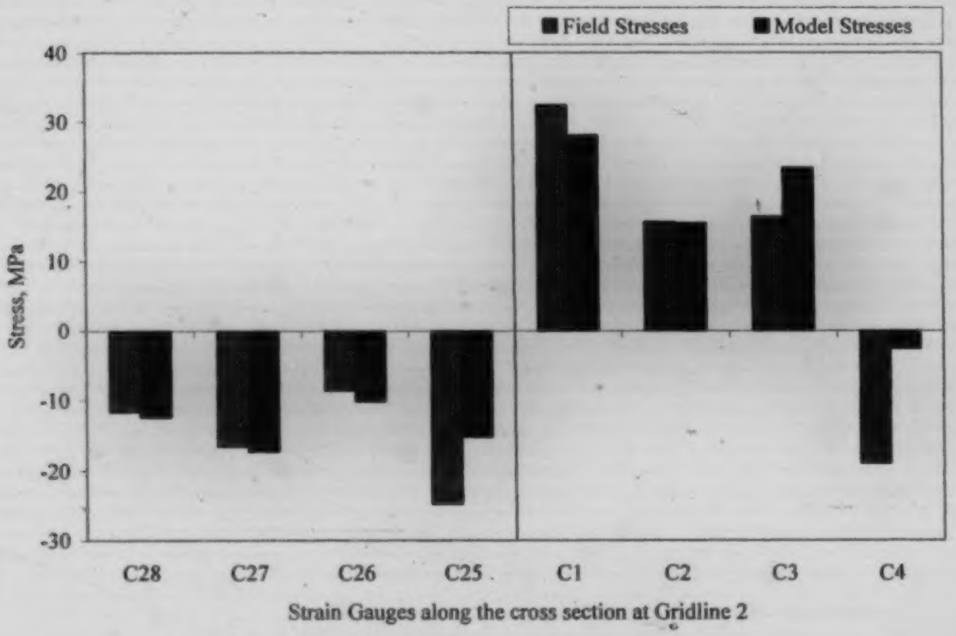

Fig. 8.10 Results matching at gridline 2

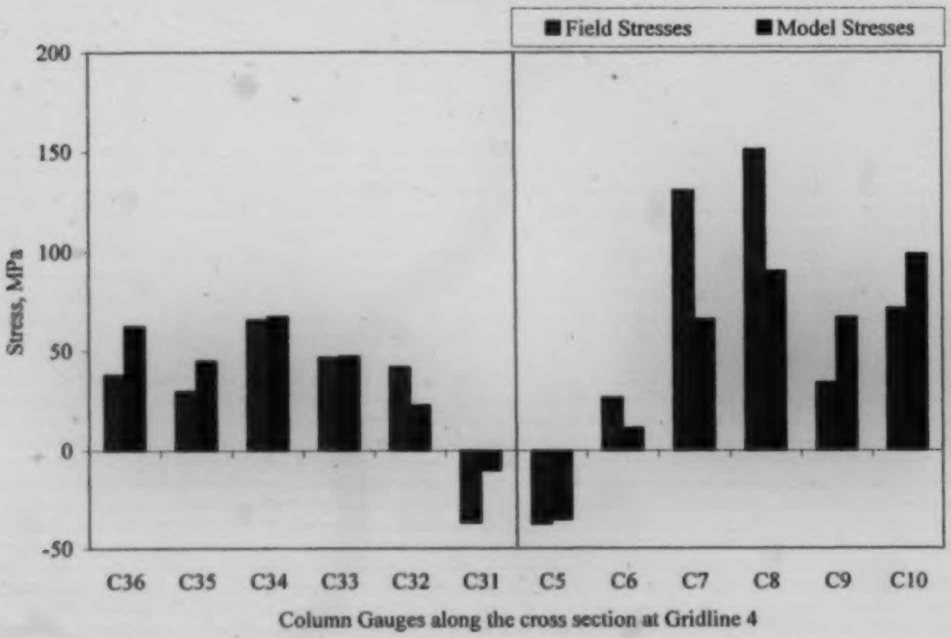

Fig. 8.11 Results matching at gridline 4

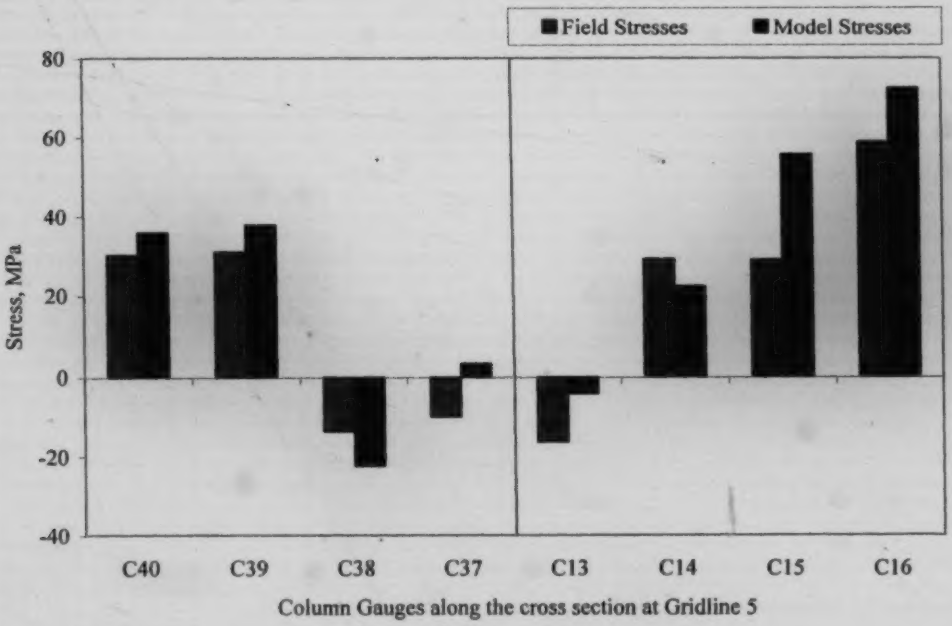

Fig. 8.12 Results matching at gridline 5

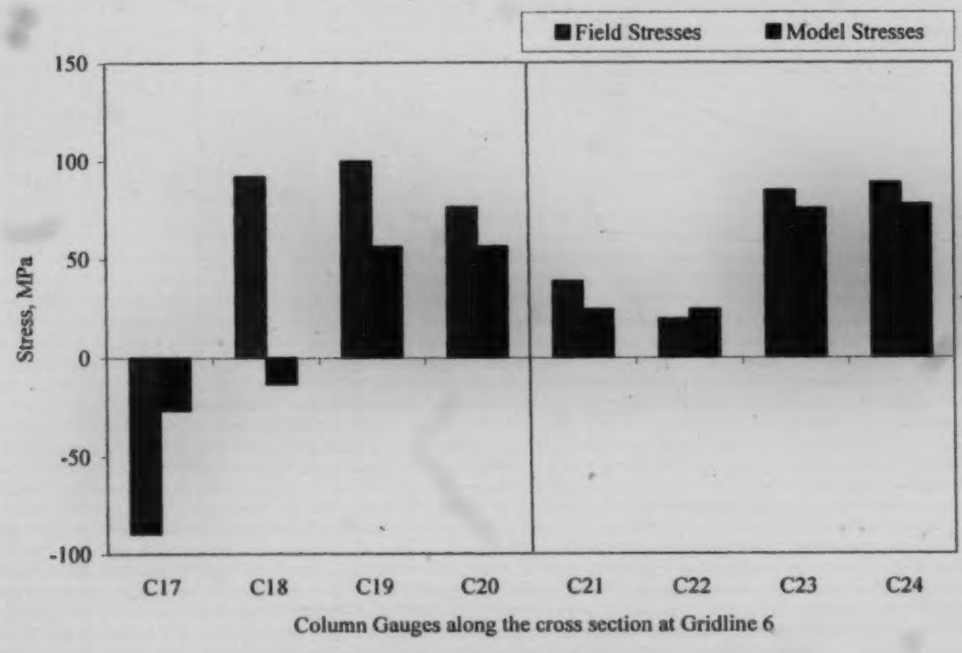

Fig. 8.13 Results matching at gridline 6

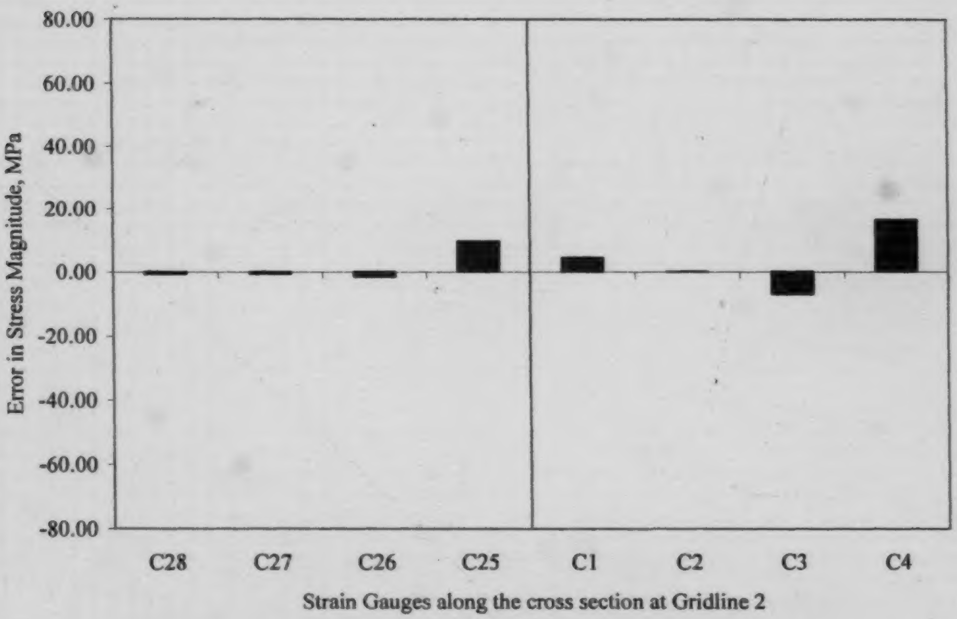

Fig. 8.14 Error between field and analysis stresses at gridline 2

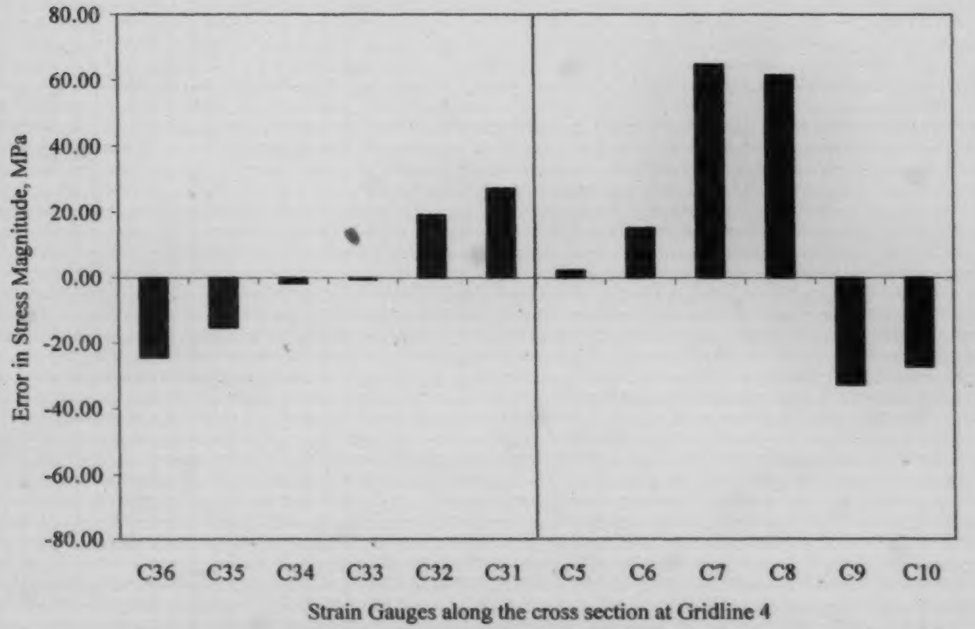

Fig. 8.15 Error between field and analysis stresses at gridline 4

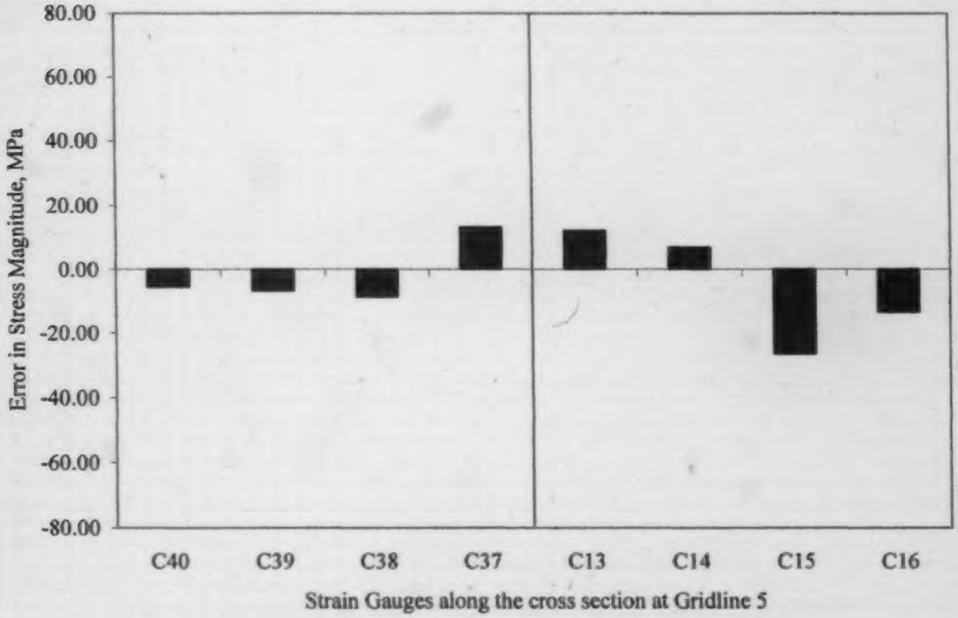

Fig. 8.16 Error between field and analysis stresses at gridline 5

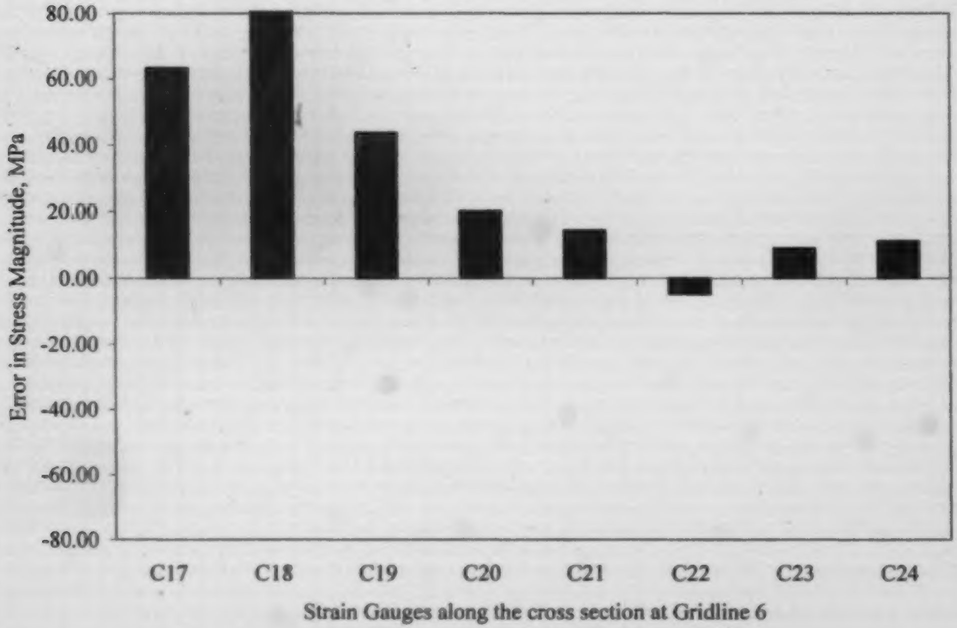

Fig. 8.17 Error between field and analysis stresses at gridline 6

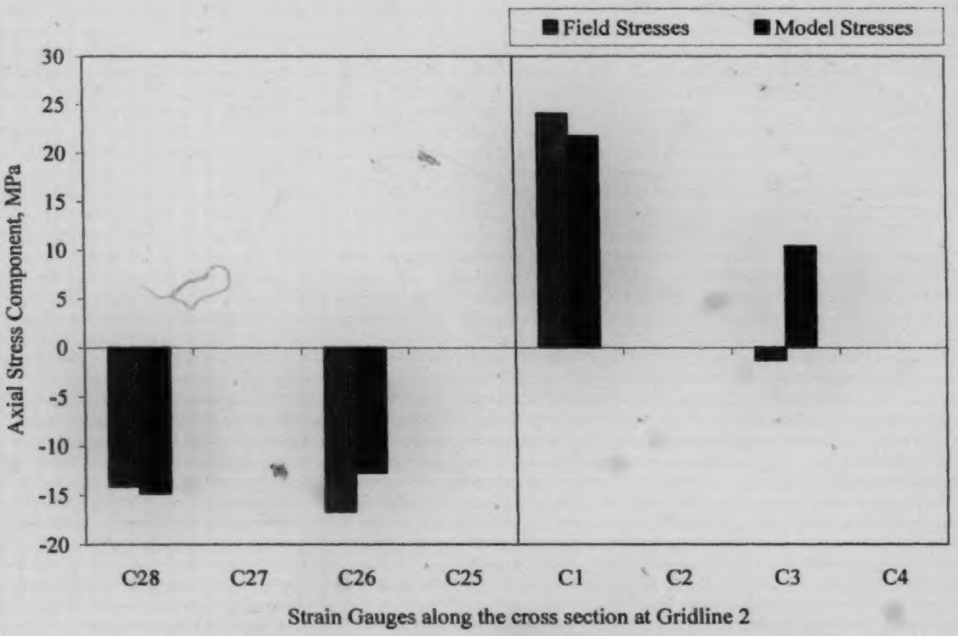

Fig. 8.18 Axial stress component matching at gridline 2

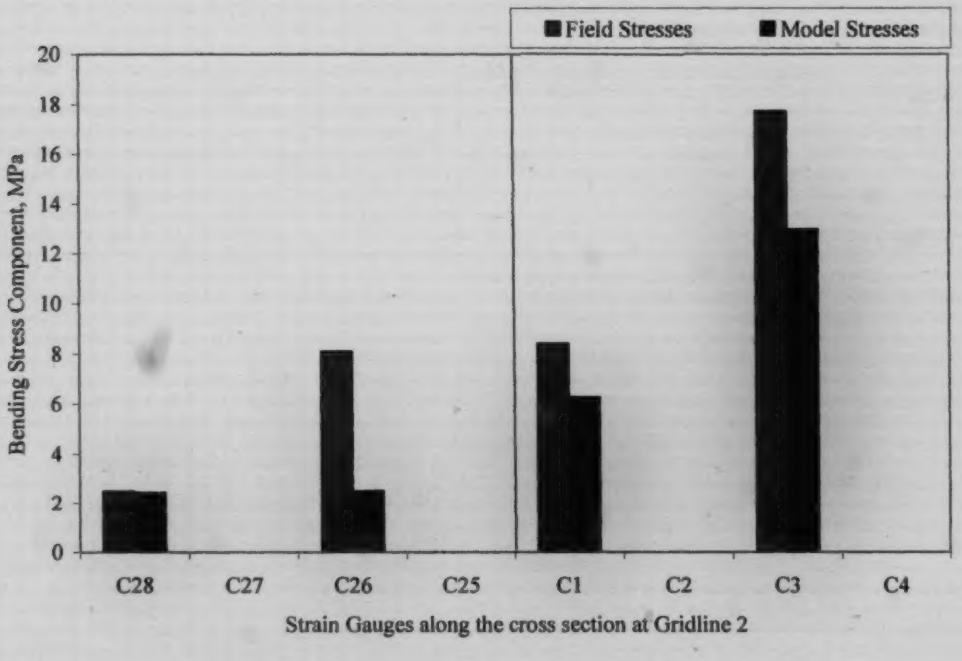

Fig. 8.19 Bending stress component matching at gridline 2

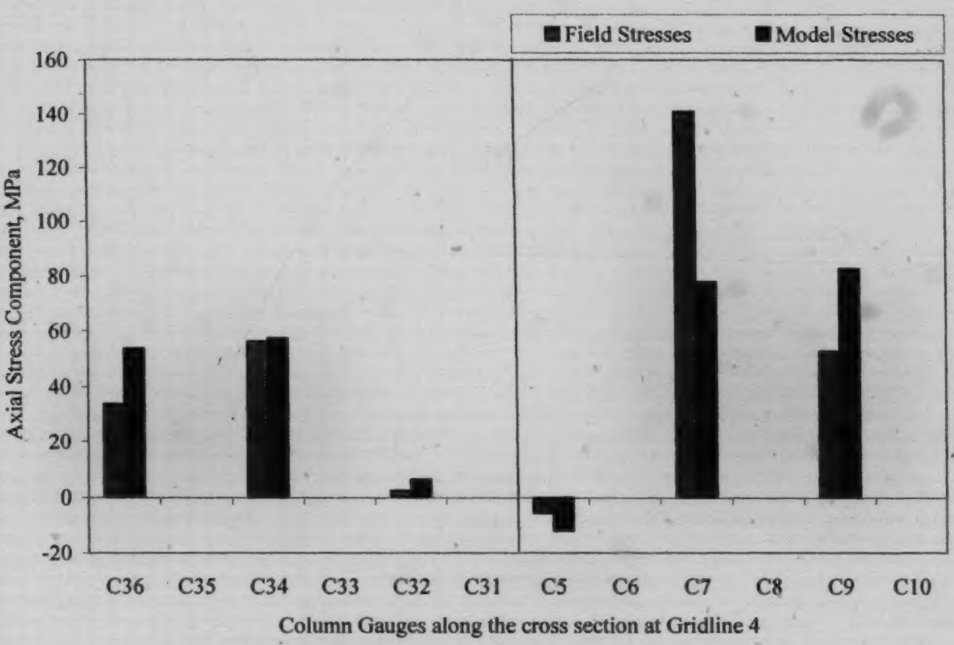

Fig. 8.20 Axial stress component matching at gridline 4

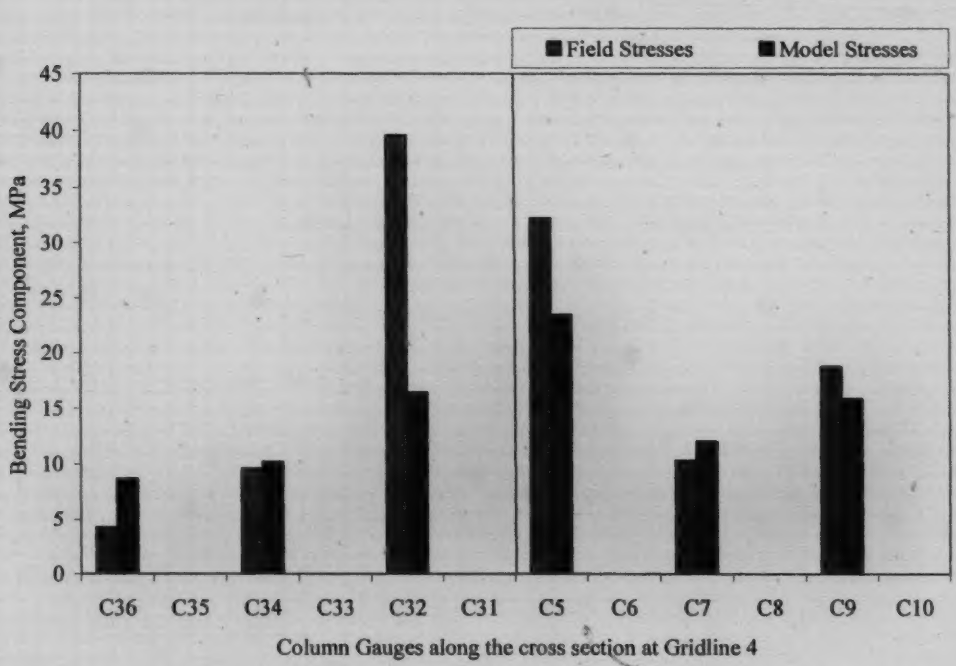

Fig. 8.21 Bending stress component matching at gridline 4

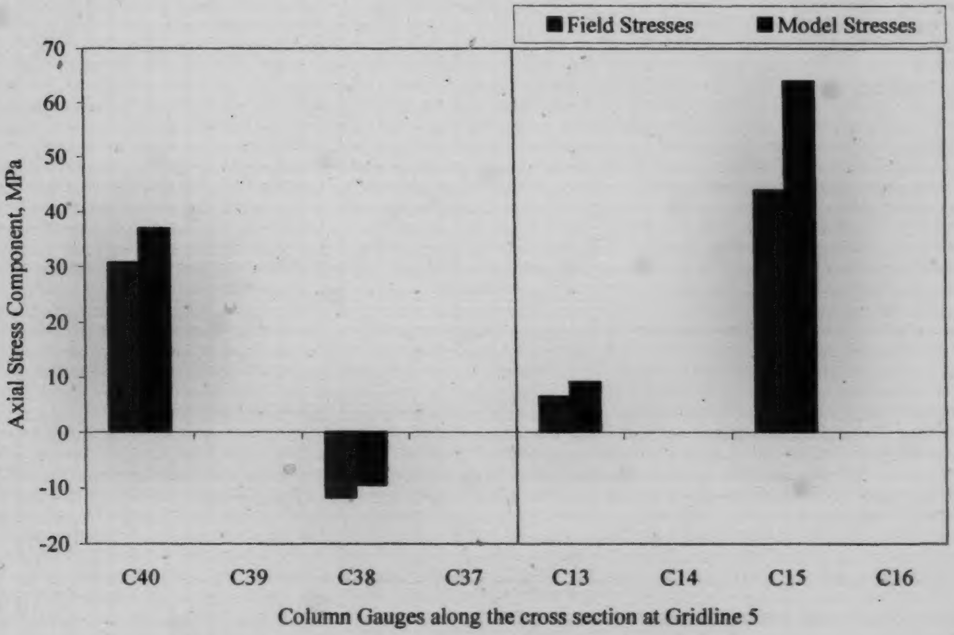

Fig. 8.22 Axial stress component matching at gridline 5

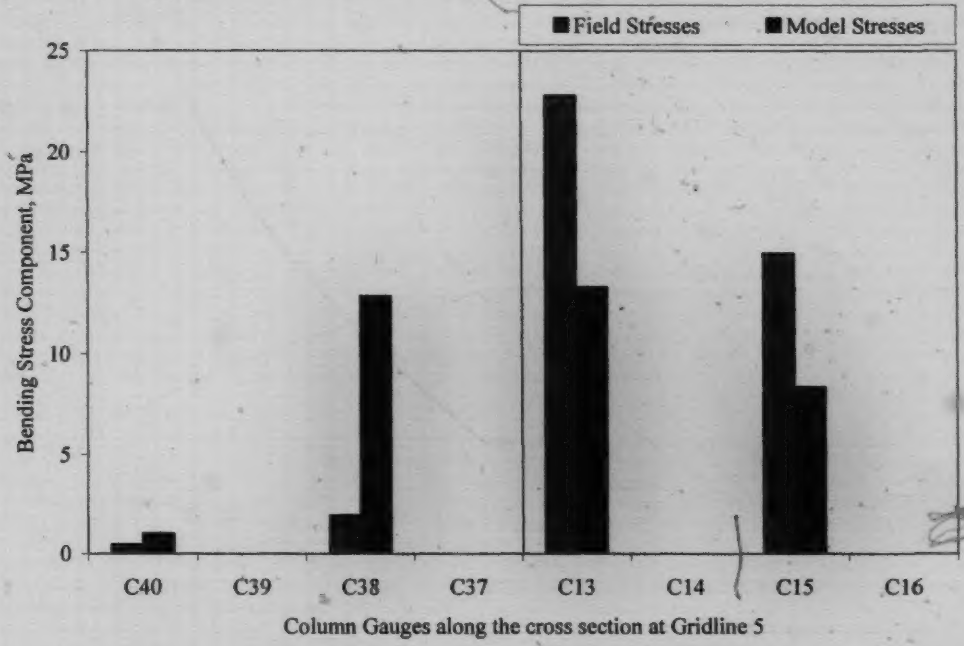

Fig. 8.23 Bending stress component matching at gridline 5

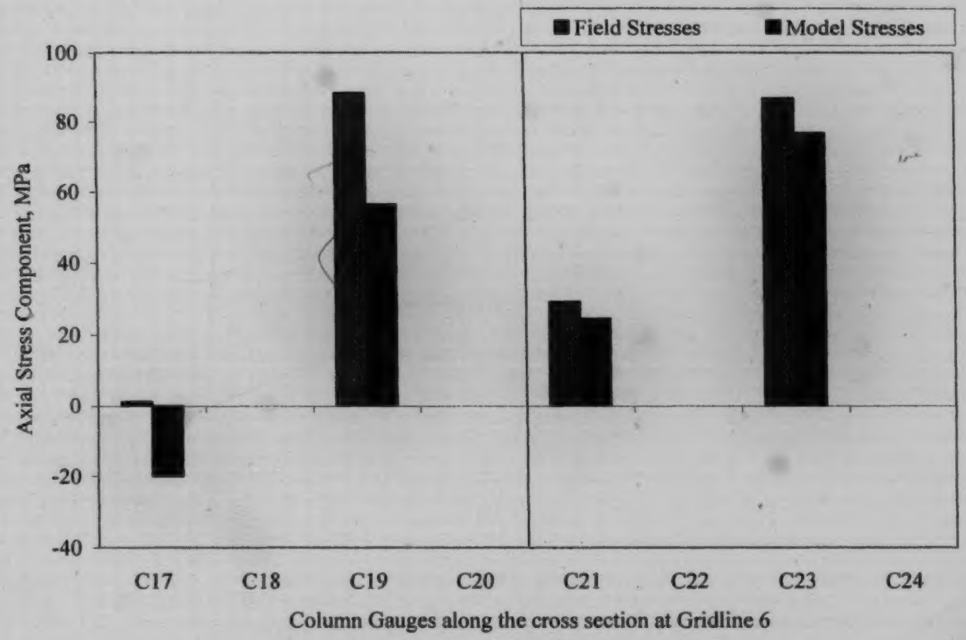

Fig. 8.24 Axial stress component matching at gridline 6

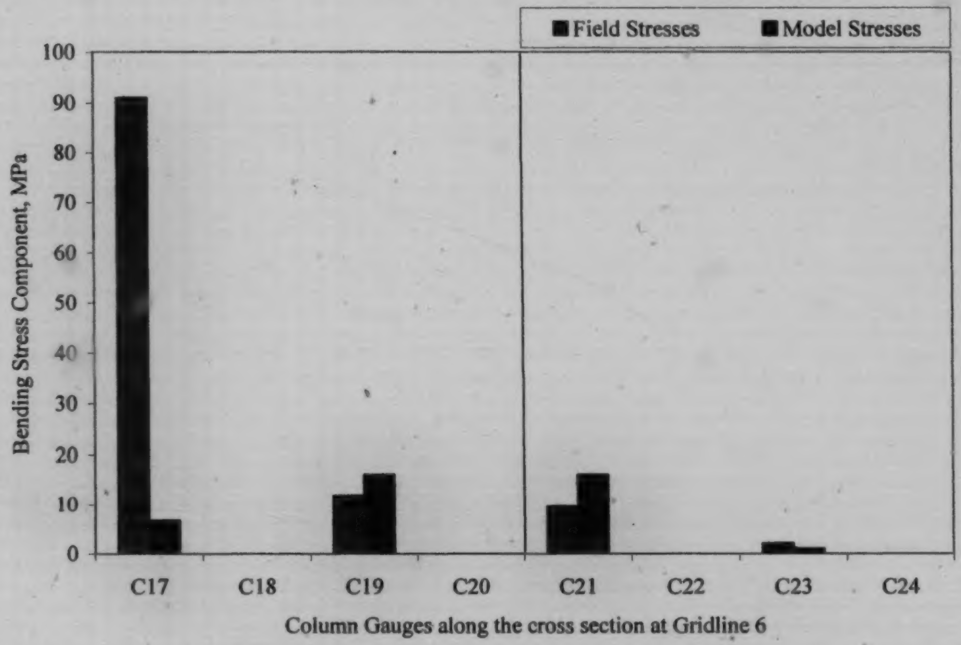

Fig. 8.25 Bending stress component matching at gridline 6

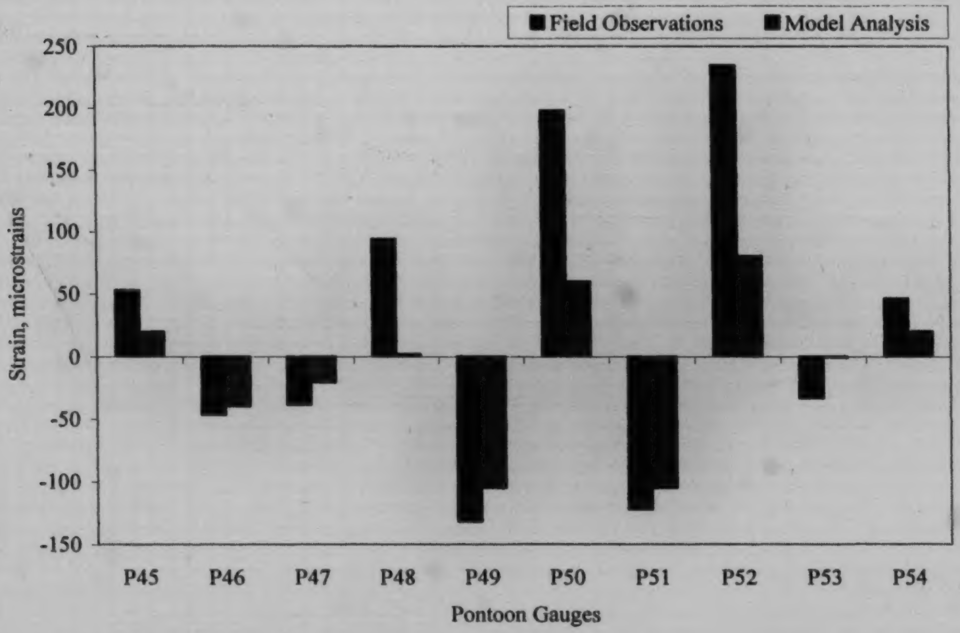

Fig. 8.26 Comparison of field and analysis strains on Pontoon

8.3.5 Stress Hot Spots from Analysis

Stress matching between field observations and model analysis results has thus far indicated good replication of field behaviour by the finite element model and the field load case devised earlier. It is not possible to instrument each and every member or nook and corner of the structure, and hence, the strain gauges may not be placed exactly where the structure is seeing highest stresses. Finite element analysis comes handy in such situations, wherein a stress contour plot gives an idea of how the stresses are varying over the structure and what the values of maximum stresses are. Figures 8.27 and 8.28 present the stress contours on the plate elements of the pontoon girder. The dark (blue) colour around the pontoon mid span represents the highest stress experienced by the pontoon, which is varying between 30 to 50 MPa (150 to 250 micro-strains). This is exactly what has been captured by the pontoon gauges. It is also worth noting that the regions of maximum stresses are centred in the neighbourhood of where the columns sit on top of the pontoon girders. It seems quite logical and natural that the contact between columns and pontoons should be the regions of maximum stress due to stress concentrations etc. Hence, the maximum stresses at column mid span are experienced where the columns are meeting the pontoon at its mid span as shown in Figures 8.27 and 8.28. The figures also show that the plates under other columns near the pontoon foundation are also experiencing high stresses. Most of the plates on the foundation are dark (blue) in colour, whereas some of the plates directly under the columns and on the edges are light (green, yellow and red) in colour. This light (red) colour is the area of highest stress in this stress contour, which peaks at 103 MPa.

Similarly, Figure 8.29 shows the stress contour on the pontoon plates as well as the vertical shear wall plates for the columns, which is placed at column gridline 3. The shear wall plate appears to be under high stresses throughout, with stresses varying from 60 MPa to 100 MPa. Figure 8.30, on the other hand, shows the stress diagram for all the columns, braces and beams of the crusher structure. The red and blue colours differentiate between compressive and tensile stresses. As clearly visible in the figure, the stresses on the edge columns and bracing members are the highest of all. As it appears, the column gauges are able to capture the peak stresses better than the hopper or pontoon gauges because of the high number of gauges used exclusively on columns that is forty gauges in total. Hence, most of the column gauges would serve as excellent monitoring tools for long term health of the structure owing to their closer proximity to true maximum stresses and also due to higher reliability. The maximum stresses obtained on the columns and bracing members are in the tune of 100 MPa to 150 MPa.

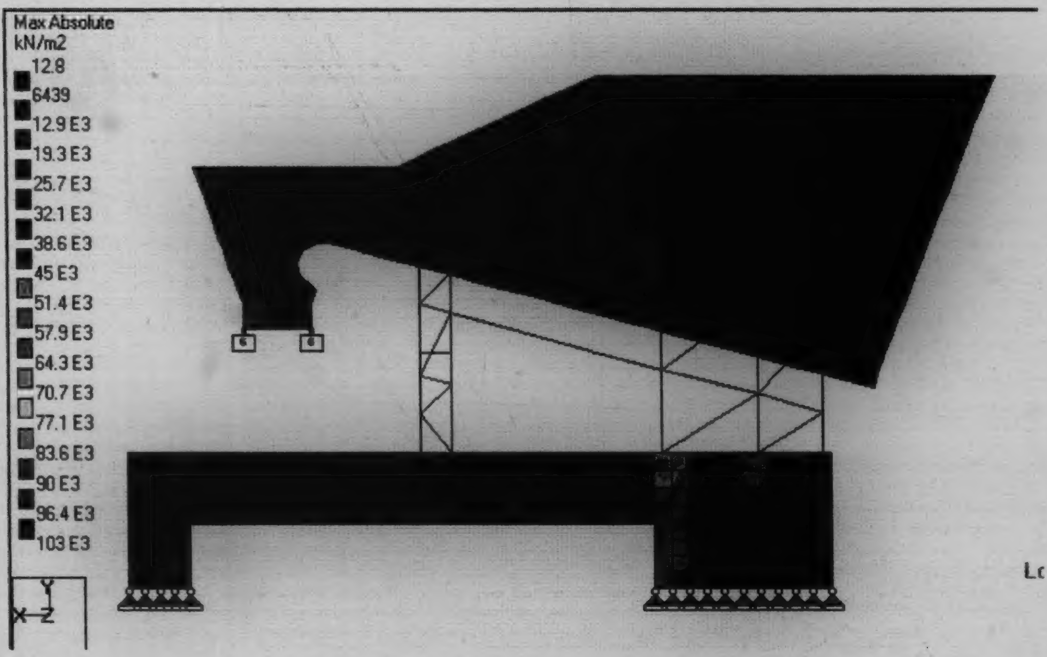
Max Absolute
kN/m2
12.8
6439
12.9 E3
19.3 E3
25.7 E3
32.1 E3
38.6 E3
45 E3
51.4 E3
57.9 E3
64.3 E3
70.7 E3
77.1 E3
83.6 E3
90 E3
96.4 E3
103 E3
Y
X
Z
Lc

Fig. 8.27 Sectional view of pontoon plates stress contour

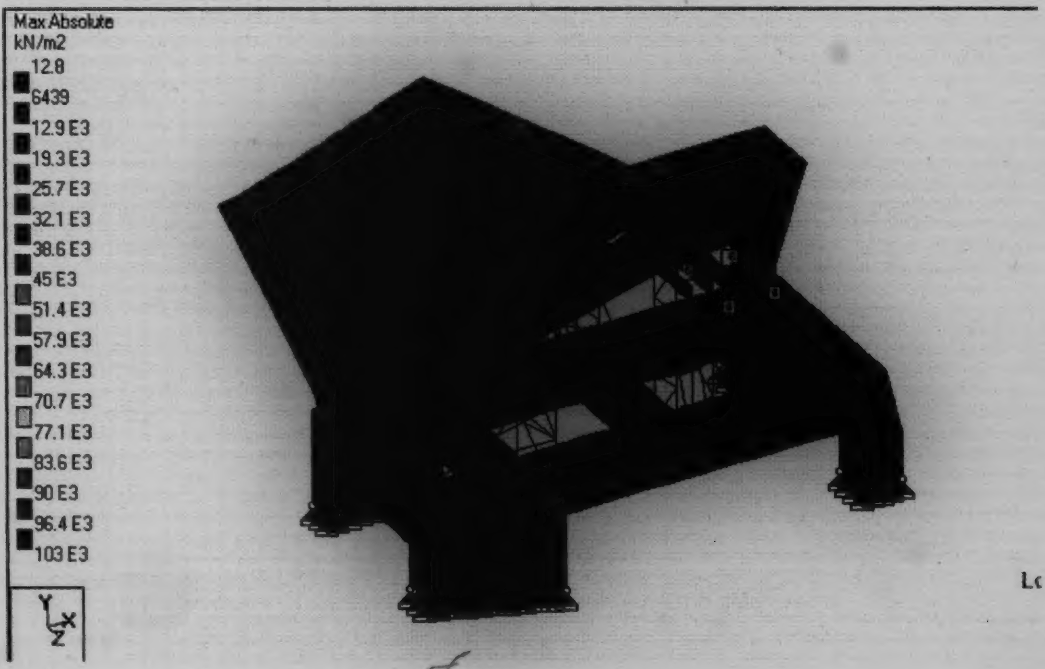
Max Absolute
kN/m2
12.8
6439
12.9 E3
19.3 E3
25.7 E3
32.1 E3
38.6 E3
45 E3
51.4 E3
57.9 E3
64.3 E3
70.7 E3
77.1 E3
83.6 E3
90 E3
96.4 E3
103 E3
Y
X
Z
Lc

Fig. 8.28 Isometric view of pontoon plates stress contour

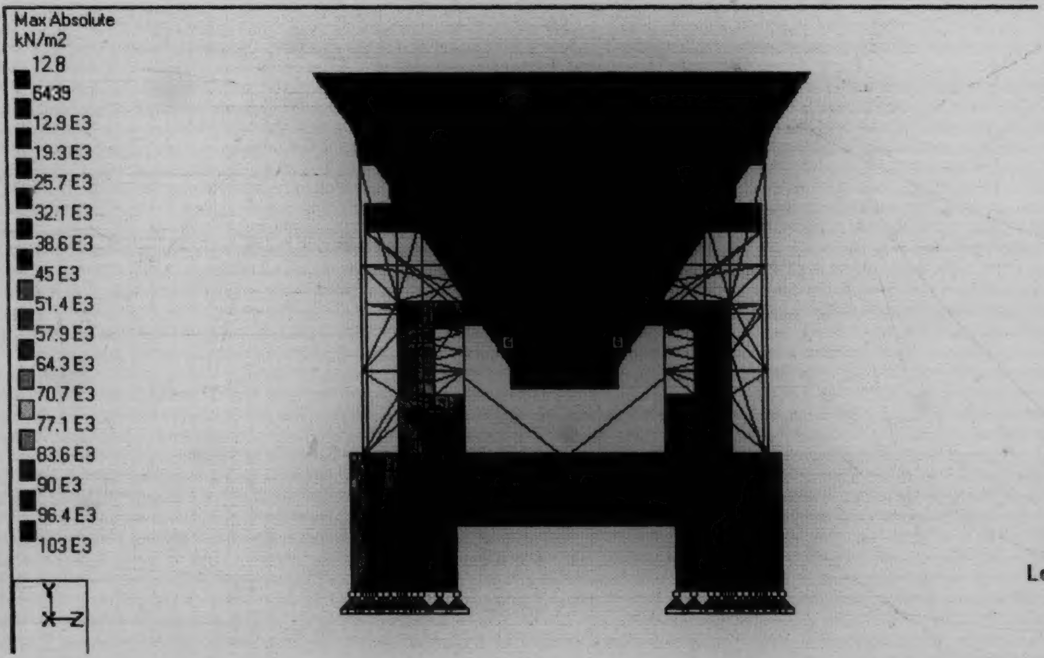
Max Absolute
kN/m2
12.8
6439
12.9 E3
19.3 E3
25.7 E3
32.1 E3
38.6 E3
45 E3
51.4 E3
57.9 E3
64.3 E3
70.7 E3
77.1 E3
83.6 E3
90 E3
96.4 E3
103 E3
Y
X Z
Lc

Fig. 8.29 Sectional view of vertical plate shear wall stresses for columns

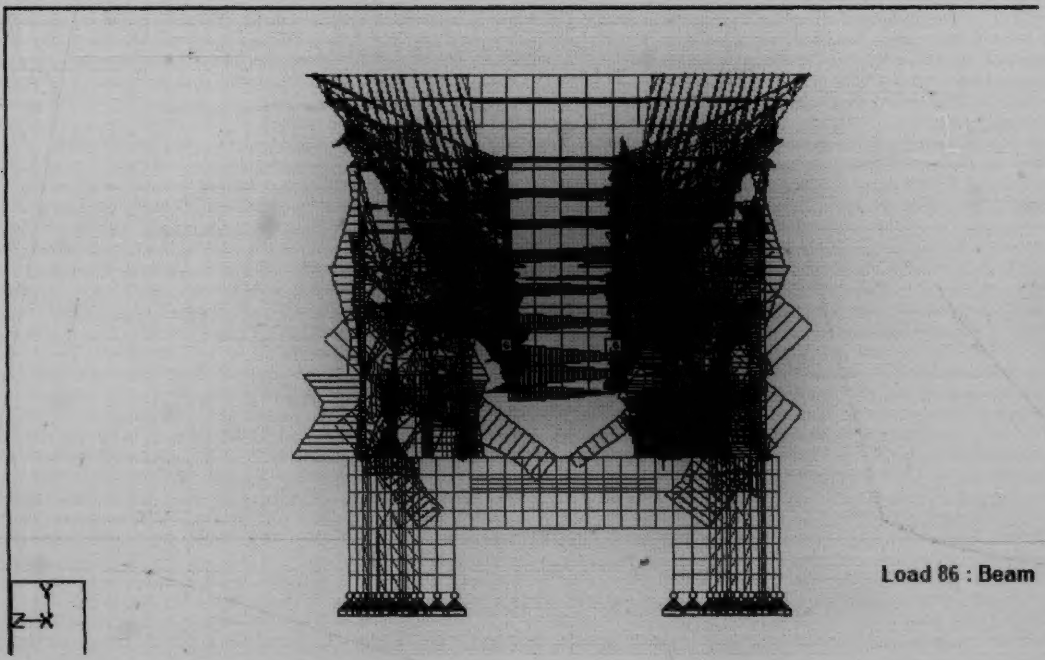
Load 86 : Beam
Y
Z X

Fig. 8.30 Sectional view of columns braces and beams stresses

Thus, the stress hot spots are identified as the area in and around the columns. Firstly, the columns are well stressed under the severe empty hopper loading condition to 100 MPa. Secondly, the column braces and shear walls are stressed up to 100 to 150 MPa. Finally, the pontoon plates in the vicinity of the columns and at the mid span are also stressed close to 100 Mpa. Although the hopper is not well instrumented and the field load case is not developed to determine hopper stresses, it is expected that the joint area between the hopper and the columns and the joint between different segments of the hopper would be highly stressed at least to the same degree of 100 to 150 MPa under severe loading conditions.

8.4 Damage Simulation

With a finite element model calibrated to field observations and the field load case proven to be a close approximation to the load due to dumping of oil sand, it is now possible to perform various types of numerical analyses that would otherwise not be possible without subjecting the structure to some form of physical damage. The damage sustained is limited to the numerical analyses conducted, which gives a probable behaviour of the structure if such damages were to happen. The benefit of these numerical damage simulation exercises rests in the ability to get a peek into the structure's response under damaged condition with relative ease and without subjecting the structure to any sort of distress. The inherent disadvantage to such numerical damage simulations is that the actual behaviour in the non-linear state of the structure may be completely different from what has been predicted. Moreover, with the presence of ample indeterminacy and scope for load redistribution in the event one member gets damaged, the effect of damage may remain quite localised and may hardly get noticed at gauges far away from it.

Nevertheless, it is of interest to expose different components of the structure to damage at different locations one by one and then see the change in response at the nearby gauge locations. Figures 8.31 to 8.34 show the influence of different damage scenarios at the column gauges at each column gridline. The first vertical bar in the bar chart represents the response of the structure in undamaged state and each bar thereafter represents a unique damage situation on the structure. Thus, the responses under different damage conditions are compared against each other and to the original undamaged state. For example, Figure 8.31 shows the response in the vicinity of the column gauges on gridline 2 obtained from numerical analysis. Response under three different damage conditions are plotted against the undamaged response, wherein under each damage condition all the columns on the right side of the hopper line of symmetry at a particular gridline are assumed to have a reduced stiffness of 50% of the original value. Such a reduction in stiffness could come from change in boundary conditions like loss of bolts converting a fixed boundary condition into a pinned boundary condition with little resistance capacity due to missing bolts. Other situations like corrosion and wear and tear or physical damage to the member might also play a role. In the first damage scenario, all the columns on the right side of line of symmetry at gridline 2 are assume damaged by 50% of stiffness value and then its response near the gridline 2 gauges are obtained from analysis. In the next damage scenario, all the columns on the right side of gridline 3 are assumed damaged; and similarly columns on the right side of gridlines 4, 5 and 6 are also assumed damaged one by one. Thus, in total five different damage scenarios have been defined for the columns.

As shown in Figure 8.31, when the damage of 50% reduction in stiffness occurs at the columns on gridline 2, those columns are able to carry lesser load and hence develop lower stresses. A clear drop in stress by 5% to 25% at all the gauge locations of gridline 2 is observed under this damage scenario of gridline 2 as compared to the undamaged response. The next bar chart in Figure 8.31 shows the stresses at those gauge locations when the columns at gridline 3 are damaged. As can be seen, this damage scenario leads to an increase in stress level at most of the gauges at gridline 2. This is because of the fact that when the columns on gridline 3 get damaged, portion of its load is transferred to the gridline 2 columns and the rest to gridline 4 columns. As shown in Figure 8.32, there is a definite increase in stresses at the location of gauges on gridline 4 in the scenario of columns on gridline 3 being damaged as well. However, as the distance of the damage location increases from the location of the gauges, its influence on the stress increase is much feeble. For example, the influence of damage at G2 is not so well felt by the gauges at column gridline 4 in Figure 8.32. Similarly, in Figure 8.34, the influence of damage to G2 or G3 columns is hardly visible at the gauges on gridline 6, whereas the damage at G4 and G5 is quite well felt there by a good increase in stress level. Obviously, in the damage scenario of G6 columns getting damaged, the stress at the gridline 6 gauges fall sharply (instead of rising) in Figure 8.34. This is simply because damage leads to a reduced capacity of carrying loads and the loads are redistributed to the columns at gridline 5.

Thus, it can be concluded that a significant and regular reduction in mean strain readings at the gauges on a particular gridline is a sign of damage at that gridline, whereas a significant increase in the mean strain at those gauges could be an indication that some of the members in its neighbourhood are damaged, transferring additional loads to this column. The statistical mean and other parameters of strain jump at each gauge location due to dumping of oil sand are obtained from statistical analyses in chapter 7. Hence, when the mean value of strain jumps at any of the gauges or group of gauges changes over the years, it would indicate some shift in structural properties or damage. Depending on whether the mean strain values are increasing or decreasing, the location of damage can be pin-pointed to some extent, although exact damage location is a much more difficult task.

In Figure 8.33 for the gauges on gridline 5, again the stress values drop from the original undamaged response when the damage scenario of G5 occurs. However, for damage scenarios of G4 and G6 the stress values rise instead because of their proximity to the gauges at gridline 5. These trends of stress increase and decrease at the various gauges will ultimately aid in damage detection in the long run, but it does need more work in this area of for detection and location with confidence. Another trend that can be observed is that when the damages to the columns are occurring on the right side of the gridline, only those gauges that are placed on the right side of the gridline show possible stress increase or decrease, whereas the stress at gauge locations that are on the left side of the gridline like gauges C31 to C36 in Figure 8.32 show little change. A similar trend can be confirmed on the left side gauge locations in Figures 8.31 and 8.33, with slight change in stress levels from the undamaged state but little variation in stress from one damage scenario to another. Hence, a change in mean strain value is definitely a sign of some permanent change in structural property. In order to locate such changes further, the trend of mean strain change over different gauges at various gridlines will be helpful. Thus, the damage simulation exercise with a few typical damage scenarios is able to lend a sneak peak into the possible changes in mean strain readings over the years and the possible strategies to deal with for their detection. This is however, not a comprehensive damage simulation exercise aimed to identify each and every possible damage scenario, rather the first step in that direction and a glimpse into the response under damaged conditions. It is also worth mentioning here that the results presented here are for the case of 50% damage on each of the columns considered. For smaller levels of damage, the results would be similar but more difficult to separate from healthy structure response.

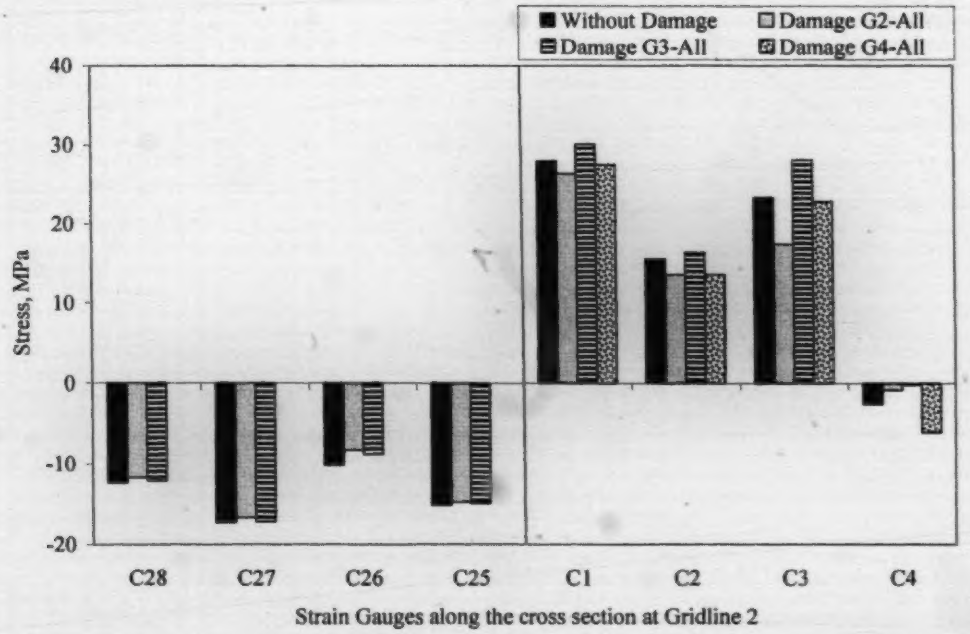

Fig. 8.31 Influence of different damage scenarios on column gauges at gridline 2

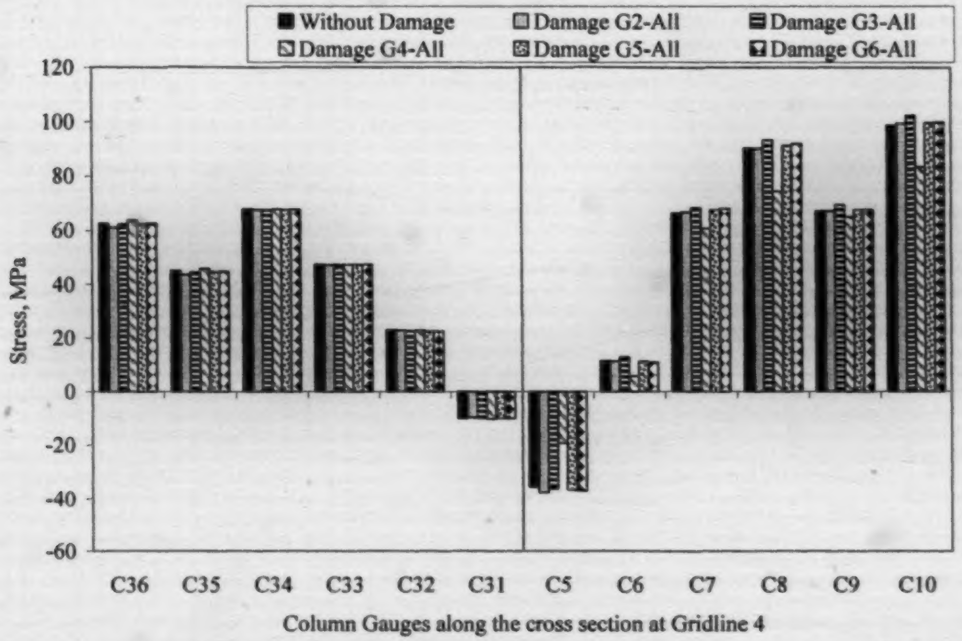

Fig. 8.32 Influence of different damage scenarios on column gauges at gridline 4

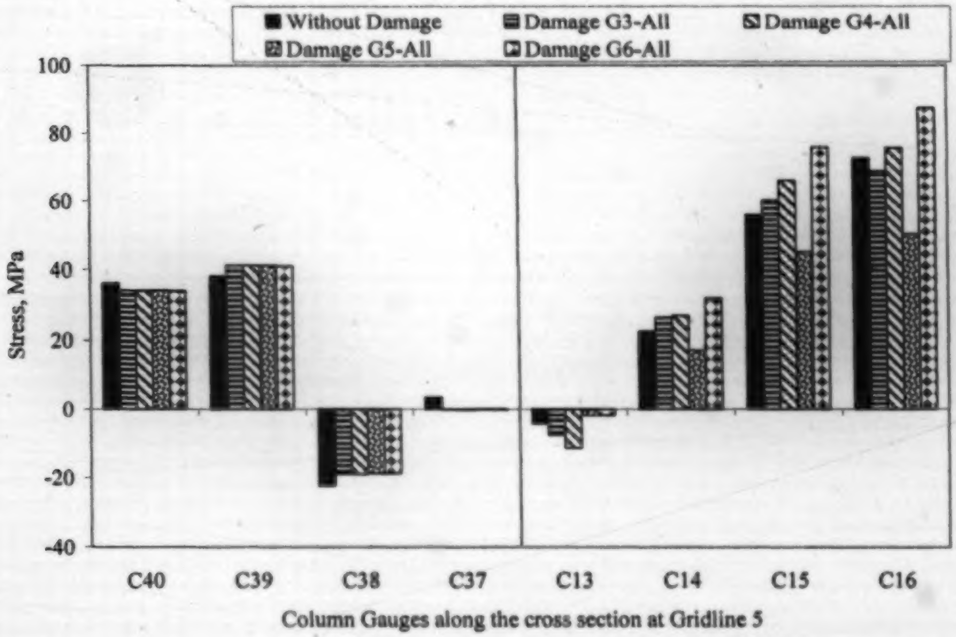

Fig. 8.33 Influence of different damage scenarios on column gauges at gridline 5

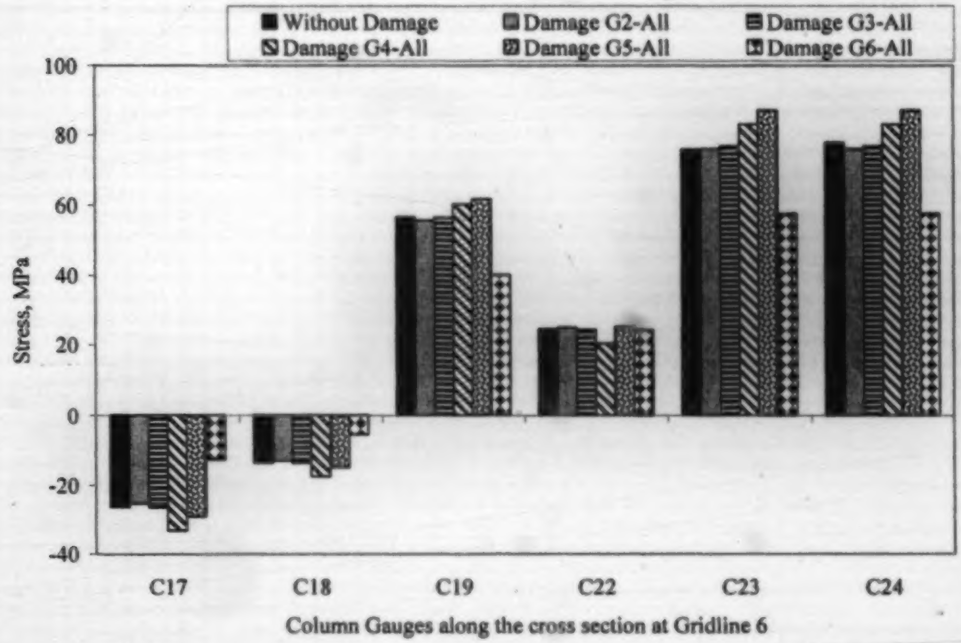

Fig. 8.34 Influence of different damage scenarios on column gauges at gridline 6

8.5 Summary

A unified finite element model of the crusher structure and its components including hopper, columns and pontoons is subjected to a field load case and results obtained by analysis are matched against field observations obtained. A good match is achieved at almost all column gridlines with error in the range of 10 to 20 MPa. The match is also tested by breaking the strain components due to bending and axial loading on the columns as well as the results obtained at pontoon plates. The field load case developed by trial and error is thus established as a close likeness of the real field loading under severe empty hopper dump condition, and is recommended to be considered in future designs of similar crushers. The stress hot spots obtained from analysis on columns, braces, and pontoon plates are analysed and presented. These hot spots would serve as the potential critical locations to be regularly inspected. Lastly, a damage simulation exercise has led to an understanding of the patterns of change in strain due to various damage scenarios and suitable strategies for long term monitoring and damage detection on the Aurora II crusher.

8.6 References

Cook, R. D., Malkus, D. S. and Plesha, M. E. 1989. Concepts and Applications of Finite Element Analysis. Third Edition, John Wiley & Sons, Inc., New York, USA.

Research Engineers International. 2003. STAAD Pro Reference Manual. NetGuru Inc., California, USA.

CHAPTER 9

SUMMARY, CONCLUSIONS AND RECOMMENDATIONS

9.1 Summary

Structural Health Monitoring (SHM) is an emerging tool aimed to take a structure from passive to an active state in terms of intelligence and self diagnosis. SHM has become a choice with a reckoning for researchers and engineering professionals throughout the world, especially for monitoring aging bridges. However, scores of issues remain to be addressed before SHM could become a readily usable and easily accessible tool. Techniques for extracting structural signatures, managing data, and detecting structural changes or damage, remain core areas of research. Application of SHM is extended beyond the conventional boundaries of bridges and buildings to industrial structures in this research project. The Aurora II crusher of Syncrude has been instrumented with 82 sensors and a state of the art data acquisition system to regularly monitor and provide a health report on demand. The project establishes a knowledge-base on crushers and the loads acting on them, especially due to dumps from 10 m height. Knowledge of current operation will not only help in reliable operation and smooth maintenance and management schedules but also lead to an improvement in future design of the crusher.

The Smart Structures Project under Structural Reliability that was conceptualized and initiated at Syncrude has Structural Health Monitoring (SHM) of Aurora2 Crusher as its important component. The Smart Structure project aims to reduce trucking costs and crusher downtime. In a bid to move to the future generation of fully mobile crushers from the present semi-mobile ones to reduce the haul time, a range of design parameters need to be tested, more detailed loading information needs to be obtained, and long term data on real field conditions are required. The SHM project of Aurora2 crusher is envisaged to be the primary feeder of all these information on loading, boundary conditions, impact factor, and stress ranges etc. to Syncrude and Krupp Canada Inc., the vendors of the crusher, who will incorporate the findings from this project into their design of the next generation of crushers.

The SHM of Aurora II oil sand crusher of Syncrude Canada Limited in Fort McMurray, Alberta, is a step out in the direction of extending the utility, application, and benefits of SHM to other civil infrastructure. The oil sand crusher is a vital component in the mining operations of oil sands, which has become a focal point of Canadian economy and is the second largest known oil deposit in the world. The crusher is primarily responsible for breaking large lumps of oil sand into easily manageable sizes of 400 mm and less for hydro-transportation to the extraction plant. It is able to collect oil sand from two haul trucks of up to 400 ton simultaneously into its diamond shaped hopper. When completely empty, the fall of oil sand into the hopper can be as much as 10 metres, causing huge impact loads on the structure. It is subjected to a myriad of loads ranging from impact, abrasion, vibration, and temperature variation of up to 80 degree Celsius. Variability and magnitude of loads under extreme climatic conditions make the project quite challenging. Lack of field performance data combined with the continuously evolving demands of the future generation of crushers and some instances of past maintenance problems reinforce the need for monitoring the crusher.

The crusher has been instrumented with 82 sensors, which includes 60 weldable strain gauges, 10 LVDT's, 10 accelerometers, and 2 thermocouples. Out of the sixty strain gauges, 10 each are welded on the south side of hopper and pontoon, whereas 40 strain gauges are put on the columns and bracings. Data collected from the 82 sensors at 100 Hz have been analysed to create a knowledge bank on the behaviour of different structural components of the crusher. Base data was collected before commissioning of the plant, which provides the datum for comparison of behaviour over the years. Some control tests have been conducted later with known weight of oil sand and other dump parameters like material level in the hopper, side and speed of dump, with video recording. Data was also collected under the influence of temperature alone when no dumping was occurring. One of the biggest challenges facing SHM projects is the huge amount of data gathered in a very short time. Significant time and resources are required to analyse the data, interpret the results, and make a decision on the management of structure and the data. Every ten minutes 11 MB of data is generated, which amounts to about 1.5 GB of disk space per day. Storing such amount of data permanently for a long term is costly, inefficient, intimidating, and defies reason; hence, an algorithm has been developed for event identification based on a metric defined as Strain Jump, a differential entity obtained as the difference between maximum and minimum strain observed in a 5 second moving window. Its differential nature not only gets rid of temperature effects, but also from effects of noise and drift over time. Once events are identified, it becomes obvious that only 10% of the collected data actually pertain to events and the rest 90% are non-event or mundane data.

The proposed event identification and data processing algorithm integrated with the database system is able to effectively process, reduce, and archive the data for easy access and long term monitoring by about 10,000 times, without losing any valuable information. The algorithm is built upon multiple layers and varieties of thresholds derived from the operating conditions and response characteristics of the structure. Much has been drawn from the many similarities existing between the structural signal under impact of oil sand and the electrical signal generated by firing of neurons. Experience of detecting neural spikes in neuroscience has been applied into the structural domain in detecting strain jump. Strain jump has served as an excellent parameter in event detection and structural monitoring, with ability to predict remaining life of the structure. Magnitude of strain jump, dump duration, inter-spike interval, average noise amplitude and time stamp of the dump have been used as the parameters for signal processing and event detection. Moving search windows of 10 second and 20 second durations have been employed in event identification and feature extraction respectively. Two separate algorithms are used for major events with higher strain jump and minor events with strain jump magnitude very close to the ambient noise. Dump events identified over multiple channels are verified against each other to a satisfactory level of verification power before writing the characteristic features of the dump into the database for each gauge location. The algorithm is robust and is able to successfully process data collected under varying operating conditions to identify all dump events with remarkable accuracy. Many checks and balances exist in the algorithm to detect potential sources of error, which are communicated to the user for rectification or improvement in the future. Histogram of strain jump at each gauge location will able to predict the fatigue life of the structure to schedule appropriate inspection and maintenance interval. Various statistical queries are able to extract information from the database at the click of a button to enhance the knowledge of the user. Hence, the proposed data processing and management algorithm has satisfactorily extracted all the pertinent information from the data and reduced it significantly to provide a platform for long term health monitoring of the structure.

Analysis of the data has shed light on the stress levels occurring at different structural components and their associated impact factors. In addition to the individual strain readings of a sensor, study of the relative strain readings on a range of nearby sensors on pontoon and columns have helped establish strain patterns to associate with certain dump types and conditions. It is this concept of individual strain magnitudes combined with their neighbourhood pattern that will aid in damage detection on the crusher. Certain strain patterns have been identified for different types of dumps. Performance of the crusher members under temperature and different types of dump loads has been assessed. Temperature variations of up to 80 degree Celsius over the year can lead to significant stresses and changes in structural behaviour. However, over 0.2 million dump-events occurring annually to maintain the crusher's production at 70% of rated capacity overshadows the influence of temperature on the structure from the point of view of fatigue and remaining life. Critical dump parameters have been explored for optimum operation. Dump in an empty hopper is responsible for the severest of strains; however, under normal operation the hopper is never empty. The strain magnitude increases with the speed of dump and fall in hopper material level. Dumps faster than 20 seconds and hopper material level less than 20% causes the strain to rise exponentially. The average impact factor and strains under normal operation and the maximum strains and impact factors during extreme loading events of controlled testing have been calculated. Based on the maximum strain jumps and impact factors observed at pontoon, columns and hopper in the crusher, they are found to be satisfactory under normal operation while some columns and bracing members experiencing slightly high stresses under severe loading. The inclined struts and braces are recommended for review in future designs owing to high stresses and bending observed under extreme loading.

Aurora II Double Roll crusher is a complex combination of hopper plates, beams, bracings, columns and supporting pontoon. It is subjected to impact loads of two 400 ton heavy haulers as continuous normal operating condition. Although, no substantial structural maintenance problems have occurred in the past on the four crusher of this category, there is little work or knowledge regarding the margin of safety in the design specifically in the impact factor estimation. This issue may become crucial in the near future when At-face slurry system demands a fully mobile crusher. Detailed investigations of the crusher behaviour under temperature, normal operation, and control testing have been carried out and the results presented.

1. Linear relationships exist between temperature and strain gauge readings at different locations within small temperature variations. Slopes of this relationship for each gauge have been plotted and they vary from 1.31 to 6.4 micro-strains per degree Celsius, which can be corrected for thermal coefficient of the gauge for larger temperature variations. Ten minute averaging interval has been adopted for eliminating noise in the thermal data.
2. The adequacy of rate of data acquisition during operation has been explored and found to be quite satisfactory by good number of data points captured in every rising arm of strain in a strain jump due to a dump event.
3. North side (left) dump has much higher influence on South pontoon than South side dump. Empty hopper dump C1-L is the most severe dump event.
4. The maximum measured absolute strain value at pontoon mid-span is 229 micro-strains. At column gauges the maximum strain observed was 450 micro-strains for vertical members and 757 micro-strains for struts and braces; whereas the maximum strain observed in hopper gauges was 200 micro-strains.
5. The strain readings measured at all column gauges were broken into bending and axial strain components. Presence of some local bending was observed in some

vertical column gauges and most of the inclined struts and braces. The bracing at gridline 6 recorded bending and axial strain components of 450 micro-strains each.

6. Maximum impact factor of 15 was measured for pontoon, 25 for columns, and 10 for hopper based on the readings of sixty strain gauges during tests in October 2003 and April 2004. These values correspond to empty hopper. For dumps on partially full hopper during normal operation, average observed impact factor were 3 for pontoon, 4 for columns and 3.6 for hopper.
7. Maximum dynamic strain due to a single dump on empty hopper is 3.3 times higher than maximum static strain due to a completely full hopper.
8. Normalized strain jump pattern along the pontoon is a good indicator of the side and type of dump. The strain jump magnitude increases rapidly with decreased dump duration below 15 seconds. It also increases rapidly with decreased hopper level below 20%. It is therefore recommended that normal operating conditions sustain these impact-reducing limits.

The nature of the load and structural response under it has been dealt with in a dynamic sense. By using Fourier transform and digital filtering tools, the natural frequencies and damping characteristics of the structure has been analysed. Power spectrum and filtering techniques re-affirmed that frequencies above 10 Hz were all noise and the structural frequencies were between 0 to 10 Hz. By trial and error with different periods of data files, data between 100 to 200 seconds long gave the best results in power spectrum, which amounted to frequency resolution of between 0.01 Hz to 0.005 Hz. The static component of the response is obtained by passing the signal through a low pass filter with cut off frequency of 0.1 Hz. The major frequency peaks identified by various power spectrum plots are: 0.24 Hz, 0.49 Hz, 0.96 Hz, 2.93 Hz, 3.417 Hz, 3.91 Hz, 5.86 Hz, and 7.81 Hz. The peak frequencies start shifting and getting blurred under dumping of oil sand into the hopper. An increase in the mass of the structure due to the added mass is the reason behind such shift and blur due to spectral leakage. Some of the low frequency modes become more prominent under dumping of oil sand, such as the frequencies of 0.24 and 0.49 Hz. Not all frequencies are captured at all gauge locations and under all loading conditions due to obvious reasons. Band filtering in the frequency bands of importance gives the amplitude of vibration due to various frequencies and their modal damping, which usually varies between 3% and 5% for the higher vibration modes. For the first three or four fundamental modes of vibration, the modal damping ratio was obtained between 11% and 15%, which indicates high damping due to many mechanical and functional components.

Statistical properties like mean, median, standard deviation, maximum and minimum values, etc. are considered of much value to SHM projects. Based on 1300 dump events encountered in April 2004 and June 2006, a certain pattern and values have been generated for each of the statistical parameter in consideration. When monitored over a long period of time, each of these statistical parameters has the potential to monitor and detect changes in performance to a certain extent. Standard error of the mean is usually quite low between 1 to 3 micro-strains. The 95% confidence interval for the mean is also within a range of 1 to 4 micro-strains, which is excellent for the magnitudes of the mean concerned. The difference between the positive and negative values of strain jump is defined as the Range, which is another useful parameter worth monitoring. Thus, any significant variation in the positive jump, negative jump, jump range, or the mean value of jump at a gauge location signals some major change in the structural stiffness or boundary conditions. Such changes if found at more than one gauge locations, would reinforce the belief that the structure has seen some major event or damage. The extreme values of strain jump encountered at various strain gauges were in the range of more than 700 micro-strains during empty hopper dumping. It was observed that the extreme values are many times larger than the mean values, which signifies that the extremes are less frequently occurring. The largest magnitudes of strain jump observed are occurring on the bracing members, like C7, C8, C16, C17, C23, C24, C34, C36, C40, etc. and the same members also happen to have the highest magnitude of mean strain jump. Thus, those members are regularly under high stress and it is not one secluded case of high stress loading. The absolute mean strain jumps at most of the gauges happen to be less than 100 micro-strains, except for a few gauges that inadvertently happen to be on the bracing members. The mean strain jumps on the rest of the gauges are varying between 20 and 100 micro-strains. These first values for the statistical parameters at each gauge location serve as the benchmark for monitoring of the structure that can be adjusted later as per future needs and behaviour. These statistical observations also help identify the structural members that are consistently under comparatively higher stresses, which would be of much help in making appropriate modifications in future designs.

Histograms are eventually able to represent the probability distribution functions for a random variable, which in this case happens to be the strain jump recorded during dump events. Thus, the frequency of occurrence of a particular strain magnitude at a particular gauge location, and consequently, its corresponding probability of occurrence can be viewed in a glance on histograms. In a statistical sense, assuming that a sufficiently large sample population has been considered, it can be argued with confidence that the sample mean would approach population mean. So, the histogram at each gauge location represents the characteristic property of structural response at that gauge location and its distribution shape and sample mean would remain similar over time. This is taken as the statistical property of the population of response at that gauge, which does not change with time and remains statistically constant, except when damage occurs. It is quite obvious from the histograms that the column gauges experience much higher strain levels more frequently than the gauges on pontoon or hopper. Gauges placed on the columns in Gridline-2 experience typically low strains, which is evident by the fact that none of the gauges on Gridline-2 feature in the list of critical gauges. Gauges on the bracing members frequently observe strain jump in the range of 200 to 400 micro-strains, and on many occasions even up to 500 and 600 micro-strains. Thus, even the average (or mean) strain jump magnitudes for these bracing gauges are higher than 100 micro-strains. It can also be noticed that most of the bracing members are subjected to compressive stresses (negative strain jump) due to most of the dumping. However, on some occasions they do as well experience tensile stresses in the range of up to 100 micro-strains. On the contrary, the strain jumps at the gauges on the vertical column members appear to be significantly lower in magnitude. Thus, the pontoon is expected to have the longest fatigue life, the vertical column members to have relatively shorter life, and the inclined column bracings to have the shortest fatigue life based on the frequency of high stress cycles they are subjected to.

Fatigue and fatigue induced fracture are the leading causes of failure of steel structures. With the repetitive nature of loading experienced by the Aurora II crusher, calculation and assessment of its fatigue life assumes much significance. Since the structure is not subjected to constant amplitude stress range at all times and the magnitude of stress can vary widely as shown by the histograms in the previous section, an equivalent stress range approach has been used for calculation of fatigue life. The equivalent stress range is calculated based on the strain histories depicted by the histograms using the equation based on the Palmgren-Miner cumulative fatigue damage rule. Based on these equations, the equivalent stresses for the column bracing members are obtained as the highest of all. The equivalent stress at gauge C24 on a bracing member is obtained as 40.71 MPa for the stress history encountered and recorded at that location. For this equivalent constant stress assuming a category E connection detail, the fatigue life of the bracing member is obtained as 5.34 million cycles. Since the crusher structure is subjected to an average of 0.203 million cycles per annum, the life of the bracing member in simple terms is obtained as 26 years. Hence, in general, the structure as a whole and the bracing members in particular happen to be acceptable from fatigue point of view based on field test results. Assuming a situation where two thirds of the bolts at a connection go missing, a new equivalent stress range of 122 MPa is obtained for the bracing members by applying a stress factor of 3. The fatigue life then is obtained as just below one year (0.98 years) for category E detail. Hence, a minimum inspection interval of one year should be maintained for detecting and correcting any loose bolts or total loss of bolts condition.

A finite element analysis and numerical damage simulation exercise is carried out to wrap up the research and present the performance of the model with respect to field observations. Finite element modeling is also a useful tool to fill in the gaps left by instrumentation and allow for simulations. A unified finite element model of the crusher structure and its components including hopper, columns and pontoons is subjected to a field load case and results obtained by analysis are matched against field observations obtained. A good match is achieved at almost all column gridlines with error in the range of 10 to 20 MPa. The match is also tested by breaking the strain components due to bending and axial loading on the columns as well as the results obtained at pontoon plates. The field load case developed by trial and error is thus established as a close likeness of the real field loading under severe empty hopper dump condition, and is recommended to be considered in future designs of similar crushers. The stress hot spots obtained from analysis on columns, braces, and pontoon plates are analysed and presented. These hot spots would serve as the potential critical locations to be regularly inspected. Lastly, a damage simulation exercise has led to an understanding of the patterns of change in strain due to various damage scenarios and suitable strategies for long term monitoring and damage detection on the Aurora II crusher.

9.2 Conclusions

This research has established a framework for Structural Health Monitoring of the Aurora II crusher in Fort McMurray, Alberta. This framework includes a network of instrumentation hardware, software, a data processing and management algorithm, response patterns based on structural behaviour, a finite element model and sufficient statistical information for long term monitoring. By integrating and building upon the techniques and information presented by this research, the industrial partners would be in a position to implement in the field. The project has established a knowledge-base on oil sand crushers and the loads acting on them. Knowledge of current operation will be instrumental in efficient management of the crusher as well as for improving future designs. Based on the analysis of the research data and information contained in it, the following conclusions are drawn.

1. The biggest challenge faced by the SHM system is to process and manage 1.5 GB of data collected everyday in an efficient and cost-effective manner. Strain Jump has been successfully used as a metric to identify and quantify dump events. This eliminates noise and temperature effects and selects the most important strain readings, discarding the rest. A data processing and management algorithm has been developed specific to the project to reduce volume of data by 10,000 times before archiving it into a database.

2. The data processing algorithm is built on layers of a series of thresholds working together to identify a dump event by using strain jump magnitude, dump duration, average noise magnitude, and inter-jump interval as the parameters with an overlapping scanning window. Selected strain gauges then verify the validity of the identified dump events before reducing the data and storing them permanently into a database of dump events. This data processing algorithm is developed for impact loading in particular but with some modifications it can cater to the needs of a wider spectrum of SHM projects.

3. Based on statistical analyses conducted on strain at each gauge location, bracing members are found to have the highest mean strain jump of 100 micro-strains and the columns on gridline 4 and 6 are the most heavily stressed. Statistical parameters have been established for monitoring any shift in their values over the years.

4. Fatigue life calculations revealed that bracing members had the lowest fatigue life during normal operation of the crusher while pontoons had the longest fatigue life. The shortest fatigue life for the critical braces was adequate at 26 years, though factors like stress concentration due to bolt loss could drop it down to 1 year. Consequently, a yearly inspection schedule is proposed for all the joints and bolts to ensure proper tightness during operation.

5. Structural behaviour of the crusher under dumping and temperature variation has been analysed to establish response patterns and peak stress levels. Empty hopper dumps produced the largest strain values, the occurrence of which is few in number each year. A certain strain pattern and impact factor has been associated with each type of dump. Dumps faster than 20 seconds caused significant rise in strain and so did material level less than 20% in the hopper. Specific recommendations to decrease loading are to ensure a minimum dump time of 20 seconds and to retain at least 20% material level in the hopper..

6. Columns on gridline 2 were the least stressed whereas those on gridlines 4 and 6 were highly stressed. The bracing members produced the highest strain of 757 micro-strains and an equivalent impact factor of 25, whereas the pontoon and hopper stresses remained much lower. The average impact factor on pontoon and hopper during severe loading was 15 and 10 respectively. The average impact factors on the pontoon, columns and hopper during normal operation, on the other hand, were much lower at 3, 4, and 3.6 respectively. Pontoon and hopper response was satisfactory, whereas some columns were highly stressed under severe loading. The inclined braces and struts were the worst affected under heavy impact owing to high stresses and presence of bending, and hence, are recommended for review in future designs to limit vibration and fatigue.

7. Power spectrum analysis revealed most of the structural frequencies were below 10 Hz. Eight peak frequencies were identified in the range, but their clarity got blurred during dumping due to changing mass and spectral leakage. Modal damping ratios for the first three or four fundamental frequencies were obtained between 11% and 15% , whereas the higher vibration modes had damping ratios between 3% to 5%

8. A unified finite element model of the Aurora II crusher was prepared using STAAD Pro software and a good match obtained with field observations to yield a new field design load case simulating the impact due to fall of oil sand into an empty hopper. A knowledge-bank has been established on performance of oil sand crushers under impact loading and the nature of the load itself. Finite element modelling also identifies the stress hot spots on the structure and provides an opportunity to conduct damage simulation to shed light on the patterns of strain changes and the strategies suitable for monitoring and damage detection on the Aurora II crusher.

9.3 Recommendations

The following recommendations are made to fill in the gaps left by and created by the current research. Since data is the back bone of any SHM system, first and foremost, continuous data collection for a number of years would be able to give a much better picture of the statistical features and their variance over time. With the availability of a data processing and management program, now it is possible to handle the huge amount of data that comes along with it. For continuous data collection at site to be possible, it would also be important for Syncrude Canada Ltd. to integrate the SHM system into its field production monitoring system so that the program is able to communicate any abnormal behaviour. With a larger volume of continuous data, it would be possible to generate statistical trends at each gauge location for each month or week of operation that would facilitate long term monitoring.

The data processing and management program also needs to be worked upon to make it more user-friendly. In its current state, it is a command prompt based program with little help for the field operators. The algorithm is also specifically applicable to only impact type of loading on the crusher. Its utility on other types of structures and loadings, like vehicle moving on a bridge, needs to be investigated. With such a feature extraction capability free from the effects of noise and temperature, which is able to statistically predict the remaining life of the structure as well as monitor its long term health, would be very interesting and desirable. A larger volume of data may also see some modifications in the algorithm to cater to the specific monitoring needs. Application and development of statistical or probabilistic damage detection techniques based on statistical knowledge gathered over many years is also envisaged.

The sensor network applied on the hopper was not dense enough to give an idea about the stress distribution in different regions of the hopper. Hence, in order to get a better picture of hopper stresses, a more detailed instrumentation is recommended. Also, a more detailed dynamic investigation with strategic placement of accelerometers along the length and height of the structure would be able to determine the mode shapes and their precise natural frequencies. A finite element model with non-linear analysis capabilities would be desirable to conduct rigorous numerical damage simulations. It is strongly recommended that similar SHM initiatives be applied to other structures of Syncrude and elsewhere based on the learning from this research. In order to limit the high strains due to impact, it is recommended that the dump truck operators do not dump into the hopper faster than 20 seconds and at all times the hopper should maintain 20% full to dampen the effect of impact from fall. It is also recommended that Krupp Canada Inc. review its design of the inclined struts and braces under extreme impact and vibrations. The vendors of the crusher are also advised of the new field design load case developed for their perusal in design of future crushers. It is recommended to Syncrude Canada Ltd. to maintain an annual inspection of all bolts and connections, tightening them if necessary, for a long and healthy service life of the crusher.

APPENDIX – A

Proposed Field Design Load Case

STAAD Input File

```
LOAD 25 VERTICAL LOADS AT GRID 5 AND 6
JOINT LOAD
438 FY -4000

LOAD 28 VERTICAL AT GRID 2
JOINT LOAD
314 FY -1000

LOAD 29 VERTICAL AT GRID 3
JOINT LOAD
352 FY -1000

LOAD 30 VERTICAL AT GRID 4
JOINT LOAD
399 FY -500

LOAD 34 HORIZONTAL LOAD GRID 2
JOINT LOAD
314 FZ -1000

LOAD 35 HORIZONTAL LOAD GRID 3
JOINT LOAD
352 FZ -1000

LOAD 38 HORIZONTAL LOAD GRID 4
JOINT LOAD
399 FZ -1000

LOAD 40 LEFT HOPPER VERTICAL G4
JOINT LOAD
939 FY -2500

LOAD 41 LEFT HOPPER HORIZONTAL G4
JOINT LOAD
939 FZ 1250

LOAD 42 VERTICAL TENSION ON LEFT HOPPER G2
JOINT LOAD
888 FY 800

LOAD 43 G6 - ADDITIONAL LOAD ON GRID 6 OUTSIDE COLUMN
```

```
JOINT LOAD
436 FY -300

LOAD COMB 86 RIGHT HOPPER COMBINED LOADING 1
28 1.8 29 2.0 30 4.0 25 0.5 34 1.0 35 1.0 38 2.0 40 0.8 41 1.5 42 1.0 43 1.0

PERFORM ANALYSIS PRINT LOAD DATA
FINISH
```